

---

# Cardiac Magnetic Resonance Studies

in

# Coronary Artery Disease

---

Thesis submitted for the degree of

Doctor of Medicine

at the University of Leicester

by

Penelope Ruth Sensky

University of Leicester

June 2002

UMI Number: U601219

All rights reserved

INFORMATION TO ALL USERS

The quality of this reproduction is dependent upon the quality of the copy submitted.

In the unlikely event that the author did not send a complete manuscript and there are missing pages, these will be noted. Also, if material had to be removed, a note will indicate the deletion.



UMI U601219

Published by ProQuest LLC 2013. Copyright in the Dissertation held by the Author.  
Microform Edition © ProQuest LLC.

All rights reserved. This work is protected against  
unauthorized copying under Title 17, United States Code.



ProQuest LLC  
789 East Eisenhower Parkway  
P.O. Box 1346  
Ann Arbor, MI 48106-1346

***In memory of David de Bono***

*in appreciation*

*of his unswerving friendship, faith, idealism,*

*and invaluable, stimulating contributions to the inception of*

*these studies*

## **Acknowledgements**

I am grateful to David de Bono, who secured initial funding for this work from the British Heart Foundation in combination with Glenfield Hospital Research and Development, and to the Wellcome Trust for awarding me a Research Fellowship.

My supervisors, Nilesh Samani and Graham Cherryman, provided unstinting practical and intellectual contributions to the studies presented. I cannot thank them enough. I am indebted to them not only for their supreme patience but also for their personal support and friendship.

I would like to express my thanks for the tireless radiological reporting that was integral to the studies. In particular I am grateful to Christine Reek for her angiographic skills, to Richard Keal for reporting the MRI wall motion scans, to Norah Hudson for evaluating the scintigraphic studies and to Graham Cherryman for qualitative MRI perfusion analysis. A special note of thanks goes to Richard and Norah for much advice, friendship and moral support. Keith Abrams kindly gave statistical support.

I am very grateful to key personnel. Mark Horsfield wrote the computer algorithms for quantitative perfusion analysis and provided generous advice on matters of MRI mathematics and physics. Julia Tranter contributed essential nursing and managerial support to the studies and conducted all symptom questionnaires. Kay Lord was the ultimate secretary.

I would like to wholeheartedly thank the MRI radiographers for their patience, advice, willingness to learn and enthusiastic participation in these studies. Their friendliness and professional attitude made these projects a pleasure to be involved in. I am also extremely grateful to the technicians and nursing staff in the department of Nuclear Medicine for their unerring cooperation and flexibility. In particular, I would like to thank Hazel Williams for advice on the pharmacological stress regimens.

I am grateful to Manuel Galinanes for making available to me the exercise test data and surgical details for the study presented in Chapter 7, and to Asvina Jivan who provided the retrospective relaxation rate data for Chapter 3.

Finally, I wish to express a special thank you to Paul, not only for his superb computer skills but also for his patience, understanding and encouragement throughout this project.

# Contents

<b>Chapter 1 Introduction.....</b>	<b>15</b>
1.1 Introduction .....	16
1.2 Coronary artery disease .....	16
1.2.1 Coronary artery revascularization.....	18
1.2.2 Coronary angiography.....	19
1.3 Non-invasive imaging techniques in coronary artery disease .....	20
1.3.1 Non-invasive assessment of myocardial perfusion.....	21
1.3.1.1 Clinical indications.....	21
1.3.1.2 Myocardial perfusion imaging .....	22
1.3.1.3 Imaging techniques for measurement of myocardial perfusion .....	23
1.3.1.3.1 Single photon emission computed tomography.....	23
1.3.1.3.2 Positron emission tomography .....	24
1.3.1.3.3 Computerized tomography (CT).....	24
1.3.1.3.4 Contrast echocardiography .....	25
1.3.1.3.5 Magnetic resonance imaging.....	25
1.3.1.3.5.1 Inversion recovery snapshot-fast low angle shot (FLASH) sequence	26
1.3.1.3.5.2 Contrast media.....	26
1.3.1.3.5.3 Clinical application .....	30
1.3.2 Non-invasive assessment of myocardial function.....	31
1.3.2.1 Clinical indications.....	31
1.3.2.2 Myocardial function imaging .....	32
1.3.2.3 Imaging techniques for measurement of myocardial function .....	32
1.3.2.3.1 Stress echocardiography .....	32
1.3.2.3.2 Magnetic resonance imaging.....	33
1.3.3 Non-invasive assessment of myocardial hibernation.....	35
1.3.3.1 Definition and clinical relevance.....	35
1.3.3.2 Identification of myocardial hibernation.....	35

1.3.3.2.1	Inotrope-induced contractile reserve .....	36
1.3.3.2.2	Preservation of perfusion and metabolism.....	37
1.3.3.2.3	Cell membrane integrity .....	37
1.4	Cardiac MRI experience in Leicester prior to thesis commencement .....	38
1.5	Thesis objective.....	39
1.6	Thesis hypotheses .....	39
1.7	Specific thesis objectives and overview .....	40
1.7.1	Development of first pass contrast-enhanced MRI technique for quantification of myocardial perfusion (Chapter 3) .....	40
1.7.2	Diagnostic potential of adenosine perfusion MRI in patients with coronary artery disease (Chapter 4) .....	41
1.7.3	MRI prediction of contractile recovery in individual myocardial segments following revascularization: translation into clinical benefit (Chapter 5).....	41
1.7.4	Restoration of myocardial blood flow following percutaneous balloon dilatation and stent implantation (Chapter 6).....	41
1.7.5	Comparison of clinical and functional effects of transmyocardial laser revascularization and thoracic sympathectomy (Chapter 7).....	42
<b>Chapter 2</b>	<b>Methods.....</b>	<b>43</b>
2.1	Ethical approval .....	44
2.2	Clinical assessment.....	44
2.3	Coronary angiography .....	44
2.3.1	Measurement of ejection fraction .....	45
2.3.2	Qualitative reporting according to the Green Lane system .....	45
2.3.3	Quantification of coronary artery stenoses.....	45
2.4	Magnetic resonance imaging.....	45
2.4.1	Magnetic resonance imager.....	45
2.4.2	Slice selection .....	46
2.5	Magnetic resonance imaging: myocardial perfusion .....	47
2.5.1	Imaging sequence .....	47
2.5.2	Scan protocol .....	48
2.5.3	Adenosine infusion.....	48

2.5.4	Quantitative analysis of MRI perfusion data.....	49
2.5.4.1	Estimation of the unidirectional transfer constant for gadodiamide ( $K_i$ ): tracer kinetic model .....	49
2.5.4.2	Relationship of tracer kinetic model to magnetic resonance imaging.....	52
2.5.4.3	Measurement of longitudinal relaxation time ( $R_1$ ): derivation of $K_i$ .....	53
2.5.4.3.1	Extraction of regional signal intensity.....	53
2.5.4.3.2	Calculation of $K_i$ .....	55
2.5.4.4	Estimation of myocardial perfusion .....	56
2.5.4.4.1	Myocardial perfusion reserve index and myocardial perfusion reserve.....	56
2.5.4.5	Bolus delivery.....	57
2.5.4.6	Signal and contrast to noise ratio.....	57
2.5.4.7	Delayed hyperenhancement.....	57
2.5.5	Qualitative analysis of perfusion images.....	57
2.6	Magnetic resonance imaging: myocardial function.....	59
2.6.1	Imaging sequence .....	59
2.6.2	Scan protocol .....	59
2.6.3	Dobutamine infusion .....	60
2.6.4	Quantitative analysis.....	61
2.6.4.1	Ejection fraction .....	61
2.6.4.2	Measurement of end-diastolic wall thickness.....	61
2.6.5	Qualitative analysis.....	61
2.6.5.1	Wall motion score.....	61
2.6.5.2	Characterization of myocardium .....	61
2.7	Magnetic resonance imaging: dual adenosine dobutamine stress (DADS) protocol .....	62
2.7.1	Scan protocol .....	62
2.8	Safety in the magnet .....	63
2.8.1	Clinical supervision .....	63
2.8.2	Electrocardiographic monitoring .....	64
2.8.3	Monitoring / Infusion equipment.....	64

2.8.4 Pharmacy.....	65
2.9 Collation of myocardial cross-sectional imaging data with coronary angiography .....	65
<b>Chapter 3 Development of first pass contrast-enhanced MRI technique for quantification of myocardial perfusion.....</b>	<b>67</b>
3.1 Introduction.....	68
3.1.1 Electrocardiographic gating .....	68
3.1.2 Gadodiamide bolus.....	69
3.1.3 Single visit stress/rest imaging.....	70
3.2 Hypothesis.....	70
3.3 Objectives.....	71
3.4 Methods.....	72
3.4.1 ECG gating.....	72
3.4.1.1 Measurement of R-R interval variability.....	72
3.4.1.2 Calculation of image position within the cardiac cycle ( $\Phi$ ).....	73
3.4.1.3 Magnetic resonance imaging: Comparison of $R_1$ values obtained from gated and non ECG-gated image acquisition.....	75
3.4.1.4 Statistics.....	76
3.4.2 Volunteer $K_i$ study.....	76
3.4.2.1 Study design .....	76
3.4.2.2 Magnetic resonance image analysis .....	77
3.4.2.3 Statistics.....	77
3.5 Results .....	78
3.5.1 ECG gating.....	78
3.5.1.1 Measurement of R-R interval variability.....	78
3.5.1.2 Calculation of image position within the cardiac cycle ( $\Phi$ ).....	79
3.5.1.3 Magnetic resonance imaging.....	80
3.5.2 Volunteer $K_i$ study .....	80
3.5.2.1 Patient demographics.....	80
3.5.2.2 Image quality .....	81
3.5.2.2.1 Bolus delivery.....	81

3.5.2.2.2	Signal and contrast to noise ratio.....	81
3.5.2.2.3	Baseline $R_1$ values .....	82
3.5.2.3	Quantitative analysis .....	83
3.6	Discussion.....	85
3.6.1	ECG gating.....	85
3.6.1.1	R-R variability with adenosine.....	85
3.6.1.2	Calculation of image position within the cardiac cycle ( $\Phi$ ).....	85
3.6.1.3	Magnetic resonance imaging: Comparison of $R_1$ values obtained from gated and non ECG-gated image acquisition.....	86
3.6.2	Volunteer $K_i$ study.....	88
3.6.2.1	Image quality.....	88
3.6.2.1.1	Bolus delivery.....	88
3.6.2.1.2	Signal and contrast to noise ratio.....	89
3.6.2.1.3	Baseline signal intensity.....	89
3.6.2.2	Quantitative analysis .....	90
3.7	Conclusion.....	91
<b>Chapter 4 Diagnostic potential of adenosine perfusion MRI in patients with coronary artery disease.....</b>		<b>93</b>
Part I: Quantitative image parameters .....		94
4.1	Introduction.....	94
4.2	Hypothesis.....	94
4.3	Objectives.....	94
4.4	Methods.....	95
4.4.1	Study design.....	95
4.4.2	Magnetic resonance image analysis.....	95
4.4.3	Collation with angiographic findings .....	96
4.4.4	Statistics.....	96
4.5	Results .....	96
4.5.1	Patient demographics.....	96
4.5.2	Magnetic resonance imaging .....	97

4.5.2.1	Haemodynamic data .....	97
4.5.2.2	Image quality .....	97
4.5.2.3	Bolus delivery.....	97
4.5.2.4	Signal and contrast to noise ratio.....	97
4.5.2.5	Baseline signal intensity .....	98
4.5.2.6	Quantitative analysis .....	98
4.5.3	Collation with angiographic findings .....	99
4.5.3.1	Receiver operator characteristic curve analysis .....	100
4.6	Discussion .....	101
4.6.1	Magnetic resonance image quality and bolus delivery .....	101
4.6.2	Collation with angiographic findings .....	102
4.7	Conclusion.....	103
Part II: Qualitative image parameters .....		104
4.8	Introduction .....	104
4.9	Hypothesis.....	104
4.10	Objectives.....	104
4.11	Methods.....	105
4.11.1	Study design.....	105
4.11.2	Magnetic resonance image analysis.....	105
4.11.3	Collation with angiographic findings .....	105
4.11.4	Statistics.....	106
4.12	Results .....	107
4.12.1	Patient demographics.....	107
4.12.2	Haemodynamics .....	107
4.12.3	Image quality .....	108
4.12.4	Detection of angiographic coronary artery disease .....	108
4.12.5	Relationship of MRI perfusion patterns to angiographic stenosis severity .....	109
4.12.5.1	Extent of perfusion deficit.....	109
4.12.5.2	Nature of perfusion deficit.....	109

4.12.5.3 Collateral circulation .....	111
4.13 Discussion .....	111
4.13.1 Patient selection .....	111
4.13.2 Magnetic resonance imaging .....	112
4.13.3 Detection of angiographic disease .....	112
4.13.4 Relationship of MRI perfusion patterns to angiographic stenosis severity .....	113
4.13.4.1 Extent of perfusion deficit .....	113
4.13.4.2 Nature of perfusion deficit.....	114
4.13.4.3 Collateral circulation .....	114
4.14 Conclusion.....	114
<b>Chapter 5 MRI prediction of contractile recovery in individual myocardial segments following revascularization: translation into clinical benefit.....</b>	<b>116</b>
5.1 Introduction .....	117
5.2 Hypothesis.....	118
5.3 Objectives.....	118
5.4 Methods.....	119
5.4.1 Study design.....	119
5.4.2 Revascularization.....	119
5.4.3 Magnetic resonance imaging .....	120
5.4.4 Regional myocardial function.....	120
5.4.5 Ejection fraction.....	120
5.4.6 End-diastolic wall thickness.....	120
5.4.7 Perfusion .....	120
5.4.8 Delayed hyperenhancement.....	121
5.4.9 Thallium scintigraphy.....	121
5.4.10 Analysis.....	121
5.4.10.1 Assessment of segmental improvement .....	121
5.4.10.2 Prediction of improvement in ejection fraction.....	122
5.4.11 Statistics.....	122

5.5	Results .....	122
5.5.1	Patient demographics.....	122
5.5.2	Revascularization.....	123
5.5.3	Identification of potential parameters of myocardial hibernation .....	123
5.5.4	Prediction of segmental improvement.....	124
5.5.5	Prediction of global improvement and clinical outcome .....	125
5.6	Discussion .....	127
5.6.1	Contractile reserve .....	128
5.6.2	Delayed hyperenhancement.....	129
5.6.3	Resting perfusion .....	130
5.6.4	Thallium scintigraphy.....	130
5.6.5	Clinical outcome.....	130
5.7	Conclusion.....	132
<b>Chapter 6 Restoration of myocardial blood flow following percutaneous balloon dilatation and stent implantation .....</b>		<b>133</b>
6.1	Introduction .....	134
6.2	Hypothesis.....	134
6.3	Objectives.....	134
6.4	Methods.....	135
6.4.1	Study design.....	135
6.4.2	Revascularization.....	135
6.4.3	Analysis of angiographic data.....	135
6.4.4	Magnetic resonance imaging .....	135
6.4.5	Collation of MRI and angiographic data .....	136
6.4.6	Statistics.....	136
6.5	Results .....	137
6.5.1	Patient demographics.....	137
6.5.2	Coronary artery revascularization.....	137
6.5.3	Clinical outcome.....	138

6.5.4	Magnetic resonance imaging .....	138
6.5.5	Image analysis.....	138
6.5.5.1	Quantitative analysis .....	138
6.5.5.2	Qualitative analysis .....	139
6.6	Discussion .....	140
6.7	Conclusion.....	142
<b>Chapter 7 Comparison of clinical and functional effects of transmymocardial laser revascularization and thoracic sympathectomy.....</b>		<b>144</b>
7.1	Introduction.....	145
7.2	Hypothesis.....	146
7.3	Objectives.....	146
7.4	Methods.....	147
7.4.1	Study design.....	147
7.4.2	Revascularization.....	147
7.4.2.1	Transmymocardial laser revascularization .....	147
7.4.2.2	Thoracic sympathectomy.....	148
7.4.3	Exercise electrocardiography .....	148
7.4.4	Magnetic resonance imaging .....	148
7.4.4.1	Myocardial perfusion.....	149
7.4.4.2	Delayed hyperenhancement.....	149
7.4.4.3	Myocardial function .....	149
7.4.5	Statistics.....	150
7.5	Results .....	150
7.5.1	Patient demographics.....	150
7.5.2	Revascularization.....	150
7.5.2.1	Transmymocardial laser revascularization .....	151
7.5.2.2	Thoracic sympathectomy.....	151
7.5.3	Clinical outcome.....	151
7.5.3.1	Symptom perception.....	151

7.5.3.2	Exercise tolerance test .....	152
7.5.4	Magnetic resonance imaging .....	152
7.5.4.1	Haemodynamic data .....	152
7.5.4.2	Myocardial perfusion.....	153
7.5.4.2.1	Quantitative analysis .....	153
7.5.4.2.2	Qualitative analysis .....	155
7.5.4.2.3	Delayed hyperenhancement.....	155
7.5.4.3	Functional cine imaging .....	155
7.5.4.3.1	Resting ejection fraction and left ventricular volumes.....	156
7.5.4.3.2	Characterization of myocardium from rest/stress scans.....	157
7.6	Discussion .....	158
7.6.1	Clinical outcome.....	158
7.6.2	Magnetic resonance imaging .....	159
7.6.2.1	Myocardial perfusion.....	159
7.6.2.2	Delayed hyperenhancement.....	159
7.6.2.3	Functional cine imaging .....	160
7.6.2.4	Placebo effect .....	160
7.7	Conclusion.....	161
<b>Chapter 8</b>	<b>Conclusions and Future Perspectives.....</b>	<b>162</b>
8.1	Conclusions.....	163
8.2	Future Perspectives .....	165
<b>Appendix</b>	<b>Publications and presentations arising from this thesis .....</b>	<b>167</b>
Papers.....		168
Book Chapters.....		168
Submitted Papers.....		168
Abstracts .....		169
<b>References</b> .....		<b>173</b>

---

# **Chapter 1**

## **Introduction**

---

## **1.1 Introduction**

In the last decade, management of coronary artery disease has become progressively more interventional. The number of patients receiving thrombolysis, percutaneous and surgical revascularization procedures continues to rise in an effort to minimize the deleterious process of myocardial ischaemia. In addition, new methods of revascularization, e.g. transmyocardial laser revascularization and targeted gene therapy, are undergoing clinical trials (Hughes *et al.*, 1999; Losordo *et al.*, 1999; Sinnaeve *et al.*, 1999; Owen & Stables, 2000). Accurate application of interventional strategies requires not only angiographic visualization of the patient's epicardial coronary anatomy, but a detailed knowledge of the effects of coronary atheroma on myocardial perfusion, function and viability. Currently available imaging modalities include scintigraphy, positron emission tomography and echocardiography. Cardiac magnetic resonance imaging (MRI) is a rapidly emerging imaging technique that is likely to prove to be an invaluable additional clinical tool for identification of the multiple end-organ effects of coronary artery disease (van der Wall *et al.*, 1995; Baer *et al.*, 1999b; Sensky & Cherryman, 2000; Sinitsyn, 2001). One of the values of cardiac magnetic resonance is the potential to evaluate perfusion, function and viability during a single examination. This thesis comprises presentation of a series of studies to evaluate the use of cardiac magnetic resonance in the diagnosis of coronary artery disease, the identification of myocardial hibernation and the assessment of revascularization procedures.

## **1.2 Coronary artery disease**

Coronary artery disease is caused by the development of atherosclerotic plaque within the arteries that supply blood to the myocardium (Fuster *et al.*, 1992). Once such areas become of sufficient size to obstruct blood flow a cascade of ischaemia is triggered (Figure 1.1) and myocardial performance is impaired (Nesto & Kowalchuk, 1987). Ischaemia is increased by physical exertion and maximal hyperaemia becomes compromised by loss of luminal area of 50% (Gould & Lipscomb, 1974). Initially, reduced coronary blood flow results in impaired perfusion

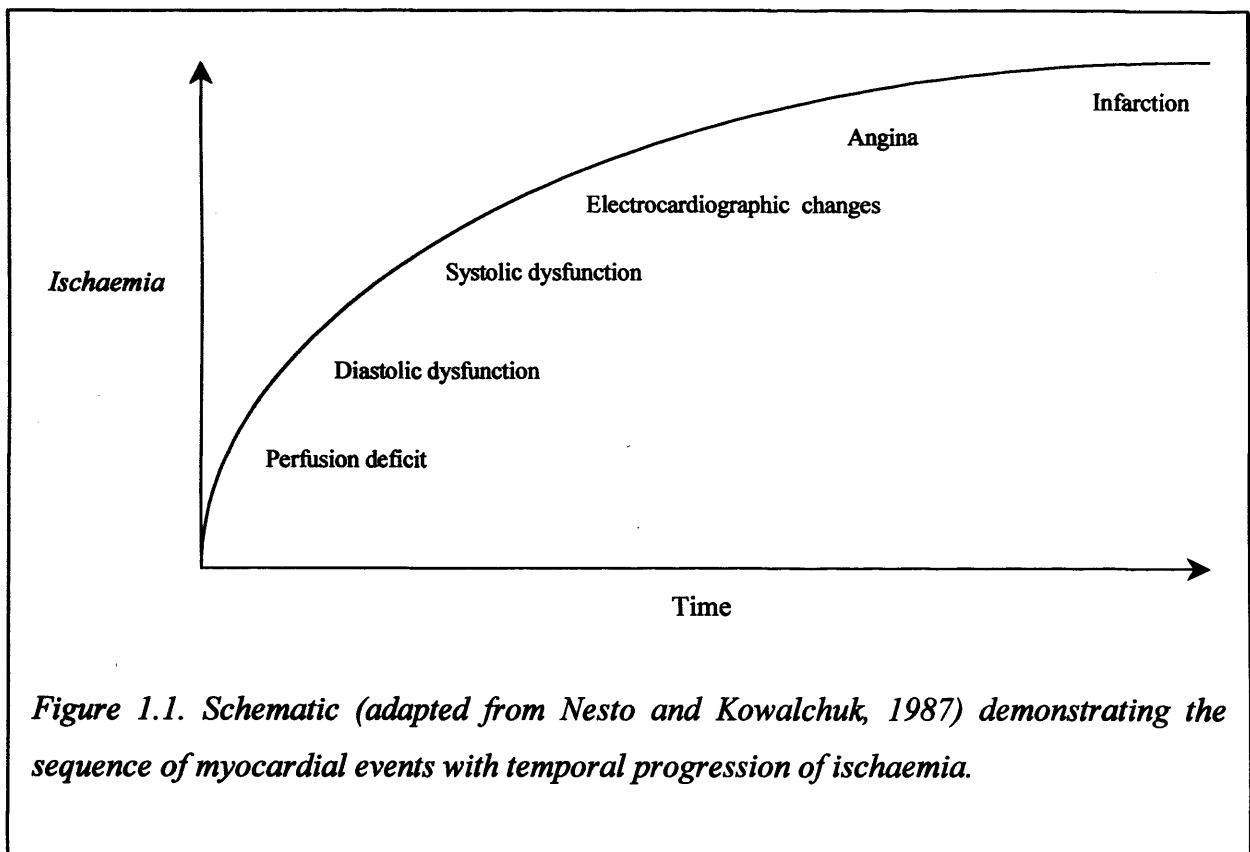
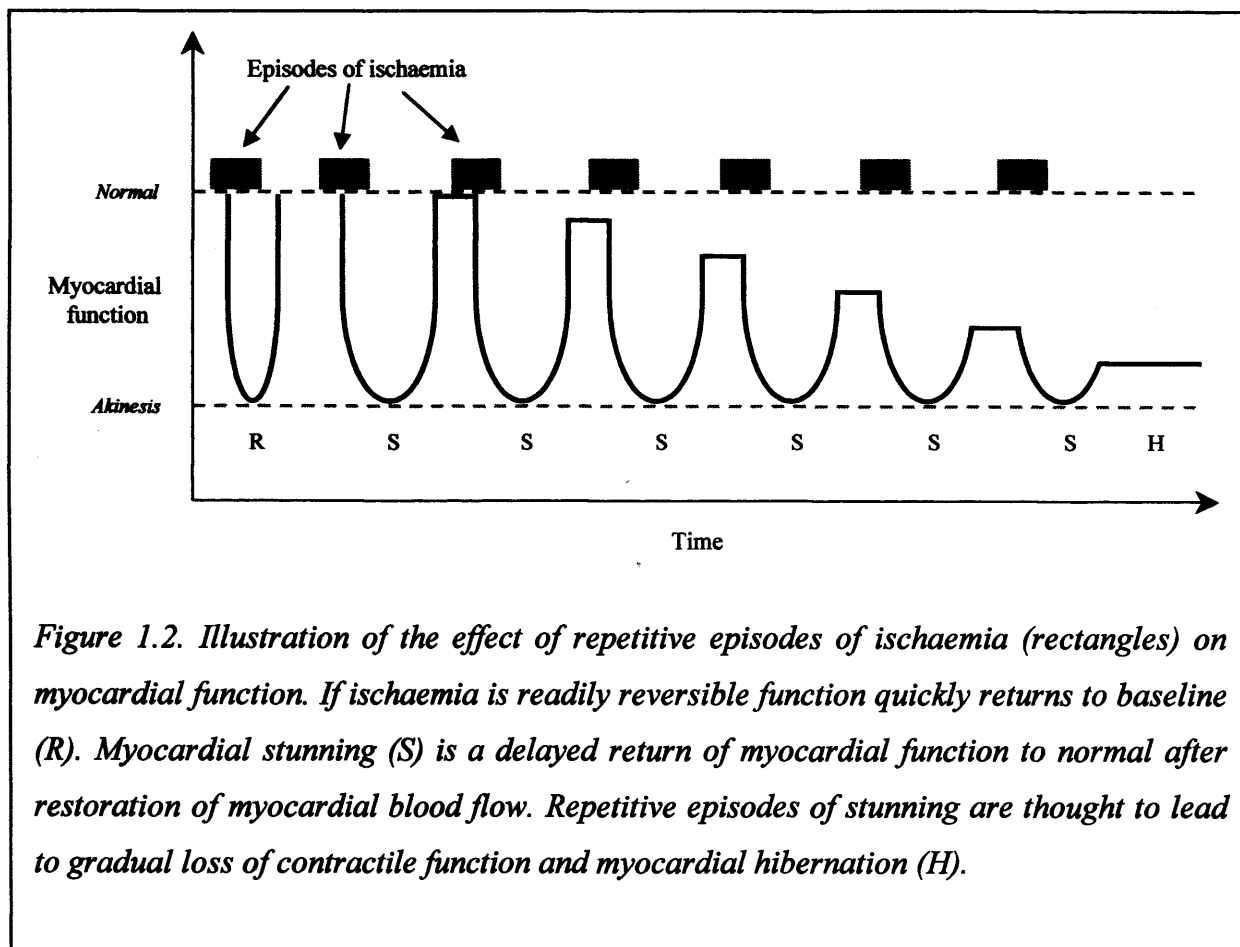


*Figure 1.1. Schematic (adapted from Nesto and Kowalchuk, 1987) demonstrating the sequence of myocardial events with temporal progression of ischaemia.*

and corresponding diminished myocardial oxygen delivery. Hypoperfusion is first seen in the subendocardial portion of the cardiac muscle (Bache & Schwartz, 1982). Impairment of diastolic and then systolic myocardial function is precipitated. The severity of regional dyssynergy is correlated with transmural blood flow {Schroder & Schultheiss 1997}. These events are precursors to electrocardiographic changes and to the clinical syndrome of angina pectoris (Nesto & Kowalchuk, 1987). If ischaemia continues unabated, death of myocardial tissue occurs and an area of infarction or scar tissue is the result. The affected territory has severely reduced perfusion and remains permanently functionless.

Restoration of blood supply to the myocardium results in reversal of these events. With readily reversible ischaemia, perfusion and function rapidly return to normal. Transient loss of myocardial function can occur following a period of ischaemia despite improvement in arterial flow and organ perfusion. This is known as myocardial stunning and function ultimately returns to baseline. Repetitive episodes of stunning and prolonged severe ischaemia that are of insufficient gravity to cause infarction may lead to a condition called myocardial hibernation (Figure 1.2)



(Ferrari *et al.*, 1999). Myocardial hibernation is characterized by a down-regulation of myocyte activity and receptors. Basal perfusion is preserved but resting dysfunction occurs (Rahimtoola, 1995). Hibernating tissue can have a similar clinical manifestation to scar tissue. However, the importance of myocardial hibernation, in contrast to myocardial infarction, is that function will recover following revascularization (Rahimtoola, 1995).

### 1.2.1 Coronary artery revascularization

Many patients with coronary artery disease are managed conservatively on medication alone. Patients at the more severe end of the disease spectrum require coronary artery revascularization. Interventions are performed in order to alleviate symptoms of chronic ischaemia, to preserve failing left ventricular function and to improve long-term prognosis (Hollman, 1992; Goldman, 1995; Lieu *et al.*, 1996; Beanlands *et al.*, 1998; Eagle *et al.*, 1999).

There are two traditional forms of coronary artery revascularization. Discrete angiographic lesions may be approached percutaneously and transluminal angioplasty, frequently accompanied by elective stent implantation, performed. Increasingly complex and diffuse lesions are being managed in this way as technology available to cardiologists improves. Coronary artery bypass surgery is an established alternative for patients with more diffuse, widespread disease.

A cohort of patients has severe diffuse disease that is unamenable to conventional percutaneous or surgical techniques. This group includes patients with small calibre vessels or those that have had previous bypass surgery but subsequently suffer graft occlusion or progression of native vessel atheroma. Such patients often present with high grade symptoms of ischaemia that are refractory to optimal medical therapy. There is therefore increasing interest in novel therapies to enhance myocardial blood flow or improve patient symptom perception. Transmyocardial laser revascularization is a relatively new surgical technique that has been documented to provide a beneficial clinical effect in this situation (Frazier *et al.*, 1995; Milano *et al.*, 1998). Research is also in progress to evaluate techniques to deliver genetically engineered growth factors to stimulate local angiogenesis within ischaemic myocardial territories (Laham *et al.*, 1999; Losordo *et al.*, 1999).

### **1.2.2 Coronary angiography**

Coronary angiography is the current gold standard for delineation of coronary artery disease. Epicardial stenoses can be visualized in multiple planes. Estimation of vessel lumen cross-sectional area loss is frequently used to predict obstruction to arterial blood flow and likely presence of reversible ischaemia. Interventional procedures can be planned with accuracy. However, information regarding the precise functional effects of specific stenoses on myocardial function and perfusion cannot be obtained objectively by angiographic interpretation alone (White *et al.*, 1984; Gould, 1988) but may be determined by use of additional invasive tests such as measurement of coronary flow reserve with intra-coronary Doppler flow wires (Ofili *et al.*, 1993; Bach *et al.*,

1995). In addition, coronary angiography requires ionizing radiation for image acquisition and is an invasive procedure with measurable risk (Johnson & Krone, 1993).

### **1.3 Non-invasive imaging techniques in coronary artery disease**

Indirect parameters of obstructive coronary atheroma displayed in the ischaemic cascade, i.e. myocardial perfusion and function, can be utilized by less invasive imaging methods to diagnose coronary artery disease and to estimate its severity. Furthermore, correlation of angiographically visualized luminal obstruction and information on resulting abnormalities of myocardial perfusion, function and viability is of clinical value in planning revascularization strategies. Serial imaging following revascularization can assess efficacy of established procedures and contribute to the understanding of developing techniques.

Imaging methods currently available in the clinical arena include echocardiography, scintigraphy and positron emission tomography. Computerized tomography has also been applied to patients with coronary artery disease but largely remains a research tool.

MRI is now well established as the gold standard for delineation of mediastinal anatomy and assessment of cardiac function (Higgins & Sakuma, 1996). Combined high specification hardware development and implementation of ultrafast imaging sequences have overcome many MRI difficulties created by respiration and cardiac cyclic motion. MRI has high spatial resolution and provides detailed soft tissue imagery. In recent years, this modality has become a genuine competitor to current clinical methods for the evaluation of myocardial perfusion, function and viability (Table 1.1). A potential advantage of MRI is that an assessment of anatomy, myocardial wall thickening and perfusion at rest and during stress could be performed in a single examination (Kramer *et al.*, 1996). No ionizing radiation is utilized and so MRI is a safe modality for serial patient studies.

Technique	Myocardial				Coronary Vasculature	Invasive	Ionizing Radiation	Spatial Resolution
	Perfusion	Function	Strain	Metabolism				
MRI	+	+	+	+	±	-	-	~1 mm
TTE	±	+	-	-	-	-	-	~1-2 mm
SPECT	+	+	-	±	-	-	+	~6-10 mm
PET	+	-	-	+	-	-	+	~5-8 mm
CA	-	+	-	-	+	+	+	~0.5-2 mm

*Table 1.1. Potential advantages and disadvantages of cardiac MRI over other imaging techniques. TTE = transthoracic echocardiography; SPECT = single photon emission computed tomography; PET = positron emission tomography; CA = coronary angiography.*

### **1.3.1 Non-invasive assessment of myocardial perfusion**

#### **1.3.1.1 Clinical indications**

Since myocardial perfusion abnormalities occur early following the onset of ischaemia, evaluation of regional myocardial perfusion heterogeneity is a sensitive marker for the presence of coronary artery disease. Clinical indications for myocardial perfusion imaging in patients with known or suspected coronary artery disease are shown in Table 1.2.

In addition to use as a diagnostic test to confirm initial or recurrent coronary artery disease and myocardial viability, perfusion imaging may be helpful to identify patients with symptoms of ischaemia but normal coronary angiography, i.e. syndrome X (Go *et al.*, 1990; Wilke *et al.*, 1997; Wieneke *et al.*, 1999). Diagnostic myocardial blood flow evaluation has also been performed in the emergency setting (Hilton *et al.*, 1994). There is a wealth of literature describing the value of nuclear imaging techniques for provision of prognostic information. Applications include categorization of patients into low or high risk groups for future cardiac events, need for further intervention and elucidation of cardiovascular risk associated with non-cardiac surgical procedures (Brown, 1995; Iskander & Iskandrian, 1998). Clarification of physiological effects of single or sequential angiographic stenoses and collateral circulation are invaluable in treatment planning

<b>Diagnosis</b>	<i>De novo</i> or recurrent ischaemic heart disease Myocardial viability Emergency evaluation of chest pain
<b>Risk Stratification</b>	Prognosis for future coronary events Post myocardial infarction Prior to non-cardiac surgery
<b>Treatment planning / evaluation</b>	Evaluation of the effects of collateral circulation Functional significance of known angiographic lesions Follow-up after medical or interventional treatment
<b>Research tool</b>	Characterization of novel revascularization strategies

*Table 1.2. Clinical indications for myocardial perfusion imaging.*

(Sabia *et al.*, 1992; Schwaiger, 1994; Uren *et al.*, 1994). Serial imaging to evaluate changes in myocardial perfusion following conventional or novel treatment strategies is a useful tool in both clinical and research settings (Versaci *et al.*, 1996; Bax *et al.*, 1997a; Kosa *et al.*, 1999; Rimoldi *et al.*, 1999).

### **1.3.1.2 Myocardial perfusion imaging**

As with all investigational methods for evaluation of ischaemia, perfusion imaging is enhanced by the addition of cardiac stress. This may be in the form of physical exercise, or with use of pharmacological stressors (Iliceto, 1995). The latter are particularly useful for imaging modalities where image acquisition is impractical during physical exercise, e.g. echocardiography or MRI, and additionally if the patient is physically unable to exercise sufficiently or presents with electrocardiogram abnormalities that prohibit accurate exercise electrocardiogram interpretation. The two most commonly used pharmacological stressors used to maximize myocardial perfusion are the vasodilators, dipyridamole and adenosine.

Adenosine is a naturally occurring purine that acts on vascular smooth muscle cell surface A<sub>1</sub> and A<sub>2</sub> adenosine receptors to produce an increase in intracellular cAMP. Dipyridamole causes a rise in interstitial adenosine concentration by inhibiting adenosine cellular uptake and metabolism. Both agents give rise to a four to five fold hyperaemia, in contrast to the two-fold vasodilatory effect of dobutamine. Thus during stress, there is a four to five fold increase in blood flow to normal myocardial territories compared with the basal state. In the presence of coronary artery stenosis, there is impaired vasodilatation, and a reduction of this stress: rest ratio. Subendocardial ischaemia may be precipitated by loss of distal arterial perfusion pressure and by redirection of endocardial blood flow to the epicardial layer. High resistance collateral flow may also be impaired because of generalized vasodilatation.

Perfusion deficits may be assessed qualitatively by visual image interpretation and categorized as either reversible (present on stress imaging alone) or fixed (present on stress and rest imaging). Some methods permit a more quantitative estimate of blood flow and the parameters coronary flow reserve and myocardial perfusion reserve have been coined to express the quantitative relationship of blood flow at rest to flow during stress (Goldstein *et al.*, 1987; Bourdarias, 1995). Coronary flow reserve is defined as the ratio of epicardial arterial blood flow during maximal hyperaemia to flow at rest. Myocardial perfusion reserve is the term applied to the ratio of blood flow within the myocardium during maximal hyperaemia to flow in basal conditions.

### **1.3.1.3 Imaging techniques for measurement of myocardial perfusion**

Single photon emission computed tomography and positron emission tomography are the traditional clinical methods for evaluation of myocardial perfusion. Contrast-enhanced computed tomography, contrast-enhanced echocardiography and MRI remain research techniques.

#### ***1.3.1.3.1 Single photon emission computed tomography***

Single photon emission computed tomography is the most commonly available clinical imaging technique for the assessment of cardiac perfusion (Hor, 1988; Keijer *et al.*, 1997). The

radioisotopes thallium-201 or technetium-99m are taken up by the myocardium in proportion to blood flow. Image analysis requires reconstruction into double oblique imaging planes and reporting techniques are usually qualitative. Since adjacent areas are compared, this methodology may limit accuracy in the presence of triple vessel disease and global ischaemia. Single photon emission computed tomography has poor spatial resolution in comparison with other techniques and artifacts frequently degrade image quality. Such artifacts include attenuation from breast tissue in the anterior wall and signal loss inferiorly, the latter predominantly in men as a result of respiratory motion and increased distance from the camera. Although quite high diagnostic sensitivities are obtained, specificity is generally less (Go *et al.*, 1990; Schwaiger, 1994).

#### ***1.3.1.3.2 Positron emission tomography***

Positron emission tomography provides the closest clinical method available for absolute quantification of perfusion (Schwaiger & Muzik, 1991; Muzik *et al.*, 1998). Radio-labelled tracers, e.g. rubidium or oxygen, are imaged dynamically as they pass through the cardiovascular circulation. Regional blood flow at rest and stress can be quantified with the use of radiotracer biodistribution kinetic modelling. The method is less prone to attenuation than single photon emission computed tomography and spatial resolution is better, but still not sufficient to delineate minor perfusion deficits or those limited to the subendocardial layer. Positron emission tomography is expensive, and only available in specialized centres.

#### ***1.3.1.3.3 Computerized tomography (CT)***

Computerized tomography has recently been shown to have potential for regional myocardial blood flow estimation (Georgiou *et al.*, 1994; Schmermund *et al.*, 1997). Dynamic imaging of iodinated contrast agents is used and preliminary results employing electron beam computerized tomography suggest that a quantitative measure of myocardial blood flow can be obtained. Multi-slice computerized tomography is now replacing this modality and is likely to become the future

computerized tomography method for perfusion evaluation. However, the technique necessitates significant exposure to ionizing radiation.

#### **1.3.1.3.4 Contrast echocardiography**

The advent of pulsed and power harmonic Doppler modalities have led to considerable advances in contrast echocardiography for myocardial perfusion imaging (Mulvagh, 2000; Senior *et al.*, 2000). Images are subject to multiple artifacts including attenuation, contrast blooming and failure of bubble opacification owing to inhomogeneous ultrasound delivery to tissue. Further work needs to be done to fully elucidate the complex interactions of the varying microbubble contrast agents and ultrasound modalities before contrast echocardiography is sufficiently robust for clinical application.

#### **1.3.1.3.5 Magnetic resonance imaging**

Whilst MRI has been proven to be an accurate means of imaging cardiac anatomy and function, dynamic contrast-enhanced first pass MRI for evaluation of myocardial perfusion is a relatively new technique (Figure 1.3) (Atkinson *et al.*, 1990; Schaefer *et al.*, 1992; Eichenberger *et al.*, 1994; Matheijssen *et al.*, 1996; Wilke *et al.*, 1997; Martin *et al.*, 1998; Cullen *et al.*, 1999b).

MRI has two potential advantages over other imaging modalities. Firstly, it is anticipated that the high spatial resolution could permit discrete visualization of the subendocardial layer, a feature that would be ideal for detection of subtle pathophysiological perfusion abnormalities. Secondly, the currently available temporal resolution facilitates rapid tracking and characterization of the first pass of a contrast agent such that quantitative estimates of myocardial blood flow can be made (Wilke *et al.*, 1997; Cullen *et al.*, 1999b). As with the other imaging modalities employed for the assessment of myocardial ischaemia, the diagnostic value of perfusion imaging with MRI is enhanced by the addition of a stressor. Most of the early work with MRI in this field was done with the use of dipyridamole. However, adenosine is the preferred agent because its short half-life is beneficial in terms of limiting patient side effects and facilitating the remainder of the examination.

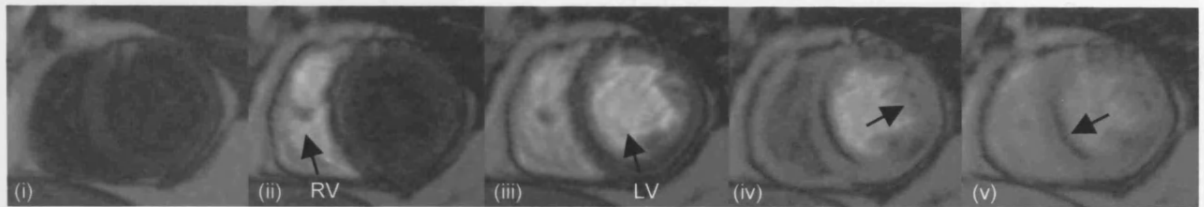


*Figure 1.3. Example of sequential first pass contrast-enhanced magnetic resonance perfusion images acquired during adenosine infusion. The bolus of gadodiamide (arrows) appears first in the right ventricle (RV, ii) and then in the left ventricular cavity (LV, iii). Normally perfused myocardium is enhanced (arrow, iv). A subendocardial perfusion deficit is the result of a severe right coronary artery stenosis (arrow, v).*

If adenosine is contra-indicated, dobutamine can be used, but a sub-maximal vasodilatory effect is obtained (Orlandi, 1996).

#### *1.3.1.3.5.1 Inversion recovery snapshot-fast low angle shot (FLASH) sequence*

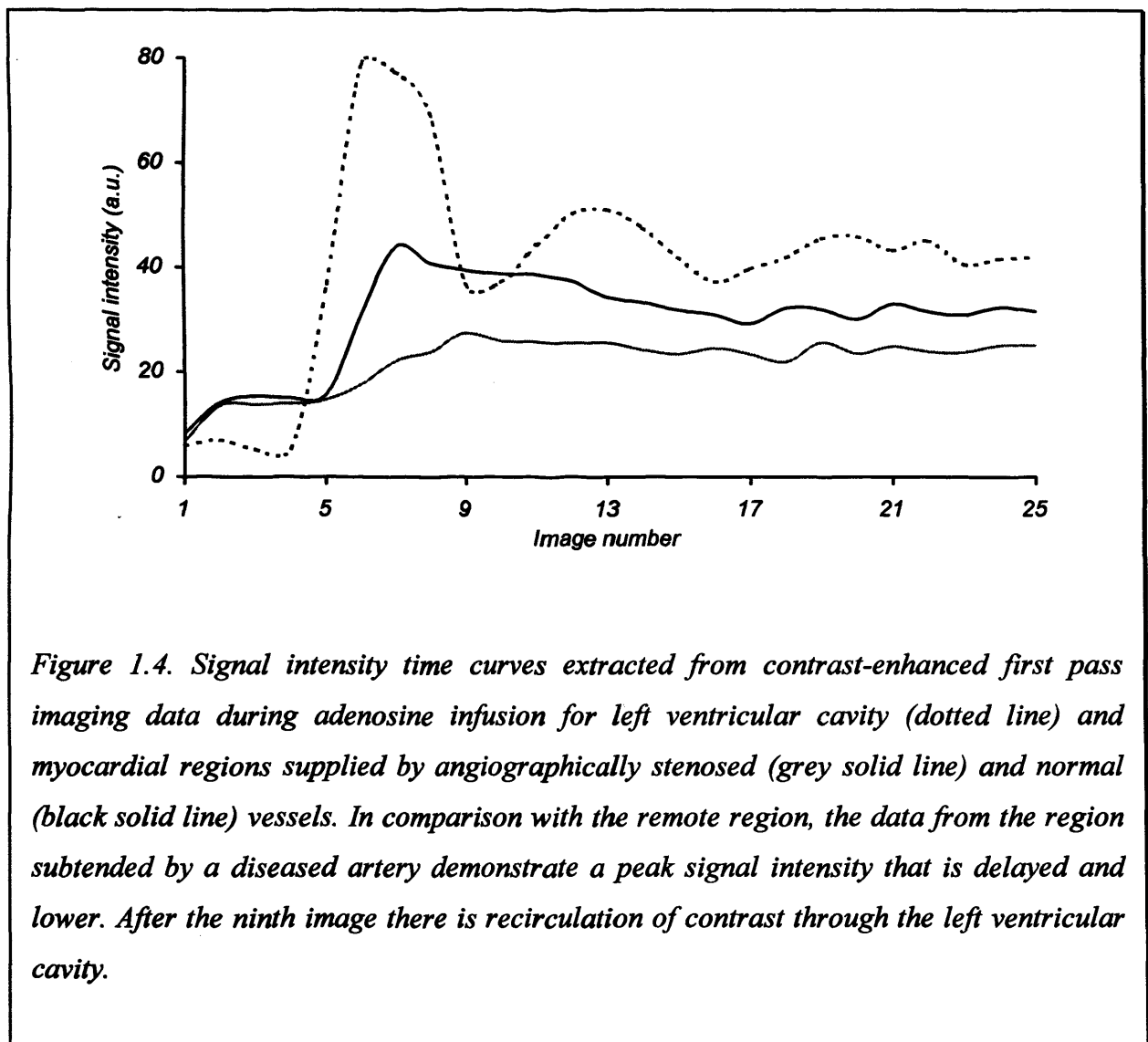
A standard sequence in use is inversion recovery snapshot-FLASH (Atkinson *et al.*, 1990; Schaefer *et al.*, 1992; Klein *et al.*, 1993; Hartnell *et al.*, 1994; Keijer *et al.*, 1995; Lauerma *et al.*, 1997; Fritz-Hansen *et al.*, 1998; Cullen *et al.*, 1999b; Al-Saadi *et al.*, 2000; Keijer *et al.*, 2000). This sequence has high signal to noise ratio and image contrast. The latter is obtained by employing a 180° inversion prepulse to null myocardial signal prior to contrast agent administration. Nulling minimizes myocardial signal intensity and thus enhances the relative signal intensity increase produced by contrast agent longitudinal relaxation rate ( $T_1$ ) shortening effects. At 1.5 Tesla, myocardium has a  $T_1$  relaxation time of 750 - 850 ms, and so the null point, i.e. time after the inversion pulse when myocardial tissue no longer has any longitudinal magnetization to be transferred into a transverse plane by a radiofrequency pulse, occurs at approximately  $0.69 \cdot T_1$  ms. This may vary in certain disease states. With the use of high performance gradients, relatively short repetition (TR) and echo (TE) times can be achieved and in combination with the inversion time and flip angle, used to maximize image contrast.

#### *1.3.1.3.5.2 Contrast media*

The contrast media employed are the gadolinium chelates, paramagnetic compounds that act by shortening the longitudinal relaxation rate of the myocardium. These agents are water soluble with relatively low molecular weights. They are therefore able to diffuse rapidly across capillary membranes into tissue extracellular space, but are unable to enter cells with intact membranes. Although approximately 30 - 50% of the first pass bolus enters myocardial interstitium following intravenous administration (Brasch, 1992; Tong *et al.*, 1993), myocardial gadolinium chelate concentration is determined primarily by coronary perfusion (Diesbourg *et al.*, 1992). Perfusion deficits are recognized as areas of reduced or delayed signal intensity. These signal intensity

changes form the basis of image analysis. Since recirculation and bolus dilution lead to rapid equilibration between vascular and extracellular compartments, gadolinium contrast media do not remain fixed in the myocardium in proportion to blood flow (Diesbourg *et al.*, 1992). There is rapid accumulation of contrast agent in the myocardial interstitium and loss of any signal intensity heterogeneity; hence the need for image acquisition during contrast agent first pass. Myocardial uptake during the initial bolus has been shown to be related to blood flow in both animal and human studies (Wilke *et al.*, 1993; Wilke *et al.*, 1997).

Quantitative estimates of myocardial blood flow require extraction of signal intensity time curve data on consecutive images from myocardial regions and the left ventricular cavity (Figure 1.4).



Attempts have been made to extract semi-quantitative parameters from the curves. For more quantitative data, mathematical models that take bolus delivery and contrast agent kinetics into consideration have been proposed to provide an estimate of myocardial perfusion reserve. Most quantitative parameters extracted from these curves require normalization of myocardial signal intensity changes in response to the contrast agent bolus (tissue function) with respect to signal intensity changes in the left ventricular cavity (input function) in order to take bolus variations into account.

Semi-quantitative parameters of blood flow include peak signal intensity, mean contrast agent transit time and curve upslope. Differentiation of regional peak signal intensities was one of the first parameters to be described in relation to myocardial blood flow (Manning *et al.*, 1991; Schaefer *et al.*, 1992). Contrast agent mean transit time has been suggested as a measure of flow as this is less affected by spatial variations in signal intensity than peak amplitude or slope (Wilke *et al.*, 1994; Keijer *et al.*, 1995; Keijer *et al.*, 2000). This approach relies on the assumption that contrast agent distribution volume is constant for both normal and ischaemic myocardium. Both these methods are dependent on a very compact bolus delivery necessitating central injection techniques. Mean transit time is affected by bolus recirculation and so extrapolation of the downslope of the input curve with the use of a gamma variate function is necessary for its estimation. Evaluation of the signal intensity time curve upslope alone ignores the kinetics of contrast agent washout and consequently avoids the need for curve downslope extrapolation (Eichenberger *et al.*, 1994; Matheijssen *et al.*, 1996; Al-Saadi *et al.*, 2000; Keijer *et al.*, 2000).

Considerable work has been done by some groups to attain absolute myocardial perfusion measurements (Larsson *et al.*, 1994; Larsson *et al.*, 1996; Wilke *et al.*, 1997). A mathematical process known as deconvolution is used to standardize the tissue function to varying bolus deliveries to the myocardium. This process is a powerful algorithm for smoothing and differentiation of two signals within the Fourier domain.

Wilke *et al.* have proposed a mathematical model that is based on characterization of the tissue residue impulse response from the measured signal intensity time curve with respect to the input function (Wilke *et al.*, 1997). With deconvolution of these two functions, the tissue residue impulse response curve can be inferred. This curve is a plot of  $R_F$  against time where  $R_F$  represents the probability that a contrast agent molecule remains in the region of interest (ROI) up to time  $t$ . This probability is maximal during the wash-in portion of the contrast agent first pass as the curve decays over time owing to tissue contrast agent wash-out. The initial height of the tissue residue impulse response is used as a measure of blood flow (Clough *et al.*, 1994; Wilke, 1998). By relating the contrast agent inflow and outflow curves by this method, extrapolation of outflow data is avoided. In order to desensitize the deconvolution process to data noise, a constraining Fermi function is employed to provide a parameterized representation of the tissue impulse response function (Jerosch-Herold *et al.*, 1998). High image temporal resolution is essential especially at high flow rates when upslope duration is shortest. This is achieved with use of the saturation recovery snapshot-FLASH sequence to permit acquisition of several data points on the flow sensitive wash-in portion of the curve. This method is also reliant on rapid uniform central injection of contrast agent in order to minimize extracellular leakage and changes in myocardial blood volume. Estimates of myocardial blood flow in animals have been validated against myocardial flow measurements with radiolabelled microspheres for flow rates of  $0.3 - 4 \text{ ml g}^{-1} \text{ min}^{-1}$ . Values of myocardial perfusion reserve calculated in patients with chest pain but normal coronary angiography correlated well with Doppler measured CFR (Wilke *et al.*, 1997).

In Leicester, there is some experience of utilizing the unidirectional transfer coefficient for gadolinium compounds over the capillary membrane ( $K_i$ ) as a determinant of perfusion. This is derived with the use of a modified two compartmental Kety model (Larsson *et al.*, 1994; Larsson *et al.*, 1996). Calibration of signal intensity in terms of contrast agent concentration is required. This is achieved by calculation of myocardial relaxation rate ( $R_1$ ) according to an analytical expression of the measured signal intensity produced by a fast gradient echo sequence, taking into

account inter-image delay (Larsson *et al.*, 1994; Larsson *et al.*, 1996; Vallee *et al.*, 1997).  $K_i$  is then determined from deconvolution of the  $R_1$  input and tissue functions.  $K_i$  can be expressed as the product of contrast agent extraction fraction (E) and flow (F), i.e.  $K_i = F \times E$ . Determined parameters describe myocardial flow and distribution volume. The Kety model was originally proposed for application to freely diffusible tracers for which E is assumed to be unity. Since gadolinium compounds are barrier limited, this assumption does not apply. Whilst  $K_i$  alone is related to perfusion, for absolute blood flow quantification this method is limited by its dependence on E as direct measurement of this factor is not possible in humans. E has been measured in animal studies for small molecular compounds in normal myocardium and corrections extrapolated from these results can be applied (Tong *et al.*, 1993). Despite this limitation, values of  $K_i$  have been shown to have a linear relationship with blood flow determined by microspheres and with positron emission tomography (Vallee *et al.*, 1998).  $K_i$  has been shown to be sensitive to changes in perfusion induced by vasodilator stress and by the presence of coronary artery stenosis (Fritz-Hansen *et al.*, 1998; Vallee *et al.*, 1998; Cullen *et al.*, 1999b). The ratio of vasodilator induced stress and rest  $K_i$  values has been presented as an index of myocardial perfusion reserve (Cullen *et al.*, 1999b). This model is less sensitive to noise and more independent of separation of first and second contrast agent passes than those described above. Use of this technique avoids patient exposure to the risks of central venous access required by the semiquantitative and quantitative methods where compact contrast agent bolus delivery is required to generate high temporal resolution of the signal intensity curve upslope. A disadvantage of this methodology is that there is insufficient temporal resolution of the upslope to allow semi-quantitative analysis in addition to application of the modified two compartmental Kety model.

#### 1.3.1.3.5.3 *Clinical application*

The diagnostic potential of perfusion imaging with magnetic resonance has been evaluated against other imaging modalities (Table 1.3). Sensitivities and specificities of MRI for detection of significant coronary angiographic lesions range from 44 - 93 % and 60 - 100 %, respectively

(Schaefer *et al.*, 1992; Klein *et al.*, 1993; Eichenberger *et al.*, 1994; Hartnell *et al.*, 1994; Bremerich *et al.*, 1997; Al-Saadi *et al.*, 2000). An inverse relationship between myocardial perfusion reserve index and severity of coronary artery stenosis as assessed by angiography has been demonstrated (Cullen *et al.*, 1999b). An excellent correlation between myocardial perfusion reserve obtained by MRI and Doppler coronary flow reserve has also been shown (Wilke *et al.*, 1997). Sensitivities and specificities for detection by MRI of perfusion deficits seen on scintigraphy images range from 56 - 90 % and 61 - 90 % respectively (Klein *et al.*, 1993; Eichenberger *et al.*, 1994; Hartnell *et al.*, 1994; Matheijssen *et al.*, 1996; Bremerich *et al.*, 1997).

Comparison	Findings	Reference
MRI vs. CA	70% agreement	(Eichenberger <i>et al.</i> , 1994)
MRI vs. SPECT	90% agreement	(Eichenberger <i>et al.</i> , 1994)
MRI vs. CA and SPECT	65% sensitivity, 76% specificity	(Hartnell <i>et al.</i> , 1994; Matheijssen <i>et al.</i> , 1996)
MRI MPR vs. CFR	Correlation: $r = 0.8$	(Wilke <i>et al.</i> , 1997)
MRI MPRI vs. CA stenosis diameter	Correlation: $r = -0.81$	(Cullen <i>et al.</i> , 1999b)

*Table 1.3. Comparison of perfusion MRI with other imaging modalities. CA = coronary angiography; SPECT = single photon emission computed tomography; MPR(I) = myocardial perfusion reserve (index); CFR = coronary flow reserve.*

### **1.3.2 Non-invasive assessment of myocardial function**

#### **1.3.2.1 Clinical indications**

Compromise of myocardial function develops later than perfusion abnormalities in the ischaemic cascade and so theoretically this parameter is a less sensitive marker for early pathology (Brown, 1995). However, evaluating the effects of ischaemia on myocardial function has proved to be of value in the assessment of patients with coronary artery disease. The clinical indications for imaging myocardial function in patients with known or suspected ischaemic heart disease are similar to those for myocardial perfusion assessment (Table 1.2). Additional information may be

gained regarding left ventricular ejection fraction and anatomical structure. This has prognostic value for survival and operative risk (Anonymous, 1983; Weiner *et al.*, 1987).

### **1.3.2.2 Myocardial function imaging**

Regional wall motion abnormalities are the trademark of myocardial ischaemia (Ross, Jr., 1986). In patients with clinically significant disease they may be present at rest, ranging from mild hypokinesia with ischaemia to dyskinesia with infarction. For the precipitation of stress-induced myocardial dysfunction secondary to ischaemia, dobutamine is the optimal agent (Iliceto, 1995). Dobutamine is a sympathomimetic agonist that acts on cardiac  $\beta_1$  receptors. Myocardial contractility and the rate-pressure product are increased resulting in an oxygen supply-demand mismatch in territories supplied by stenosed coronary vessels.

In a similar fashion to stress perfusion imaging, regional wall abnormalities may be either reversible (present on stress imaging alone) or fixed (present at rest and with stress). The concept of dobutamine-induced contractile reserve, typical of myocardial hibernation is discussed below (Section 1.3.3). Qualitative analysis of images is most commonly performed.

### **1.3.2.3 Imaging techniques for measurement of myocardial function**

The most accessible clinical tool for the evaluation of myocardial function in the context of coronary artery disease is stress echocardiography. Radionuclide ventriculography is an alternative modality but rarely used to evaluate regional function. Cine computerized tomography has also been presented as a potential tool. However, obligatory doses of radiation render these techniques undesirable for stress imaging.

#### **1.3.2.3.1 Stress echocardiography**

Stress echocardiography has been well characterized as a diagnostic test for coronary artery disease (Krahwinkel *et al.*, 1997a). The modality can also provide prognostic information with similar applications to those obtained by assessment of myocardial perfusion with radionuclide

techniques (Picano *et al.*, 1997). The extent of myocardial jeopardy arising from specific angiographic anatomy can be estimated. Serial imaging is safe as no ionizing radiation is required and so longitudinal studies to evaluate the effects of disease progression or therapeutic manoeuvres are practical (Donovan *et al.*, 1997). An important advantage of echocardiography over the other imaging modalities is that it is portable and can be effectively applied at the bedside. However, it is limited by its reliance on patient acoustic windows (Nagel *et al.*, 1999). It has also been suggested that the technique is open to observer subjectivity (Hoffmann *et al.*, 1996).

#### **1.3.2.3.2 Magnetic resonance imaging**

The high spatial resolution of MRI and the ability to image in any orientation permits finely detailed delineation of cardiac structures and morphology (Higgins & Sakuma, 1996). Intra-cardiac and extra-cardiac structures such as masses, thrombi and pericardial abnormalities can be visualized readily (Figure 1.5). Magnetic resonance images acquired throughout the cardiac cycle facilitate evaluation of regional and global myocardial function. Epicardial and endocardial borders of the heart can be defined with ease. Sequential images can be presented in a cine format and subjected to frame by frame analysis for qualitative or quantitative assessment of myocardial thickening (van Ruge *et al.*, 1993). Current gradient echo cine magnetic resonance sequences favour “white blood imaging” where flowing blood is depicted as a bright signal, rather than as the signal void, i.e. “black blood imaging” seen with spin echo sequences (Fisher *et al.*, 1985; Sechtem *et al.*, 1987). Repeated short axis slices, encompassing the entire myocardium, can be stacked to calculate left and right ventricular mass, ejection fraction and cardiac volumes. When measured by MRI, these variables have been shown to be accurate and highly reproducible, reflecting precise myocardial border discrimination and whole heart coverage (Bellenger *et al.*, 2000). Thus, the reliance on geometric assumptions required by echocardiography and ventriculography is not needed.

As with echocardiography, the accuracy of cine MRI for the diagnosis of coronary artery disease is augmented by increasing the cardiac workload. In a conventional clinical scanner, there

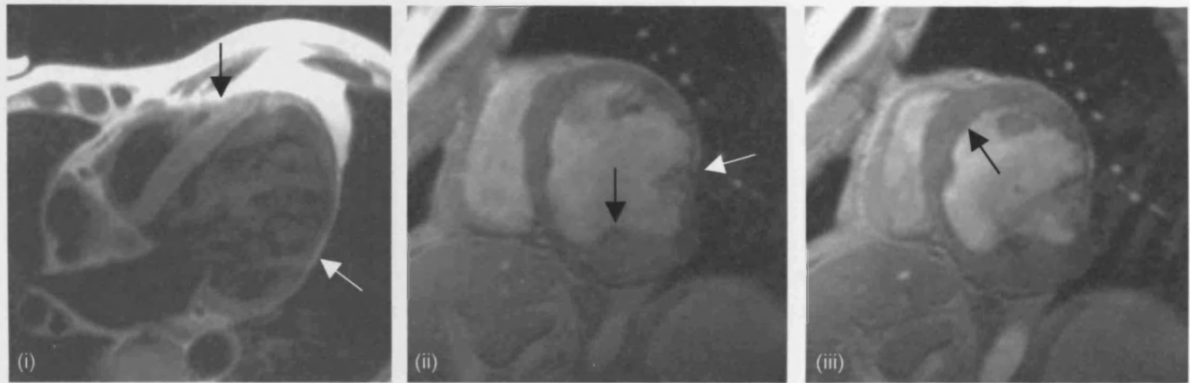


*Figure 1.5. Example of magnetic resonance images for the evaluation of cardiac structure and function. These images are from a patient with a remote inferolateral myocardial infarction. A spin echo horizontal long axis view (i) demonstrates preserved septal thickness (black arrow) but an extremely thin lateral wall (white arrow, i). This is also seen in the gradient echo cine images (white arrow, ii). End-diastolic (ii) and systolic (iii) short axis cine frames reveal inferolateral akinesia but some contractility in the anterior wall (arrow, iii). The inferior wall appears thickened owing to the presence of laminated thrombus (black arrow, ii).*

is limited room for the subject to perform physical exercise. Thus pharmacological stress agents have to be employed. At the inception of this thesis, long imaging times and difficulty in ECG-gating during inotrope-induced tachycardias hampered initial stress work with MRI. However, despite the use of only a modest dose of dobutamine, MRI demonstrated comparable diagnostic sensitivities and specificities compared with those with stress echocardiography and scintigraphy (Table 1.4).

Modality	Sensitivity	Specificity	Reference
Dobutamine wall motion MRI	91%	80%	(van Ruggie <i>et al.</i> , 1994)
Exercise electrocardiography	64%	30%	(Senior <i>et al.</i> , 1994)
Dobutamine echocardiography	72 - 86%	77 - 95%	(Krahwinkel <i>et al.</i> , 1997a)
Dobutamine MIBI-SPECT	95%	71%	(Senior <i>et al.</i> , 1994)

*Table 1.4. Comparison of dobutamine MRI with other diagnostic techniques for the diagnosis of coronary artery disease. MIBI-SPECT = technetium-99m single photon emission computed tomography.*

Modern MR sequences have reduced image acquisition times so that images can be acquired during a subject's breath-hold. These techniques have facilitated the use of optimal stress regimens, with multi-dose administration of dobutamine equivalent to that recommended by echocardiographers. With the use of a high dose dobutamine-atropine protocol, Nagel *et al.* found MRI to be superior to dobutamine stress echocardiography for the detection of CAD (Nagel *et al.*, 1999). MRI had an 86% positive (98% in patients with three-vessel disease) and an 86% negative predictive accuracy for the detection of CAD. In their study, transthoracic echocardiography had a 74% positive and 70% negative diagnostic accuracy. The favourable MRI result appeared to be attributable entirely to the excellence of image quality. The difficulties with suboptimal acoustic windows and subendocardial delineation that plague stress echocardiography were surmounted.

### **1.3.3 Non-invasive assessment of myocardial hibernation**

#### **1.3.3.1 Definition and clinical relevance**

Hibernating myocardium is a state of persistent left ventricular contractile dysfunction that is fully reversible with reperfusion (Rahimtoola, 1995). It appears to reflect repeated stunning in tissue with adequate perfusion to maintain viability at rest but inadequate flow reserve to preclude ischaemia with physiological stress (Ferrari *et al.*, 1999). Its identification is vital in the assessment of patients with global or regional myocardial impairment because in comparison with behaviour of myocardial scar tissue, territories consisting predominantly of hibernating tissue show functional improvement following successful revascularization. Although the identification of myocardial hibernation is important in the assessment of patients after myocardial infarction, it is of greatest consequence in patients with significant left ventricular dysfunction being considered for revascularization procedures (Di Carli *et al.*, 1995; Di Carli *et al.*, 1998). The coronary artery surgery study (CASS) demonstrated the benefit of surgical revascularization compared with medical therapy in patients with low ejection fractions. However, patients with left ventricular impairment have substantial peri-operative morbidity and mortality (Alderman *et al.*, 1983). Thus, the decision to proceed with a revascularization procedure needs to be based on sound criteria. Information required by the surgeon ideally includes accurate assessment of ejection fraction, the site of regional wall dysfunction, the extent of myocardial hibernation and scar, and the extent and reversibility of regional perfusion abnormalities. Thus, integrated examination of cardiac structure, function and perfusion is likely to be particularly valuable.

#### **1.3.3.2 Identification of myocardial hibernation**

The identification of myocardial hibernation is based on the following properties: a recruitable contractile reserve accompanying increased perfusion or transiently increased stimulation, preserved basal perfusion and metabolism, and preserved cell membrane integrity. Traditionally applied imaging modalities include echocardiography and the radionuclide techniques (Table 1.5).

Modality	Sensitivity	Specificity	Standard Parameter	Reference
Dobutamine echocardiography	94%	80%	LV recovery*	(Haque <i>et al.</i> , 1995)
Dobutamine transoesophageal echocardiography	77%	81%	FDG-PET	(Baer <i>et al.</i> , 1996b)
Dobutamine transoesophageal echocardiography	92%	88%	LV recovery*	(Baer <i>et al.</i> , 1996a)
Thallium reinjection scintigraphy	100%	80%	LV recovery*	(Haque <i>et al.</i> , 1995)
Thallium redistribution	91%	50%	LV recovery*	(Haque <i>et al.</i> , 1995)
Positron emission tomography	96%	69%	LV recovery*	(Baer <i>et al.</i> , 1996a)
Dobutamine MRI	89%	94%	LV recovery*	(Baer <i>et al.</i> , 1998)
Dobutamine MRI	81%	95%	FDG-PET	(Baer <i>et al.</i> , 1995)

*Table 1.5 Comparison of techniques available for the assessment of myocardial hibernation. FDG-PET = <sup>18</sup>F-deoxyglucose positron emission tomography; \* = post revascularization.*

### **1.3.3.2.1 Inotrope-induced contractile reserve**

A key diagnostic feature of hibernating myocardium is a recruitable contractile reserve following stimulation with low doses of agents with positive inotropic effects. Stress echocardiography is employed traditionally to detect this (Haque *et al.*, 1995; Baer *et al.*, 1996a; Baer *et al.*, 1996b) but it is both subject and operator dependent (Cigarroa *et al.*, 1993; Afridi *et al.*, 1995; Armstrong & Bossone, 1997; Krahwinkel *et al.*, 1997b). When this series of studies was commenced, there was very little work evaluating this parameter with MRI (Baer *et al.*, 1995; Baer *et al.*, 1996b; Baer *et al.*, 1998). Baer *et al.* tested single dose dobutamine-induced contractile reserve as assessed by MRI against both transoesophageal echocardiography and positron emission tomography with good agreement with both modalities (Baer *et al.*, 1995; Baer *et al.*, 1996b). Subsequently this group has conducted a further study evaluating the use of this parameter to predict improvement in myocardial segments affected by myocardial infarction and subsequent revascularization of the infarction vessel (Baer *et al.*, 1998). All patients had revascularization of

the infarction-related vessel only. They found 89% sensitivity and 94% accuracy for prediction of segmental recovery and subsequent improvement of ejection fraction. More recently Gunning *et al.* have demonstrated dobutamine MRI to be more sensitive (81%) but less specific (45%) than radionuclide scintigraphy for improvement of ejection fraction following revascularization in patients with chronic left ventricular dysfunction (Gunning *et al.*, 1999).

#### **1.3.3.2 Preservation of perfusion and metabolism**

The preservation of sufficient perfusion to sustain myocardial metabolism and cell membrane integrity is essential for cell viability. Classically, positron emission tomography is the modality employed to determine this but this technique is restricted in clinical application because of limited availability. Myocardial territories that demonstrate abnormally low uptake of a perfusion tracer, e.g. ammonia or potassium, in association with preserved or abnormally high metabolism as depicted by  $^{18}\text{F}$ -deoxyglucose uptake, are defined as hibernating (Bax *et al.*, 1997b). Biochemical data and evidence from positron emission tomography studies suggest that a minimum resting blood flow of  $0.25 - 0.3 \text{ ml g}^{-1} \text{ min}^{-1}$  is required to maintain cell viability (Gewirtz *et al.*, 1994). At present there are no data evaluating quantitative perfusion parameters determined by MRI in hibernating myocardium.

#### **1.3.3.3 Cell membrane integrity**

Single photon emission tomography is widely available. Perfusion tracer uptake, e.g. thallium-201, requires not only normal perfusion, but also cell membrane integrity and preserved metabolic function. Myocardial territories that are viable but have slow blood flow may be seen initially as an area of relatively poor tracer activity reflecting either reduced coronary artery blood flow, myocardial infarction or both. Repeated imaging may reveal the presence of delayed tracer uptake (Lomboy *et al.*, 1995). These techniques demonstrate good sensitivity but relatively poor specificity for the identification of myocardial hibernation (Haque *et al.*, 1995).

Delayed contrast enhanced MRI may be a marker for non-viable myocardium. This principle exploits the low molecular weight of MRI contrast media and the resulting free distribution of contrast between the intravascular and extracellular spaces. A breach in cell membrane integrity increases interstitial accumulation of contrast medium and changes the tissue signal characteristics. Measurement of the contrast fractional distribution has been proposed as a means of distinguishing normal from necrotic myocardial tissue (Wendland *et al.*, 1999). During the period of study this parameter has been proven to have significant potential as a marker for myocardial necrosis and is presented in more detail in Chapter 5 (Kim *et al.*, 1999; Kim *et al.*, 2000).

## **1.4 Cardiac MRI experience in Leicester prior to thesis commencement**

The departments of radiology and cardiology in Leicester have an ongoing programme of cardiac MRI. In 1993, a study of 103 patients with acute myocardial infarction was started, comparing resting perfusion MRI against ECG, thallium and echocardiography (Cherryman *et al.*, 1999a; Cherryman *et al.*, 1999b). A first pass contrast-enhanced inversion recovery snapshot-FLASH sequence was employed. A quantitative measurement of myocardial perfusion based on Larsson's model (Larsson *et al.*, 1994; Larsson *et al.*, 1996) was examined in the same patient group by Dr. Asvina Jivan in association with Dr. Mark Horsfield. In particular, the technical problems in obtaining accurate measurements of myocardial relaxation rate changes were examined in detail (Jivan *et al.*, 1997). Subsequently, Dr. James Cullen developed a two-day adenosine rest/stress perfusion protocol to evaluate myocardial ischaemia. This was tested in volunteers and applied to a cohort of patients with coronary artery disease (Cullen *et al.*, 1999b). These projects were completed with the use of a 1.0 Tesla imager (*Magnetom*<sup>TM</sup>, Siemens, Erlangen, Germany) at Leicester Royal Infirmary. In 1996, a 1.5 Tesla imager (*Vision*<sup>TM</sup>, Siemens, Erlangen, Germany) was installed at Glenfield Hospital. This represented a major hardware upgrade with a dedicated phased array cardiac coil and 25 mTesla M<sup>-1</sup> gradients.

## **1.5 Thesis objective**

The principle underlying the concept of this thesis was to customize the current state of the art cardiac MRI techniques available and then to apply them to a range of clinical applications in patients with coronary artery disease. The protocol designs aim to facilitate utilization of the multi-faceted capabilities of magnetic resonance in the evaluation of myocardial perfusion and function within the same examination. This should be possible as the higher specifications of the 1.5 Tesla imager permit faster image acquisition times and produce superior image quality.

## **1.6 Thesis hypotheses**

1. The temporal resolution of the inversion recovery snapshot-FLASH sequence can be enhanced by image acquisition with a constant total repetition time ( $TR_0$ ), rather than by gating to the electrocardiogram, without loss of image or data quality. A low dose of contrast agent can be utilized to facilitate quantitative data acquisition. Two repeated dynamic measurements of perfusion can be made within the same examination despite the presence of residual contrast agent from the first study. Results are reproducible from same day assessments and between image acquisitions on different days.
2. A single visit adenosine stress and rest protocol for assessment of myocardial perfusion can be designed. Quantitative data for research use and qualitative data, more suited to clinical application, can be extracted and used to detect angiographic coronary artery disease.
3. A protocol combining the adenosine stress and rest perfusion assessment with a dobutamine breath-hold cine sequence can be designed to optimize information on myocardial perfusion and function gained during a single examination. This can be applied to patients with left ventricular function to determine parameters of myocardial hibernation. Dobutamine-induced contractile reserve, end-diastolic wall thickness, preserved basal perfusion and

delayed contrast hyperenhancement are predictors of segmental and global myocardial recovery following revascularization.

4. The adenosine perfusion protocol can be used to identify perfusion changes following revascularizing interventions. Early and late improvements in perfusion following percutaneous transluminal angioplasty can be demonstrated. This technique can also detect changes in myocardial perfusion and ischaemic burden, as documented by concurrent dobutamine cine MRI, following transmyocardial laser revascularization and thoracic sympathectomy.

## **1.7 Specific thesis objectives and overview**

To avoid repetition, methodology common to more than one study is presented in detail in Chapter 2. Methods specific to individual studies are described within the relevant chapter. The thesis is divided into five main studies, described in Chapters 3 - 7. Specific results are discussed within each individual chapter. An overview of the results and future perspectives are presented in the final section.

### **1.7.1 Development of first pass contrast-enhanced MRI technique for quantification of myocardial perfusion (Chapter 3)**

This study describes adaptation and upgrade of the inversion recovery snapshot-FLASH sequence for acquisition of myocardial perfusion data as a precursor to the design of a single visit adenosine stress and rest protocol. The aims are firstly to investigate the approach of image acquisition with a constant total repetition time rather than gating to the electrocardiogram, and use of a low contrast agent dose. The image acquisition sequence is then applied at rest to normal volunteers to establish reproducibility of the technique for calculation of the extraction fraction of gadodiamide,  $K_1$ , during the same examination and between examinations conducted on separate days.

### **1.7.2 Diagnostic potential of adenosine perfusion MRI in patients with coronary artery disease (Chapter 4)**

A single visit adenosine stress and rest protocol for perfusion imaging is utilized. The first study aims to test the diagnostic accuracy of quantitative perfusion parameters for the identification of coronary artery disease in patients with single and multi-vessel disease. The second study aims to test the diagnostic potential of a qualitative reporting method and to assess whether specific qualitative perfusion patterns are associated with severity of coronary artery stenosis, remote myocardial infarction and presence or absence of collateral flow.

### **1.7.3 MRI prediction of contractile recovery in individual myocardial segments following revascularization: translation into clinical benefit (Chapter 5)**

The initial aim of this study is to incorporate a multi-stage dobutamine cine protocol into the adenosine stress and rest perfusion acquisition sequence to create a comprehensive examination of myocardial structure, function and perfusion. Such a protocol would allow examination of potential parameters of myocardial hibernation, i.e. end-diastolic wall thickness, dobutamine-induced contractile reserve, myocardial perfusion and delayed hyperenhancement. The second aim is to use this protocol to perform a definitive study in patients with left ventricular dysfunction undergoing revascularization to determine if these parameters are predictive of segmental and global functional recovery.

### **1.7.4 Restoration of myocardial blood flow following percutaneous balloon dilatation and stent implantation (Chapter 6)**

The adenosine stress perfusion protocol is used to determine whether qualitative and quantitative image data can identify early perfusion changes following percutaneous transluminal angioplasty and establish their persistence six months after the procedure.

### **1.7.5 Comparison of clinical and functional effects of transmyocardial laser revascularization and thoracic sympathectomy (Chapter 7)**

The remit of this final study is to use the dual adenosine-dobutamine stress protocol to evaluate any changes in myocardial function and perfusion following transmyocardial revascularization and thoracic sympathectomy.

---

## **Chapter 2**

### **Methods**

---

## 2.1 Ethical approval

Approval was obtained from Leicester Health Authority Ethics Committee for all studies (Table 2.1). The nature of the study and all procedures were explained to all subjects verbally and with the use of patient information leaflets. Informed written consent was obtained prior to recruitment.

Ethics Application Title	EC No.
Low dose contrast cardiac MRI	5154
Contrast enhanced myocardial perfusion using MRI in patients with ischaemic heart disease	3661
Dobutamine stress cine MRI for quantitative regional wall motion analysis	4822
MRI for the evaluation of hibernating myocardium	5108
MRI following percutaneous transluminal angioplasty	5274
Comparative study on the beneficial effect of transmyocardial laser revascularization and thoracic sympathectomy	4834

*Table 2.1. Leicester ethics committee approval numbers (EC No.) for the studies presented in this thesis.*

## 2.2 Clinical assessment

A patient symptom questionnaire was carried out by an experienced cardiac nurse practitioner, blinded to other study data. Patient symptoms of angina and dyspnoea were assessed according to New York Heart Association criteria (Goldman *et al.*, 1981).

## 2.3 Coronary angiography

All coronary angiography was undertaken on clinical grounds and performed with a standard Judkins' approach (Judkins, 1967). Quantitative measurements were performed on line with Quantcor software (Quantcor™ QCA, Siemens, Erlangen, Germany (Haase *et al.*, 1993)).

### 2.3.1 Measurement of ejection fraction

End-diastolic and end-systolic frames of the left ventriculogram were identified. The myocardial contour was traced and end-diastolic and end-systolic volumes estimated by the software. Ejection fraction was calculated (Equation 2.1).

$$\text{Equation 2.1.} \quad EF = \frac{EDV - ESV}{EDV} \%$$

### 2.3.2 Qualitative reporting according to the Green Lane system

All angiograms were reported qualitatively according to the Green Lane reporting system (Brandt *et al.*, 1977) in order to take into account individual variations in coronary artery anatomy. This is discussed in more detail below (Section 2.9). Stenoses were visually graded from at least 2 views. A coronary vessel was defined as having significant disease by presence of one or more stenoses causing greater than 50% reduction in cross-sectional area. Conversely, a functionally “normal” coronary artery was defined as having no stenoses greater than 50%.

### 2.3.3 Quantification of coronary artery stenoses

The diameter of any diseased vessels was measured at the site of the stenosis (c) or stent (d) and at two reference points, i.e. above (a) and below (b) the lesion (Figure 2.1). Stenosis was then calculated as percent reduction in cross-sectional area. Mean reference diameters pre-intervention ( $r_1$ ) and post-intervention (stent implantation,  $r_2$ ) were defined as  $(a + b) / 2$ . Where stenting was employed, acute stent gain was defined as  $d/r_1 - c/r_2$ .

## 2.4 Magnetic resonance imaging

### 2.4.1 Magnetic resonance imager

All scans were conducted with the use of a 1.5 Tesla *Vision™* imager (Siemens, Erlangen, Germany) in the MRI unit at Glenfield General Hospital, Leicester. A cardiac dedicated phased

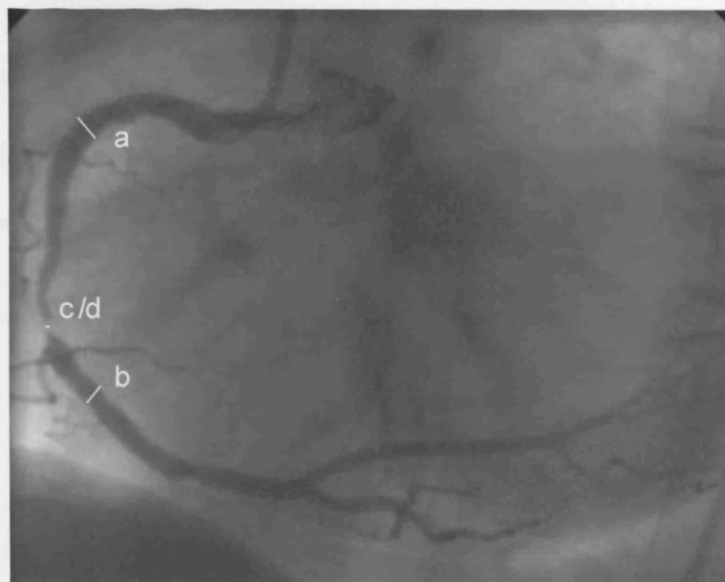


*Figure 2.1. Quantification of angiographic coronary artery stenosis. Reference diameters above (a), below (b) and at the site of a lesion (c, or d if stented) are illustrated.*

array radiofrequency surface coil was used to optimize image quality by increasing signal to noise ratio and maximizing spatial resolution. Purpose-designed fiberoptic cables compatible with the magnetic field and imaging system provided a continuous electrocardiogram (ECG). All subjects were screened with a standard questionnaire to exclude contra-indications to MRI, contrast agent or stressors (Table 2.2) prior to entry into the Faraday cage.

---

Metallic implants	Clinical instability
Intra-cranial clips	Pacemakers/Internal cardiac defibrillators
Intra-ocular foreign bodies/implants	Temporary pacing wires/Swan-Ganz catheters
Cochlear implants	Pregnancy/breast feeding
Shrapnel	Severe claustrophobia
Dehiscent Starr-Edwards prosthetic valves (1960 – 1964)	
Contraindications to adenosine or dobutamine	
Contraindications to gadodiamide, i.e. known allergy or severe renal impairment	

---

*Table 2.2. Contraindications to stress contrast-enhanced MRI.*

#### **2.4.2 Slice selection**

Standard scouting views were acquired to localize the heart and to derive subsequent imaging planes. For both perfusion and functional cine imaging three short axis planes at the cardiac base, mid-papillary level and apex were selected (Figure 2.2). The angle of the short axis was positioned parallel to the plane of the mitral valve. Slice separation was determined by centering the middle slice at mid-papillary level. The outer two slices were positioned equidistant to the mid-plane so that the apical plane retained left ventricular cavity and the basal slice did not encroach into the left ventricular outflow tract.

Additional horizontal and vertical long axis planes were acquired for functional imaging to facilitate evaluation of the cardiac apex (Figure 2.3). Where perfusion and functional cine imaging were performed in the same subject short axis views were matched exactly. When subjects attended for serial imaging, imaging plane parameters were referenced to the scouting views from

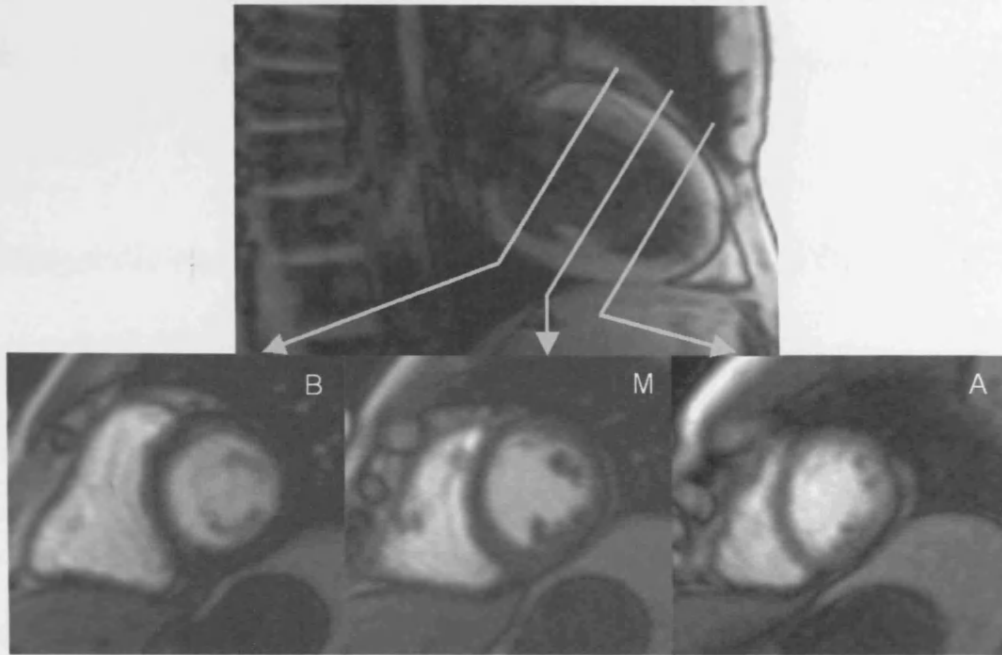


*Figure 2.2. Positioning of basal (B), mid-papillary (M) and apical (A) short axis planes from vertical long axis localizer.*

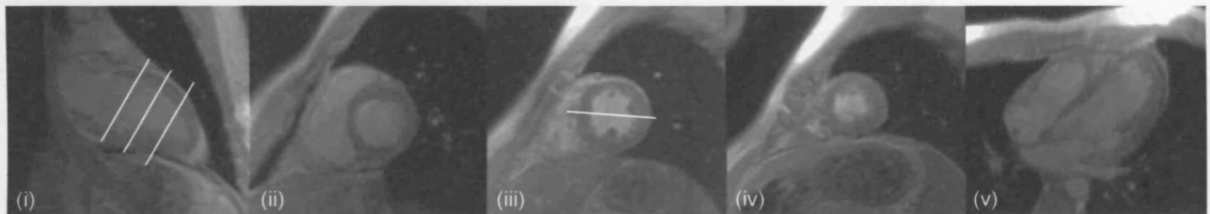


*Figure 2.3. Cine images showing derivation of imaging planes. The vertical long axis (i) is used to obtain the short axis views. The three parallel lines indicate the image planes for the three levels: left = basal (ii), centre = mid-papillary (iii), right = apical (iv) short axes. The mid-papillary short axis (iii) is then bisected, as illustrated, to give the horizontal long axis view (v).*

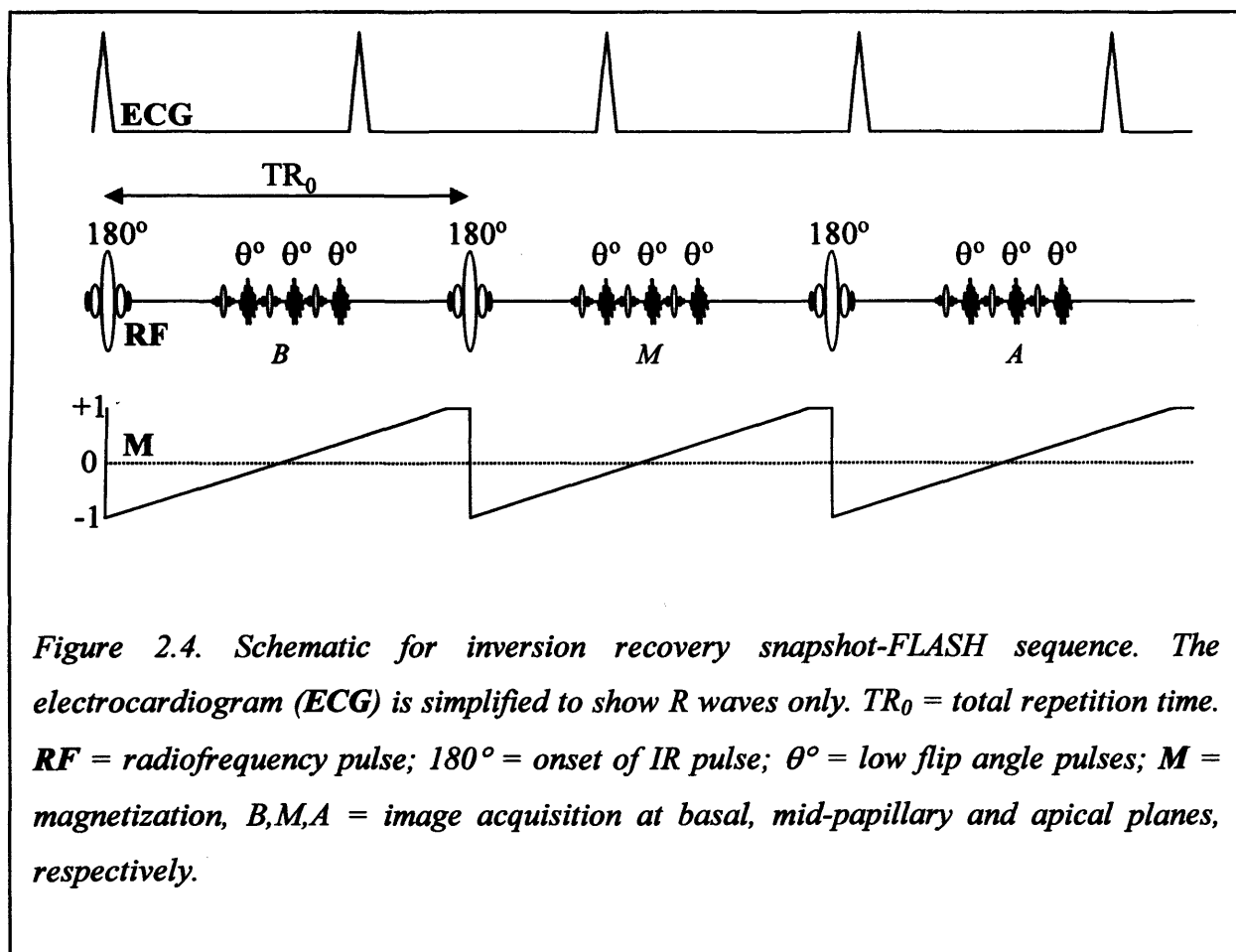
the initial scan to ensure identical slice positioning. For all image analysis the juncture of the right ventricular free wall and the left ventricle was used as an anatomical reference landmark to register cardiac orientation.

## 2.5 Magnetic resonance imaging: myocardial perfusion

Contrast-enhanced first pass MRI was used to evaluate myocardial perfusion.

### 2.5.1 Imaging sequence

An inversion recovery snapshot-fast low angle shot (FLASH) sequence was utilized (Figure 2.4) (Haase, 1990). A  $180^\circ$  inversion prepulse was used to null myocardial signal prior to gadodiamide administration, thus enhancing the relative signal intensity increase produced by contrast agent  $T_1$  shortening effects. The sequence was run with a constant total repetition time



rather than with gating to the electrocardiogram. This approach is discussed further in Chapter 3. The imaging sequence parameters are displayed in Table 2.3.

<b>Repetition time (TR)</b> = 4.5 ms	<b>Flip angle (<math>\alpha</math>)</b> = 8°
<b>Total repetition time (TR<sub>0</sub>)</b> = 1080 ms	<b>Field of view (FOV)</b> = 300 mm <sup>2</sup>
<b>Inversion time (TI)</b> = 300 ms, effective TI (TI <sub>eff</sub> ) = 516 ms	<b>Slice thickness</b> = 9 mm
<b>Echo time (TE)</b> = 2 ms	<b>Matrix</b> = 96 x 128

*Table 2.3. MRI parameters for inversion recovery snapshot-FLASH sequence. TI and TI<sub>eff</sub> are the times from the inversion pulse to the first and mid lines of k-space, respectively.*

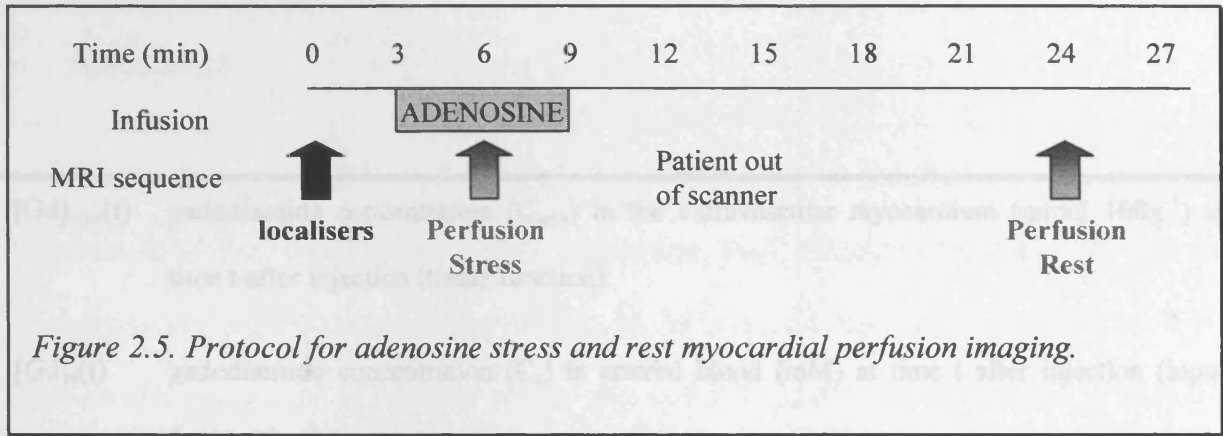
### 2.5.2 Scan protocol

First pass contrast-enhanced perfusion MRI was performed at rest and 3 minutes after commencement of an adenosine infusion. Approximately twenty minutes separated the two scans. During this time the patient was withdrawn from the imager bore but remained immobile on the couch so that the localizer scans were not distorted. In the rare occurrence of significant patient motion, planes were relocalized with reference to the initial scouting images.

A proton density image ( $M_0$  image) after full longitudinal relaxation was obtained in each plane prior to each application of the sequence to enable calculation of the longitudinal relaxation rate ( $R_1$ ). A low dose gadodiamide bolus (0.025 mmol kg<sup>-1</sup>, *Omniscan*, Nycomed Amersham, Amersham, UK) was given by rapid hand injection via the ante-cubital vein after the third measurement of each plane. The 3 short axis slices were acquired sequentially (25 measures). The protocol for adenosine perfusion imaging is shown in Figure 2.5.

### 2.5.3 Adenosine infusion

Adenosine (Adenoscan, Sanofi Winthrop Ltd., France) was administered for a total of 6 minutes according to a standard regimen of 140 µg kg<sup>-1</sup> min<sup>-1</sup>. The infusion was terminated if the patient developed intolerable side effects, ischaemia or if any adverse events occurred. Substances



containing caffeine were stopped 12 hours before administration. Dipyridamole was withdrawn 48 hours prior to scanning.

## 2.5.4 Quantitative analysis of MRI perfusion data

### 2.5.4.1 Estimation of the unidirectional transfer constant for gadodiamide ( $K_i$ ): tracer kinetic model

The unidirectional transfer constant for gadodiamide ( $K_i$ ) was used as a measure of perfusion. The derivation of the tracer kinetic model is described in detail by Larsson *et al.* (Larsson *et al.*, 1994; Larsson *et al.*, 1996). A brief description is included below. Abbreviations of the parameters expressed in the tracer kinetic model equations are displayed in Table 2.4 (overleaf).

Equation 2.2 is the first order differential equation that describes the transport of gadodiamide across the capillary membrane (Kety, 1951).

$$\text{Equation 2.2.} \quad \frac{d[Gd]_{myo}(t)}{dt} = K_i[Gd]_a(t) - k_2[Gd]_{myo}(t)$$

The fact that gadodiamide is a diffusible substance that is distributed in the extracellular space without interaction with other macromolecules (Weinmann *et al.*, 1984; Prato *et al.*, 1988) is assumed to hold true within myocardium. Equation 2.2 can therefore be rewritten (Equation 2.3).

---

$[Gd]_{myo}(t)$	gadodiamide concentration ( $C_{myo}$ ) in the extravascular myocardium ( $mmol\ 100g^{-1}$ ) at time $t$ after injection (tissue function)
$[Gd]_a(t)$	gadodiamide concentration ( $C_a$ ) in arterial blood ( $mM$ ) at time $t$ after injection (input function)
$K_i$	the unidirectional influx constant that determines the transport of gadodiamide across the capillary membrane ( $ml\ 100g^{-1}\ min^{-1}$ )
Hct	Haematocrit
$\lambda$	volume ( $ml\ 100g^{-1}$ ) of distribution of gadodiamide within the myocardium
$k_2$	$K_i (1-Hct)/\lambda =$ transfer constant for the back diffusion of gadodiamide across the capillary membrane
$\otimes$	mathematical operation of convolution
E	unidirectional extraction fraction (dimensionless) of gadodiamide during its initial passage across the capillary membrane
F	blood perfusion ( $ml\ 100g^{-1}\ min^{-1}$ )
PS	permeability-surface area product ( $ml\ 100g^{-1}\ min^{-1}$ )
$R_1(t)$	longitudinal relaxation rate at time $t$ after injection ( $sec^{-1}$ )
$R_1(0)$	longitudinal relaxation rate before injection ( $sec^{-1}$ )
$\beta$	relaxivity of gadodiamide ( $L\ mmol^{-1}\ s^{-1}$ )

---

*Table 2.4. Definition of parameters expressed in tracer kinetic model.*

$$\text{Equation 2.3.} \quad \frac{d[Gd]_{myo}(t)}{dt} = K_i \left[ [Gd]_a(t) - \frac{1-Hct}{\lambda} [Gd]_{myo}(t) \right]$$

Equation 2.3 states that the infinitesimal change in myocardial gadodiamide concentration is proportional to the arterial gadodiamide concentration. Back diffusion of gadodiamide into the vascular system is proportional to concentration in the interstitial space of the myocardium. If the concentration within the myocardium at time zero is 0 ( $[Gd]_{myo}(0) = 0$ ), the solution to Equation 2.3 is shown in Equation 2.4.

$$\text{Equation 2.4.} \quad C_{myo}(t) = K_i \int C_a(t) e^{-\frac{(1-Hct)K_i(t)}{\lambda}} dt$$

This can be further described (Equation 2.5) by a convolution operation of the residue impulse response of the myocardium ( $K_i \exp^{-(1-Hct)K_i(t)/\lambda}$ , tissue function) and the arterial gadodiamide concentration (input function).

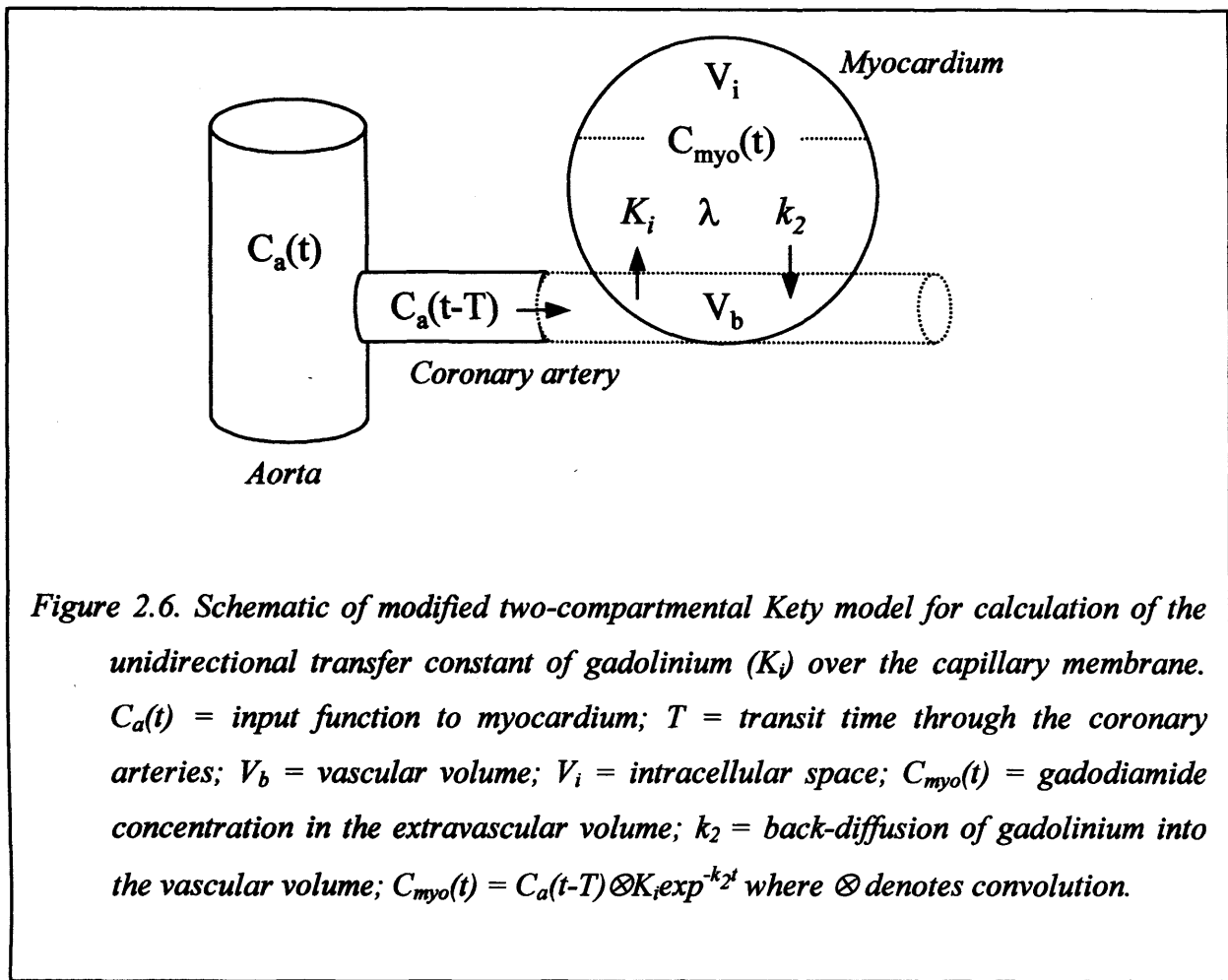
$$\text{Equation 2.5.} \quad C_{myo}(t) = C_a(t) \otimes K_i e^{-\frac{(1-Hct)K_i(t)}{\lambda}}$$

This function is based on the single capillary model (Figure 2.6). This assumes that (i) all capillaries within a ROI are identical with uniform dimensions and permeabilities and (ii) that  $K_i$  and  $\lambda$  are constant throughout the period of measurement.

$K_i$  is related to the extraction fraction of gadodiamide across the capillary membrane and blood perfusion (Equation 2.6) (Renkin, 1959; Crone, 1963).

$$\text{Equation 2.6.} \quad K_i = E \cdot F = F \left( 1 - e^{-\frac{PS}{F}} \right)$$

The model was originally proposed for application to freely diffusible tracers for which E is assumed to be unity. Since gadodiamide is barrier limited, this assumption does not apply. Direct measurement of the extraction fraction of gadodiamide is difficult in humans. E has been measured for technetium-99, a compound of equivalent molecular weight to gadodiamide in humans at rest



( $E = 0.5$ ) and during vasodilation ( $E = 0.4$ ) (Svendsen *et al.*, 1992; Tong *et al.*, 1993) and so these factors could be used to correct  $K_i$  to extrapolate absolute values for flow (Fritz-Hansen *et al.*, 1998).

#### 2.5.4.2 Relationship of tracer kinetic model to magnetic resonance imaging

In order to relate the tracer kinetic model to MRI, the following assumptions have to be made:

- (i) The effect of gadodiamide within the vascular compartment (7 - 8% of the two compartments) and possible exchange effects between the intravascular and extravascular compartments are ignored.
- (ii) Fast exchange, i.e. rapid transition of protons between compartments and a very short residence time in each compartment in relation to the relaxation rate and measuring time,

exists between intracellular and extracellular water. The relaxation rate is therefore a weighted average of the relaxation rates of the different compartments.

- (iii) The change in longitudinal relaxation rate is linearly related to the change in gadodiamide concentration.

The change in relaxation rate for a myocardial ROI following administration of gadodiamide is shown in Equation 2.7 (Lauffer, 1987).

$$\text{Equation 2.7.} \quad R_1(t) = R_1(0) + \beta[Gd]_{myo}(t)$$

The relaxivity of gadodiamide is a constant and set at  $4.3 \text{ L mmol}^{-1} \text{ s}^{-1}$  at 1.5 Tesla field strength (Weinmann *et al.*, 1984; Lauffer, 1987; Tweedle *et al.*, 1988). Equation 2.7 can then be substituted into Equation 2.5 (Equation 2.8).

$$\text{Equation 2.8.} \quad \Delta R_1(t) = R_1(t) - R_1(0) = C_a(t) \otimes \beta \cdot K_i \cdot e^{-\frac{(1-Hct)K_i}{\lambda}(t)}$$

If myocardial relaxation rates before and after gadodiamide injection are measured together with the arterial concentration of contrast agent, then  $\beta \cdot K_i$  and  $K_i/\lambda$  can be estimated by a least-squares fitting procedure (Patlak *et al.*, 1983).

#### 2.5.4.3 Measurement of longitudinal relaxation time ( $R_1$ ): derivation of $K_i$

First pass contrast-enhanced images were transferred to a Sun workstation (Sun Microsystems, Mountainview, California) for further analysis with the use of image software Analyze AVW 2.5 (Mayo Foundation, Rochester, Minnesota). The dynamic images from each anatomical plane were placed in temporal sequence to create rest and stress studies for each short axis slice.

##### 2.5.4.3.1 Extraction of regional signal intensity

Definition of epicardial and endocardial borders was graded as being of either sufficient or insufficient quality for placement of analytical contours. These borders were then contoured by

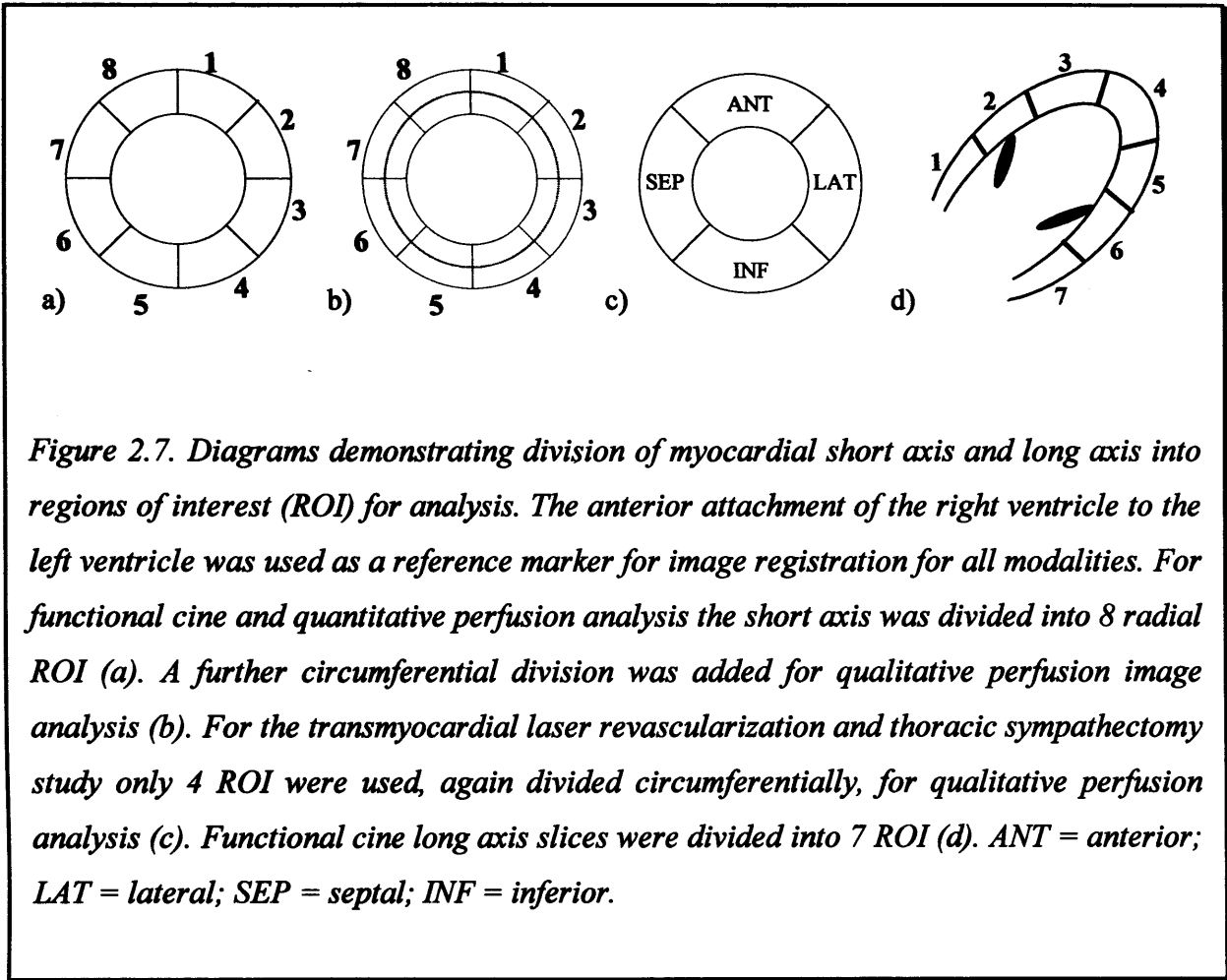


*Figure 2.7. Diagrams demonstrating division of myocardial short axis and long axis into regions of interest (ROI) for analysis. The anterior attachment of the right ventricle to the left ventricle was used as a reference marker for image registration for all modalities. For functional cine and quantitative perfusion analysis the short axis was divided into 8 radial ROI (a). A further circumferential division was added for qualitative perfusion image analysis (b). For the transmyocardial laser revascularization and thoracic sympathectomy study only 4 ROI were used, again divided circumferentially, for qualitative perfusion analysis (c). Functional cine long axis slices were divided into 7 ROI (d). ANT = anterior; LAT = lateral; SEP = septal; INF = inferior.*

hand. Care was taken to exclude any signal from either the left ventricular cavity or adjacent non-myocardial structures from the contoured area. The myocardium was then divided radially into 8 equal ROI (Figure 2.7a). The only exception to this was that for the final study presented in Chapter 7, 4 ROI were utilized (Figure 2.7c). The anterior attachment of the right ventricle to the left ventricle was used as a reference marker for image registration. The image analysis software had insufficient spatial resolution to separate subendocardial and epicardial layers in the majority of patients studied and so transmural perfusion only was assessed by this method.

Images were then sampled to give a mean signal intensity-time curve for each ROI over the 25 dynamic images and mean regional signal intensity values for the proton density image. A signal intensity-time curve for the contrast agent bolus was also generated from a spherical ROI placed in the centre of the left ventricular cavity in the corresponding basal short axis slice.

### 2.5.4.3.2 Calculation of $K_i$

The extracted signal intensities were used to derive  $R_1$  values over time for each myocardial ROI (tissue function) and for the left ventricular cavity (input function) for each mid-papillary slice (Jivan *et al.*, 1997) (Figure 2.8). The tissue and input functions were entered into a deconvolution algorithm to calculate the unidirectional transfer constant,  $K_i$ , for gadodiamide for each myocardial ROI (Equation 2.8). For this function, haematocrit was assumed to be 0.5, and the relaxivity of gadodiamide in blood was assumed to be similar to that in myocardial water. The computer

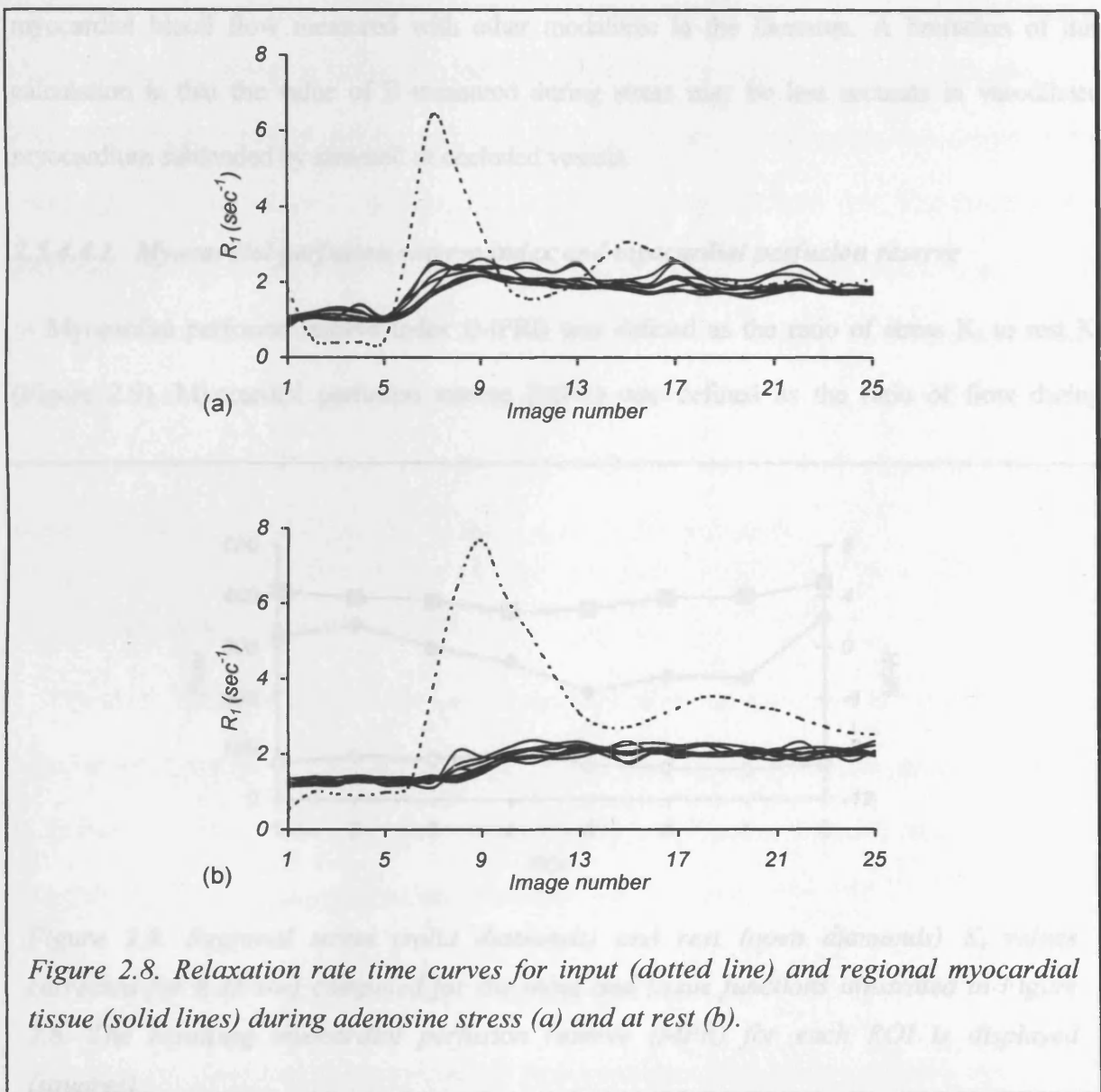


Figure 2.8. Relaxation rate time curves for input (dotted line) and regional myocardial tissue (solid lines) during adenosine stress (a) and at rest (b).

algorithms necessary for these computations were written in C programming language by Dr. Mark Horsfield.

#### 2.5.4.4 Estimation of myocardial perfusion

The reported values of  $E$  described above were introduced to attempt to relate  $K_i$  more accurately to myocardial perfusion. Rest and stress  $K_i$  values were therefore corrected for  $E$  values of 0.5 and 0.4, respectively, so that resulting values for flow gave as close an approximation to absolute myocardial blood perfusion as could be achieved with use of this tracer kinetic model. This data is presented in addition to the  $K_i$  data to facilitate comparison with absolute values for myocardial blood flow measured with other modalities in the literature. A limitation of this calculation is that the value of  $E$  measured during stress may be less accurate in vasodilated myocardium subtended by stenosed or occluded vessels.

##### 2.5.4.4.1 Myocardial perfusion reserve index and myocardial perfusion reserve

Myocardial perfusion reserve index (MPRI) was defined as the ratio of stress  $K_i$  to rest  $K_i$  (Figure 2.9). Myocardial perfusion reserve (MPR) was defined as the ratio of flow during

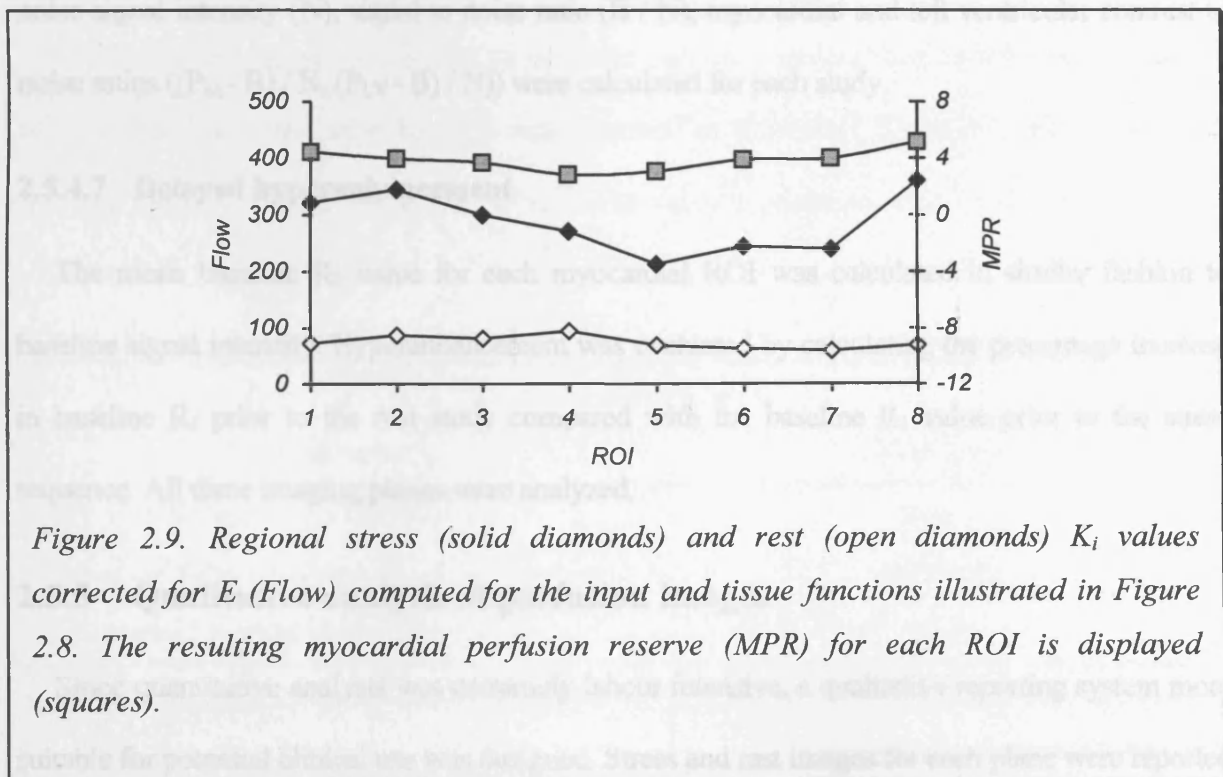


Figure 2.9. Regional stress (solid diamonds) and rest (open diamonds)  $K_i$  values corrected for  $E$  (Flow) computed for the input and tissue functions illustrated in Figure 2.8. The resulting myocardial perfusion reserve (MPR) for each ROI is displayed (squares).

adenosine stress to that at rest (Equation 2.9). These parameters were calculated for each ROI.

$$\text{Equation 2.9.} \quad MPR = \frac{(SK_i / 0.4)}{(RK_i / 0.5)}$$

#### **2.5.4.5 Bolus delivery**

Adequacy of bolus delivery to the left ventricular cavity was determined by identification of the peak left ventricular  $R_1$  value image frame number.

#### **2.5.4.6 Signal and contrast to noise ratio**

Peak myocardial ( $P_M$ ) and left ( $P_{LV}$ ) ventricular signal intensities were defined as the maximum signal intensity achieved in any of the myocardial ROI and left ventricular cavity, respectively for each study. Study baseline signal intensity, i.e. prior to contrast administration, was defined as the mean signal intensity from the second, third and fourth images for each ROI. The first image in each study was ignored as unrepresentative of steady state. Regional values were averaged to give the overall baseline signal intensity,  $B$ . The contribution of noise to signal intensity in each image was measured by placing a spherical ROI onto an artefact-free area outside the patient. The mean noise signal intensity ( $N$ ), signal to noise ratio ( $B / N$ ), myocardial and left ventricular contrast to noise ratios ( $(P_M - B) / N$ ,  $(P_{LV} - B) / N$ ) were calculated for each study.

#### **2.5.4.7 Delayed hyperenhancement**

The mean baseline  $R_1$  value for each myocardial ROI was calculated in similar fashion to baseline signal intensity. Hyperenhancement was evaluated by calculating the percentage increase in baseline  $R_1$  prior to the rest study compared with the baseline  $R_1$  value prior to the stress sequence. All three imaging planes were analyzed.

### **2.5.5 Qualitative analysis of perfusion images**

Since quantitative analysis was extremely labour intensive, a qualitative reporting system more suitable for potential clinical use was designed. Stress and rest images for each plane were reported

together on line. Initially, image quality was assessed for diagnostic acceptability. Factors considered to render images of insufficient quality for analysis were lack of definition of epicardial and endocardial borders, e.g. partial volume effects, motion artefact, lack of distinction from the pericardial layer, and presence of artefacts overlapping cardiac structures. The quality and character of the gadodiamide bolus was appreciated. At each level, the myocardium was divided into 8 radial ROI. Each ROI was then divided circumferentially into inner and outer layers (Figure 2.7b). Perfusion in each ROI was classed as being normal or abnormal. Abnormal perfusion was defined as visually evident reduced and/or delayed peak signal intensity following contrast agent enhancement (Table 2.5).

Contrast enhancement pattern		Perfusion assessment
Enhancement	Peak signal	
Normal	Satisfactory	Normal
Slow	Satisfactory	Abnormal
Slow	Low	Abnormal
None		Abnormal

*Table 2.5. Qualitative parameters to define normal and abnormal myocardial perfusion.*

If a perfusion deficit was limited to the inner layer it was described as subendocardial. If it affected both inner and outer layers it was described as transmural. Stress and rest images were reported together to allow recognition of reversible (only apparent on stress) and fixed (similar on stress and rest) defects Table 2.6.

Perfusion: Rest vs. Stress	
Enhancement	Evaluation
Normal at rest and on stress	Normal
Increased delay or hypoenhancement on stress	Reversible
Impaired, equivalent at rest and on stress	Fixed

*Table 2.6. Qualitative parameters for definition of reversible and fixed regional myocardial perfusion deficits.*

## 2.6 Magnetic resonance imaging: myocardial function

### 2.6.1 Imaging sequence

A breath-hold cine gradient echo sequence gated to the electrocardiogram was used to image myocardial function. A sequence diagram is shown in Figure 2.10. Imager parameters are displayed in Table 2.7.

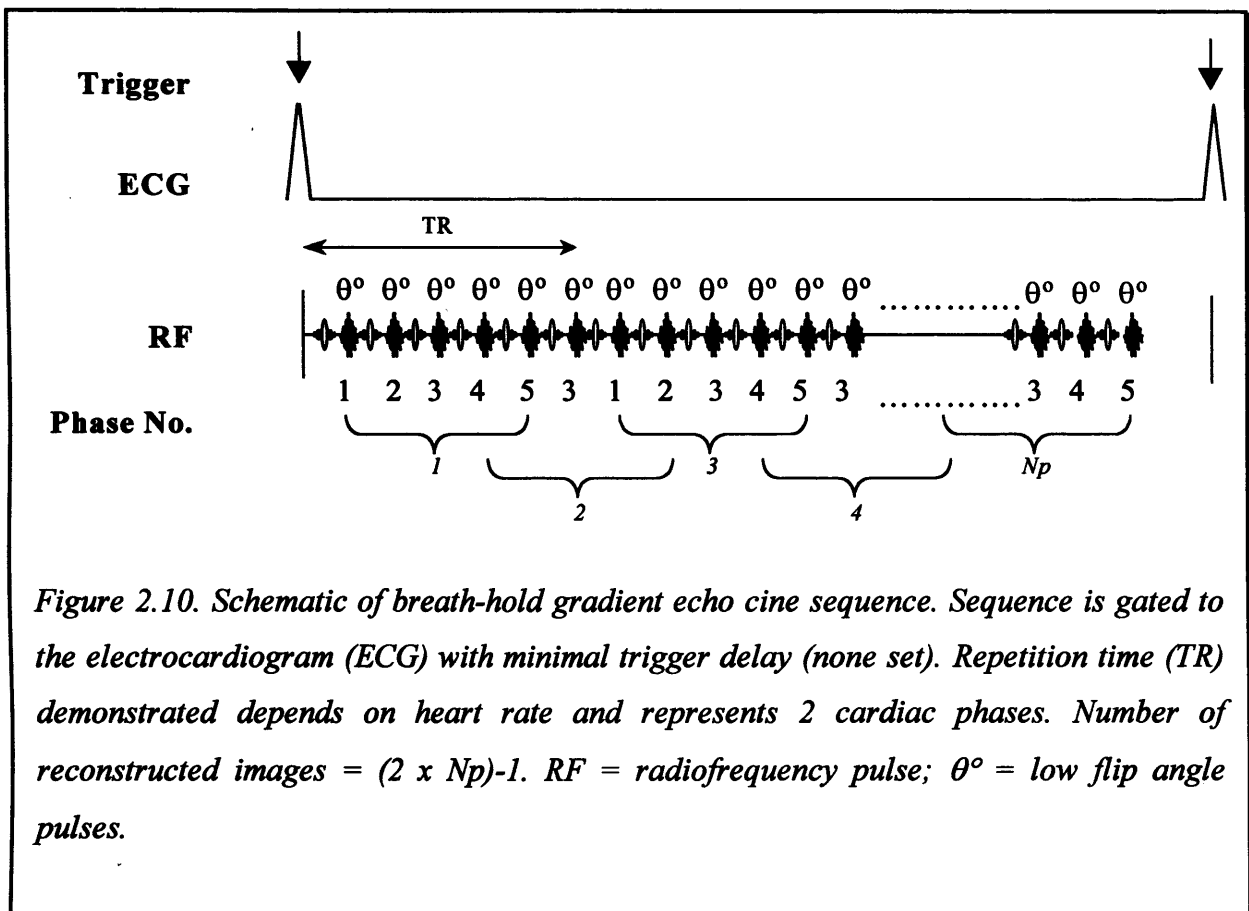


Figure 2.10. Schematic of breath-hold gradient echo cine sequence. Sequence is gated to the electrocardiogram (ECG) with minimal trigger delay (none set). Repetition time (TR) demonstrated depends on heart rate and represents 2 cardiac phases. Number of reconstructed images =  $(2 \times N_p) - 1$ . RF = radiofrequency pulse;  $\theta^\circ$  = low flip angle pulses.

### 2.6.2 Scan protocol

Images in the five planes were acquired at rest, and then repeated during dobutamine stress (Figure 2.11).

**Repetition time (TR)** = 60 ms

**Echo time (TE)** = 4.8 ms

**Flip angle** = 20°

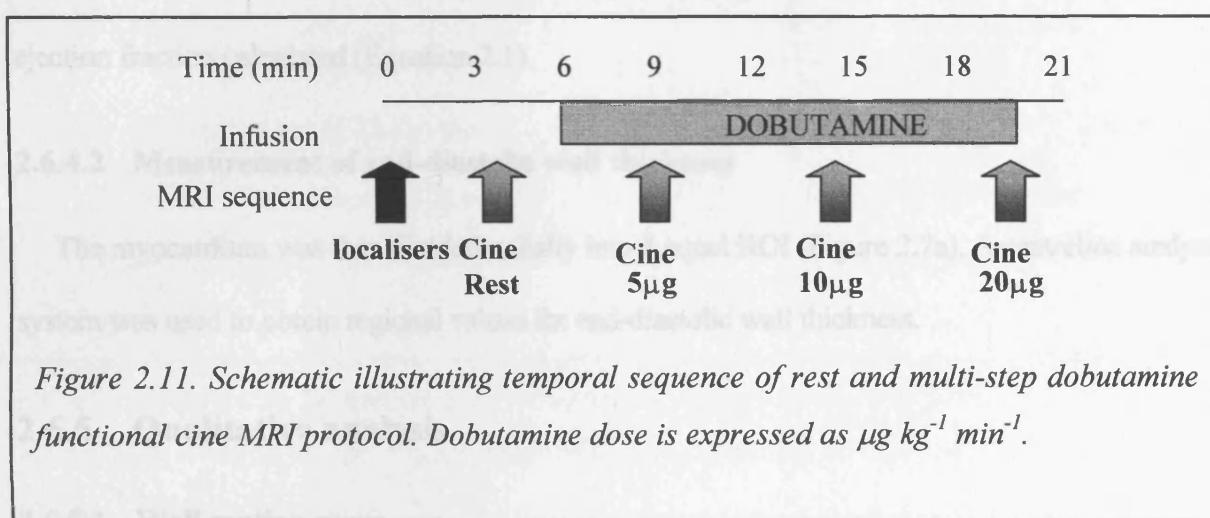
**Field of view (FOV)** = 300 mm x 300 mm (short axis); 420 mm x 315 mm (long axis)

**Slice thickness** = 6 mm

**Matrix** = 96 x 128

**Acquisition time** = 15, 19 or 23 heart beats (ECG-gated)

Table 2.7. MRI parameters for breath-hold gradient echo cine sequence.



### 2.6.3 Dobutamine infusion

A multistep low dose steady state dobutamine (Dobutamine Hydrochloride Infusion, Phoenix Pharmaceuticals Ltd., Gloucester, UK) infusion was used. Dobutamine was commenced at  $5 \mu\text{g kg}^{-1} \text{min}^{-1}$  increasing to  $10 \mu\text{g kg}^{-1} \text{min}^{-1}$  and then  $20 \mu\text{g kg}^{-1} \text{min}^{-1}$ . Imaging was performed after three minutes at each dose in order to achieve a steady state. The infusion was stopped if the patient developed intolerable side effects, hypotension, clinical and/or electrocardiographic changes of significant ischaemia or arrhythmia, severe chest pain or breathlessness, systolic blood pressure  $> 220$  mmHg, diastolic pressure  $> 120$  mmHg or if new myocardial systolic thickening abnormalities occurred in more than one contiguous ROI during dobutamine (see below). Beta-blockers were withheld for 48 hours prior to each scan.

## **2.6.4 Quantitative analysis**

Functional images were transferred to a Sun workstation (Sun Microsystems, Mountainview, California) for further analysis with the use of image software Argus II (Siemens, Erlangen, Germany). The short axis slices were used for quantitative analysis. End-diastolic and end-systolic images were selected. Epicardial and endocardial borders were contoured by hand. Care was taken to exclude papillary muscle from the measured area.

### **2.6.4.1 Ejection fraction**

End-diastolic (EDV) and end-systolic volumes (ESV) were measured and left ventricular ejection fraction calculated (Equation 2.1).

### **2.6.4.2 Measurement of end-diastolic wall thickness**

The myocardium was then divided radially into 8 equal ROI (Figure 2.7a). A centreline analysis system was used to obtain regional values for end-diastolic wall thickness.

## **2.6.5 Qualitative analysis**

### **2.6.5.1 Wall motion score**

A qualitative reporting system was devised to assess regional systolic wall thickening. Images were viewed as a video loop on line. Diagnostic quality was assessed as the images could be susceptible to quality loss from poor triggering or motion artefact if the subject had difficulty breath-holding. The myocardial short and long axes were divided into 8 and 7 radial regions of interest, respectively (Figure 2.7a and d). Systolic wall thickening was graded according to the criteria shown in Table 2.8.

### **2.6.5.2 Characterization of myocardium**

Characterization of myocardial regions of interest as normal, ischaemic, hibernation or scar tissue was achieved by comparing systolic wall thickening on stress and rest functional cine images (Table 2.9).

<b>Systolic wall thickening</b>	<b>Score</b>
Normal	0
Mild hypokinesis	1
Moderate hypokinesis	2
Severe hypokinesis	3
Akinesis	4
Dyskinesis	5

*Table 2.8. Wall motion score for qualitative assessment of cine images.*

<b>Systolic wall thickening</b>	
<b>Rest v Stress</b>	<b>Evaluation</b>
Normal at rest and on stress	Normal
Normal at rest, dysfunction on stress	Reversible dysfunction
Dysfunction at rest, improved on stress	Hibernation
Dysfunction at rest, unchanged on stress	Scar

*Table 2.9. Definition of myocardial evaluation as normal, ischaemic (reversible dysfunction) hibernating or scar by assessment of systolic wall thickening at rest and during dobutamine stress.*

## **2.7 Magnetic resonance imaging: dual adenosine dobutamine stress (DADS) protocol**

The imaging sequences described above were combined to provide an assessment of myocardial perfusion and function in a single examination. This was referred to as the dual adenosine dobutamine stress (DADS) protocol.

### **2.7.1 Scan protocol**

Following scouting images, myocardial perfusion imaging was performed during adenosine infusion. The patient was then withdrawn from the magnet bore for 10 minutes in order to allow the effects of the adenosine to subside. Resting functional cine images were then obtained,

succeeded by a rest perfusion scan. A multi-step dobutamine infusion was then commenced with further acquisition of functional cine images at each dose level.

A schematic of DADS protocol is shown in Figure 2.12.

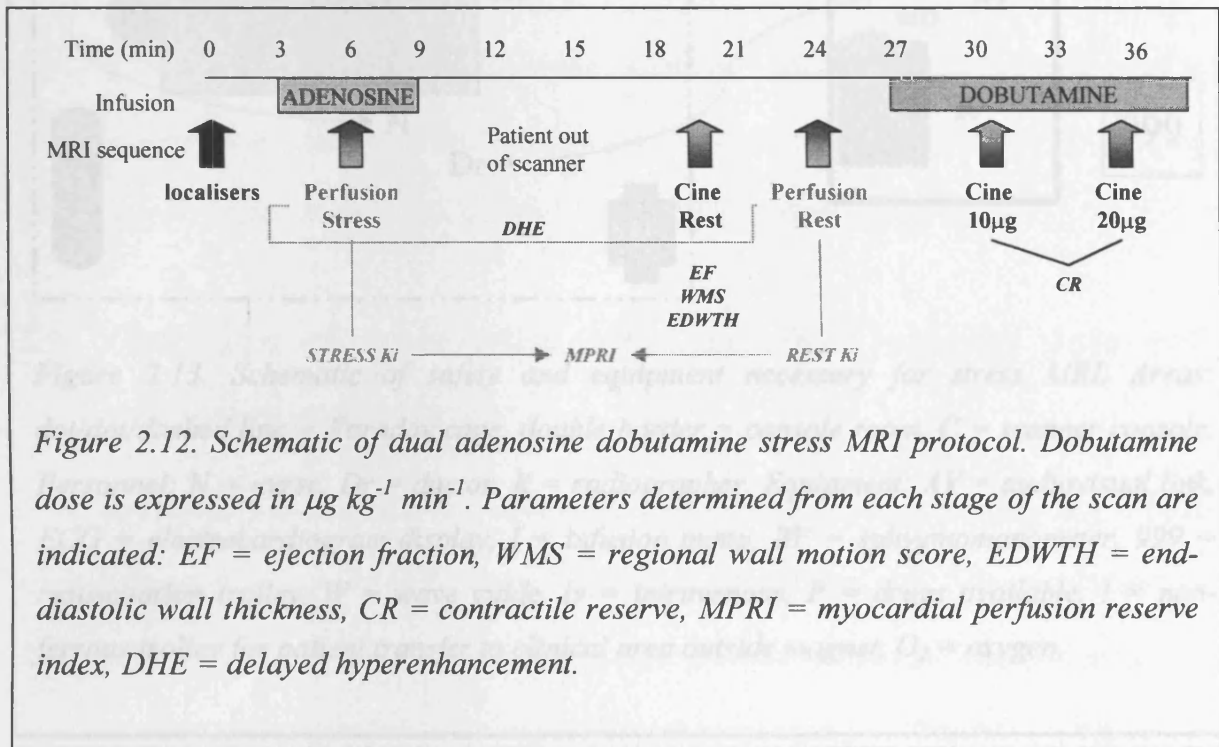


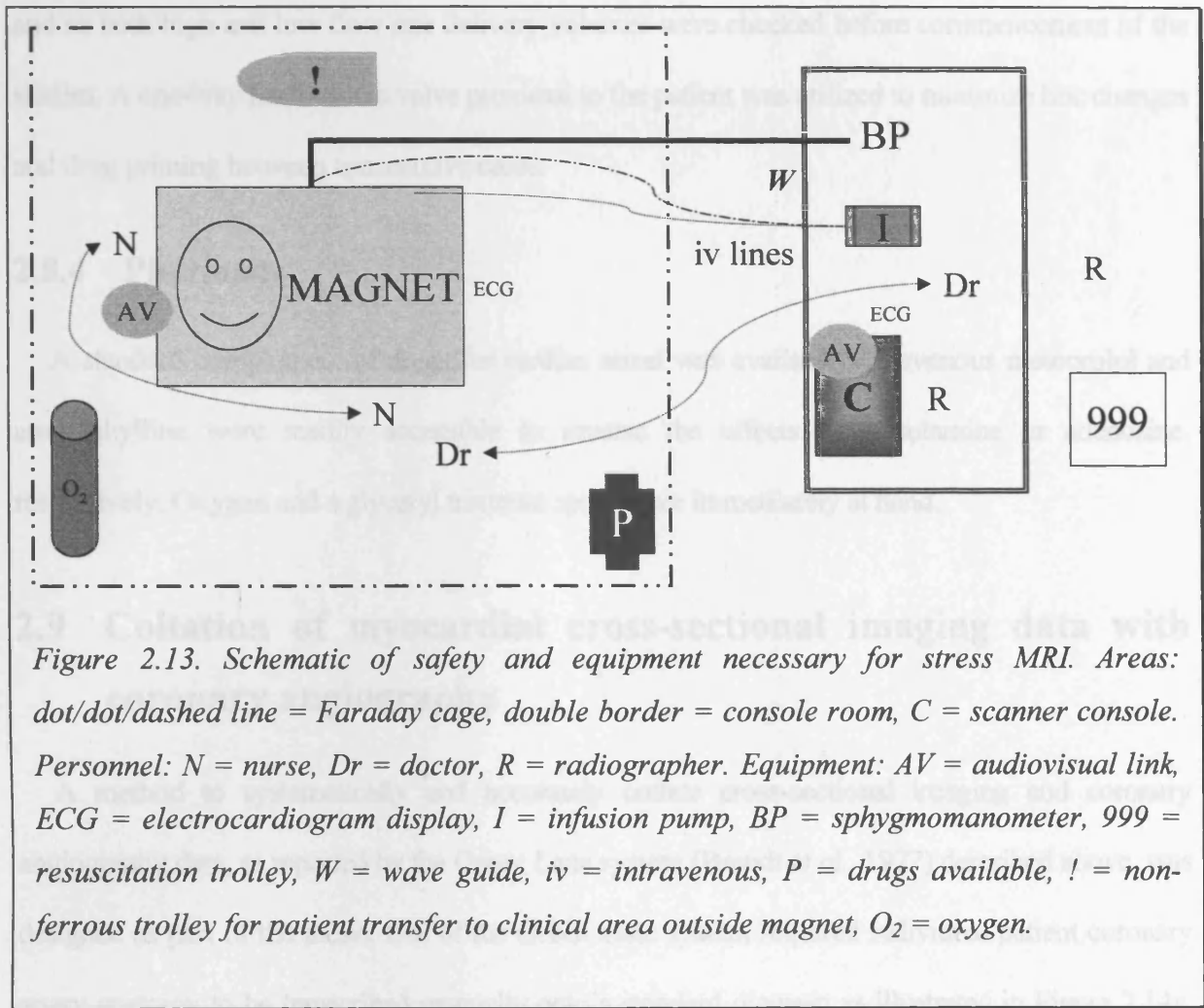
Figure 2.12. Schematic of dual adenosine dobutamine stress MRI protocol. Dobutamine dose is expressed in  $\mu\text{g kg}^{-1} \text{min}^{-1}$ . Parameters determined from each stage of the scan are indicated: EF = ejection fraction, WMS = regional wall motion score, EDWTH = end-diastolic wall thickness, CR = contractile reserve, MPRI = myocardial perfusion reserve index, DHE = delayed hyperenhancement.

## 2.8 Safety in the magnet

The majority of clinical studies conducted for this research necessitated recruitment of patients with severe coronary artery disease. Patient safety within the magnet was therefore a paramount concern.

### 2.8.1 Clinical supervision

All scans were medically supervised with the support of an experienced cardiac nurse. A minimum of two radiographers, trained in rapid extraction of the patient from the magnet and cardiopulmonary resuscitation, were present at all times. A clinical area containing resuscitation equipment immediately outside the Faraday cage was available should any adverse events arise. A direct audio-video link connected the patient and control console (Figure 2.13).



## 2.8.2 Electrocardiographic monitoring

A continuous trace of the patient's electrocardiogram (ECG) permitted monitoring of cardiac rate and rhythm during stressor administration. Within the environment of the imager, the ECG is subject to artifacts from a variety of sources rendering the ST segment non-diagnostic. Close clinical supervision and immediate on-line review of cine images were performed to monitor for development of ischaemia.

## 2.8.3 Monitoring / Infusion equipment

Blood pressure and oxygen saturation measurements were recorded during stressor administration. The sphygmomanometer and drug delivery system were incompatible with use within the Faraday cage and so the equipment was operated from the imager control room with tubing passing through the wave guide. This necessitated the use of long infusion lines (32 feet),

and so both high and low flow rate delivery volumes were checked before commencement of the studies. A one-way haemostatic valve proximal to the patient was utilized to minimize line changes and drug priming between consecutive cases.

#### **2.8.4 Pharmacy**

A standard complement of drugs for cardiac arrest was available. Intravenous metoprolol and aminophylline were readily accessible to reverse the effects of dobutamine or adenosine, respectively. Oxygen and a glyceryl trinitrate spray were immediately at hand.

### **2.9 Collation of myocardial cross-sectional imaging data with coronary angiography**

A method to systematically and accurately collate cross-sectional imaging and coronary angiography data, as reported by the Green Lane system (Brandt *et al.*, 1977) described above, was designed as part of the thesis. Use of the Green Lane system required individual patient coronary artery anatomy to be transcribed manually onto a standard diagram as illustrated in Figure 2.14a. The relative size and distribution of the vessels were reported precisely in order to accommodate anatomical variation, severity of all stenoses visualized and in addition, to incorporate an assessment of collateral flow.

MRI ROI (Figure 2.7) were transcribed onto a polar map (Figure 2.14b), with the outer ring representing the cardiac base, the middle ring, the mid-papillary plane and the inner ring the section just above the apex. The true apex is depicted at the map centre. The polar map was then overlaid with a Green Lane diagram (Figure 2.14b,c), modified to match the diagonal, obtuse marginal, inferior and septal territories with the anterior, lateral, inferior walls and septum, respectively, on the MRI data. The triangle representing the right ventricle is placed to the left of the schematic. Using the notation described by Brandt *et al.* (Brandt *et al.*, 1977), the coronary anatomy was drawn on to this diagram (Figure 2.14d). The MRI regions that each coronary artery supplies

become immediately apparent (Figure 2.14e). Three patients are presented in Figure 2.15 to illustrate use of this system.

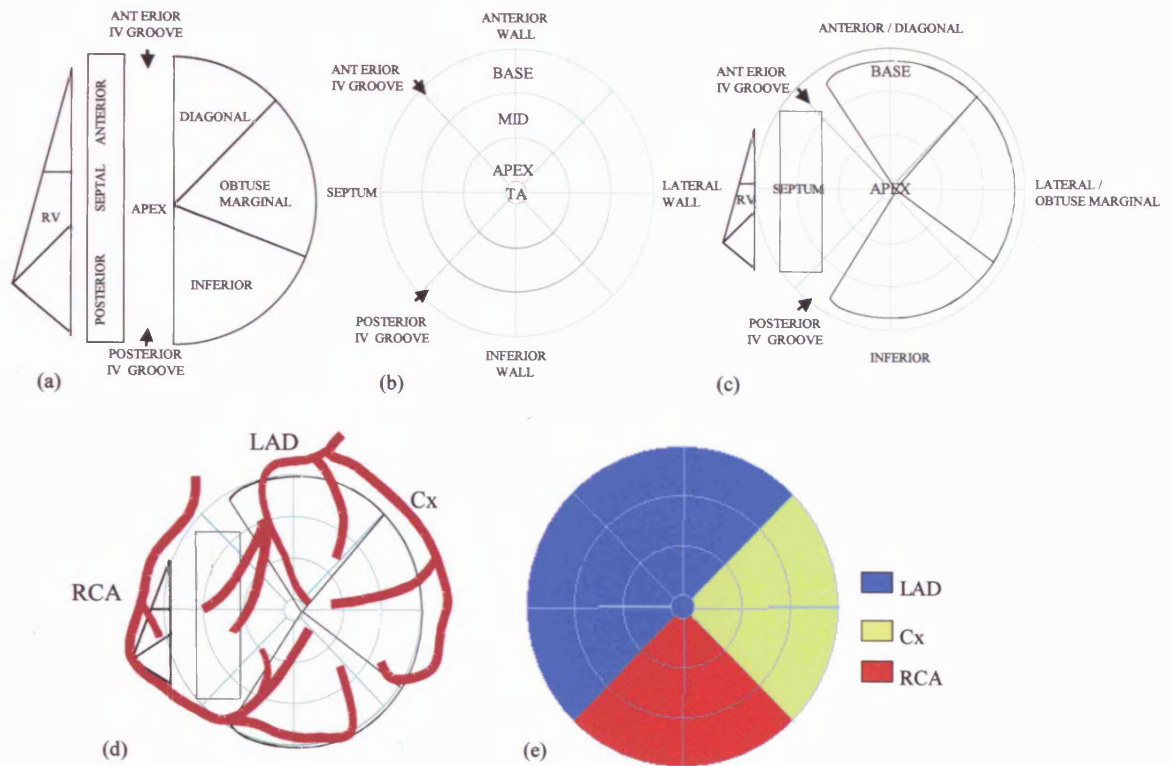


Figure 2.14. Schematic demonstrating collation of regional MRI and angiographic reporting systems. (a) A representation of the original Green Lane diagram. The semicircle represents the left ventricular free wall and is divided into diagonal, obtuse marginal and inferior coronary territories. These correspond to anterior, lateral and inferior walls seen on MRI. The septum is represented by an oblong, and the right ventricle (RV) is indicated by a small triangle. (b) Polar map illustration of MRI regions of interest (ROI). The outer concentric ring represents the cardiac base, the middle ring the mid-papillary short axis, and the inner ring the level just above the apex. The centre of the plot is the true apex (TA). The position of the anterior and posterior inter-ventricular grooves is indicated. (c) The MRI polar map is then overlaid with a Green Lane diagram modified to match the left ventricular free wall, septum and interventricular grooves. (d) The coronary artery anatomy is drawn on to the hybrid polar map. In this example, the left anterior descending artery meets the posterior descending artery at the cardiac apex. (e) The MRI ROI are then easily assigned to the appropriate vessel. LAD = left anterior descending artery; Cx = circumflex artery; RCA = right coronary artery.

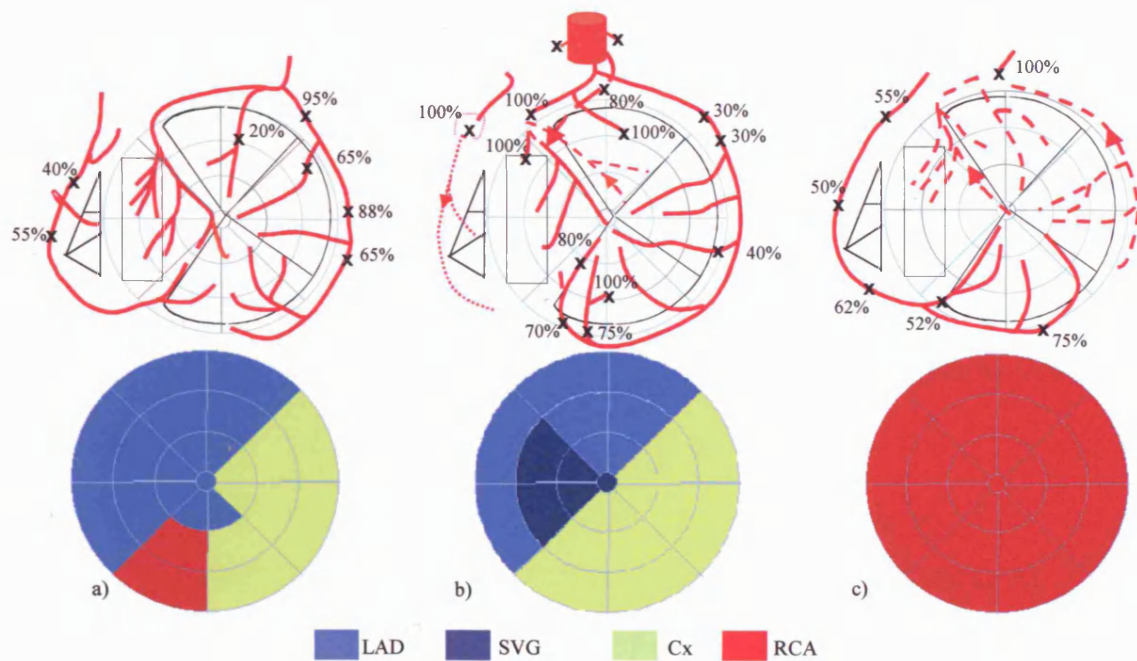


Figure 2.15. Clinical examples detailing angiographic anatomy in accordance with the Green Lane system onto hybrid polar maps (above) and the subsequent allocation of MRI regions of interest (ROI) to each major vessel (below). The coronary arteries with antegrade flow are transcribed onto the polar map as solid red lines. Retrograde flow is indicated by a dashed red line, and slow antegrade flow denoted by a dotted red line. Angiographic stenoses are denoted by an *x* and the % reduction in cross-sectional area. LAD = left anterior descending artery; SVG = saphenous vein graft; Cx = circumflex artery; RCA = right coronary artery.

a) A patient with blood supply to the inferior wall from all three major vessels; b) a patient with a very small RCA that does not reach the left ventricle, and also displaying a saphenous vein graft (arrow) to the mid LAD territory; c) a patient with an occluded left main stem but with the entire left coronary system filling retrogradely via collaterals from the RCA. For revascularization purposes, the coronary anatomy follows the same pattern as in the schematic in Figure 2.14.

---

## **Chapter 3**

### **Development of first pass contrast-enhanced MRI technique for quantification of myocardial perfusion**

---

## 3.1 Introduction

The determination of myocardial longitudinal relaxation rate ( $R_1$ ) is the first step towards perfusion quantification by MRI (Section 2.5.4). Improving accuracy of  $R_1$  calculation is therefore paramount for reliable estimation of blood flow. Two approaches are considered to achieve this: firstly, increasing the temporal resolution of image acquisition by using a constant repetition time ( $TR_0$ ) rather than gating to the electrocardiogram (ECG), and secondly, using low dose gadodiamide to ensure proportionality of contrast agent concentration to myocardial signal intensity. Finally, the ability to perform two scans, i.e. stress and rest during the same examination would improve clinical efficiency. These proposed changes to the existing perfusion protocol in Leicester (Cullen *et al.*, 1999b) are made possible because of the cardiac specifications of the Glenfield imager (Section 1.4).

### 3.1.1 Electrocardiographic gating

Typically, dynamic image acquisition is ECG-gated to mid or late diastole, which in subjects with normal resting heart rates occupies the latter 50% of the cardiac cycle. In principle, this should reduce motion artefact caused by cardiac movement (Hawkes *et al.*, 1981; Lanzer *et al.*, 1985). There are several disadvantages associated with ECG-gating. The insertion of a trigger delay into the imaging sequence increases image acquisition time, thus reducing the temporal resolution of the signal intensity time curve. When the change in myocardial  $R_1$  is being measured, the correction of the error due to magnetization saturation relies on a constant  $TR_0$  between acquisition of image slices. This correction can only be made effectively when the heart rate is constant (Jivan *et al.*, 1997).

Accurate ECG-gating requires repeated and precise recognition of the subject's R wave in order to trigger image acquisition consistently. The ECG trace within the environment of the magnetic resonance imager is subject to several artefacts that may cause erratic triggering. Such artefacts

include distortion from the switching magnetic field gradient, radiofrequency pulsing and patient movement (Roth *et al.*, 1985). ECG configurations such as low voltage R waves from previous myocardial infarction, high amplitude T waves, aberrant conduction patterns, and baseline ECG distortion from large vessel flow may also result in poor R wave recognition.

All subjects have a natural heart rate variability arising from normal variation in the balance of the autonomic nervous system. Heart rate variability varies with age and also in some disease states (Stein & Kleiger, 1999). There are little data in the literature describing the effect of vasodilator stressors on heart rate variability (Rongen *et al.*, 1999). However, adenosine and dipyridamole both induce a significant increase in heart rate (Reid *et al.*, 1990; Salustri *et al.*, 1992), and the trigger delay used to gate a two minute dynamic sequence at its initiation may be inaccurate towards the end of acquisition as the heart rate increases in response to the stressor. In addition, baseline arrhythmias, e.g. atrial fibrillation or ventricular ectopy, are common in patients with ischaemic heart disease. Varying intervals between successive R waves on the electrocardiogram will give rise to initial difficulty in choosing an appropriate trigger delay, leading to inconsistencies of scan placement within the cardiac cycle during the dynamic image run and inaccuracies in the calculation of  $R_1$ . Acquiring the images at a constant  $TR_0$ , i.e. non ECG-gated acquisition, could overcome some of these difficulties.

### **3.1.2 Gadodiamide bolus**

At clinical doses gadodiamide compounds create image contrast as a result of their  $T_1$  relaxation shortening properties, i.e. by reducing the time course of return of tissue longitudinal magnetization to equilibrium following a radiofrequency pulse application (Higgins *et al.*, 1993). Signal intensity is enhanced in areas of myocardium into which gadodiamide is delivered by blood flow. Where quantitative imaging is carried out, a dose of 0.02 – 0.025 mmol  $kg^{-1}$  is optimal. This ensures that measured changes in signal intensity are linearly proportional to changes in gadodiamide concentration within the myocardium (Strich *et al.*, 1985; Weinmann *et al.*, 1990; Manning *et al.*,

1991; Wilke *et al.*, 1993; Weinmann *et al.*, 1990). Above this concentration saturation effects occur and this relationship no longer applies. This is particularly important when signal intensity changes of the bolus within the left ventricle are used to normalize myocardial blood flow (Larsson *et al.*, 1994; Larsson *et al.*, 1996). Since gadodiamide concentration within the left ventricle is relatively high the linear relationship threshold may be breached and flow calculations compromised (Eichenberger *et al.*, 1994; Keijer *et al.*, 1995). With transfer of image acquisition to the higher performance scanner, it should be possible to utilize a lower gadodiamide dose in order to optimize quantification of myocardial perfusion without loss of image quality.

### **3.1.3 Single visit stress/rest imaging**

In order to calculate myocardial perfusion reserve, two contrast-enhanced dynamic MRI scans are required. One is required during pharmacological vasodilator stress, and the second during rest. Practically, it would be most economical to undergo these two scans during the same examination. Previously in Leicester, stress and rest imaging was performed 24 hours apart in order to allow gadodiamide to clear from the system before the second examination (Cullen *et al.*, 1999b). Since calculation of the extraction fraction of gadodiamide across the capillary membrane,  $K_i$ , is based on knowledge of the change in gadodiamide concentration within the myocardium over time rather than the actual concentration *per se* (Section 2.5.4), theoretically this time delay should not be required (Larsson *et al.*, 1994; Larsson *et al.*, 1996). Stress and rest perfusion imaging with MRI should be possible within a half-hour examination. As with any imaging modality prior to clinical application, repeatability and reproducibility of results should be determined.

## **3.2 Hypothesis**

Image acquisition without ECG-gating improves temporal resolution and is applicable to patients with arrhythmias and heart rate changes from stressors. Images acquired with a constant  $TR_0$  and with low dose contrast agent bolus are of sufficient quality for quantitative perfusion analysis. Calculation of  $K_i$  is not affected by the presence of residual gadodiamide from a low dose

bolus given earlier during the same examination. Calculated  $K_i$  values are repeatable at the same examination and reproducible between subject visits.

### 3.3 Objectives

The objectives of the work presented in this chapter are:

1. To examine the potential inaccuracies that arise from non ECG-gated stress and rest image acquisition and to compare these with those occurring with a typical ECG-gated protocol by:
  - a. measurement of sample R-R interval variability in patients at rest and during adenosine stress to determine the effects of adenosine and common arrhythmias on heart rate variability;
  - b. calculation of the temporal resolution and variability in the position within the cardiac cycle of image acquisition with (i) ECG-gating to diastole and (ii) image acquisition with a constant  $TR_0$  in patients with sinus rhythm and arrhythmias;
  - c. retrospective review of image data from a previous cohort of subjects with comparison of  $R_1$  values obtained from images acquired by (i) ECG-gating and (ii) with a constant  $TR_0$  with values obtained using multiple inversion time (TI) inversion-recovery (IR) snapshot FLASH imaging.
2. To conduct a first pass contrast-enhanced study in volunteers with use of a non ECG-gated technique and low dose gadodiamide bolus to:
  - a. determine whether image quality and bolus delivery are acceptable for quantitative analysis;
  - b. to establish the change in myocardial background  $R_1$  values for different imaging time delays after the first contrast agent bolus;
  - c. to determine repeatability and reproducibility of  $K_i$  values.

## 3.4 Methods

### 3.4.1 ECG gating

#### 3.4.1.1 Measurement of R-R interval variability

Four consecutive patients in sinus rhythm attending for adenosine stress scintigraphy were studied. Mean age was 59 years (range 45 - 73 years). A Holter monitor was used to record the patient's ECG (lead V<sub>1</sub>) continuously for 3 minutes at rest and for the duration of a 6 minute adenosine infusion (140 µg kg<sup>-1</sup> min<sup>-1</sup>). Two anonymous 4 minute continuous ambulatory ECG recordings at rest from patients with atrial fibrillation and multiple ventricular ectopy, respectively, were added to the study data. The intervals between successive R waves of the QRS complex were measured by ECG sampling using the software package Pathfinder 700 (Reynolds, Hertfordshire, U.K.). Any transient arrhythmias such as ectopic beats were included. ECG recordings and R-R interval measurements were filtered by hand and errors made by the software, e.g. misreading high amplitude T waves as R waves, thus recording the R-T and T-R interval as 2 R-R intervals, were corrected (R-R interval = R-T + T-R). This occurred with frequency in one patient, and the original data set was kept as "errored" data set (Figure 3.1).

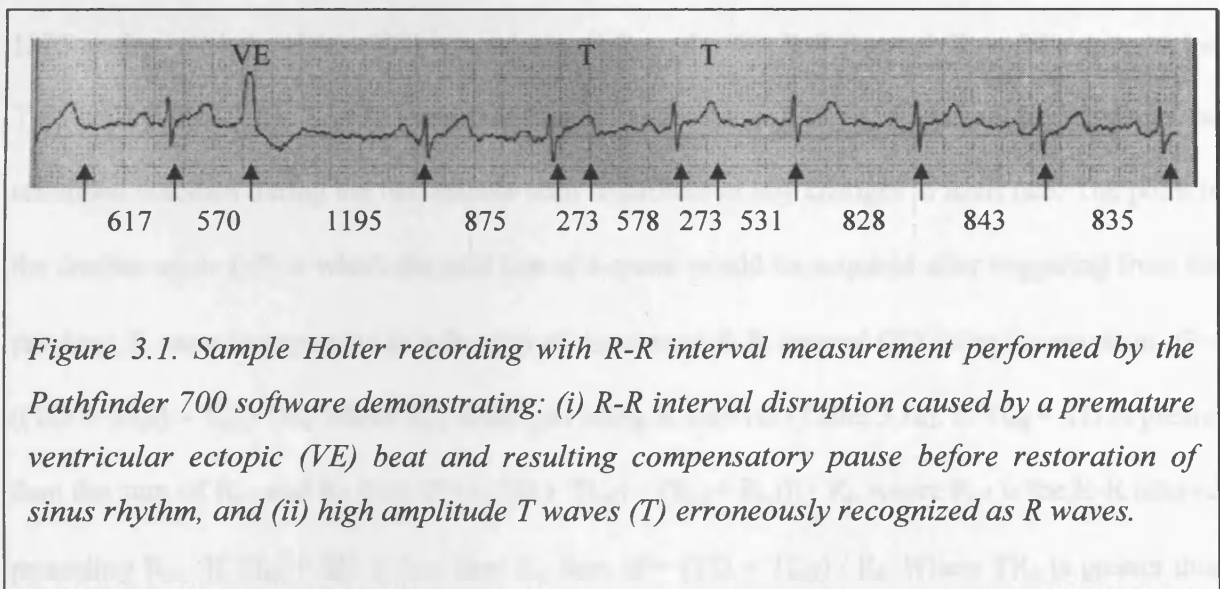


*Figure 3.1. Sample Holter recording with R-R interval measurement performed by the Pathfinder 700 software demonstrating: (i) R-R interval disruption caused by a premature ventricular ectopic (VE) beat and resulting compensatory pause before restoration of sinus rhythm, and (ii) high amplitude T waves (T) erroneously recognized as R waves.*

The mean  $\pm$  standard deviation (SD) R-R intervals at rest, during the total adenosine infusion, and for the first three minutes and latter 3 minutes of the adenosine infusion were calculated.

### 3.4.1.2 Calculation of image position within the cardiac cycle ( $\Phi$ )

The point of the cardiac cycle ( $\Phi$ ) at which the mid line of  $k$ -space is acquired for each image during a 2 minute single slice  $T_1$ -weighted IR-snapshot FLASH sequence was calculated both for ECG-gated image acquisition and for images acquired with a constant  $TR_0$ . Two minutes of resting R-R interval data were used from 2 patients in sinus rhythm, i.e. those with the lowest and highest R-R interval variation, the “errored” data set and the R-R interval values from the patients with atrial fibrillation and multiple ventricular ectopy. The number of images that would be acquired over each two-minute period was counted in order to compare the temporal resolution for both ECG-gated and non ECG-gated techniques. Parameters of the IR-snapshot FLASH sequence on the *Vision*<sup>TM</sup> imager were used for this computation (Table 2.3). Schematics of the sequences are illustrated (Figure 3.2).

The time to acquire 96 lines of  $k$ -space and complete image acquisition (IA) is 432 ms ( $n_k \times TR$ ). This is followed by a dead time, required for data transfer and storage (specific to the sequence and imager) of approximately 348 ms ( $c$ ) before further images can be acquired. For ECG-gating, a trigger delay (TD) was calculated from the first R-R interval ( $R_0$ ) of the data set, i.e.  $TD = (1.3 * R_0) - TI_{\text{eff}}$ . This TD was calculated to place the mid-line of  $k$ -space in mid-diastole and remained constant during the two-minute scan regardless of any changes in heart rate. The point in the cardiac cycle ( $\Phi$ ) at which the mid line of  $k$ -space would be acquired after triggering from the previous R wave is expressed as a fraction of the current R-R interval ( $R_t$ ) using the equation:  $\Phi = ((TD + TI_{\text{eff}}) - R_{t-1}) / R_t$ , where  $R_{t-1}$  is the preceding R interval (Table 3.1a). If  $TI_{\text{eff}} + TD$  is greater than the sum of  $R_{t-1}$  and  $R_t$ , then  $\Phi = ((TD + TI_{\text{eff}}) - (R_{t-1} + R_{t-2})) / R_t$ , where  $R_{t-2}$  is the R-R interval preceding  $R_{t-1}$ . If  $TI_{\text{eff}} + TD$  is less than  $R_t$ , then  $\Phi = (TD + TI_{\text{eff}}) / R_t$ . Where  $TR_0$  is greater than

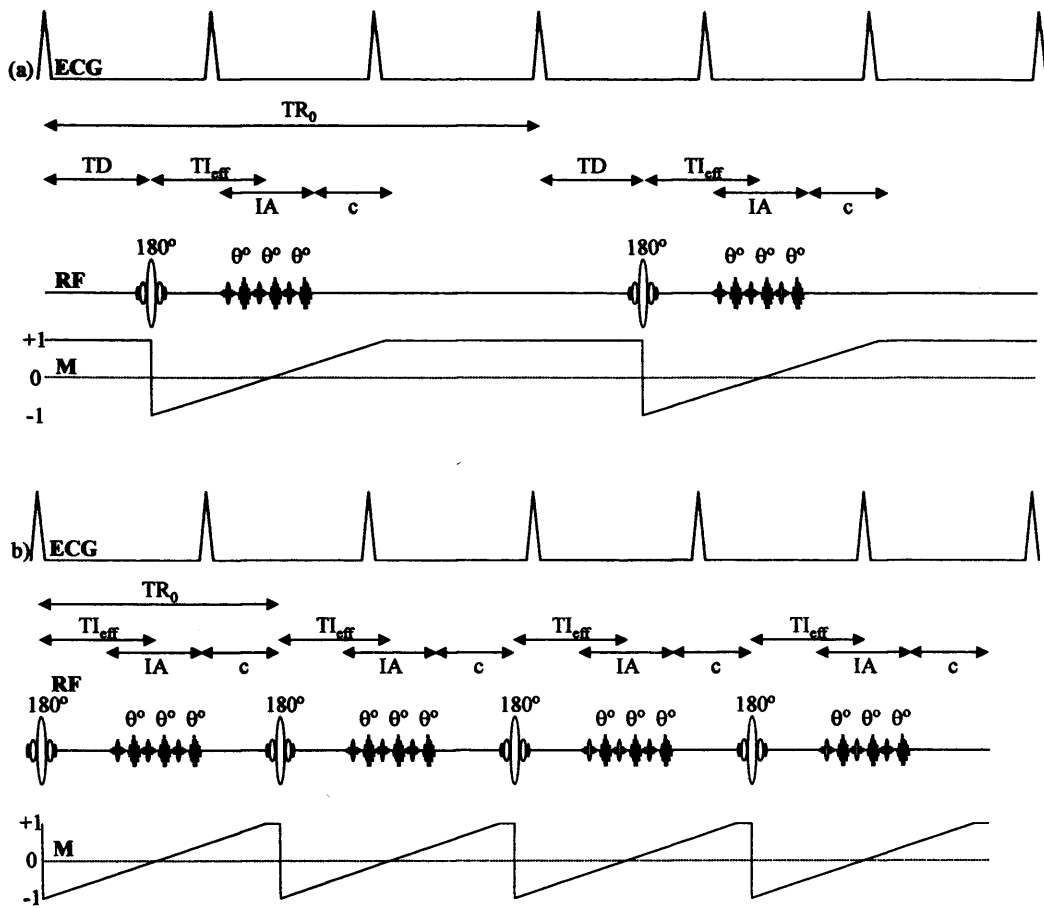


Figure 3.2. Inversion recovery-snapshot FLASH sequence showing: (a) ECG-gated and (b) non ECG-gated image acquisition schematics. For simplicity the electrocardiogram (ECG) shows R waves only. The duration of each component of the sequence has been calculated for a constant R-R interval of 750 ms.  $TR_0$  = total repetition time (1080 ms);  $TD$  = trigger delay (calculated, see text);  $Tl_{eff}$  = time from inversion pulse to mid-line of k-space;  $IA$  = image acquisition time (432 ms);  $c$  = dead time (348 ms);  $RF$  = radiofrequency pulse;  $180^\circ$  = onset of inversion pulse;  $\theta^\circ$  = low flip angle pulses;  $M$  = magnetization.

$(R_{t-1} + R_t)$ , then triggering for the next measure will occur on the next available R wave ( $R_{t+1}$ ).  $TR_0 = (TD + Tl_{eff} + (IA / 2) + c)$ .

For non ECG-gated images the time interval prior to image acquisition is constant ( $TR_0 = Tl_{eff} + IA / 2 + c = 1080$  ms). A cumulative summation list of R-R intervals and image acquisition times was made (Table 3.1b). For each image time, where  $Tl_{i(cum)}$  is greater than  $R_{t-1(cum)}$ , the time within

the cardiac cycle is calculated for each image acquisition:  $(T_{i(cum)} - R_{t-1(cum)}) / R_t$ , where  $T_{i(cum)}$  is the sum of the preceding image acquisition times, and  $R_{t-1(cum)}$  is the sum of preceding R-R intervals. Where  $T_{i(cum)}$  is less than  $R_{t-1(cum)}$ , then the R-R interval is skipped.

(a) ECG-gated			(b) Non ECG-gated			
R-R (ms)	TD (ms)	$\Phi$	R-R (ms)	R-R <sub>cum</sub> (ms)	T <sub>i(cum)</sub> (ms)	$\Phi$
992			992	992	0	
929	774	0.32	929	1921	1080	0.09
945			945	2866	2160	0.25
914	774	0.38	914	3780	3240	0.41
945			945	4725	4320	0.57
960	774	0.36	960	5685	5400	0.70
968			968	6653	6480	0.82
945	774	0.34	945	7598	7560	0.96

Table 3.1. Calculation of the position in the cardiac cycle ( $\Phi$ ) that the mid line of k-space is acquired for sample R-R interval data for (a) ECG-gated and (b) non ECG-gated methods. R-R = list of consecutive R-R intervals; TD = trigger delay; R-R<sub>cum</sub> = cumulation of R-R intervals; T<sub>i(cum)</sub> = cumulation of imaging times.

### 3.4.1.3 Magnetic resonance imaging: Comparison of R<sub>1</sub> values obtained from gated and non ECG-gated image acquisition

Image data, previously acquired with the 1.0 Tesla *Magnetom*<sup>TM</sup> imager from five healthy volunteers (mean age 29 years, four males, one female) were kindly made available by the radiology department. Patients had been imaged three times with eleven measures first with ECG gating, i.e. with the incorporation of a TD, calculated as above, to obtain an image approximately every two R-R intervals and then with a constant TR<sub>0</sub> to acquire an image every 1080 ms. Finally, ECG-gated images had been obtained with the inversion time altered from 1.93 s to 0.15 s in thirteen steps with full relaxation allowed between each image acquisition (Haase, 1990; Jivan *et*

*al.*, 1997). A proton density image after full longitudinal relaxation was acquired prior to each application of the sequence to enable calculation of  $R_1$ .

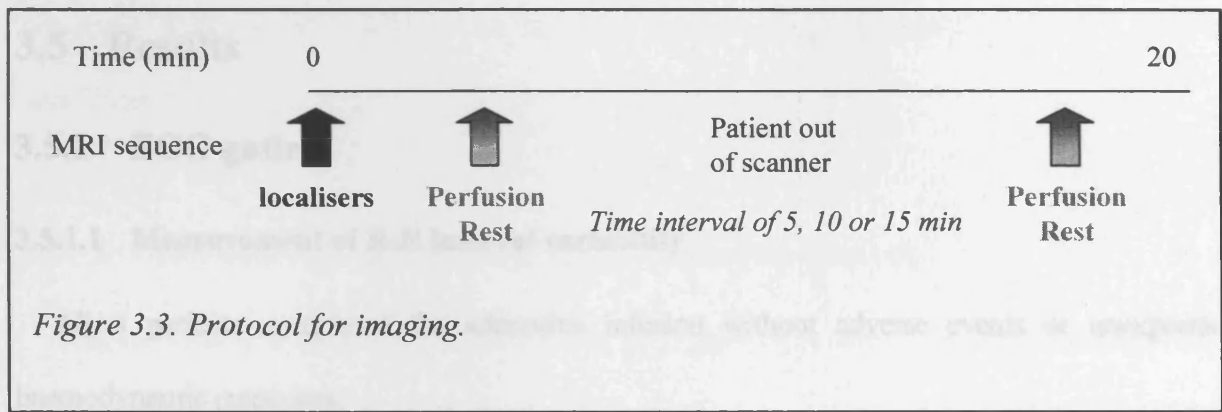
#### **3.4.1.4 Statistics**

A paired Student's  $t$  test was used for the haemodynamic data and to evaluate the  $R_1$  measurement agreements. The mean and standard deviation were calculated for all sets of R-R interval data, and an  $F$  test for two-sample variance was used to evaluate differences in variance. The  $F$  test was also used to compare the ECG-gated and non ECG-gated values of  $\Phi$ . The  $R_1$  values obtained from ECG-gated and non ECG-gated imaging for each ROI were compared with the  $R_1$  measurements obtained with the “gold standard” multiple inversion pulse imaging using the Bland-Altman test of agreement (Bland & Altman, 1986). All data are presented as mean  $\pm$  standard deviation.

### **3.4.2 Volunteer $K_1$ study**

#### **3.4.2.1 Study design**

Five healthy volunteers from the cardiac catheter laboratory staff were recruited for the study by poster advertisement. All volunteers were low risk for presence of coronary artery disease, i.e. they had no history of hypertension, hypercholesterolaemia, or diabetes. All were lifelong non-smokers and had normal 12-lead electrocardiogram. First pass contrast-enhanced MRI (1.5 Tesla *Vision*<sup>TM</sup>, Section 2.5.1) was performed at rest on three separate days, with single slice image acquisition at the mid-papillary level. A low dose gadodiamide bolus was used (0.025 mmol kg<sup>-1</sup>). On each occasion, imaging was repeated with a differing time interval between the two imaging sequences i.e. 5, 10 and 15 minutes, respectively (Figure 3.3). The study had to be conducted outside normal working hours and so scans were conducted either at approximately 8 a.m. or 6 p.m..



### 3.4.2.2 Magnetic resonance image analysis

Images were assessed for diagnostic acceptability and adequacy of bolus delivery. The potential presence of signal intensity saturation was investigated by comparing the peak signal intensity in the right and left ventricular cavities, respectively. Signal and contrast to noise ratios were calculated (Section 2.5.4.6). Increase in baseline  $R_1$  following the first gadodiamide bolus prior to the second dynamic sequence was noted. The unidirectional transport coefficient for gadodiamide over the capillary membrane,  $K_i$ , was calculated for each ROI (Section 2.5.4). Correction for the extraction fraction of gadodiamide over the capillary membrane,  $E$ , was applied.

### 3.4.2.3 Statistics

Unpaired Student's  $t$  tests were used to compare peak right and left ventricular signal intensities and diurnal variation of  $K_i$  values. Paired Student's  $t$  tests were used to compare background signal intensities and calculated  $K_i$  values for each visit. Analysis of variance was used to compare these parameters between visits. Consistency of  $K_i$  values between the first and second scans, and between the initial scans from each of the three visits, was also examined by Bland Altman plots (Bland & Altman, 1986).

## 3.5 Results

### 3.5.1 ECG gating

#### 3.5.1.1 Measurement of R-R interval variability

All 4 patients completed the adenosine infusion without adverse events or unexpected haemodynamic responses.

a) R-R interval (ms)			b) Variance comparison		
Data set	n	mean $\pm$ SD	Data sets	F	p
Rest	844	834 $\pm$ 122	Rest; AD1	1.41	< 0.001
AD1	897	721 $\pm$ 103	Rest; AD2	1.74	< 0.001
AD2	1006	672 $\pm$ 93	Rest; AD	1.47	< 0.001
AD	1903	695 $\pm$ 101	AD1; AD2	1.23	< 0.001
AF	363	609 $\pm$ 145	AF; rest	1.41	< 0.001
VE	259	820 $\pm$ 267	VE; rest	4.75	< 0.001

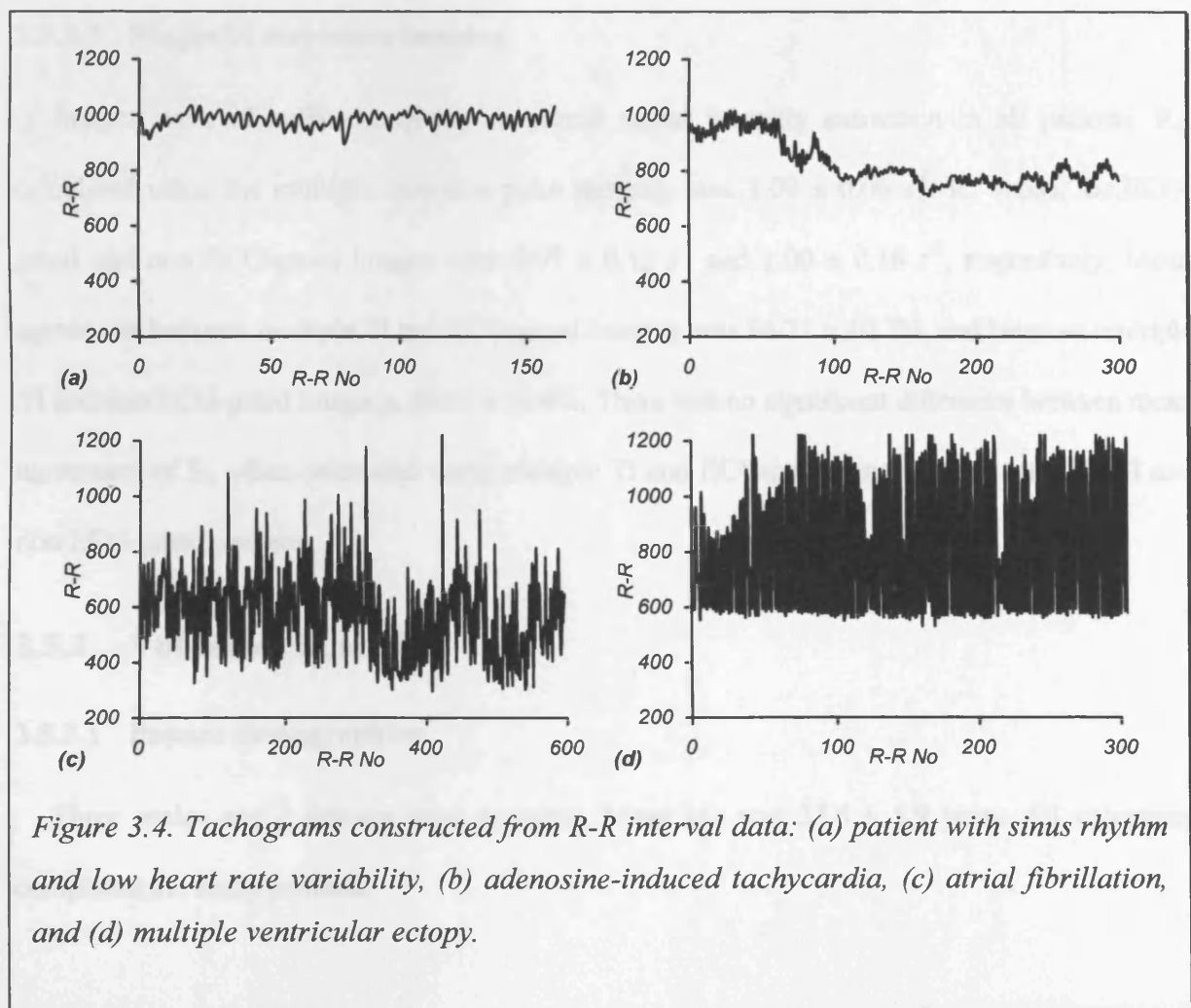
*Table 3.2. a) R-R interval data at rest, during the first half (AD1), second half (AD2) and total length (AD) of the adenosine infusion, and from the patients with atrial fibrillation (AF) and ventricular ectopy (VE). n = the number of data points for each rhythm strip. b) The F test data for comparisons between specified data sets are shown where p represents statistical significance of the test.*

The R-R interval data from rest and adenosine stress, together with comparison of variance are shown in Table 3.2. There was significantly greater variance of the R-R interval data at rest than with either the first three minutes, second three minutes or all six minutes of the adenosine infusion ( $p < 0.001$  in all cases). There was also greater R-R interval variance observed in the first half of the adenosine infusion than in the second half ( $p < 0.001$ ). In the two patients with arrhythmia, i.e. atrial fibrillation and multiple ventricular ectopy, there was a much greater variance in the duration of successive R-R intervals than in the patients with resting sinus rhythm ( $p < 0.001$  in both

instances). This variance can be appreciated from tachograms constructed from the R-R interval data (Figure 3.4).

### 3.5.1.2 Calculation of image position within the cardiac cycle ( $\Phi$ )

The results from the 2-minute sections of the ECG recordings used for hypothetical calculation of  $\Phi$  for comparison of ECG-gated and non ECG-gated image acquisition are shown in Table 3.3. When the difference in variance between ECG-gated and non ECG-gated data are examined, there is only a significant difference in patient 1 ( $p < 0.001$ ). There is no significant difference in the variance in image acquisition position in the cardiac cycle between the ECG-gated and non ECG-gated protocol in any of the other examples presented.



Data Set	ECG-gated			Non ECG-gated		Gating v non-gating
	n	R-R (ms)	$\Phi$	n	$\Phi$	p
Pt 1 rest	53	982 ± 27	0.31 ± 0.03	97	0.51 ± 0.29	< 0.001
Pt 4 rest	44	828 ± 176	0.58 ± 0.23	104	0.50 ± 0.28	ns
Errored	65	575 ± 250	0.55 ± 0.30	103	0.48 ± 0.28	ns
AF	65	626 ± 124	0.38 ± 0.31	96	0.52 ± 0.29	ns
VE	65	806 ± 245	0.40 ± 0.26	102	0.52 ± 0.29	ns

*Table 3.3. F test data for variance of image placement in the cardiac cycle ( $\Phi$ ) and temporal resolution of image acquisition with and without ECG-gating in patients with low R-R interval variability (Pt 1 rest), high variability (Pt 4 rest), the errored data set, and the arrhythmias, i.e. atrial fibrillation (AF) and ventricular ectopy (VE). Values for R-R and  $\Phi$  are mean ± SD; n = the number of image acquisitions within the time period; p = statistical significance.*

### 3.5.1.3 Magnetic resonance imaging

Images were of sufficient quality to permit signal intensity extraction in all patients.  $R_1$ , calculated using the multiple inversion pulse imaging, was  $1.09 \pm 0.06 \text{ s}^{-1}$ .  $R_1$  values for ECG-gated and non ECG-gated images were  $0.97 \pm 0.13 \text{ s}^{-1}$  and  $1.00 \pm 0.16 \text{ s}^{-1}$ , respectively. Mean agreement between multiple TI and ECG-gated imaging was  $86.71 \pm 10.7\%$ , and between multiple TI and non ECG-gated imaging,  $86.03 \pm 10.4\%$ . There was no significant difference between mean agreement of  $R_1$  when calculated using multiple TI and ECG-gated imaging and multiple TI and non ECG-gated imaging.

## 3.5.2 Volunteer $K_i$ study

### 3.5.2.1 Patient demographics

Three males and 2 females were recruited. Mean age was  $33.6 \pm 5.9$  years. All volunteers completed the study protocol.



*Figure 3.5. First pass contrast-enhanced MRI sequence from normal volunteer. Images were acquired with a constant total repetition time. Note myocardial enhancement in final image.*

### 3.5.2.2 Image quality

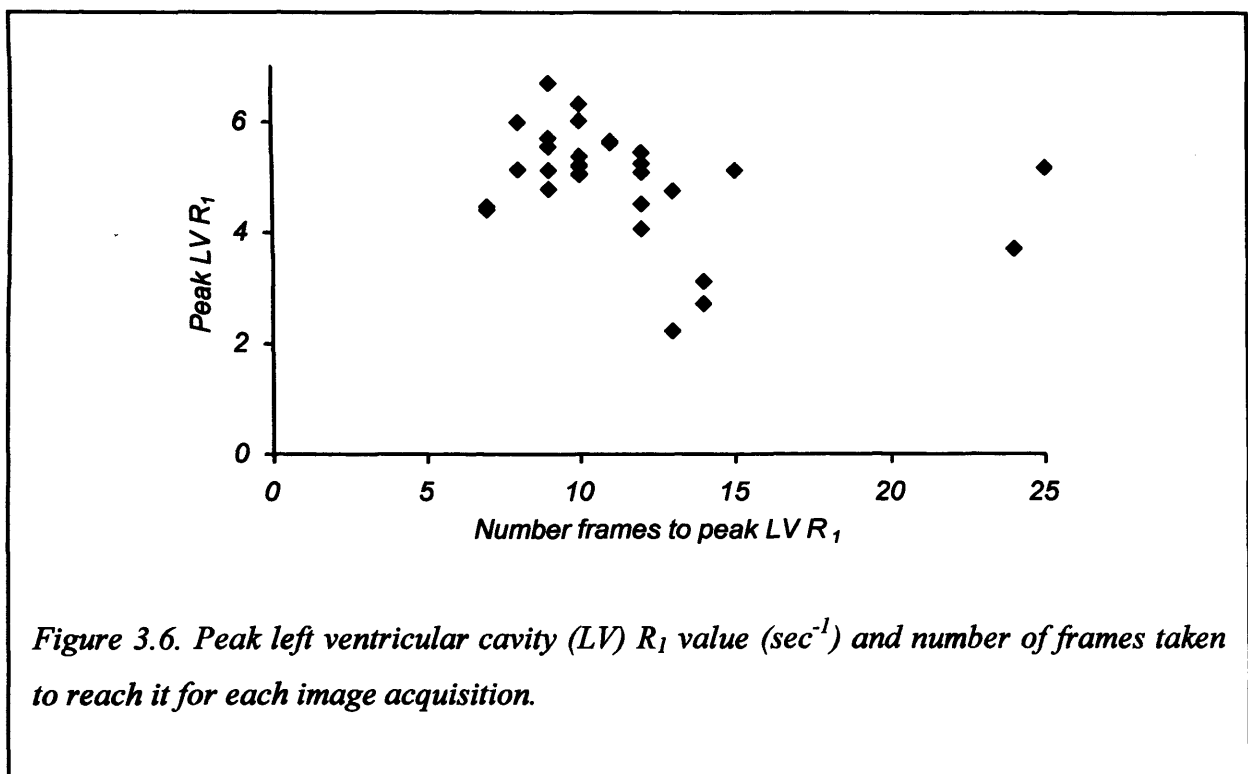
Image quality was adequate (Figure 3.5) except those where bolus delivery was poor (see below).

#### 3.5.2.2.1 Bolus delivery

The peak bolus  $R_1$  value achieved within the left ventricular cavity was  $4.96 \pm 0.99 \text{ sec}^{-1}$ . The number of image frames taken to reach the peak  $R_1$  value was  $11.6 \pm 4.1$ . The variation in bolus quality is depicted in Figure 3.6. An effective bolus (Figure 3.7a) was delivered in 28/30 image acquisitions. In the remaining 2, gadodiamide was very slow to reach the left ventricular cavity, only reaching a peak  $R_1$  value towards the end of the image run (Figure 3.7b). These were therefore excluded from quantitative analysis.

#### 3.5.2.2.2 Signal and contrast to noise ratio

Peak right ventricular signal intensity was higher than peak left ventricular signal intensity in all studies, i.e.  $116.2 \pm 22.2$  vs.  $94.8 \pm 24.1$  arbitrary units (a.u.),  $p < 0.001$ .



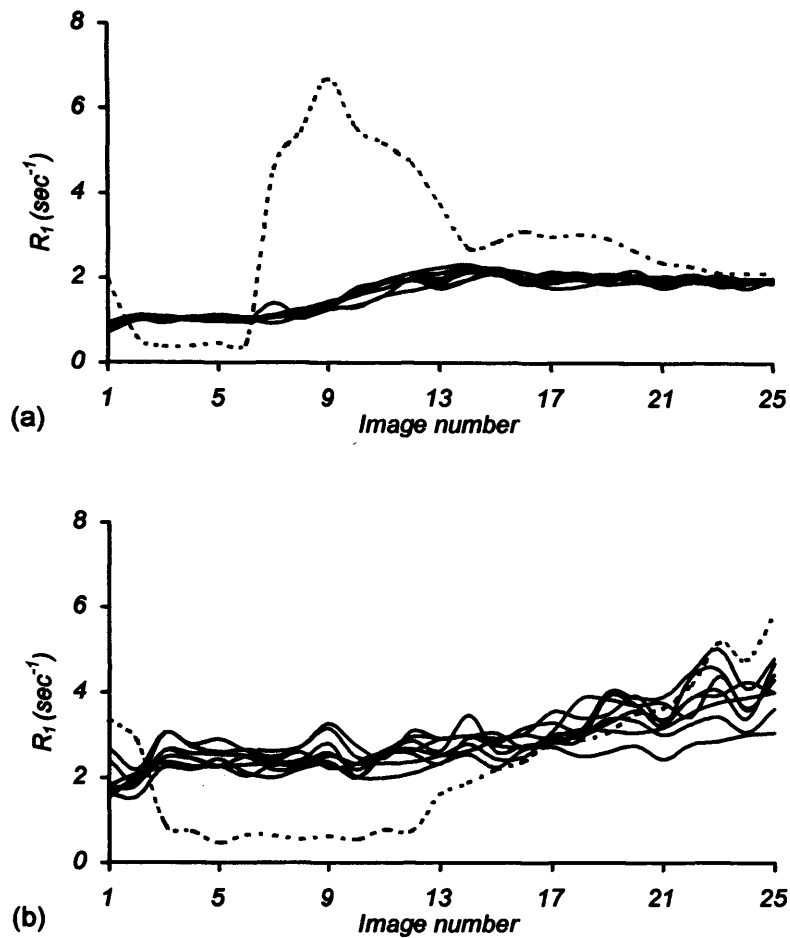


*Figure 3.7. Relaxation rate time ( $R_1$ ) curves for input (dotted line) and regional myocardial tissue (solid lines) demonstrating adequate (a) and poor (b) bolus delivery of gadodiamide to the left ventricle.*

Mean study contribution of noise to signal intensity was  $4.92 \pm 0.67$  a.u.. Baseline myocardial signal to noise ratio was  $4.74 \pm 1.41$ . Myocardial contrast to noise ratio for all studies was  $7.27 \pm 2.05$ . Contrast to noise ratio within the left ventricular cavity was  $15.02 \pm 4.82$ .

### **3.5.2.2.3 Baseline $R_1$ values**

Baseline  $R_1$  values prior to the first and second contrast agent boluses are shown in Table 3.4. In each case, the baseline  $R_1$  value prior to the second scan was greater than that prior to the initial gadodiamide bolus ( $p < 0.001$  for all time intervals). A trend towards a lower percent increase in the myocardial baseline  $R_1$  before the second scan with lengthening of the interscan time interval

was seen (Table 3.4). The percent increase was significantly greater when only 5 minutes separated the two scans compared with either a 10 or 15 minute time delay between image acquisitions ( $p < 0.001$ ). Percent increase in baseline  $R_1$  after a 10 or 15 minute delay was similar.

Time delay between image acquisitions	Baseline $R_1$ pre-gadodiamide	Baseline $R_1$ pre-second scan	% increase
5	$1.02 \pm 0.06$	$1.47 \pm 0.05^\ddagger$	$31.0 \pm 4.8^\ddagger$
10	$1.06 \pm 0.06$	$1.38 \pm 0.08^\ddagger$	$23.0 \pm 5.8$
15	$1.05 \pm 0.05$	$1.33 \pm 0.06^\ddagger$	$20.7 \pm 5.1$

*Table 3.4. Comparison of mean  $\pm$  SD baseline  $R_1$  values prior to first and second resting scans, respectively for each visit ( $^\ddagger p < 0.001$ ), and the percentage increase in second baseline  $R_1$  compared with initial measurement ( $^\ddagger p < 0.001$ , compared with percentage increase after both 10 and 15 minute time delays).*

### 3.5.2.3 Quantitative analysis

$K_i$  values could be computed in 213/ 240 (88%) ROI owing to the two incidences of suboptimal bolus delivery. In the remaining 11 ROI,  $K_i$  could not be calculated because the deconvolution algorithm could not resolve input and tissue functions.

Overall,  $K_i$  values for all the baseline scan and second acquisitions were similar, i.e.  $37.6 \pm 11.3$  and  $35.5 \pm 10.4$  ml  $100g^{-1}$  min $^{-1}$ , respectively. For each visit,  $K_i$  values for the second scan were unchanged from baseline, regardless of the time interval between the two scans (Table 3.5). A Bland Altman scatter plot is presented for combined data from all three visits (Figure 3.8). Mean difference was  $2.2 \pm 9.5$  ml  $100g^{-1}$  min $^{-1}$ . The coefficient of repeatability was 52%.

Figure 3.9 contains the Bland-Altman scatter plots for the initial scans on each of the 3 examinations. Mean differences were 3, 5.3 and 10.5 ml  $100g^{-1}$  min $^{-1}$  and coefficients of reproducibility were 81%, 74% and 76% respectively for the 3 graphs presented.

When baseline  $K_i$  values were compared,  $K_i$  was lower at the second visit (10 minute interscan interval) than on the remaining occasions ( $p < 0.001$ , Table 3.5). No difference in  $K_i$  values were

seen between early morning and evening i.e.  $35.0 \pm 7.2$  and  $37.3 \pm 12.2$  ml  $100\text{g}^{-1} \text{min}^{-1}$ , respectively.

Given the variation in the baseline scan  $K_i$  values, it was not possible to compare the three second scan acquisitions directly to assess the affect of time interval on the parameter.

Time delay between image acquisitions	$K_i$		F	
	1 <sup>st</sup> acquisition	2 <sup>nd</sup> acquisition	1 <sup>st</sup> acquisition	2 <sup>nd</sup> acquisition
5	$39.8 \pm 10.1$	$37.6 \pm 11.3$	$63.7 \pm 36.9$	$58.2 \pm 37.5$
10	$33.0 \pm 7.9^\ddagger$	$31.2 \pm 7.7$	$62.7 \pm 21.2$	$49.9 \pm 28.7$
15	$41.2 \pm 14.2$	$39.6 \pm 17.2$	$82.3 \pm 28.4$	$73.0 \pm 24.4$

Table 3.5.  $K_i$  (ml  $100\text{g}^{-1} \text{min}^{-1}$ ) values obtained at baseline and at 5, 10 and 15 minutes after 1<sup>st</sup> acquisition  $K_i$  values are corrected for extraction fraction to give estimates of myocardial flow (F, ml  $100\text{g}^{-1} \text{min}^{-1}$ ).  $^\ddagger p < 0.001$ , compared with initial  $K_i$  values from scans on the other two visits.

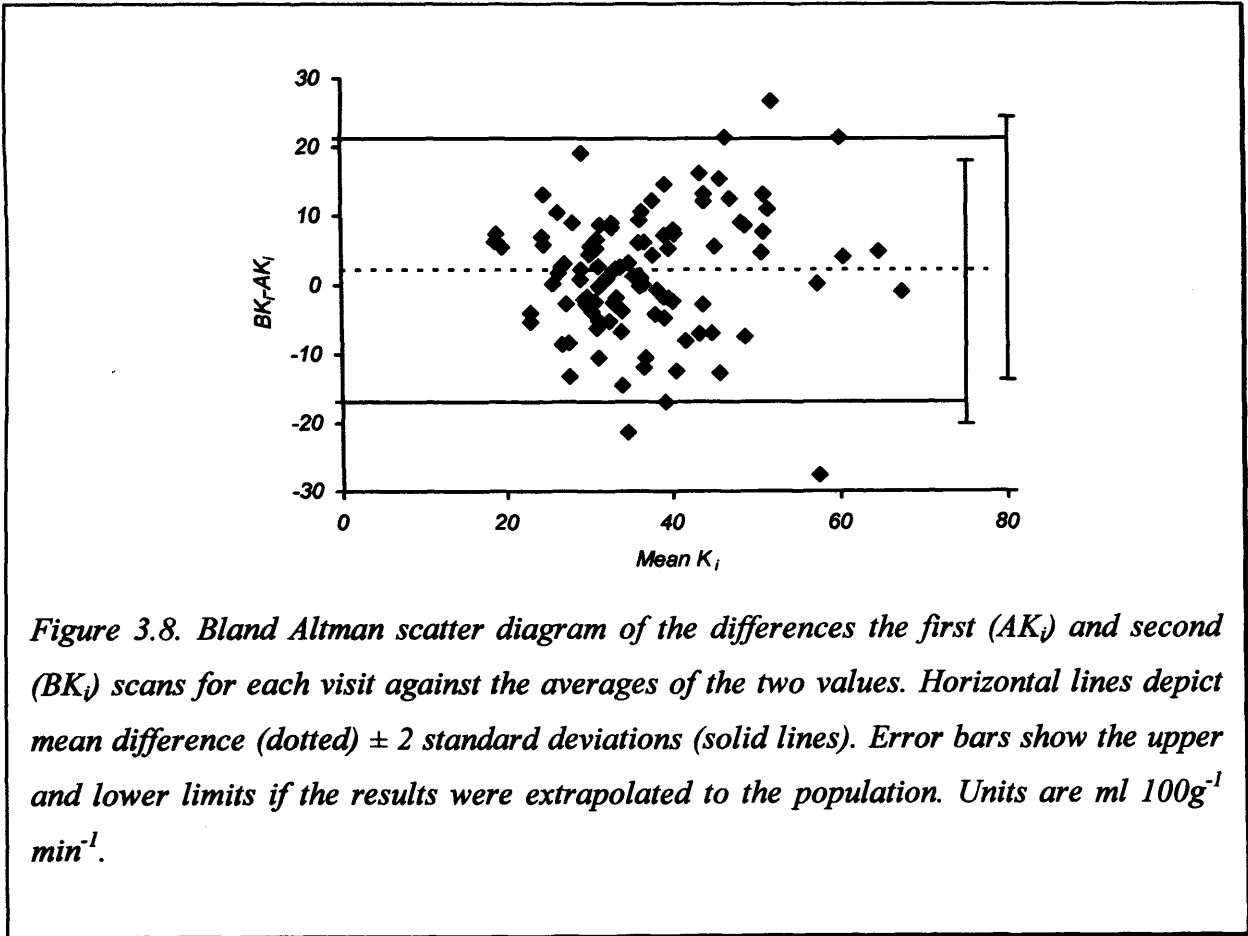
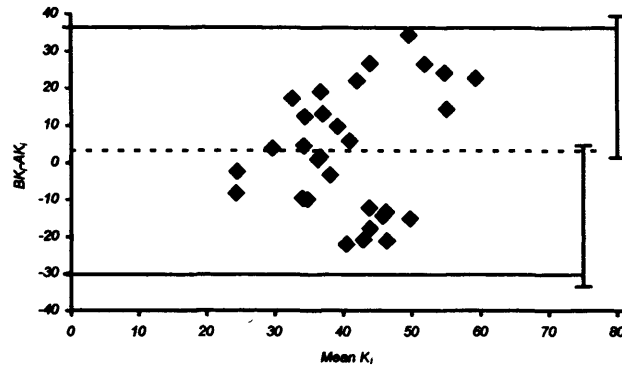
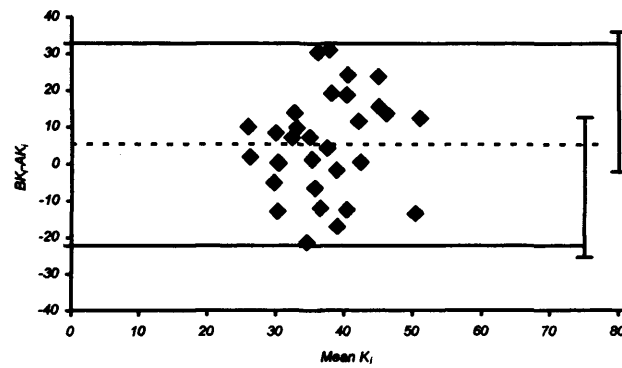


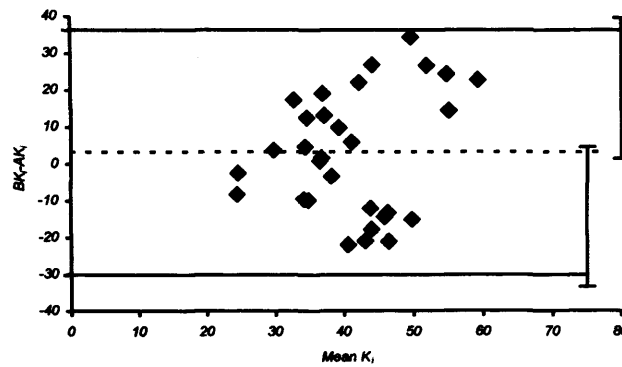
Figure 3.8. Bland Altman scatter diagram of the differences the first ( $AK_i$ ) and second ( $BK_i$ ) scans for each visit against the averages of the two values. Horizontal lines depict mean difference (dotted)  $\pm 2$  standard deviations (solid lines). Error bars show the upper and lower limits if the results were extrapolated to the population. Units are ml  $100\text{g}^{-1} \text{min}^{-1}$ .



(a) 5 vs. 15



(b) 5 vs. 10



(a) 5 vs. 15

Figure 3.9. Bland Altman scatter diagrams of the differences between  $K_i$  values derived from the initial scan at each visit. 5, 10 and 15 represent the examination where 5, 10 and 15 minutes separated the two scans. Horizontal lines depict mean difference (dotted)  $\pm$  2 standard deviations (solid lines). Error bars show the upper and lower limits if the results were extrapolated to the population. Units are  $\text{ml } 100\text{g}^{-1} \text{min}^{-1}$ .

## **3.6 Discussion**

### **3.6.1 ECG gating**

#### **3.6.1.1 R-R variability with adenosine**

The reduction in R-R interval variability seen in the patients during adenosine infusion is in line with previously reported data in volunteers (Rongen *et al.*, 1999). It is therefore unlikely that cardiac gating would be detrimentally influenced by stressor-induced changes in heart rate variability. However, when a tachycardia is induced after the trigger delay has been set and imaging commenced, as the heart rate increases, image acquisition is pushed later into diastole. This may result in loss of temporal resolution as the image acquisition and dead times continue into the next R-R interval. Motion artefact is likely to be exacerbated as some of the image acquisition time may be during systole. This is more likely when dobutamine is used as the stressor as a greater tachycardia is typically induced (Al-Saadi *et al.*, 1999).

#### **3.6.1.2 Calculation of image position within the cardiac cycle ( $\Phi$ )**

The calculation of the variation in position of image acquisition within the cardiac cycle was based on R-R intervals measured from clinical patients with low and high R-R interval variability and sample arrhythmias. Atrial and ventricular ectopy have a relatively high incidence in patients with coronary artery disease, cardiomyopathy or valvular heart disease (Zipes, 2000). Patients with these pathologies were included as they form a high proportion of those referred for clinical perfusion imaging. In many cardiac MRI studies, protocols exclude patients who are not in sinus rhythm and so ECG-gating issues in these patients are avoided. The “errored” data set was similarly included since, with the difficulties that can arise in obtaining an adequate and sustained ECG trace in the magnetic environment, this type of artefact and resultant ECG-gating error could easily occur.

The data from patient 1 shows that ECG-gating to diastole is extremely consistent when heart rate variability is low. In contrast, a non ECG-gated approach produces high variation in  $\Phi$ . The

effect of varied R-R intervals on ECG-gating is seen by the increased range of  $\Phi$  in the patients with high R-R variability, arrhythmias, and the artefactual (errored) data, respectively. This variation in  $\Phi$  is not significantly different to that obtained with a constant  $TR_0$ . However, the temporal resolution of the ECG-gated images is only half that obtained with non ECG-gated acquisition as a significant increase in  $TR_0$  is incurred by the need to add a trigger delay. In addition, with ECG-gating, an R-R interval greater or less than  $TI_{\text{eff}} + TD$  results in further loss of temporal resolution. This occurs through postponement to a third R-R interval, or by premature imaging in an abnormally long R-R interval with subsequent delay in triggering on the next R wave because of image acquisition duration. This problem is not applicable to non ECG-gated images since  $TR_0$  is constant, and unaffected by any patient parameters. ECG-gating will therefore provide less information about the first pass of the contrast agent through the myocardium. There is more chance of failing to image temporally close to the bolus peak in the left ventricle, and also of differentiating between any varying times to maximum signal intensity in regional myocardial territories. Calculation of the unidirectional influx constant for gadolinium ( $K_i$ ) relies on the combined characteristics of the input and tissue  $R_1$  time curves (Larsson *et al.*, 1996; Cullen *et al.*, 1999b). Obviously, the estimated  $K_i$  will be more accurate if there are more data points available. Temporal resolution becomes worse when multi-slice imaging is attempted, since, for example, if three short axis slices are acquired as in this magnetic resonance protocol and the patient has a heart rate of less than 70 beats/min, the maximum temporal resolution between successive ECG-gated images at each level is six R-R intervals. For heart rates in excess of 70 beats/min, image acquisition declines to every ninth R-R interval. For non ECG-gated imaging, temporal resolution remains a constant  $3 \times TR_0$  (approximately 3 seconds) for each imaged slice.

### **3.6.1.3 Magnetic resonance imaging: Comparison of $R_1$ values obtained from gated and non ECG-gated image acquisition**

Motion artefact was not found to be a more significant problem with non ECG-gated images than with ECG-gated scans. The total time for image data acquisition was 432 ms, i.e.  $4.5 (TR) \times$

96 (lines of  $k$ -space). Ideally, all  $k$ -space lines should be acquired during diastole, and the ECG-gated sequence was timed so that the mid-line occurred at mid-diastole. Whilst significant motion during the middle  $k$ -space lines will cause gross motion artefacts, cardiac motion between the first and last lines of  $k$ -space will cause a loss of fine image detail and a spreading of the signal from these lines in the phase-encoded direction. Once the heart rate is over 50 beats per minute, it is impossible for all lines to be acquired during diastole, and some image acquisition will occur in systole. This effect is more noticeable during stress, since not only is the heart rate increased, but also the diastolic component of the cardiac cycle becomes proportionally less, reducing the time of minimal cardiac motion available for imaging (Ganong W.F., 2000). An attractive alternative approach is to ECG-gate image acquisition to systole since myocardial thickening increases the number of pixels available for analysis. However, systole only occupies approximately a third of the cardiac cycle and has a much shorter isovolumic phase than diastole. Once the heart rate exceeds 40 beats per minute, image acquisition time will encroach into diastole and motion blurring is inevitable. Thus artefact from cardiac motion is likely to be a problem, regardless of whether the imaging sequence is ECG-gated. However, if an image acquired during an ECG-gated sequence were blurred, its omission from the data set could cause a greater loss of temporal resolution than the omission of two or even three non ECG-gated images.

There is a small change in blood volume between diastole and systole that may theoretically give rise to a source of error in  $R_1$  calculation on images acquired during systole. However, this change has been estimated to amount to only 5% (Spaan *et al.*, 1981). A further concern is that torque and through plane myocardial motion may lead to an error in the placement of ROI on consecutive images in a series when imaging in varying parts of the cardiac cycle (Matter *et al.*, 1996). Torque may be compensated for during image analysis with the use of anatomical landmark registration to a reference marker and according adjustment of sampling areas. Through plane motion requires correction by myocardial tracking, a hardware feature only available on dedicated

cardiac imagers (Kuijjer *et al.*, 1999). These difficulties are also encountered with the use of ECG-gated sequences when patient parameters displace image acquisition outside diastole.

Despite the reservations regarding motion artefact with non ECG-gated image acquisition, the image quality from non ECG-gated images from the volunteers was sufficient in all cases to enable the subendocardial and epicardial borders to be delineated for signal intensity extraction and subsequent  $R_1$  calculation. The  $R_1$  values obtained by ECG-gating or non-ECG gating have a high level of agreement with the  $R_1$  “gold standard” values obtained by the multiple TI technique. This implies that the quantitative information obtained from images acquired without ECG-gating can be used reliably for quantitative perfusion calculations.

### **3.6.2 Volunteer $K_1$ study**

#### **3.6.2.1 Image quality**

As with the images conducted on the previous generation scanner, image quality was not impaired by acquisition with a constant  $TR_0$ . The temporal resolution of generated time curves was 1080 ms seconds. This improves on single slice temporal resolution of 2 R-R intervals previously published with this imaging sequence (Cullen *et al.*, 1999b).

##### **3.6.2.1.1 Bolus delivery**

In the majority of cases bolus delivery to the left ventricular cavity was consistent despite utilization of peripheral venous access and hand injection of the contrast agent. Poor bolus delivery with very delayed peak occurred in one subject rendering both image runs from the examination void. This could be owing to venous access siting in a small vein or bolus passage through a tortuous venous system resulting in slow contrast agent flow into the circulation.

Some workers prefer to use mechanical injection of gadodiamide into an intracaval catheter (Wilke *et al.*, 1997). Quality of the bolus curve is then determined by pulmonary and cardiac circulation haemodynamics (Blomley *et al.*, 1993). Central contrast agent administration in a

subject with normal right and left ventricular function results in compact bolus delivery to the coronary circulation. However, injection in patients with cardiac dysfunction will be compromised by any right ventricular impairment, abnormality in left ventricular filling parameters or valvular incompetence. The advantage of central injection is then lost with additional risk of catheter insertion complications. The model for quantification of myocardial blood flow used in this study is less sensitive to noise and more independent of separation of first and second contrast agent passes than models relying predominantly on interpretation of the upslope of the signal intensity curves (Eichenberger *et al.*, 1994; Matheijssen *et al.*, 1996; Wilke, 1998; Al-Saadi *et al.*, 2000; Keijer *et al.*, 2000). Thus peripheral venous injection for bolus delivery can be utilized. The technique is potentially applicable to patients with impaired circulatory haemodynamics.

#### **3.6.2.1.2 Signal and contrast to noise ratio**

The peak  $R_1$  value that was measured in the right ventricle was consistently greater than that measured in the left ventricular cavity, implying that no signal saturation was occurring. This enabled the bolus concentration change within the left ventricle to be utilized as the input function. The low dose of gadodiamide was however sufficient to provide good contrast to noise ratio in the left ventricular cavity and in the myocardium. Data obtained were therefore suitable for quantitative analysis.

#### **3.6.2.1.3 Baseline signal intensity**

The half-life of gadodiamide within plasma is approximately 90 minutes, assuming normal renal function. The presence of residual gadodiamide within the myocardium prior to the second examination on each visit was therefore unsurprising. The increase in background  $R_1$  values demonstrated were for presumed normal myocardium and as expected, this increase declined with time from bolus delivery. There is some evidence to suggest that gadodiamide clearance may be impaired by loss of myocyte integrity (Tong *et al.*, 1993). In patients with coronary artery disease

such hyperenhancement may suggest the presence of myocardial infarction (Kim *et al.*, 2000). This concept is evaluated further in Chapters 4 and 5.

### 3.6.2.2 Quantitative analysis

The values of resting  $K_i$  observed are in keeping with those previously obtained by other investigators with use of a similar MRI sequence (Fritz-Hansen *et al.*, 1998; Cullen *et al.*, 1999b). When corrected for E, absolute values for resting blood flow are similar to those measured in normal subjects with positron emission tomography (Muzik *et al.*, 1998).

Although higher baseline  $R_1$  values were present prior to the second scan at each visit this did not adversely affect calculation of  $K_i$ . Similar  $K_i$  values were obtained at each visit regardless of the time interval between scans. This was expected since derivation of  $K_i$  is based on the change in gadodiamide concentration within the myocardium over time, rather than gadodiamide concentration per se (Equation 2.4) (Larsson *et al.*, 1994; Larsson *et al.*, 1996). For accuracy of repeated  $K_i$  calculation on the same day, the actual time interval separating the two scans is not crucial. Stress and rest perfusion imaging could therefore be performed during a single patient visit rather than on two separate days as published previously (Cullen *et al.*, 1999b).

It was endeavoured to evaluate the repeatability of  $K_i$  measurement during a single visit by presentation of a Bland Altman scatter plot. This proved difficult to determine accurately because of the population size. For clinical imaging, the second measurement would be during vasodilator stress and so  $K_i$  would be increased three to five fold. Thus the margin of error demonstrated between the resting measurements could be acceptable where myocardial perfusion reserve is estimated.

No data evaluating reproducibility of perfusion imaging with MRI have yet been published. The difference in the  $K_i$  values obtained from the initial scan at the 10 minute visit was not numerically large but proved to be significantly lower than the values obtained on the other two occasions. Since the  $K_i$  values were relatively reproducible within the same visit this implies that this variation

was visit rather than technique related. Myocardial perfusion is influenced by heart rate, myocardial afterload and contractility and so varies in accordance with subject haemodynamic parameters, metabolic states and response to pharmacological interventions. These factors are difficult to keep static within subjects especially in the context of serial examinations. A further complexity in identifying a normal range of values is that autoregulatory mechanisms that govern myocardial perfusion are not homogeneous across the myocardium giving rise to a natural spatial variation of flow (Falsetti *et al.*, 1975; Bassingthwaighte *et al.*, 1989; Austin *et al.*, 1990). Unfortunately the analytical software did not have sufficient spatial resolution to allow subdivision of the myocardium into epicardial and subendocardial layers for quantitative analysis. Qualitative assessment of these layers is presented in Chapter 4. The data were examined for presence of diurnal variation in  $K_i$  values but no evidence of this was found. Specific instructions regarding dietary intake, e.g. caffeine or physical activity prior to image acquisition were not given. The number of volunteers was small and the data may have been affected by volunteer behaviour immediately before and during the scan. Definition of a normal range of myocardial perfusion values and acceptable limits for reproducibility is therefore difficult because of the potentially dynamic range of perfusion parameters.

### **3.7 Conclusion**

For dynamic first pass imaging, ECG-gating image acquisition to diastole has the theoretical advantage that motion artefact may be reduced. However, because of the mandatory duration of image acquisition and dead times, this advantage is only realized for subjects with low heart rates and minimal R-R interval variability. In clinical practice, increased heart rate variability, ectopic activity and arrhythmias cause errors in ECG-gating that lead to the same degree of variance in the placement of image acquisition within the cardiac cycle as those images acquired with a constant  $TR_0$ . Although heart rate variability reduces with vasodilator stress, the induced tachycardia and change in the duration of the diastolic and systolic components of the cardiac cycle may also be a source of ECG-gating error. The temporal resolution of image acquisition using the ECG-gated

technique is much less than that of the non ECG-gated method. Furthermore, any triggering errors have the effect of delaying image acquisition and reducing temporal resolution even further. Calculation of regional myocardial  $R_1$  values from images acquired at a constant  $TR_0$  have a similar high level of agreement to the “gold standard”  $R_1$  measures as  $R_1$  values obtained from ECG-gated images. Thus a non ECG-gated technique for dynamic perfusion imaging gives equivalent quantitative data, offers a higher temporal resolution, and is subject to fewer errors than ECG-gated image acquisition.

The quality of magnetic resonance images acquired without ECG-gating and utilizing a low dose bolus of gadodiamide is acceptable for quantitative analysis. There is adequate contrast to noise ratio both within the myocardium and left ventricular cavity for perfusion parameters to be assessed without signal intensity saturation. Perfusion imaging during a single visit appears to be repeatable regardless of the time interval between image acquisitions. This implies that values of  $K_i$  obtained at rest and during adenosine stress at a single examination could be presented in relation to each other as a parameter of myocardial perfusion, i.e. myocardial perfusion reserve. Some inter-visit difference in  $K_i$  values was seen. This did not appear to be technique-related and may represent natural variation in myocardial flow. In the context of the degree of hyperaemia seen with adenosine stress, this variation may not be of clinical significance in application of the technique to stress imaging in patients with coronary artery disease.

---

## **Chapter 4**

# **Diagnostic potential of adenosine perfusion MRI in patients with coronary artery disease**

---

## **Part I: Quantitative image parameters**

### **4.1 Introduction**

The data from the volunteers presented in Chapter 3 suggest that  $K_i$  calculations from two dynamic imaging sequences, one at stress and one at rest, within the same examination may be sufficiently robust to provide useful information regarding myocardial ischaemia. The first portion of this chapter reports a pilot study evaluating the diagnostic potential of this quantitative technique in patients with coronary artery disease. A potential concern is whether MRI with adenosine stress could be tolerated by patients with left ventricular dysfunction. The haemodynamics of bolus delivery to a compromised left ventricle may vary because of raised left ventricular end-diastolic pressure and functional atrioventricular regurgitant jets. To date, there is very little literature assessing the application of adenosine stress first pass contrast-enhanced MRI in patients with cardiac impairment.

### **4.2 Hypothesis**

Quantitative analysis of adenosine stress and rest first pass contrast-enhanced magnetic resonance images can be used to detect angiographically significant coronary artery disease in patients with single and multi-vessel disease and with either normal or impaired left ventricular function.

### **4.3 Objectives**

The objectives of this study are:

1. to test the feasibility of single visit adenosine stress and rest first pass contrast-enhanced MRI with image acquisition with a constant total repetition time and low dose gadodiamide bolus;

2. to test the potential diagnostic performance of quantitative image analysis to detect angiographic coronary artery disease in a pilot group of patients with single and multi-vessel coronary artery disease and with both normal and impaired left ventricular function.

## **4.4 Methods**

### **4.4.1 Study design**

Three groups of patients were recruited for the study: (i) group A, defined as subjects with normal coronary angiography, left ventriculography and 12-lead electrocardiogram (ECG), (ii) group B, i.e. patients with single vessel coronary artery disease with normal left ventricular function and 12-lead ECG, and (iii) group C, defined as patients with multi-vessel coronary artery disease with regional or global left ventricular impairment, with or without 12-lead ECG abnormalities. Twelve patients were recruited in total: group A, n = 2; group B, n = 5; group C, n = 5. All patients underwent adenosine stress and rest first-pass contrast-enhanced MRI as described in Section 2.5.1. Images were acquired at basal, mid-papillary and apical levels.

### **4.4.2 Magnetic resonance image analysis**

Images were assessed for diagnostic acceptability. Adequacy of bolus delivery in group C patients was compared with that attained in patients in groups A and B (Section 2.5.4.5). Signal and contrast to noise ratios were calculated (Section 2.5.4.6). Increase in baseline  $R_1$  following the first gadodiamide bolus prior to the second dynamic sequence was noted (Section 2.5.4.7). The unidirectional transport coefficient for gadodiamide over the capillary membrane,  $K_i$ , was calculated for each ROI (Section 2.5.4). Stress/rest  $K_i$  ratios were calculated to give an index of myocardial perfusion reserve (MPRI) for each ROI. Correction for the extraction fraction of gadodiamide over the capillary membrane,  $E$ , was applied.

### **4.4.3 Collation with angiographic findings**

Coronary angiograms were analyzed by an experienced cardiac radiologist, blinded to MRI perfusion data (Section 2.3.2). MRI ROI were then assigned to the appropriate supplying coronary artery territory according to the angiogram report (Section 2.9).

### **4.4.4 Statistics**

A paired Student's *t* test was used for the haemodynamic data. Unpaired *t* tests were used to compare baseline  $R_1$  data and perfusion parameters in the different patients groups. 95% confidence intervals are calculated for sensitivity and specificity values. All data are presented as mean  $\pm$  SD. Receiver operator characteristic (ROC) curves were constructed for the values of myocardial perfusion reserve obtained to establish the potential sensitivity and specificity of the resulting threshold myocardial perfusion reserve for the detection of a significant coronary artery stenosis. Sensitivities and specificities are expressed with 95% confidence intervals.

## **4.5 Results**

### **4.5.1 Patient demographics**

Mean age was  $59 \pm 10$  years (range 41 - 72 years). Body mass index was  $27 \pm 2.6$  kg m<sup>-2</sup>. All patients were male. In group B, two patients had disease in the left anterior descending artery, two patients had right coronary artery disease and the fifth patient had circumflex artery disease. Ejection fraction on ventriculography in groups A and B was  $72 \pm 4\%$ . In group C, two patients had two vessel disease. The remaining three patients had three vessel disease although in one patient the right coronary artery was small and did not supply the left ventricle. Three patients in group C had sustained myocardial infarction more than six months prior to study commencement. Ejection fraction in this group was  $38 \pm 5\%$ .

## 4.5.2 Magnetic resonance imaging

### 4.5.2.1 Haemodynamic data

All patients completed the scan protocol within 30 minutes. No adverse events occurred and there were no unexpected responses to adenosine (Table 4.1). Heart rate increased ( $p < 0.001$ ) and systolic pressure decreased ( $p < 0.05$ ). Diastolic and mean arterial blood pressure also decreased during the infusion but the fall was insignificant.

Parameter	P	SBP	DBP	MAP
Rest	$68 \pm 15$	$135 \pm 19$	$77 \pm 13$	$95 \pm 14$
Adenosine	$80 \pm 14^\ddagger$	$126 \pm 20^*$	$70 \pm 13$	$89 \pm 14$

Table 4.1. Change in haemodynamic parameters in response to adenosine stress. P = pulse; SBP = systolic blood pressure; DBP = diastolic blood pressure; MAP = mean arterial pressure. \* $p < 0.05$ ,  $^\ddagger p < 0.001$ .

### 4.5.2.2 Image quality

Endocardial and epicardial contours were sufficiently defined (Figure 4.1) and without degradation by artefact to allow placement of analytical contours on all images.

### 4.5.2.3 Bolus delivery

The peak bolus  $R_1$  value achieved within the left ventricular cavity was unaffected by left ventricular function, i.e.  $6.32 \pm 0.74 \text{ s}^{-1}$  in groups A and B, and  $6.36 \pm 1.78 \text{ s}^{-1}$  in group C. The number of frames to required to reach peak  $R_1$  was greater in the patients with poor left ventricular function than in those with normal left ventricular function, i.e. group C,  $4 \pm 1$  and groups A and B,  $3 \pm 1$  ( $p < 0.05$ ).

### 4.5.2.4 Signal and contrast to noise ratio

Mean study contribution of noise to signal intensity was  $4.86 \pm 0.36$  arbitrary units (a.u.). Baseline myocardial signal: noise ratio (SNR) was  $4.74 \pm 1.4$ . Myocardial contrast to noise ratio

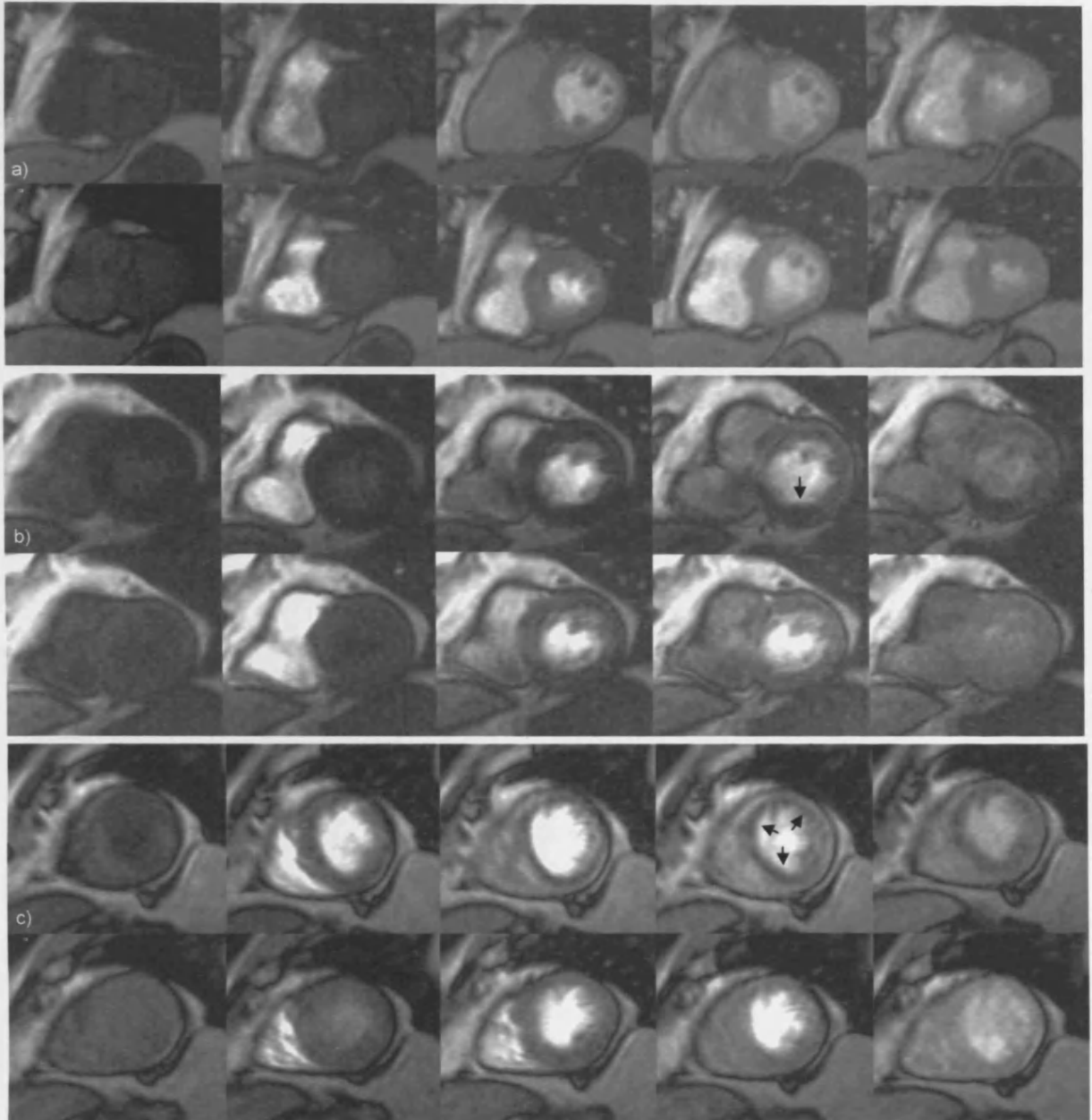


*Figure 4.1. Paired stress (upper sequence) and rest (lower sequence) perfusion MRI scans: a) normal subject; b) patient with single vessel right coronary artery stenosis demonstrating inferior transmural reversible perfusion deficit (arrow); c) widespread reversible subendocardial perfusion deficit (arrows) in patient with triple coronary artery disease.*

for all studies was  $8.75 \pm 1.5$  (range 5.75 - 11.12). Contrast to noise ratio within the left ventricular cavity was  $20.44 \pm 2.78$  (range 15.54 –25.91).

#### 4.5.2.5 Baseline signal intensity

The time interval between the first images of the stress and rest dynamic sequences was  $23 \pm 5$  minutes (range 15 - 32 minutes). Baseline  $R_1$  prior to stress and rest contrast imaging are shown in Table 4.2. Overall there was a 21% increase in baseline  $R_1$  values on the resting images ( $p < 0.001$ ). This increase was less in groups A and B than in group C. The patients from group C with previous myocardial infarction had a higher resting baseline  $R_1$  increase, than those patients in group C without previous infarction ( $p < 0.001$ ). There was no significant difference in the baseline  $R_1$  increase at rest between the latter group and patients in groups A and B (Table 4.2).

Patient group	Baseline $R_1$ pre-stress	Baseline $R_1$ pre-rest	% increase
Normal LV (groups A & B)	$1.08 \pm 0.08$	$1.32 \pm 0.06$	$19.0 \pm 6.0$
Abnormal LV (group C)	$1.01 \pm 0.05$	$1.37 \pm 0.21$	$25.0 \pm 8.9^\ddagger$
Previous MI (from group C)	$1.00 \pm 0.06$	$1.44 \pm 0.25$	$29.2 \pm 8.3^\ddagger$
No previous MI (from group C)	$1.03 \pm 0.04$	$1.27 \pm 0.08$	$18.8 \pm 5.6$

*Table 4.2. Mean  $\pm$  SD baseline  $R_1$  values prior to stress and resting contrast imaging, and the rest/stress ratio expressed as % increase in rest baseline  $R_1$  compared with stress imaging. LV = left ventricle; MI = myocardial infarction.  $^\ddagger p < 0.001$ : normal LV vs. abnormal LV, and previous MI vs. no previous MI.*

#### 4.5.2.6 Quantitative analysis

Stress and rest  $K_i$  values could be computed in 96/98 and 97/98 ROI, respectively. MPRI was therefore calculated for 95/98 ROI. Average time taken for analysis for each patient was 90 minutes.

### 4.5.3 Collation with angiographic findings

Coronary artery (Group, no. ROI)	Rest $K_i$	Stress $K_i$	MPRI	Stress F	Rest F	MPR
Normal (A, 16)	40.4 ± 7.2	128.9 ± 36.5	3.21 ± 0.58	322.1 ± 91.3	80.7 ± 14.3	4.01 ± 0.72
Normal (B, 26)	41.1 ± 10.6	83.2 ± 46.7 (nA <sup>†</sup> )	2.02 ± 0.94 (nA <sup>‡</sup> )	207.9 ± 116.6	82.3 ± 21.3	2.52 ± 1.18
Normal (C, 5)	56.4 ± 30.4	84.3 ± 32.3 (nA <sup>†</sup> )	1.59 ± 0.28 (nA <sup>‡</sup> )	210.8 ± 80.7	112.8 ± 60.8	1.99 ± 0.35
Stenosis (B, 14)	41.2 ± 13.9 (sC*)	49.5 ± 26.5 (nA <sup>‡</sup> , nB*)	1.42 ± 0.86 (nA <sup>‡</sup> , nB*)	123.7 ± 66.1	82.3 ± 27.9	1.77 ± 1.08
Stenosis (C, 39)	30.7 ± 14.2 (nA <sup>‡</sup> )	43.9 ± 27.6 (nA <sup>†</sup> )	1.56 ± 0.67 (nA <sup>‡</sup> )	106.9 ± 70.3	61.3 ± 28.3	1.90 ± 0.88

Table 4.3. Mean ± SD rest  $K_i$ , stress  $K_i$  and index of myocardial perfusion reserve (MPRI). Mean ± SD stress and rest  $K_i$  ( $\text{ml } 100\text{g}^{-1} \text{min}^{-1}$ ), estimate of flow (F) during stress and rest ( $\text{ml } 100\text{g}^{-1} \text{min}^{-1}$ ), myocardial perfusion reserve index (MPRI) and estimate of absolute myocardial perfusion reserve (MPR). Data are presented for regions of interest (ROI) from normal coronary artery territories and those subtended by stenosed arteries for each patient group. \* $p < 0.05$ , <sup>†</sup> $p < 0.01$ , <sup>‡</sup> $p < 0.001$ . nA = compared with normal ROI from group A; nB = compared with normal ROI from group B; sC = compared with ROI supplied by stenosed vessels in group C.

The values for resting and stress  $K_i$  and calculated myocardial perfusion reserve index are shown in Table 4.3. The MPRI in the ROI supplied by angiographically normal coronary arteries in groups B and C was significantly lower than the MPRI seen in group A ( $p < 0.001$  for both groups). There was no significant difference between the resting  $K_i$  values in these territories. The stress  $K_i$  was significantly greater in group A than in the normal regions in both group B ( $p < 0.01$ ) and group C ( $p < 0.05$ ).

The MPRI in the ROI supplied by stenosed vessels in group B was significantly less than MPRI in group A ( $p < 0.001$ ) and normal ROI in group B ( $p < 0.05$ ). There was no difference in the resting  $K_i$ . The stress  $K_i$  in the ROI supplied by a stenotic vessel was significantly lower than in group A ( $p < 0.001$ ) and the normal ROI in group B ( $p < 0.05$ ).

The MPRI in the ROI supplied by stenotic vessels in group C was less than the MPRI in group A ( $p < 0.001$ ) but not significantly different from the ROI subtended by normal vessels in group C. In these ROI, both rest and stress  $K_i$  were lower than those in group A ( $p < 0.001$ ,  $p < 0.05$ ). In the ROI supplied by stenotic vessels the resting  $K_i$  was lower in group C than in group B ( $p < 0.05$ ).

#### 4.5.3.1 Receiver operator characteristic curve analysis

Patient groups	Parameter MPRI $\leq 2$	CAD		Sensitivity (%)	Specificity (%)
		+	-		
<b>A and B</b>	+	11	13	79	68
	-	3	28	(52 - 92)	(53 - 80)
<b>A, B and C</b>	+	37	17	77	62
	-	11	28	(63 - 86)	(47 - 74)

*Table 4.4. Sensitivity and specificity tables (with 95% confidence intervals) for the ability of myocardial perfusion reserve index of  $\leq 2$  to detect angiographic coronary artery disease (CAD).*

For groups A and B, a myocardial perfusion reserve index of  $\leq 2$  had the best discriminatory capacity for detecting regions of interest supplied by a stenosed coronary artery, i.e. sensitivity of 79 (52 - 92)% and specificity of 68 (53 - 80)% (Table 4.4). If the  $K_i$  values are corrected for the extraction fraction, E, the absolute myocardial perfusion reserve is 2.25. When the data from group C patients were included in the analysis, the threshold myocardial perfusion reserve index for the identification of a diseased vessel remained the same, with a sensitivity of 77 (63 - 86)% and specificity of 62 (47 - 74)%.

## 4.6 Discussion

### 4.6.1 Magnetic resonance image quality and bolus delivery

This pilot study confirmed that performing rest and stress scans during a single patient visit was feasible. This is more practical for patients and more economical on imager time. The non ECG-gated image acquisition sequence consistently provided artefact-free images of sufficient quality for signal intensity extraction. Adequate bolus delivery was obtained, as reflected by the contrast to noise ratios and the consistency in the peak  $R_1$  values detected within the left ventricular cavity. These were equivalent to those seen in the volunteers (Chapter 3). The myocardial baseline signal to noise and maximum contrast to noise ratios demonstrated that the low dose of contrast produced sufficient change in signal intensity for perfusion abnormalities to be recognized above the noise contribution to the image. The contrast agent bolus in the patients in group C took longer to achieve peak concentration from baseline, undoubtedly a result of raised left ventricular end-diastolic pressure in this group. However, the peak  $R_1$  value in the left ventricular cavity was similar to the patients with normal left ventricular function. The slower rise to peak does not affect calculation of  $K_i$  as this computation is more independent of separation of first and second contrast agent passes than tracer kinetic models reliant on upslope of the signal intensity curve alone (Eichenberger *et al.*, 1994; Matheijssen *et al.*, 1996; Wilke, 1998; Al-Saadi *et al.*, 2000; Keijer *et al.*, 2000).

The baseline  $R_1$  values were increased on the rest study as a result of the previous contrast agent bolus administration for stress imaging. This increase was minimal in patients with normal left ventricular function and equivalent to the level found in normal volunteers (Chapter 3). The significantly higher value that is seen in patients with previous myocardial infarction is in keeping with delayed hyperenhancement of infarcted territories described in the literature (Kim *et al.*, 2000; Choi *et al.*, 2001; Simonetti *et al.*, 2001). This change was not uniform across all regions of the myocardium. This observation may be of value in the distinction of viable territories from scar

tissue and merits further study and discussion (Chapter 5). Theoretically, this difference in baseline  $R_1$  between stress and rest imaging should not affect perfusion quantification since the residual gadodiamide is bound and does not affect the change in gadodiamide concentration seen with a subsequent bolus.

#### **4.6.2 Collation with angiographic findings**

The values for myocardial perfusion reserve that we obtained in the ROI from the two normal patients are in keeping with those previously reported in volunteers both with MRI and positron emission tomography (Bergmann *et al.*, 1989; Chan *et al.*, 1992; Merlet *et al.*, 1993; Cullen *et al.*, 1999b). A limitation of this study is that the sensitivity and specificity for the detection of significant angiographic coronary artery disease are calculated with disease-free arteries from patients with one or two-vessel coronary artery disease included in the “normal” vessel population. A reduced MPRI in these vessels is unsurprising and is likely to reflect early arterial dysfunction (Sambuceti *et al.*, 1993). Despite this, there was a clear reduction in MPRI detected in ROI supplied by coronary arteries containing significant stenoses. The obtained MPRI cut-off value of  $\leq 2$  is in line with previously reported values in the literature (Sambuceti *et al.*, 1993; Picano *et al.*, 1994; Cullen *et al.*, 1999b; Al-Saadi *et al.*, 2000).

In the few published studies evaluating the sensitivity and specificity of perfusion MRI against coronary angiography, there is variation in the definition of a significant angiographic stenosis. Sensitivity and specificity values (angiographic cut-off value) were 90% and 83% ( $> 75\%$ ) (Al-Saadi *et al.*, 2000), 72% and 80% ( $> 70\%$ ) (Wolff *et al.*, 1999), and 80% and 83% ( $> 70\%$ ) (Arai *et al.*, 1999), respectively. Although a broader stenosis definition is taken here, no significant difference in sensitivity or specificity is demonstrated with the use of a non ECG-gated technique of image acquisition. The reduction in specificity in patients with multi-vessel disease and left ventricular dysfunction is partly a result of the contribution of the heterogeneous nature of myocardial disease in this group. Perfusion parameters may represent territories of infarction,

dysfunction with perfusion down-regulation and microvascular disease. This is illustrated by the lower resting  $K_i$  in the ROI subtended by diseased vessels in group C. A consequence of this was an artificially high MPRI in these territories. This parameter needs to be interpreted in the context of rest and stress  $K_i$  findings. In addition to being of diagnostic value in this type of patient, perfusion quantification may be useful to evaluate differing myocardial states and the effects of collateral blood flow.

## 4.7 Conclusion

Single visit adenosine stress and rest first pass contrast-enhanced MRI with the use of the image acquisition technique developed in Chapter 3 is feasible. The entire scan can be completed within 30 minutes, increasing acceptability of the technique to patients and physicians. The non ECG-gated approach increases the temporal resolution of a standard technique without apparent detriment to image quality, loss of quantitative parameters or diagnostic information and without need for invasive central cannulation. The kinetic model used takes into account the inevitable variable bolus delivery on repeated examinations and can be applied to patients with left ventricular dysfunction.

The perfusion parameters of stress  $K_i$  and myocardial perfusion reserve index proved sensitive not only to the presence of coronary artery stenosis, but also to possible early coronary arterial dysfunction and loss of vasodilator reserve. Sensitivity and specificity for the detection of angiographically significant luminal obstruction was 77% and 62%. This is in keeping with previously published figures for perfusion MRI. The results suggest that this technique could be applied to further research studies. Larger prospective studies including a true “normal” population to further evaluate the diagnostic potential of this technique would be of value.

## **Part II: Qualitative image parameters**

### **4.8 Introduction**

The ideal clinical investigation to assess myocardial perfusion would provide a semi-quantitative or quantitative measurement of cardiac blood flow (Larsson *et al.*, 1996; Wilke *et al.*, 1997; Fritz-Hansen *et al.*, 1998; Cullen *et al.*, 1999b). However, these methods require labour intensive image analysis that is impractical for general clinical use. Until accurate and fully automated edge detection software is developed such techniques are likely to remain research tools. As with SPECT and PET imaging, current clinical need for rapid reporting appears likely to be only met by qualitative analytical methods. MRI scanners routinely available for clinical work are now capable of producing perfusion images of sufficient quality for this approach to be investigated. The high spatial resolution permits assessment of transmural perfusion variations. Since the epicardial coronary artery system makes the subendocardial region most susceptible to reduced coronary artery perfusion (Hoffman, 1987), qualitative perfusion MRI has potential to be a valuable investigative tool for patients with coronary artery disease.

### **4.9 Hypothesis**

A protocol for qualitative analysis of first pass contrast-enhanced magnetic resonance images acquired during adenosine stress and at rest can be designed that is rapid to perform. This approach can be used to detect angiographically significant coronary artery disease, to provide a measure of disease severity and to assess the functional effects of collateral blood flow.

### **4.10 Objectives**

The objectives of this part of the study were:

1. to design a qualitative reporting method for the combined analysis of adenosine stress and rest first pass contrast-enhanced MRI for assessment of myocardial perfusion;

2. to test the potential diagnostic performance of qualitative image analysis to detect angiographically significant coronary artery disease in a heterogeneous group of patients ;
3. to establish whether perfusion patterns seen on MRI are related to coronary artery disease severity and presence of remote myocardial infarction;
4. to determine whether the influence of collateral vessels on regional myocardial perfusion is detectable.

## **4.11 Methods**

### **4.11.1 Study design**

Thirty consecutive patients attending for evaluation of myocardial perfusion by MRI with significant angiographic coronary artery disease in one or more vessels were recruited for the study. No patients had sustained a myocardial infarction within the six months preceding the study. First pass contrast-enhanced magnetic resonance was performed during adenosine stress and at rest (Section 2.5.1.).

### **4.11.2 Magnetic resonance image analysis**

An experienced radiologist, blinded to clinical and angiographic data, reviewed the images at each level. Image quality was assessed for diagnostic acceptability (Section 2.5.5). Each myocardial short axis slice was divided into 8 radial regions of interest (ROI) and then divided circumferentially into inner and outer layers (Figure 2.7b). Qualitative perfusion parameters were then assessed according to the designed protocol described in Section 2.5.5.

### **4.11.3 Collation with angiographic findings**

Coronary angiograms were analyzed by an experienced cardiologist, blinded to MRI perfusion data (Section 2.3.2). Identified stenoses were divided into proximal, mid or distal main vessel or branch occlusions. The most severe stenosis in each native vessel or graft was assigned to one of 5

Green Lane categories according to reduction in cross-sectional area: 1) 100%, 2) 90 - 99%, 3) 75 - 89%, 4) 50 - 74% and 5) < 50%. Where a graft was occluded, the most severe stenosis in the native vessel was assessed. Infarction-related coronary vessels were identified from the clinical history, ECG and angiographic findings. They were assigned to two groups according to the degree of residual stenosis: 1) completely occluded and 2) stenosed. The presence and degree of collateral supply to the region were scored according to Green Lane criteria, i.e. no collateral flow (0), tiny collateral vessels (1), small to moderate collateral vessels (2), large collateral vessels (3).

MRI and angiographic data were collated (Section 2.9). For each coronary artery territory perfusion was reported as abnormal if a reversible or fixed perfusion deficit was detected in one or more MRI ROI. The sensitivity and specificity of perfusion imaging for the detection of a significant angiographic stenosis was calculated. Patterns of hypoenhancement (Tables 2.5 and 2.6) seen were compared in vessels with differing degrees of stenosis. All vessels were initially included but data are also given excluding regions assigned to infarction-related coronary arteries. Vessels with total occlusion were divided into those related to previous myocardial infarction and those associated with normally functioning myocardium. Regional perfusion parameters for these two groups of arteries was compared. Finally perfusion parameters for vessels receiving varying support from collateral circulation were evaluated.

#### **4.11.4 Statistics**

A paired Student's *t* test was used to evaluate haemodynamic data. Regional perfusion data are presented from combined analysis of stress and rest images. Perfusion parameters are expressed using 95% confidence intervals for proportions.

## 4.12 Results

### 4.12.1 Patient demographics

All thirty patients completed the protocol. Patient demographics are shown in Table 4.5.

Patient characteristic	n
Male:Female	27:3
Age (range)	62 (36 - 74) years
1VD / 2VD / 3VD	5 / 6 / 19
Previous myocardial infarction	21
Previous CABG x1 / PTCA	5 / 0

*Table 4.5. Patient demographics. 1VD = single vessel disease; 2VD = 2 vessel disease; 3VD = triple vessel disease; CABG = coronary artery bypass grafting; PTCA = percutaneous transluminal coronary angioplasty.*

### 4.12.2 Haemodynamics

All patients completed the scan protocol. The procedure was well tolerated. No adverse events occurred and there were no unexpected responses to adenosine (Table 4.6). Heart rate increased ( $p < 0.001$ ) whereas systolic, diastolic and mean arterial blood pressure all decreased during the infusion ( $p < 0.01$ ,  $p < 0.001$  and  $p < 0.001$ , respectively).

Parameter	P	SBP	DBP	MAP
Rest	69 ± 16	135 ± 21	77 ± 10	98 ± 13
Adenosine	80 ± 15 <sup>†</sup>	128 ± 22 <sup>†</sup>	72 ± 9 <sup>‡</sup>	91 ± 12 <sup>‡</sup>

*Table 4.6. Change in haemodynamic parameters in response to adenosine stress. P = pulse; SBP = systolic blood pressure; DBP = diastolic blood pressure; MAP = mean arterial pressure. <sup>†</sup> $p < 0.01$ , <sup>‡</sup> $p < 0.001$ .*

### 4.12.3 Image quality

Image quality was sufficient for qualitative reporting in 705/720 (98%) ROI. Only 15/720 (2%) ROI, occurring in 2 patients, were considered to be of less than diagnostic quality. The majority of these ROI (12/15) were degraded by susceptibility artefact or partial volume effects. Extreme myocardial thinning prevented analysis of the perfusion characteristics in the other three. Reporting time was approximately 10 minutes per patient.

### 4.12.4 Detection of angiographic coronary artery disease

A total of 86 coronary artery territories were assessed. In 4 patients the right coronary artery was anatomically small and did not supply the left ventricle. Angiographically significant disease was present in 71/86 vessels. The relationship between hypoperfusion and angiographic stenosis in the 86 coronary artery territories is shown in Table 4.7. The sensitivity and specificity for detection of an angiographically significant stenosis for the total group are 93% (CI 85 - 97%) and 60% (CI 36 - 80%), respectively. These values do not change significantly when infarction-related vessels are excluded from analysis.

	Total vessels (n = 86)		Infarction-related vessels excluded (n = 65)	
	Disease +	Disease -	Disease +	Disease -
MRI +	66	6	46	6
MRI -	5	9	4	9

*Table 4.7. Number of abnormal coronary artery territories detected by MRI for all vessels and all vessels excluding infarction-related vessels. Disease + = angiographic stenosis present; Disease - = no angiographic stenosis present; MRI + = abnormal perfusion reported on MRI; MRI - = no perfusion abnormality seen on MRI.*

There was an overall false positive rate of  $7 \pm 3\%$  (n = 6) and false negative rate of  $6 \pm 3\%$  (n = 5). These non-concordant territories were further evaluated. In 3 of the false positive territories, septal perfusion deficits extended further than predicted from angiogram analysis. In one patient with an occluded left anterior descending artery, a perfusion deficit in the anterior wall extended

into the apical territory of the normal right coronary artery. Reversible subendocardial perfusion deficits were reported in 2 angiographically normal territories. In two territories that were reported as false negative, i.e. having no perfusion deficit despite the presence of angiographic disease, an extensive epicardial collateral supply was seen. A further normal MRI territory was supplied by a vessel in which a distal branch lesion only was present. The last two patients with false negative results in a single CA territory had severe triple vessel disease. In one, gadodiamide bolus quality was sub-optimal.

#### **4.12.5 Relationship of MRI perfusion patterns to angiographic stenosis severity**

The majority of the most severe angiographic stenoses (63/71) were located proximally in the vessels. Coronary artery bypass graft occlusion was seen in 9/12 grafts. Distribution and type of MRI perfusion abnormality is shown in Table 4.8 according to stenosis severity.

##### **4.12.5.1 Extent of perfusion deficit**

The proportion of ROI showing abnormal enhancement increased with the level of stenosis, from 31% with < 50% stenosis to 65% with CA occlusion ( $p < 0.05$  between all levels except 90 - 99% and 100%). This trend was also seen if infarction-related vessels were excluded.

##### **4.12.5.2 Nature of perfusion deficit**

Territories supplied by stenosed vessels contained a higher proportion of ROI displaying subendocardial perfusion deficits than territories supplied by occluded CAs ( $p < 0.05$  occlusion versus all other categories). Where subendocardial perfusion deficits were seen, they were much more likely to be reversible than fixed ( $p < 0.05$ ).

In CA territories affected by previous infarction, there was a greater proportion of full thickness perfusion deficits (75% vs. 54%,  $p < 0.05$ ). When occluded non-infarction-related (A) and infarction-related vessels (B) were compared, the likelihood of reversible ischaemia was greater in

Stenosis	CA (n)	Total ROI	Normal ROI	Abnormal ROI	SE		FT		ROI na
					Rev	Fix	Rev	Fix	
<i>All vessels</i>									
100%	29	255	81 (32) <sup>†</sup>	167 (65)	39 (23)	5 (3)	75 (45)	48 (29)	7
90 - 99%	13	120	41 (34)	73 (61)	32 (44)	1 (1)	25 (34)	15 (21)	6
75 - 89%	15	149	65 (44)	82 (55)	36 (44)	2 (2)	43 (52)	1 (1)	2
50 - 74%	14	90	51 (57)	39 (43)	20 (51)	0	12 (31)	7 (18)	0
< 50%	15	106	73 (69)	33 (31)	17 (52)	0	8 (24)	8 (24)	0
<i>Non MI-related vessels</i>									
100% (A <sup>§</sup> )	18	147	40 (27)	100 (68)	30 (30)	4 (4)	45 (45)	21 (21)	7
90 - 99%	9	72	26 (36)	44 (61)	23 (52)	0	13 (30)	8 (18)	2
75 - 89%	10	92	46 (50)	44 (48)	23 (52)	2 (5)	18 (41)	1 (2)	2
50 - 74%	13	84	49 (58)	35 (42)	18 (51)	0	10 (29)	7 (20)	0
< 50%	15	106	73 (69)	33 (31)	17 (51)	0	8 (24)	8 (24)	0
<i>MI-related vessels</i>									
100% (B <sup>§</sup> )	11	108	41 (38)	67 (62)	9 (13)	1 (1)	30 (45)	27 (40)	0
< 100% (C <sup>§</sup> )	10	111	36 (32)	71 (64)	24 (34)	1 (1)	39 (55)	7 (10)	4

*Table 4.8. Distribution of perfusion patterns according to stenosis severity. Data are for absolute number of regions of interest (ROI). CA = coronary artery; SE = subendocardial; FT = full thickness; Rev = reversible; Fix = fixed; na = not assessable; <sup>†</sup>Figures in parentheses represent percentage total ROI (normal and abnormal) and percentage abnormal ROI (SE, FT); MI = myocardial infarction; <sup>§</sup>A = occluded non-MI related vessels; B = occluded MI-related vessels; C = stenosed MI-related vessels.*

group A, i.e. 75% vs. 58% ( $p < 0.05$ ). This was owing to a greater frequency of subendocardial abnormalities in group A.

When infarction-related vessels were examined, likelihood of reversible ischaemia was greater in stenosed vessels (C) than in occluded vessels (B), i.e. 89% vs. 58% ( $p < 0.05$ ). This was a result of an increase in both subendocardial and full thickness reversible perfusion abnormalities in group C.

Examples of reversible subendocardial and fixed full thickness MRI perfusion patterns are shown in Figure 4.2.

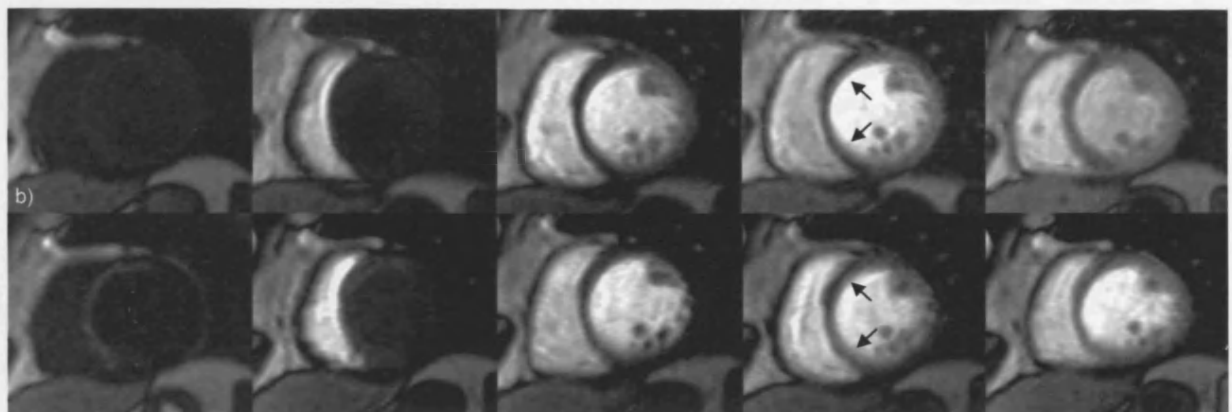
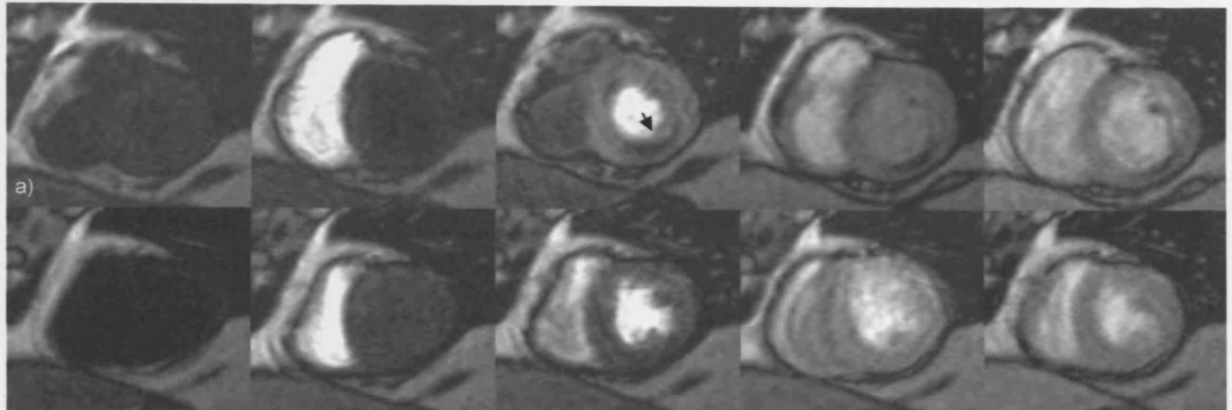


*Figure 4.2. Paired stress (upper sequence) and rest (lower sequence) perfusion MRI scans demonstrating a) inferior subendocardial reversible perfusion deficit (arrow); b) fixed transmural anteroseptal perfusion deficit (arrows).*

### 4.12.5.3 Collateral circulation

Angiographically visible collateral circulation was seen in 30 territories. Collateral circulation was graded as 1 in 18 territories, 2 in 9 territories and 3 in 3 territories. In 27/30 territories with collateral supply the original vessel was occluded. Territories supplied by occluded vessels but supported by grade 2 or 3 collaterals contained a higher proportion of normally perfused ROI compared with those only supported by grade 1 or no collaterals (44% vs. 25%,  $p < 0.05$ , Table 4.9A). In territories of occluded vessels supported by collaterals, significantly more reversible perfusion deficits were seen in territories not affected by previous myocardial infarction (74% vs. 58%,  $p < 0.05$ , Table 4.9B).

	Patient group	CA (n)	Total	Normal	Abnormal	SE rev	SE fix	FT rev	FT fix	na
A	0 + 1	19	162	40 (25) <sup>†</sup>	122 (75)	29 (24)	2 (2)	54 (44)	35 (29)	5
	2 + 3	10	93	41(44)	52 (56)	10 (21)	3 (6)	21 (40)	13 (25)	2
B	MI+ C+	10	96	33 (34)	63 (66)	9 (14)	1 (2)	28 (44)	25 (40)	0
	MI- C+	17	141	38(27)	103 (73)	30 (31)	4 (4)	41 (43)	21 (22)	7

*Table 4.9. A. Distribution of perfusion patterns according to collateral grade in occluded coronary artery territories. B. Distribution of perfusion patterns according to presence or absence of myocardial infarction in occluded coronary artery territories supported by collateral vessels. Data are for absolute number of regions of interest (ROI). \*CA = coronary artery; SE = subendocardial; FT = full thickness; Rev = reversible; Fix = fixed; na = not assessable; <sup>†</sup>Figures in parentheses represent percentage total ROI (normal and abnormal) and percentage abnormal ROI (SE, FT).*

## 4.13 Discussion

### 4.13.1 Patient selection

The majority of published studies assessing myocardial perfusion with MRI have been performed in patients with isolated single vessel disease and / or normal myocardial function (Eichenberger *et al.*, 1994; Matheijssen *et al.*, 1996; Lauerma *et al.*, 1997; Wilke *et al.*, 1997; Al-Saadi *et al.*, 2000). In this study, the MRI technique has been evaluated in a more typical

heterogeneous population of patients with ischaemic heart disease. Unfortunately no opportunity arose to study more patients with normal angiography.

#### **4.13.2 Magnetic resonance imaging**

In contrast to previously published quantitative analytical methods, images were purposely reviewed on line with the use of a grey scale to assess signal intensity to avoid time-consuming image post-processing procedures (Jerosch-Herold & Wilke, 1997; Penzkofer *et al.*, 1999; Cullen *et al.*, 1999b; Al-Saadi *et al.*, 2000; Schwitter *et al.*, 2001). Image quality was consistently sufficiently high to make qualitative reporting of scans possible despite the presence of artefact from sternal wires in patients who had undergone previous bypass surgery. Similarly, two patients had intra-coronary stents *in situ*. An epicardial signal void was seen, but there was no interference with the myocardial signal.

#### **4.13.3 Detection of angiographic disease**

The sensitivity and specificity obtained have to be judged within the characteristics of the study group. In this population there was a high prevalence of coronary artery disease and thus high sensitivity would be expected. Myocardial ischaemia was demonstrated in all patients. A distinguishing feature of this study is the method employed to collate MRI and angiographic data (Section 2.9). This is in contrast to previous MRI studies that have excluded areas of possible overlap from the analysis or used small hand drawn ROI (Klein *et al.*, 1993; Cullen *et al.*, 1999b). A few anatomical inconsistencies were seen, particularly in the septal region where hypoenhancement extended further than predicted on the angiogram. This has been reported previously with MRI (Cullen *et al.*, 1999a). In addition, the relationship between perfusion bed size, degree of anterograde and collateral flows is complex. Coronary artery territories are interdependent and may overlap (Kaul *et al.*, 1991; Qian *et al.*, 1999).

In the patient with left anterior descending artery occlusion where visualized hypoperfusion extended into adjacent territories, it is likely that the size of the myocardial area originally supplied

by this vessel was underestimated. In two patients subendocardial deficits seen in angiographically normal territories may represent occult ischaemia. Impairment in coronary flow reserve suggestive of endothelial dysfunction has been described in angiographically normal vessels in patients with isolated left anterior descending artery stenosis (Sambuceti *et al.*, 1993). Similarly, quantitative estimates of myocardial perfusion reserve with MRI in territories supplied by disease free vessels on angiography in patients with coronary artery disease are lower than those in normal volunteers (Cullen *et al.*, 1999b). In two patients in whom normal perfusion was reported on MRI but angiographic disease was present, the extensive epicardial collateral circulation noted may have protected the myocardium from stress-induced ischaemia (Tanabe *et al.*, 1980). In a further two patients extensive triple vessel disease may have led to a reporting error in that mild hypoenhancement appeared normal in comparison with the severe hypoenhancement seen in adjacent ROI. This is also a common reporting problem with SPECT imaging. The fifth patient had a distal branch occlusion that may have been insufficient to generate a perfusion defect.

A frequent criticism of the currently available perfusion MRI techniques is that in order to gain adequate temporal resolution to follow the first pass of a contrast bolus, the number of myocardial slices that can be imaged is restricted (Jerosch-Herold & Wilke, 1997). The most important limiting factor with MRI is that it is not possible to visualize the apex directly. As can be seen from the high sensitivity in this study, three short axis slices can give a reasonable sampling of the myocardial area. In practice SPECT scanning is interpreted qualitatively on the basis of the same ROI that we have used. However with SPECT, an additional evaluation of the apex can be made.

#### **4.13.4 Relationship of MRI perfusion patterns to angiographic stenosis severity**

##### **4.13.4.1 Extent of perfusion deficit**

In most territories angiographic stenosis was proximal and likely to have maximal effect on perfusion and to affect a significant area of myocardium. This distribution may explain the trend

seen between the extent of the perfusion deficit as measured by the number of abnormally perfused ROI and maximal angiographic stenosis.

#### **4.13.4.2 Nature of perfusion deficit**

The high spatial resolution of MRI facilitates visual distinction between subendocardial and transmural perfusion deficits. The results conform to the theory of stepwise progression of hypoperfusion initially affecting the subendocardium and subsequently extending through the myocardial layer to the epicardium as myocardial flow is increasingly jeopardized (Bache & Schwartz, 1982; Hoffman, 1987). The more severe pattern of perfusion deficit related to infarction is also demonstrated. The difference between the types of perfusion deficits seen in infarction territories supplied by occluded vessels compared with those supplied by stenosed vessels may be important when examining residual viability within infarction zones. To some extent the latter group appeared to be protected against development of fixed full thickness deficits and demonstrated more reversible ischaemia. As residual coronary artery patency following infarction is an important prognostic factor and may be an indicator of viability, it is possible that these MRI findings may also be helpful in establishing myocardial integrity (Lamas *et al.*, 1995; Gensini *et al.*, 1999).

#### **4.13.4.3 Collateral circulation**

Collateral circulation existed predominantly to support those vessels that were occluded. The presence of grade 2 or 3 collateral vessels appeared to partially limit the extent of perfusion deficit in these territories. However in this group of patients, the nature of the perfusion deficit was mainly determined by prior myocardial infarction.

### **4.14 Conclusion**

The designed criteria for qualitative evaluation of perfusion abnormalities with the use of combined analysis of stress and rest scans were straightforward to apply. Reporting was quicker

than with the quantitative method and had the advantage that image analysis was not as a consequence restricted to the mid-papillary slice. A limitation of this study is that the opportunity did not arise to evaluate intra-observer or inter-observer reproducibility of scan interpretation. Within this population, a high sensitivity and moderate specificity for the detection of angiographic coronary artery stenosis was achieved. Additional information was obtainable from the patterns of perfusion deficit relating to angiographic lesion severity, prior myocardial infarction and the presence or absence of collateral flow. Thus this technique may be suitable for application for *de novo* diagnosis of coronary artery disease, and as a complementary modality to angiography for assessment of the significance of a given angiographic lesion and effects of collateral flow. Further studies employing a prospective study design and incorporating assessments of intra-observer and inter-observer reproducibility are necessary.

---

## **Chapter 5**

# **MRI prediction of contractile recovery in individual myocardial segments following revascularization: translation into clinical benefit**

---

## 5.1 Introduction

Percutaneous and surgical revascularization techniques are becoming increasingly available for the treatment of coronary artery disease. It is now well established that patients with left ventricular dysfunction may attain symptomatic, functional and prognostic benefit from such procedures (Alderman *et al.*, 1983). This patient group is however, at risk from increased peri-operative morbidity and mortality (Jones *et al.*, 1978; Pigott *et al.*, 1985; Elefteriades *et al.*, 1993). Identification of individual patients that are likely to benefit from revascularization is dependent on pre-operative assessment of regional dysfunctional myocardium for evidence of myocardial hibernation (Rahimtoola, 1989). Hibernating myocardium is characterized by preserved perfusion and metabolism but chronically reduced resting contractility that improves transiently with inotropic stimulation and more long-term following restoration of coronary blood flow (Rahimtoola, 1995; Heusch & Schulz, 1996). This is in contrast to myocardial territories composed predominantly of scar tissue where regional dysfunction is unaffected by revascularization. Since coronary artery disease gives rise to heterogeneous myocardial pathology, scar tissue and hibernation may coexist within the same heart. In order to estimate the risk: benefit ratio of proposed procedures, it is of value to assess the extent of potentially reversible myocardial dysfunction (Sheiban *et al.*, 1995; Pagley *et al.*, 1997; Di Carli *et al.*, 1998).

Current clinical techniques to identify myocardial hibernation include thallium-201 imaging, positron emission tomography and stress echocardiography (Melin *et al.*, 1988; Watada *et al.*, 1994; Tamaki *et al.*, 1995). Radionuclear techniques demonstrate preserved basal perfusion or metabolism. They are limited by relatively poor spatial resolution and requirement for ionizing radiation exposure. Also, positron emission tomography is only accessible in specialized centres. Stress echocardiography is used to elicit the presence of inotrope-enhanced contractility but optimal acoustic windows necessary for complete examination remain elusive in some patients.

MRI has the potential to demonstrate cardiac anatomy, function, perfusion, membrane integrity and metabolism (Baer *et al.*, 1999a; Sensky & Cherryman, 2000; Sinitsyn, 2001). With the use of this imaging modality, several approaches for identification of myocardial hibernation have been proposed. These include assessment of resting diastolic wall thickness, inotrope-enhanced contractility, basal perfusion and myocardial tissue characterization (Baer *et al.*, 1995; Kim *et al.*, 1996; Baer *et al.*, 1996b; Di Carli *et al.*, 1998; Watzinger *et al.*, 2001).

A dual adenosine dobutamine stress (DADS) cardiac MRI protocol was designed to optimize information gained on myocardial function, perfusion and hibernation during a single patient visit (Section 2.7). This technique was tested successfully in a pilot group of patients (Sensky *et al.*, 2000). The aim of this study was to use this protocol to evaluate potential MRI parameters of myocardial hibernation in patients with chronic ischaemic left ventricular dysfunction and to determine their predictive value for segmental myocardial recovery following revascularization. Subsequently, an attempt was made to establish whether regional parameters could be translated into prediction of improvement in ejection fraction and clinical status in order to determine whether they could be successfully applied to the prediction of benefit in individual patients.

## **5.2 Hypothesis**

The following MRI parameters are indicative of myocardial hibernation and will predict regional and global left ventricular recovery after myocardial revascularization: a) dobutamine-induced contractile reserve, b) preserved diastolic wall thickness, c) normal resting myocardial perfusion d) absence of delayed hyperenhancement.

## **5.3 Objectives**

The objectives were to use a customized MRI protocol (DADS):

1. to identify and propose MRI parameters of myocardial hibernation;

2. to evaluate their sensitivity and specificity for the prediction of regional and global left ventricular recovery following revascularization;
3. to determine whether the presence of these parameters can be translated into prediction of clinical benefit (or lack of) following revascularization.

## **5.4 Methods**

### **5.4.1 Study design**

Twenty-eight consecutive patients, accepted for either surgical or percutaneous coronary artery revascularization, were recruited for the study. Inclusion criteria were the presence of angiographic coronary artery disease anatomically suitable for revascularization, and left ventricular dysfunction on ventriculography. The latter was defined as the presence of at least two contiguous akinetic segments according to Green Lane criteria (Brandt *et al.*, 1977). Exclusion criteria were contraindications to MRI, radionuclide exposure, adenosine or dobutamine infusions. No other selection criteria were applied. Patients were evaluated within four weeks prior to revascularization (visit A) and six months after the procedure (visit B). At visit A, the patient underwent (i) clinical assessment (Section 2.2) (ii) adenosine stress MRI to evaluate myocardial perfusion (iii) rest and dobutamine cine MRI to assess myocardial function and (iv) rest/delayed rest thallium scintigraphy. At visit B, the following evaluations were repeated: (i) clinical assessment (ii) adenosine stress MRI and (iii) resting cine imaging.

### **5.4.2 Revascularization**

Reference and lesion diameters of any diseased vessel were measured on the angiographic view demonstrating maximal stenosis (Section 2.3). Patients electively received either coronary artery bypass grafting or percutaneous coronary angioplasty and stent implantation. This decision was made independently of the study by the patient's cardiologist according to angiographic anatomy and distribution of diseased vessels.

### **5.4.3 Magnetic resonance imaging**

The dual adenosine dobutamine stress protocol was employed (Section 2.7).

### **5.4.4 Regional myocardial function**

An experienced radiologist, blinded to other MRI data, reported regional myocardial function on line (Section 2.6.5). Regional systolic wall thickening at rest and during dobutamine stress was scored according to the criteria in Section 2.6.5.1 (Table 2.8). A dysfunctional region of interest (ROI) was defined as scores 3 - 5. Change in resting regional qualitative scores of systolic wall thickening after revascularization was used to indicate segmental myocardial functional recovery. If the post-operative score had improved by 1 or more the region was determined to have shown recovery. If the score was the same or had deteriorated, the region was determined to have demonstrated no recovery.

### **5.4.5 Ejection fraction**

Ejection fraction was calculated from the cine images (Section 2.6.4.1). This was used as the reference standard for overall change in ejection fraction following revascularization.

### **5.4.6 End-diastolic wall thickness**

For pre-operative studies, end-diastolic wall thickness was measured on the short axis frames (Section 2.6.4.2).

### **5.4.7 Perfusion**

Quantitative analysis was independently performed on the mid-papillary slice from each examination. The unidirectional transport coefficient for gadodiamide over the capillary membrane,  $K_i$ , was calculated for each dysfunctional ROI (Section 2.5.4). Stress/rest  $K_i$  ratios were calculated to give an index of myocardial perfusion reserve (MPRI).

## **5.4.8 Delayed hyperenhancement**

The percent increase in regional baseline  $R_1$  values prior to the second contrast-enhanced image sequence (rest perfusion) compared with prior to the first image acquisition sequence (stress perfusion) was calculated to detect any delayed myocardial tissue hyperenhancement (Section 2.5.4.7). All 3 short axis slices were analyzed.

## **5.4.9 Thallium scintigraphy**

Rest/redistribution thallium scintigraphy was performed (Siemens Diacam gamma camera, Erlangen, Germany). Seventy MBq intravenous thallium-201 was given 5 minutes after the administration of 800  $\mu$ g sublingual glyceryl trinitrate spray. Single photon emission computerized tomography images were acquired 30 minutes and approximately 5 hours after injection of the isotope. Images were processed with dedicated software (Icon, Siemens, Erlangen, Germany). Initial and delayed images were carefully aligned for comparison. Basal, mid-papillary and apical short axis and horizontal and vertical long axis reconstructions, comparative with those obtained by MRI and divided into equivalent ROI, were reported by an experienced radiologist, blinded to MRI and clinical data. Regional thallium uptake in both sets of images was scored according to the following criteria: 0 = normal, 1 = mildly reduced, 2 = moderately reduced, 3 = absent.

## **5.4.10 Analysis**

### **5.4.10.1 Assessment of segmental improvement**

The following MRI parameters were proposed as potential indicators of regional myocardial hibernation: (i) contractile reserve, defined as improved wall motion score of greater than or equal to 1 with dobutamine, (ii) reduced end-diastolic wall thickness, (iii) preserved basal perfusion, (iv) lack of contrast hyperenhancement on delayed imaging. Normal resting thallium uptake or improved uptake (> 50%) on delayed imaging was used to identify myocardial hibernation on scintigraphy. Receiver operator characteristic (ROC) analysis was performed for all quantitative

parameters (ii-iv) in order to identify test cut-off values. For each tested parameter, sensitivity and specificity for prediction of segmental left ventricular recovery was determined.

#### **5.4.10.2 Prediction of improvement in ejection fraction**

Patients were divided into those in whom ejection fraction improved by  $\geq 5\%$  (group I) and those in whom it remained unchanged or had deteriorated (group II). Clinical status and parameters of myocardial perfusion in dysfunctional ROI were compared between these two groups. The proportion of dysfunctional ROI exhibiting each parameter for individual patients was determined and plotted. ROC analysis was applied to establish sensitivity and specificity of each tested parameter for the determination of individual patient benefit.

#### **5.4.11 Statistics**

Data are expressed as mean  $\pm$  standard deviation unless stated otherwise. Paired Student's *t* tests were used to compare MRI haemodynamic data and ejection fraction. Analysis of variance was used for comparison of pre-and post-operative clinical and perfusion data between groups I and II.

### **5.5 Results**

#### **5.5.1 Patient demographics**

Twenty-eight patients, 26 male and 2 female, aged  $64 \pm 6$  years were recruited into the study. Five patients had single vessel disease, 6 patients had two-vessel disease and 17 patients had triple vessel disease. Twenty-one patients had suffered myocardial infarction more than six months prior to study commencement. Ejection fraction on left ventriculography was  $38.4 \pm 9.8\%$ . Twenty-five patients underwent coronary artery bypass grafting and 3 received percutaneous angioplasty and stent implantation.

All patients completed the initial MRI assessment. The haemodynamic data from the stress MRI are displayed in Table 5.1. No unexpected responses to either stressor were seen. Seven

patients were unable to complete the post-operative examination because of the following reasons: death, 3; severe orthopnoea, 1; post-operative insertion of permanent pacemaker contra-indicating MRI, 1; hospitalization for digoxin toxicity, 1; patient withdrawal, 1. Consequently data are presented from the 21 patients that completed follow-up.

		P	SBP	DBP	MAP	P*SBP
Scan A	Rest	76 ± 14	131 ± 23	76 ± 10	94 ± 13	9930 ± 2249
	Adenosine	87 ± 11 <sup>‡</sup>	122 ± 20 <sup>‡</sup>	71 ± 10 <sup>†</sup>	88 ± 13 <sup>‡</sup>	10547 ± 2190*
	Dobutamine	96 ± 17 <sup>‡</sup>	138 ± 30	73 ± 14	95 ± 17	13035 ± 2777 <sup>‡</sup>
Scan B	Rest	71 ± 10	132 ± 31	77 ± 11	95 ± 17	9436 ± 2764
	Adenosine	82 ± 12 <sup>‡</sup>	125 ± 24	72 ± 11 <sup>†</sup>	89 ± 14*	10284 ± 2688

*Table 5.1. Change in haemodynamic parameters in response to adenosine and dobutamine stressors. P = pulse; SBP = systolic blood pressure; DBP = diastolic blood pressure; MAP = mean arterial pressure; P\*SBP = rate-pressure product. \*p < 0.05, †p < 0.01, ‡p < 0.001.*

### 5.5.2 Revascularization

The total number of coronary artery territories available for evaluation was 63 (21 x 3). Forty-nine (77.7%) of these had significant stenotic disease. 41/49 (84.8%) territories were revascularized. Thirty-eight (92.7%) were surgically grafted (left internal mammary artery, 13; radial artery, 2; saphenous vein grafts, 23). Three (7.3%) vessels underwent percutaneous coronary artery angioplasty and stenting. Of the 8 diseased vessels not revascularized, 2 were small non-dominant right coronary arteries and 6 were determined to be unsuitable for grafting at operation because of small calibre or presence of diffuse inoperable disease.

### 5.5.3 Identification of potential parameters of myocardial hibernation

Parameters of contractile reserve (Figure 5.1a) and thallium scintigraphy were evaluated for all imaging planes. Of 798 ROI, 345 (43.2%) showed severe contractile dysfunction (wall motion scores 3 - 5). Of these 137 (39.7%) showed improved function on post-operative assessment. Dobutamine cine MRI data were available for 328 (95.1%) dysfunctional ROI of which 133

(40.6%) demonstrated recovery. 5% of data were lost because of poor image quality. On thallium scintigraphy, 307 (88.9%) ROI with dysfunction were evaluated (1 patient failed to attend) of which 128 (41.7%) showed improved contractile function.

Quantitative MRI parameters, i.e. end-diastolic wall thickness and delayed hyperenhancement (Figure 5.1b), were assessed on the short axis slices. Of 504 ROI, 213 (42.3%) were dysfunctional of which 86 (40.4%) showed recovery. End-diastolic wall thickness data were assessable in 201 (98.6%) dysfunctional ROI, of which 85 (40.5%) improved function. Delayed hyperenhancement data were available for 200 (93.8%) dysfunctional ROI, of which 84 (42%) demonstrated recovery postoperatively. Analysis of perfusion was limited to the mid-papillary slices. Resting cine images for this plane contained 77/168 (35.7%) dysfunctional ROI of which 32 (41.5%) improved postoperatively.

Construction of ROC curves for the quantitative parameters showed that the optimum cut-off values for prediction of regional myocardial recovery for end-diastolic wall thickness, delayed hyperenhancement and resting  $K_i$ , were  $\geq 6.5$  mm,  $< 40\%$  increase from baseline and  $\geq 25$  ml  $100g^{-1} min^{-1}$ , respectively.

#### **5.5.4 Prediction of segmental improvement**

Table 5.2 shows the sensitivity and specificity of the tested parameters obtained from pre-operative images for the prediction of segmental myocardial recovery. Contractile reserve appears to be the best predictor followed by end-diastolic wall thickness and delayed hyperenhancement. Sensitivities for these modalities were 77, 71 and 68% and specificities were 74, 48 and 68% respectively. Rest  $K_i$  had a high sensitivity (78%) but relatively poor specificity (42%). Thallium scintigraphy appeared to be the poorest regional determinant for identification of myocardial hibernation with a sensitivity of only 44% and specificity of 48%.

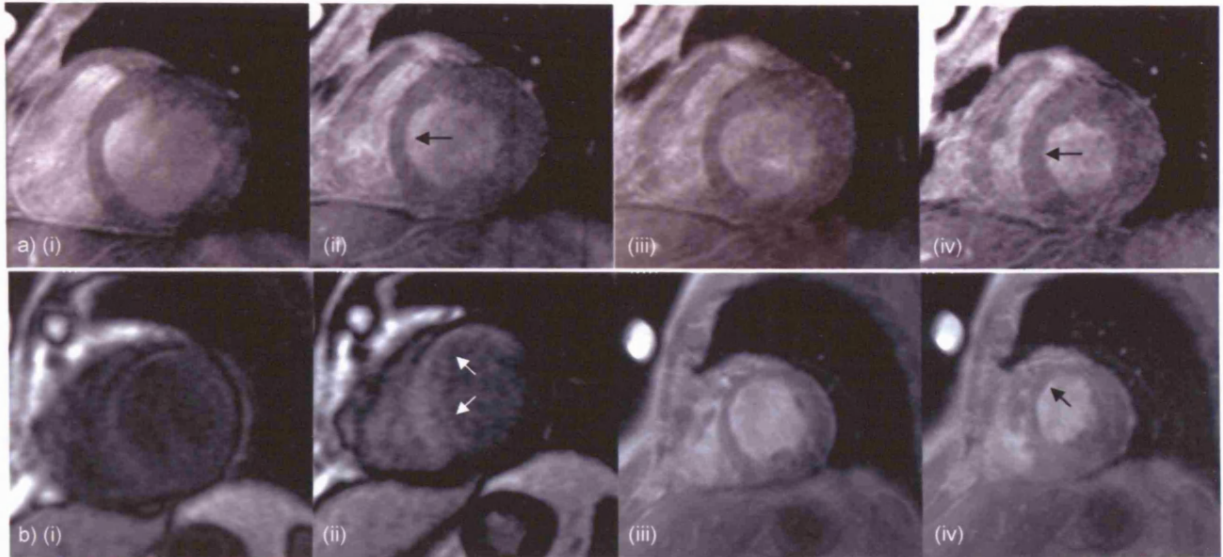


*Figure 5.1. a) Basal short axis gradient echo cine views of rest diastole (i) and systole (ii), showing septal akinesia (arrow, ii). Septal systolic function is unaffected by  $5 \mu\text{g kg}^{-1} \text{min}^{-1}$  dobutamine (iii) but a contractile reserve is demonstrated with a higher inotrope dose (arrow, iv). Note the preserved wall thickness of the akinetic area. B) Apical short axis view demonstrating delayed contrast hyperenhancement of the anteroseptal walls (ii, arrows) compared with pre-contrast images (i). The cine images (iii, diastole, iv, systole) show this area to be thin-walled and akinetic (arrow, iv) in contrast to the inferolateral walls.*

Parameter		Recovery		Sensitivity	Specificity
		+	-	(%)	(%)
<b>CR (Score &gt; 1)</b>	+	102	52	76.7	73.5
	-	31	143	(68.8 – 83.1)	(66.7 – 79.0)
<b><sup>201</sup>Tl (Normal or delayed)</b>	+	57	97	44.5	48.1
	-	71	90	(36.2 – 53.2)	(41.1– 55.3)
<b>EDWTH (<math>\geq 6.5</math> mm)</b>	+	60	37	70.1	68.1
	-	25	79	(60.2 – 79.2)	(59.2 – 75.9)
<b>DHE (&lt; 40% increase)</b>	+	57	51	67.9	56.0
	-	27	65	(57.3 – 76.9)	(47.0 – 64.7)
<b>Rest <math>K_i</math> (<math>\geq 25</math> ml <math>100g^{-1}</math> <math>min^{-1}</math>)</b>	+	21	19	77.8	42.4
	-	6	14	(59.2 – 89.4)	(27.2 – 59.2)

*Table 5.2 Sensitivity and specificity tables (with 95% confidence intervals) for contractile reserve (CR), thallium scintigraphy (<sup>201</sup>Tl), end-diastolic wall thickness(EDWTH), delayed hyperenhancement (DHE) and rest  $K_i$  for the prediction of segmental myocardial recovery following revascularization.*

### 5.5.5 Prediction of global improvement and clinical outcome

The pre-operative ejection fraction for the 21 patients that completed follow-up was  $37.6 \pm 10.3\%$ . Ten patients (group I) showed improved ejection fraction  $\geq 5\%$ , ( $32.2 \pm 15.1\%$  to  $43.9 \pm 12.6$ ,  $p < 0.01$ ). In 11 patients (group II), ejection fraction did not change or declined ( $33.7 \pm 12.9\%$  to  $27.2 \pm 10.2\%$ ,  $p < 0.01$ ).

Both groups I and II demonstrated benefit in angina status following revascularization. However, symptoms of dyspnoea were only significantly improved in Group I patients (Table 5.3). There was no significant difference in rest  $K_i$  between the groups either at baseline or follow-up in dysfunctional ROI or in stress  $K_i$  pre-operatively. However, following revascularization, stress  $K_i$  improved significantly in group I ( $p < 0.05$ ) but not in Group II (Table 5.3). This was reflected in a trend towards improvement in MPRI but this did not achieve statistical significance.

Parameter	Group I		Group II	
	Visit A	Visit B	Visit A	Visit B
NYHA CP	2.5 ± 1.4	1.4 ± 0.9*	2.2 ± 0.9	1.2 ± 0.6*
NYHA SOB	2.5 ± 1.0	1.2 ± 0.4 <sup>‡</sup>	2.3 ± 0.6	2.0 ± 0.8
Rest K <sub>i</sub>	40.0 ± 35.7	38.4 ± 20.9	46.1 ± 29.9	47.5 ± 33.6
Stress K <sub>i</sub>	36.1 ± 19.5	58.0 ± 30.6*	48.4 ± 22.1	51.6 ± 23.7
MPRI	1.54 ± 1.53	1.81 ± 1.02	1.51 ± 0.86	1.63 ± 1.22

*Table 5.3. Change in symptom status for angina (CP) and dyspnoea (SOB) following revascularization according to New York Heart Association (NYHA) criteria and perfusion parameters for dysfunctional regions of interest for groups I and II. MPRI = myocardial perfusion reserve index. Units for K<sub>i</sub> values are ml 100g<sup>-1</sup> min<sup>-1</sup>. \*p < 0.05, †p < 0.01, ‡p < 0.001.*

The success of the examined parameters in predicting overall improvement in ejection fraction in individual patients is shown in Figure 5.2. There was considerable partitioning of the groups for all parameters except resting K<sub>i</sub>. Possible criteria extracted from ROC analysis of these data can be proposed as indicators that an individual patient would benefit from revascularization (Table 5.4). The majority of patients that demonstrated improvement in ejection fraction had more than 35% dysfunctional ROI demonstrating contractile reserve. Preserved diastolic wall-thickness is required to be present in over 80% of dysfunctional ROI before it becomes a useful predictor of individual improvement. The presence of hyperenhancement in more than 50% of dysfunctional ROI appears to be a possible criterion for lack of individual patient benefit. No cut-off level for individual benefit is apparent from the resting perfusion data. Thallium scintigraphy suggests that all segments need to be recognized as viable in order to reasonably predict global left ventricular recovery.

Three patients died from post-operative pump failure. Their data are also illustrated in Figure 5.2. All had parameters that fell below the proposed criteria. No operative benefit in terms of improved left ventricular function or clinical status would have been predicted in these subjects.

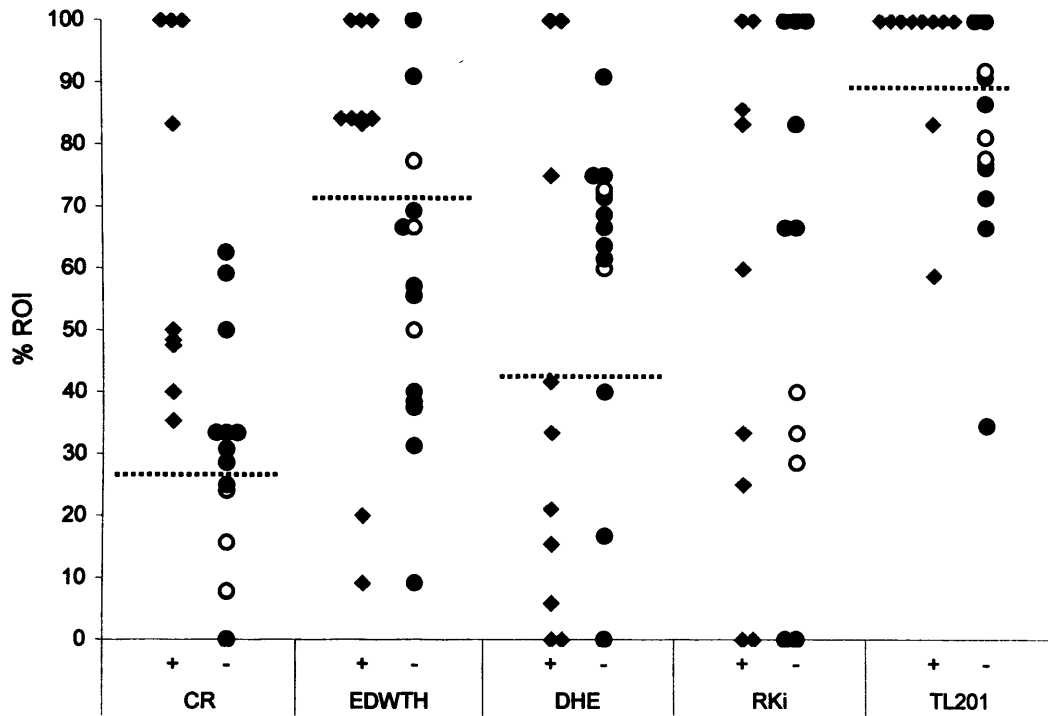


Figure 5.2. Percentage of dysfunctional regions of interest (% ROI) for each individual patient positive for each test parameter plotted against recovery (+) or no recovery (-) of ejection fraction following revascularization. CR = contractile reserve; EDWTH = end-diastolic wall thickness; DHE = delayed hyperenhancement;  $RK_i$  = rest  $K_i$ ; TL201 = rest/redistribution thallium scintigraphy. Suggested criteria for an individual patient that would indicate successful surgery for an individual patient for the varying parameters (except rest  $K_i$ ) are indicated by dotted lines. Open circles indicate post-operative deaths.

Parameter	% myocardium parameter positive	Sensitivity	Specificity	Specificity including deaths
CR	> 35%	100.0 (70.1– 100.0)	72.8 (43.4 – 90.3)	78.6 (52.4 – 92.4)
<sup>201</sup> Tl	100%	80.0 (49.0-94.3)	80.0 (52.3 – 94.9)	84.6 (60.0 – 96.0)
EDWTH	> 80%	80.0 (39.7-89.2)	81.8 (43.4 – 90.3)	85.6 (52.4 – 92.4)
DHE	> 50%	70.0 (49.0-94.3)	72.7 (43.4 – 90.3)	78.6 (57.8 – 95.7)

*Table 5.4. Sensitivities and specificities (with 95% confidence intervals) for individual patient recovery of ejection fraction based on identification of contractile reserve (CR) in more than 35%, end-diastolic wall thickness (EDWTH)  $\geq$  6.5 mm in > 80%, delayed hyperenhancement (DHE) increase in  $R_1 < 40\%$  in > 50% and identification of viability by delayed/rest thallium scintigraphy (<sup>201</sup>Tl) of 100% of dysfunctional regions of interest. Specificity is also given inclusive of post-operative deaths.*

## 5.6 Discussion

Previous studies have reported MRI parameters that may predict segmental recovery or global improvement in cardiac function following revascularization (Baer *et al.*, 1995; Kim *et al.*, 1996; Baer *et al.*, 1996b; Di Carli *et al.*, 1998; Watzinger *et al.*, 2001). This study is distinctive in that MRI parameters of contractile reserve, end-diastolic wall thickness and delayed hyperenhancement have been demonstrated to be not only predictive of segmental myocardial functional recovery, but also been translated into predictive parameters of clinical and functional benefit on an individual patient basis. MRI parameters are also demonstrated to be superior to thallium scintigraphy in predicting segmental recovery and at least equivalent in predicting global improvement following revascularization. The validity of the analysis is supported by the observation that there was a demonstrable increase in myocardial blood flow under stress in dysfunctional ROI in individuals in whom there was an improvement in ejection fraction.

### 5.6.1 Contractile reserve

The presence of an inotrope-induced contractile reserve as an indicator of myocardial hibernation has been well documented by stress echocardiographic techniques (Cigarroa *et al.*, 1993; Armstrong & Bossone, 1997; Krahwinkel *et al.*, 1997b). There are relatively few studies evaluating dobutamine MRI (Baer *et al.*, 1995; Baer *et al.*, 1996b; Baer *et al.*, 1998; Gunning *et al.*, 1999; Sandstede *et al.*, 1999; Trent *et al.*, 2000). Baer *et al.* tested single dose dobutamine-induced contractile reserve as assessed by MRI against both transoesophageal echocardiography and positron emission tomography with good agreement with both modalities (Baer *et al.*, 1995; Baer *et al.*, 1996b). These workers conducted a further study evaluating the use of this parameter to predict improvement in myocardial segments affected by myocardial infarction and subsequent revascularization of the infarction vessel (Baer *et al.*, 1998). All patients had revascularization of the infarction-related vessel only. They found 89% sensitivity and 94% accuracy for prediction of segmental recovery and subsequent improvement of ejection fraction. Further studies obtained sensitivities of 61%, 60% and 79% and specificities of 90%, 73% and 58%, respectively for prediction of segmental recovery after revascularization with dobutamine MRI (Sandstede *et al.*, 1999; Trent *et al.*, 2000). As in this study, a potential problem in assessing parameters to predict functional improvement in patients with multi-vessel disease rather than a single infarction related artery is that not all vessels are anatomically suitable for revascularization and so specificity is adversely affected.

The sensitivities and specificities for contractile reserve and preserved end diastolic wall thickness as predictors of segmental and global myocardial recovery presented in this study are in keeping with previous reports. The finding that dobutamine MRI is more sensitive but less specific than thallium scintigraphy support previous data by Gunning *et al.* (Gunning *et al.*, 1999). For the detection of myocardial ischaemia, dobutamine MRI has been demonstrated to be superior to echocardiography primarily owing to superior image quality (Nagel *et al.*, 1999). Larger

comparative studies are needed to determine whether dobutamine MRI may similarly be more successful in the prediction of left ventricular recovery than stress echocardiography.

### **5.6.2 Delayed hyperenhancement**

Delayed hyperenhancement is a relatively new MRI technique that is likely to prove an accurate means with which to identify scar tissue (Kim *et al.*, 1999; Fieno *et al.*, 2000; Choi *et al.*, 2001; Simonetti *et al.*, 2001). Animal work has demonstrated that delayed contrast hyperenhancement imaging accurately reflects acute or remote infarction size as confirmed by *ex vivo* analysis. Conversely, myocardium that is stunned by transient ischaemia without infarction demonstrates no delayed contrast hyperenhancement (Kim *et al.*, 1999; Fieno *et al.*, 2000). These findings have also been validated in human subjects following acute infarction (Choi *et al.*, 2001; Simonetti *et al.*, 2001). In patients with remote myocardial infarction, Klein *et al.* demonstrated that contrast enhanced imaging showed excellent agreement with positron emission tomography determination of viability (Klein *et al.*, 2002). Following revascularization of patients with either acute or chronic MI, the transmural extent of myocardium demonstrating hyperenhancement was the best predictor for return in contractile function post revascularization (Kim *et al.*, 2000; Choi *et al.*, 2001).

The results are in keeping with these findings. In this study only moderate sensitivity and specificity for the identification of post-operative segmental recovery was obtained. However, with application of the criterion stated for prediction of global recovery, these values improved but still remained lower than previously reported (Kim *et al.*, 2000). The cut-off value that we obtained was in keeping with results obtained in the volunteers presented in Chapter 3 (Section 3.5.2.2.3). At present differing techniques for contrast administration and image acquisition have been proposed. The methodology that we used was suboptimal for assessment of delayed hyperenhancement but allowed concurrent acquisition of first pass perfusion data for this research protocol. A higher contrast agent dose and employment of an image acquisition sequences available on a higher specification imager, such as that described by Simonetti *et al.*, is likely to provide a greater

diagnostic accuracy (Simonetti *et al.*, 2001). Multi-centre studies in larger groups of patients are necessary to fully determine the potential of this modality.

### **5.6.3 Resting perfusion**

The presence of preserved basal perfusion as an indicator of segmental recovery is in keeping with positron emission tomography data (Gewirtz *et al.*, 1994). The cut-off level identified for resting  $K_i$  is just below the level of basal perfusion obtained with this method in normal volunteers (Larsson *et al.*, 1996; Fritz-Hansen *et al.*, 1998; Cullen *et al.*, 1999b). This parameter proved to be a relatively poor indicator of myocardial recovery and was also limited to the mid-papillary slice by the labour intensity of analysis. Development of more accurate automated software will increase the availability of quantitative analytical techniques and also extend perfusion assessment to the subendocardial layer.

### **5.6.4 Thallium scintigraphy**

Thallium scintigraphy was the least accurate predictor of segmental myocardial recovery. The data suggest that all dysfunctional myocardial segments need to be positively identified as consisting of potentially viable tissue in order for individual benefit to be predicted. A recognized problem with this modality is lack of specificity for identification of tissue viability (Haque *et al.*, 1995). This is owing to relatively poor spatial resolution giving rise to failure to accurately delineate subendocardial infarction.

### **5.6.5 Clinical outcome**

Prediction of recovery of individual ROI is only useful when the data can be combined to predict likely improvement in ejection fraction and ultimate clinical benefit. There has been little attempt to determine the amount of myocardium required to be identified as hibernating in order to predict global left ventricular recovery on an individual patient basis. In this study, criteria for several parameters are provided that would indicate a successful clinical outcome. Of the

parameters, contractile reserve seems to be the most sensitive. This is reflected by the requirement of only 35% of dysfunctional myocardium needing to be positive for this parameter to translate into clinical benefit. This is compared with 50% for delayed hyperenhancement, 80% for preserved end-diastolic wall thickness and 100% for thallium scintigraphy.

The fact that the unselected study population could be divided into two groups with respect to change in post-intervention left ventricular function highlights the need for pre-operative assessment prior to revascularization procedures. The risk of surgery in this group of patients is further illustrated by an overall mortality rate of 10.7% (3/28 subjects). If revascularization had been performed solely with the purpose of prognostically improving ejection fraction rather than alleviating symptoms of angina, 50% of the patients could have been exposed to procedural risks unnecessarily. This is reflected in lack of improvement in symptoms of dyspnoea or in successful restoration of perfusion to dysfunctional ROI in the patients in group II. It should be noted that there was no difference in pre-operative ejection fraction between groups I and II indicating that this was not responsible for the difference in outcome and by itself not a useful predictive factor. While lack of improvement in ejection fraction could perhaps be tolerated, especially when there is mixed indication for revascularization that includes angina, it is of course essential to avoid peri-operative mortality. When data from the three patients who died are examined, it can be seen that for studied parameters, they could all be predicted to show no recovery with revascularization with the proposed criteria (Figure 5.2).

Inevitably development of criteria and cut-off values placed some patients inaccurately as having the potential to gain clinical benefit from revascularization (Figure 5.2). More detailed analysis of these patients revealed that in these subjects less than 50% of the dysfunctional ROI could be revascularized. If full revascularization had been possible, it is likely that higher specificities for each modality would have been obtained. This observation highlights the need to consider the MRI findings in combination with angiographic data and feasibility of revascularization.

There are several further issues that need to be considered in the application of these data. First, validation of the findings and the criteria developed are required in larger populations, ideally performed as multi-centre studies with standardized protocols. Second, analysis of the quantitative parameters is moderately labour intensive. Fortunately, the parameter with the best characteristics (contractile reserve) can be rapidly appreciated from visual image inspection. However, a limitation of this technique is that patients with significant left ventricular dysfunction prone to ventricular dysrhythmias are unsuitable for study because of potential safety issues within the magnet bore. Finally, there are developments in MRI that may improve the applicability of some of the criteria. In particular, the recently published optimized technique for delayed hyperenhancement image acquisition is likely to significantly improve diagnostic accuracy of MRI for the assessment of myocardial hibernation (Simonetti *et al.*, 2001).

## **5.7 Conclusion**

Several MRI parameters have moderate to high sensitivities and specificities for the prediction of regional left ventricular recovery post revascularization. These can be translated into prediction of improvement of ejection fraction and symptoms of cardiac dysfunction, on an individual basis. In addition, it may be possible to readily identify patients with a high risk of poor peri-operative outcome. An optimized MR examination possibly consisting of evaluation of contractile response to dobutamine, end diastolic wall thickness and assessment of delayed hyperenhancement could be a strong competitor to radionuclide and echocardiographic techniques for the detection of myocardial hibernation. It may succeed current imaging techniques because of the ability to concurrently perform assessment of myocardial perfusion and performance.

---

## **Chapter 6**

# **Restoration of myocardial blood flow following percutaneous balloon dilatation and stent implantation**

---

## **6.1 Introduction**

In Chapter 4, quantitative and qualitative methods of analyzing MRI first pass perfusion data were evaluated to determine their diagnostic accuracy for the presence of angiographically significant coronary artery disease. Since perfusion MRI is a non-invasive technique and requires no ionizing radiation for image acquisition, it is an ideal modality for serial imaging. The ability to identify changes in myocardial perfusion over time would be of clinical value in patient assessment following revascularization procedures, e.g. percutaneous angioplasty or coronary artery bypass surgery. There are few published reports describing sequential perfusion imaging with MRI (Manning *et al.*, 1991; Lauerma *et al.*, 1997).

## **6.2 Hypothesis**

Changes in myocardial perfusion following revascularization with PTCA occur early after the procedure and can be assessed by serial stress first pass contrast enhanced MRI. Improvements in perfusion can be detected by both quantitative and qualitative image reporting techniques.

## **6.3 Objectives**

The objectives of this study were:

1. to determine whether serial adenosine stress first pass contrast-enhanced MRI is able to detect regional changes in myocardial perfusion following percutaneous coronary angioplasty and direct stent implantation in patients with single vessel coronary artery disease;
2. to evaluate use of quantitative and qualitative image analytical techniques for the detection of any perfusion changes seen.

## **6.4 Methods**

### **6.4.1 Study design**

Nine consecutive patients attending for elective percutaneous balloon dilatation and direct stent implantation were recruited. Inclusion criteria were the presence of angiographic single vessel disease (Section 2.3.2) that was suitable for percutaneous revascularization, and exercise electrocardiography suggestive of myocardial ischaemia. Adenosine stress and rest first pass contrast-enhanced MRI was performed to assess myocardial perfusion within 7 days prior to revascularization (visit A), within 7 days following the procedure (visit B), and 6 months later (visit C). A clinical assessment was performed at each visit (Section 2.2).

### **6.4.2 Revascularization**

Standard diagnostic coronary angiography was performed (Section 2.3). Revascularization of the target vessel was achieved with conventional balloon dilatation and stent implantation techniques. Balloon inflation numbers and pressures were operator-determined according to angiographic results. In addition to established medication, all patients received 300 mg aspirin, 300 mg clopidogrel, a heparin bolus ( $100 \text{ units kg}^{-1}$ ) immediately prior to the procedure, continued aspirin ( $150 \text{ mg day}^{-1}$ ) and a one month regime of clopidogrel ( $75 \text{ mg day}^{-1}$ ).

### **6.4.3 Analysis of angiographic data**

Angiograms were analyzed quantitatively before and after PTCA by an experienced cardiologist, blinded to MRI perfusion data to determine acute stent gain (Section 2.3.3).

### **6.4.4 Magnetic resonance imaging**

First pass contrast-enhanced magnetic resonance was performed during adenosine stress and at rest at each visit (Section 2.5). Myocardial perfusion parameters were evaluated with the use of quantitative and qualitative image analytical techniques. The unidirectional transport coefficient for

gadodiamide over the capillary membrane,  $K_i$ , was calculated for each ROI (Section 2.5.4). Stress/rest  $K_i$  ratios were calculated to give an index of myocardial perfusion reserve (MPRI) for each ROI. Correction for the extraction fraction of gadodiamide over the capillary membrane,  $E$ , was applied. An experienced radiologist, blinded to clinical and angiographic data, performed qualitative image analysis (Section 2.5.5).

#### **6.4.5 Collation of MRI and angiographic data**

MRI ROI were then assigned to the appropriate supplying coronary artery territory according to the angiogram report (Section 2.9).

#### **6.4.6 Statistics**

A paired Student's  $t$  test was used to evaluate haemodynamic and angiographic parameters. An unpaired Student's  $t$  test was used to compare remote and target vessel quantitative parameters. Analysis of variance was used to assess quantitative MRI data between the three visits. Data are presented as mean  $\pm$  SD except for qualitative MRI data. The latter is expressed as mean (- 95% - + 95%) confidence intervals for proportions. The number of ROI for each qualitative perfusion category was expressed as a proportion of the total number of ROI supplied by the relevant subtending vessel. Chi-squared test was used to determine the statistical significance of qualitative data change.

## 6.5 Results

### 6.5.1 Patient demographics

Three patients were withdrawn from the study following the initial scan because of the following reasons: patient withdrawal at visit B (n = 1); clinical decision not to proceed with revascularization at time of scheduled PTCA (n = 2). Data are consequently presented for the 6 patients that completed the study protocol.

Patient demographics are shown in Table 6.1. Mean age was 57 (range 41 - 69) years, and mean body mass index was 29 (range 25.9 – 32.6). All patients had grade 2 or 3 symptoms of angina.

Sex	Age	BMI	Angiographic EF	Target vessel for PTCA	NYHA CP/ SOB		
					Visit A	Visit B	Visit C
M	54	25.9	No EF	LAD	2 / 1	0 / 0	0 / 0
M	41	32.7	75	Cx	3 / 1	0 / 0	0 / 0
M	46	26.1	71	LAD	3 / 1	0 / 0	3 / 0
M	69	29.4	75	RCA	3 / 1	0 / 0	0 / 0
M	64	29.3	No EF	LAD	2 / 2	0 / 0	0 / 0
F	67	30	No EF	Cx	3 / 3	0 / 0	0 / 0

*Table 6.1. Demographics of patients completing study protocol. BMI = body mass index. Initial and follow-up symptom assessment of angina (CP) and dyspnoea (SOB) according to New York Heart Association criteria (NYHA), and the target vessel for revascularization (PTCA) are detailed. LAD = Left anterior descending artery; Cx = circumflex artery; RCA = right coronary artery; EF = ejection fraction.*

### 6.5.2 Coronary artery revascularization

All patients had successful PTCA on immediate angiographic criteria. Reference vessel diameter remained unchanged following PTCA, i.e.  $2.78 \pm 0.74$  mm (A) and  $2.69 \pm 0.26$  mm (B). Minimal luminal diameter increased from  $0.5 \pm 0.51$  mm (A) to  $2.82 \pm 0.52$  mm (B,  $p < 0.001$ ). Acute stent gain was  $87 \pm 13$  %.

### 6.5.3 Clinical outcome

All patients reported resolution of ischaemic symptoms at visit B. This improvement was still maintained at visit C except for one patient, who reported recurrence of grade 3 angina (Table 6.1). Data from this subject were not included in visit C analysis but are presented separately.

### 6.5.4 Magnetic resonance imaging

All patients completed the scan protocol. No adverse events occurred and there were no unexpected responses to adenosine. Heart rate increased ( $p < 0.001$ ) whereas systolic, diastolic and mean arterial blood pressure all decreased during the infusion ( $p < 0.05$ ,  $p < 0.01$  and  $p < 0.01$ , respectively, Table 6.2).

Parameter	P	SBP	DBP	MAP
Rest	63 ± 11	129 ± 11	74 ± 8	95 ± 8
Adenosine	79 ± 18 <sup>‡</sup>	119 ± 18*	67 ± 11 <sup>†</sup>	84 ± 12 <sup>†</sup>

Table 6.2. Change in haemodynamic parameters in response to adenosine stress. P = pulse; SBP = systolic blood pressure; DBP = diastolic blood pressure; MAP = mean arterial pressure. \* $p < 0.05$ , <sup>†</sup> $p < 0.01$ , <sup>‡</sup> $p < 0.001$ .

### 6.5.5 Image analysis

#### 6.5.5.1 Quantitative analysis

Quantitative MRI data are presented in Table 6.3. At visit A, stress  $K_i$  and MPRI were higher in remote vessel territories than in those supplied by stenotic arteries ( $p < 0.01$  and  $p < 0.05$ , respectively). Following revascularization at visit B, in stented ROI there was an increase in both stress  $K_i$  ( $p < 0.001$ ) and MPRI ( $p < 0.001$ ) to values similar to those seen in remote ROI (Figure 6.1). This was maintained at visit C. Perfusion parameters remained unchanged in the remote ROI over time. Relaxation rate time curves and derived regional perfusion values are illustrated in Figure 6.1. Perfusion parameters and images from the patient presenting late with in-stent restenosis are depicted in Figure 6.2 and Figure 6.3.

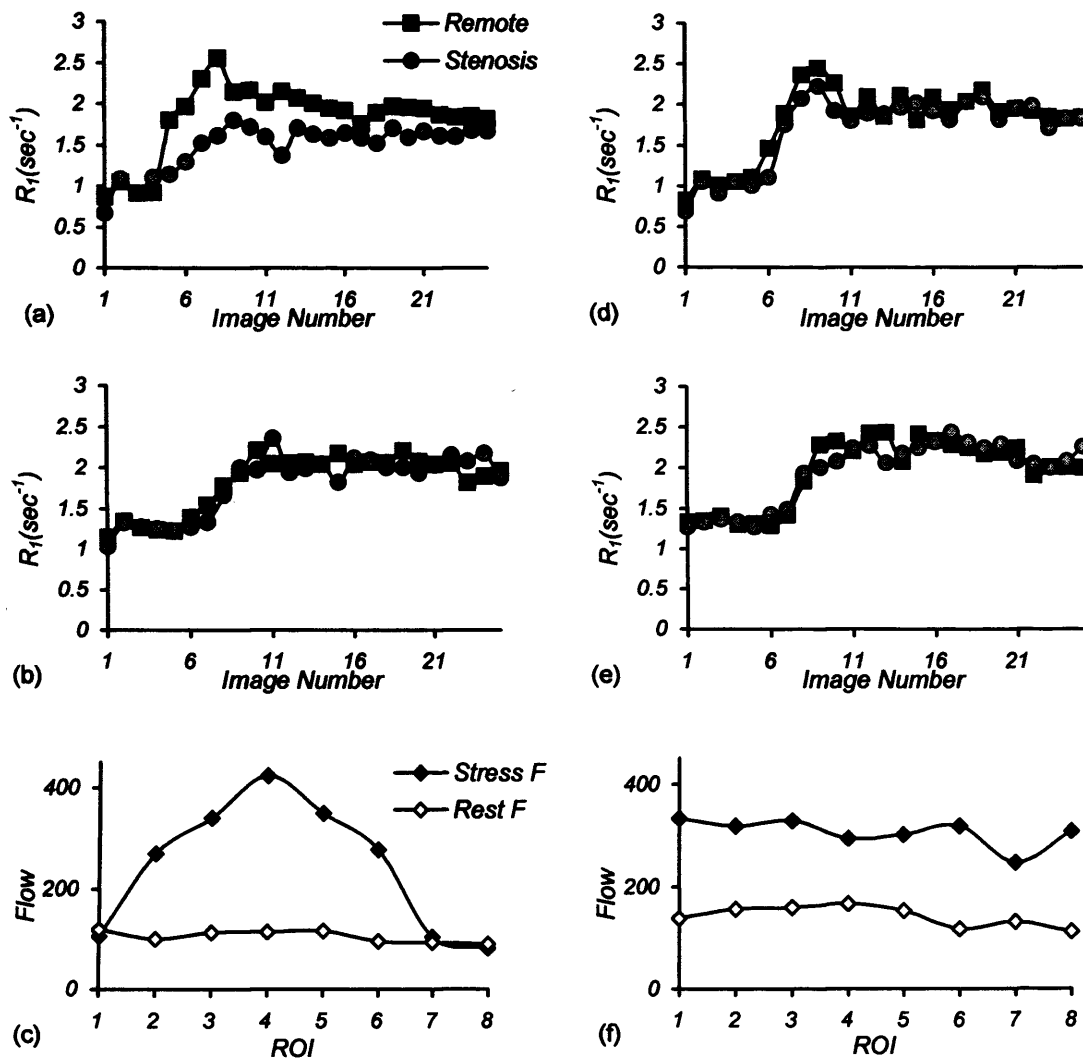


Figure 6.1. Longitudinal relaxation rate ( $R_1$ ) time curves during adenosine stress (a, d), at rest (b, e) and calculated myocardial blood flow ( $F$ ; c, f) for remote and stenosed regions of interest (ROI) pre (a, b, c) and post (d, e, f) PTCA to circumflex artery. Pre-PTCA, a delayed and lower peak  $R_1$  is seen during adenosine in the stenosed area (a). Reduced myocardial blood flow during stress is seen in ROI supplied by the diseased circumflex vessel (c, ROI 1, 7, 8). Following revascularization the stress  $R_1$  time curve is similar to that seen in the remote ROI (d) and there is a consequent increase in myocardial blood flow during stress and thus myocardial perfusion reserve index in the stented ROI (f, ROI 1, 7, 8). Resting  $R_1$  time curves (b, e) and resting myocardial flow values (c, f) are similar pre and post procedure.

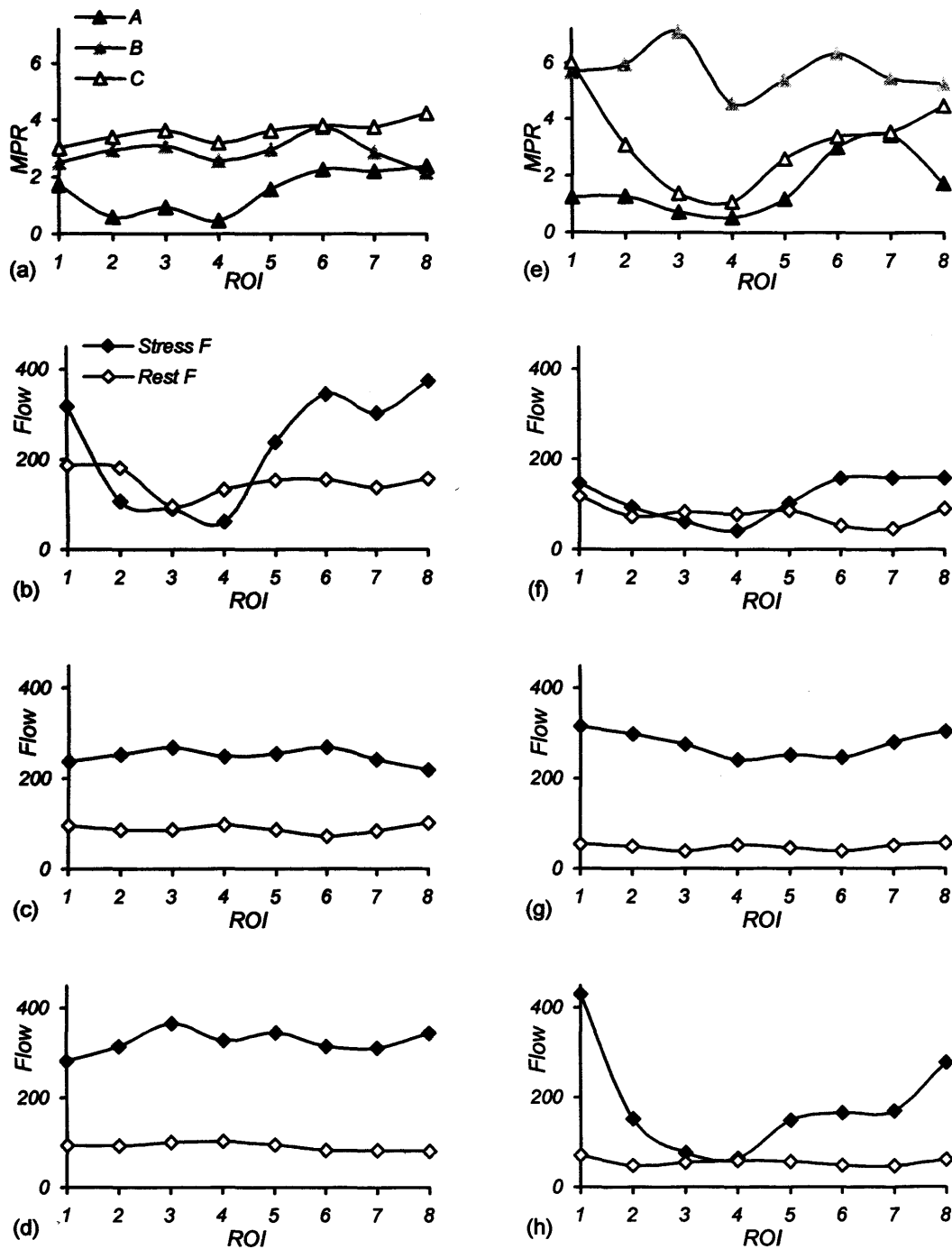
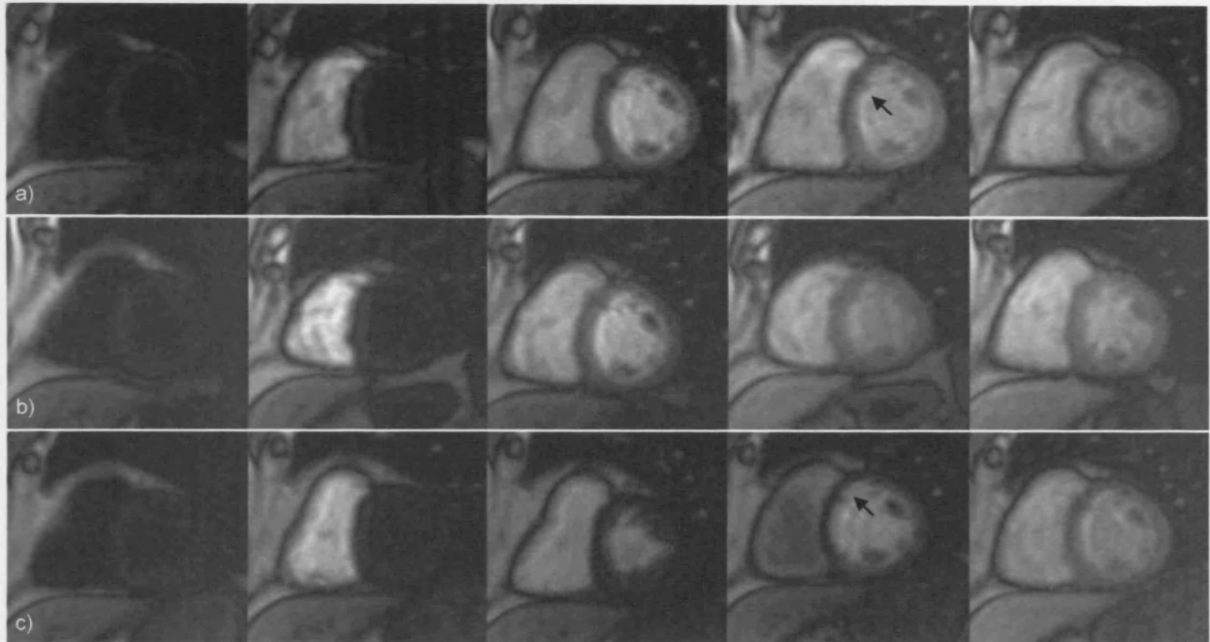


Figure 6.2. Myocardial perfusion reserves (MPR) (a, e) derived from stress and rest myocardial flow for visits A (b, f), B (c, g) and C (d, h) from 2 patients undergoing PTCA to left anterior descending artery. Flow during stress is particularly reduced in regions on interest (ROI) 2 - 4 (anteroseptum) at visit A (b, f) but shows improvement at visit B (c, g). However, the patient on the left shows continued improvement at visit C (d). The second patient (right) represented with further angina and shows marked deterioration in stress flow at visit C (h). In-stent restenosis was confirmed angiographically. These changes are reflected in MPR.



*Figure 6.3. First pass contrast enhanced perfusion image sequences acquired during adenosine stress pre (a), 1 week (b) and six months post PTCA (c) to left anterior descending artery. The anteroseptal perfusion defect seen in the pre-PTCA images (arrow, a) resolves immediately after PTCA. The recurrence of the defect (arrow, c) at six months was confirmed clinically and angiographically to be a result of in-stent restenosis.*

Territory	Visit	Stress $K_i$	Rest $K_i$	MPRI	Stress F	Rest F	MPR
Remote	A	88.6 ± 44.9 <sup>†</sup>	42.3 ± 19.4	2.47 ± 1.75*	221.5 ± 112.3	84.6 ± 38.8	3.09 ± 2.18
Remote	B	100.3 ± 28.3	38.5 ± 19.8	2.94 ± 1.08	250.8 ± 70.7	77.0 ± 39.6	3.68 ± 1.35
Remote	C	99.7 ± 46.7	46.8 ± 21.8	2.52 ± 1.46	249.3 ± 116.8	93.6 ± 43.5	3.15 ± 1.83
Stenosis	A	49.3 ± 23.5	49.2 ± 19.5	1.23 ± 1.06	123.2 ± 58.8	98.3 ± 38.9	1.54 ± 1.32
Stented	B	93.3 ± 31.8 <sup>‡</sup>	35.9 ± 13.2	2.78 ± 1.19 <sup>‡</sup>	233.2 ± 79.5	71.9 ± 26.5	3.48 ± 1.5
Stented	C	93.1 ± 68.8	42.8 ± 23.1	2.42 ± 2.04	232.8 ± 169.5	85.6 ± 46.1	3.03 ± 2.55

Table 6.3. Mean ± SD stress and rest  $K_i$  ( $ml\ 100g^{-1}\ min^{-1}$ ), estimate of flow (F) during stress and rest ( $ml\ 100g^{-1}\ min^{-1}$ ), myocardial perfusion reserve index (MPRI) and estimate of absolute myocardial perfusion reserve (MPR). Data are presented for remote regions of interest and those originally supplied by stenosed arteries from the mid-papillary short axis for each patient visit. \* $p < 0.05$ , <sup>†</sup> $p < 0.01$ , <sup>‡</sup> $p < 0.001$  vs. stenosis.

#### 6.5.5.2 Qualitative analysis

Qualitative MRI data are shown in Table 6.4. Reporting time was on average 10 minutes per patient. At visit A, there was a greater proportion of ROI demonstrating normal perfusion in remote territories than in the stenosed ROI ( $\chi^2 = 10.59$ ,  $p < 0.001$ ). Conversely, a significantly higher

Territory	Visit	Normal ROI	Reversible ROI	Fixed ROI
Remote	A	77.4 (67.9 - 84.7) <sup>‡</sup>	22.6 (15.3 - 32.1)	0.0 (0.0 - 4.0)
Remote	B	84.9 (76.3 - 90.8)	15.1 (9.20 - 23.7)	0.0 (0.0 - 4.0)
Remote	C	89.2 (81.3 - 91.4)	9.70 (5.20 - 17.4)	1.30 (0.20 - 6.90)
Stenosis	A	51.0 (37.7 - 61.4)	47.1 (34.1 - 60.5)	1.96 (0.30 - 10.3)
Stented	B	74.5 (61.1 - 84.5) <sup>†</sup>	23.5 (14.0 - 36.8)	1.96 (0.30 - 10.3)
Stented	C	84.3 (72.0 - 91.8) <sup>‡</sup>	13.7 (6.80 - 25.7)	0.0 (0.0 - 8.40)

Table 6.4. The proportion of ROI/total ROI for each coronary artery demonstrating normal perfusion, reversible or fixed perfusion deficits (expressed as mean with ± 95% confidence intervals for proportions) for remote territories and those supplied by stenosed / stented arteries as reported by visual rating. \* $p < 0.05$ , <sup>†</sup> $p < 0.01$ , <sup>‡</sup> $p < 0.001$  vs. stenosis.

incidence of ROI with reversible perfusion deficits was seen in coronary territories supplied by stenosed arteries. Following revascularization, in stented coronary artery territories there was an increased number of ROI demonstrating normal perfusion ( $\chi^2 = 6.04$ ,  $p < 0.01$ ) and a reduction in the incidence of reversible ischaemia to parameters similar to those seen in remote vessels (Figure 6.4). This difference was maintained at visit C ( $\chi^2 = 14.52$ ,  $p < 0.001$ ). No significant differences in perfusion parameters were seen in remote territories.

## 6.6 Discussion

Detection of coronary artery stenosis and early improvement of perfusion after PTCA was seen with both qualitative and quantitative reporting methods. These results are in keeping with perfusion changes following percutaneous revascularization as assessed with angiographic criteria, scintigraphy and positron emission tomography (Haude et al., 1996; Versaci et al., 1996; Kosa et al., 1999). Perfusion parameters improved following PTCA on stress imaging compared with rest. This was reflected in the reduction in the number of ROI exhibiting qualitative reversible perfusion deficits and in the increase in the stress  $K_i$  values seen. Both qualitative and quantitative parameters showed improvement bringing them into line with remote territories.

The presence of some residual reversible perfusion deficits following PTCA, despite normal angiographic appearances, has been reported previously (Versaci *et al.*, 1996). Since an optimal anatomical result was seen in all subjects on angiography, these findings may represent microvascular circulatory impairment associated with balloon dilatation. Potential mechanisms that have been proposed to explain this include distal abnormalities, e.g. microembolism, vessel constriction produced by a sudden increase in post-stenotic pressure following revascularization, wall damage resulting in platelet aggregation and vasoactive substance release or presence of endothelial dysfunction (Misra *et al.*, 1997; Badimon *et al.*, 1998; Kurz *et al.*, 2000).

As expected, perfusion parameters remained unchanged in remote vessels where no intervention took place. The incidence of reversible perfusion deficits within remote territories was

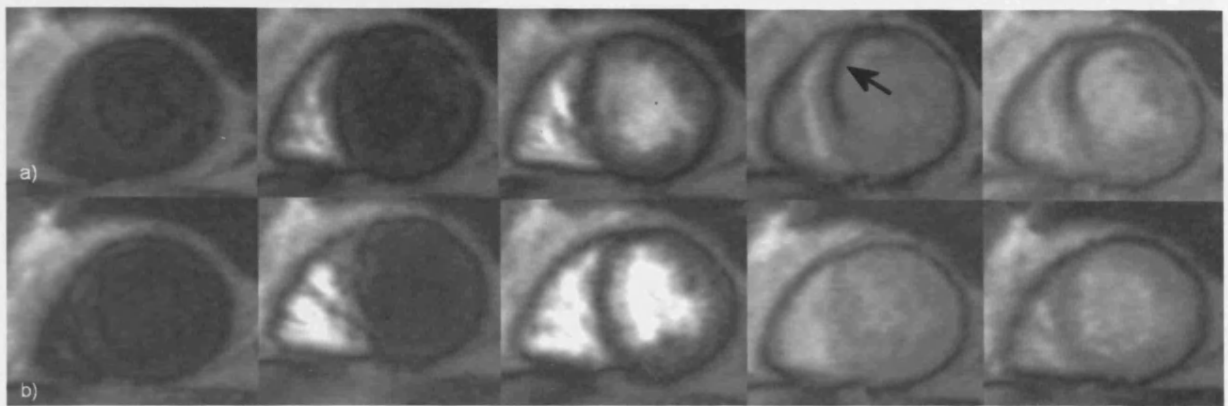


*Figure 6.4. First pass contrast enhanced perfusion image sequences acquired during adenosine stress pre (a) and post (b) PTCA to left anterior descending artery. The anteroseptal perfusion defect seen with in the pre-PTCA images (arrow) resolves after PTCA.*

relatively high. This may be because of the existence of early coronary artery dysfunction or microvascular disease that was undetectable by angiography. Impairment in coronary flow reserve has been described in remote vessels (Sambuceti *et al.*, 1993). With the use of this quantitative MRI method, Cullen *et al.* reported MPRI in normal volunteers to be  $4.21 \pm 1.16$  (Cullen *et al.*, 1999b). In contrast, in angiographically normal vessels in patients with coronary artery disease MPRI was significantly reduced to  $2.80 \pm 0.77$ . Reduced MPRI in remote territories from single vessel disease compared with normal territories in patients without any coronary artery disease was demonstrated in Chapter 4, Part I. MPRI values in the remote vessels in this study are in keeping with those previously published and support the presence of coronary endothelial dysfunction. The high spatial resolution of MRI improves visualization of the subendocardial layer where subtle perfusion abnormalities are most likely to occur. Some ROI may have been reported as abnormal because of a limitation in the method of myocardial division into 8 ROI. Although ROI were assigned to their supplying vessel as accurately as possible with the use of the Green Lane reporting system, there may have been some overlap in coronary artery territories. There is evidence that the size of perfusion beds may alter in relation to change in obstructive significance of coronary lesions following PTCA (Kaul *et al.*, 1991). This is difficult to take into account, and so allocation of ROI was kept identical on pre and post PTCA images.

Qualitative reporting is relatively quick, and can be performed immediately after image acquisition. This makes it applicable for clinical use, as it is economical on time and resources. Considerable experience is required to assess the quality of the contrast agent bolus as it arrives in the left ventricle and the subsequent flow-related myocardial signal intensity changes, and so the method may be subject to observer bias. It relies on identification of relative signal enhancement in each region of interest. Use of an inversion recovery snapshot FLASH sequence provides optimum image contrast for visual image assessment. Myocardial nulling with a  $180^\circ$  inversion prepulse enhances relatively small changes in signal intensity produced by contrast agent within the myocardium. Rarely, images acquired with this sequence may contain susceptibility artefacts

mimicking myocardial signal loss. Furthermore, lack of normally perfused regions for comparison in patients with multi-vessel disease may hinder recognition of global ischaemia.

This is the first study to demonstrate changes in  $K_i$  following a revascularisation procedure. However, serial use of quantitative techniques to measure perfusion is subject to several limitations. Quantitative analysis is extremely labour intensive because of lack of reliable myocardium detection software. Myocardial perfusion is influenced by heart rate, myocardial afterload and contractility and so varies in accordance with patient haemodynamic parameters, metabolic states and response to pharmacological interventions; these factors may well vary between examinations. Changes in intramyocardial blood volume, arterial pressure or left ventricular dysfunction induced by stressors will also affect quantitative results. A wide range of normal values for myocardial blood flow has been demonstrated with the use of positron emission tomography (Schwaiger & Hutchins, 1995) and a definite distinction between normal perfusion and ischaemia is difficult to make since parameters frequently overlap. A further complexity in identifying a normal range is that autoregulatory mechanisms governing myocardial perfusion are not homogeneous across the myocardium, giving rise to natural spatial variations of flow (Falsetti *et al.*, 1975; Bassingthwaight *et al.*, 1989; Austin *et al.*, 1990).

## 6.7 Conclusion

Both qualitative reporting and measurement of the unidirectional transfer constant of gadodiamide over the capillary membrane ( $K_i$ ) were sensitive to presence of coronary stenosis and changes in perfusion following PTCA. Qualitative analysis is quick to perform and economical for clinical use. At present, quantification of myocardial blood flow with MRI is cumbersome and limited to research applications. Any advantage over qualitative reporting needs to be established before it can be introduced into routine radiological practice.

Despite the limitations, the results suggest that serial MRI evaluation of myocardial perfusion is likely to have clinical as well as research applications, particularly with improved imager hardware

and analysis software. Perfusion imaging prior to intervention provides a functional basis for undertaking procedures and facilitates identification of target lesions for revascularization. Imaging immediately post-procedure can set a diagnostic standard for subsequent non-invasive assessment of late in-stent restenosis. Further larger clinical studies are necessary to evaluate both post-processing methods for the detection of in-stent restenosis, and longitudinal evaluation of patients following percutaneous and surgical revascularization procedures.

---

## **Chapter 7**

# **Comparison of clinical and functional effects of transmyocardial laser revascularization and thoracic sympathectomy**

---

## 7.1 Introduction

Some patients with severe coronary artery disease may not be candidates for conventional revascularization procedures, i.e. coronary bypass graft surgery or percutaneous transluminal angioplasty. Diseased vessels may be anatomically unsuitable for mechanical procedures because of small calibre or presence of diffuse disease. In patients presenting with recurrent ischaemia who have already undergone a bypass procedure, repeated cardiac surgery has increased operative risk and may be technically impossible because of native vessel disease progression. There is much interest in developing alternative forms of therapy for this type of patient. Transmyocardial laser revascularization (TMR) is a new surgical approach offered to patients with refractory angina without other interventional options.

TMR was pioneered in 1981 by Mirhoseini and Cayton (Mirhoseini & Cayton, 1981). Small transmyocardial channels are created in ischaemic territories by laser ablation. Randomized studies evaluating TMR have demonstrated relief of angina and improvement in exercise tolerance (Allen *et al.*, 1999; Burkhoff *et al.*, 1999; Frazier *et al.*, 1999; Schofield *et al.*, 1999). The cause of these beneficial effects is unclear. An attractive hypothesis is that TMR may augment myocardial perfusion by promoting angiogenesis. An increase in myocardial perfusion following TMR has been reported in animals but these results have not been consistently reproducible in clinical studies (Frazier *et al.*, 1995; Horvath *et al.*, 1997; Kohmoto *et al.*, 1998; Pelletier *et al.*, 1998; Allen *et al.*, 1999; Burkhoff *et al.*, 1999; Frazier *et al.*, 1999; Schofield *et al.*, 1999).

Thoracic sympathectomy (TS) has been reported to be an effective means with which to ameliorate angina (Claes *et al.*, 1996). This procedure involves destruction of the sympathetic chain that relays afferent nerve fibres responsible for perception of angina to the sensory cortex. Since TMR also gives rise to at least partial myocardial denervation it is possible that this mechanism may contribute to the clinical efficacy of the procedure (Kwong *et al.*, 1997; Al-Sheikh

*et al.*, 1999). At present there are no published reports comparing the clinical and functional outcomes of these two procedures.

Studies evaluating the effect of TMR on myocardial perfusion have to date been limited to nuclear modalities (Burkhoff *et al.*, 1999; Frazier *et al.*, 1999; Gruning *et al.*, 1999; Rimoldi *et al.*, 1999; Lutter *et al.*, 2000) However, the spatial resolution of both scintigraphy and positron emission tomography is insufficient to delineate the subendocardial layer of cardiac muscle. Since this is the portion of myocardium most significantly affected by ischaemia, use of these techniques may underestimate myocardial perfusion changes (Iskandrian *et al.*, 1994). Assessment with MRI may prove to be a useful modality with which to study the effects of TMR. A quantitative estimate of myocardial perfusion may be obtained and although software limitations restrict perfusion quantification to the transmural layer, visual appreciation of the subendocardium is possible (Chapters 4 and 6). In addition concurrent assessment of regional and global left ventricular function can be performed (Chapter 5).

## **7.2 Hypothesis**

Clinical benefit seen in patients undergoing TMR is associated with regional improvement in myocardial perfusion and function. TS has no effect on these regional myocardial parameters since clinical outcome is a result of cardiac denervation. Neorevascularization rather than cardiac denervation is the mechanism underlying the clinical efficacy of TMR.

## **7.3 Objectives**

The objectives of this study were:

1. to compare the efficacy of TMR and TS to alleviate myocardial ischaemia in patients with severe coronary artery disease not amenable to conventional revascularization;

2. to investigate whether either technique is associated with improvement in myocardial function or perfusion as evaluated by MRI;
3. to evaluate whether any differences seen in clinical outcome following the two procedures can shed light on the possible mechanisms underlying TMR.

## **7.4 Methods**

### **7.4.1 Study design**

Twenty consecutive patients referred and accepted by the cardiothoracic surgical department for consideration of either TMR or TS for relief of unremitting angina were recruited. Inclusion criteria were the presence of severe coronary artery disease not amenable to conventional percutaneous or surgical revascularization, ejection fraction of greater than 30% on left ventriculography and refractory symptoms of ischaemia despite optimal medical treatment. Ten patients were prospectively randomized to TMR, and the remaining ten were randomized to TS.

All patients were underwent clinical assessment (Section 2.2), formal exercise testing and dual adenosine-dobutamine MRI within two weeks prior to the elected surgical procedure and six months post-operatively.

### **7.4.2 Revascularization**

All patients received standard pre-medication and anaesthetic technique.

#### **7.4.2.1 Transmyocardial laser revascularization**

TMR was performed through a left anterolateral thoracotomy in the fifth intercostal space. A pulsed holmium: YAG laser (Cardiogenesis Corporation, Sunnyvale, California, USA, radiation wavelength 2.1  $\mu\text{m}$ , energy 2 Joules per pulse, pulse duration 350  $\mu\text{s}$ , 365  $\mu\text{m}$  flexible fibre delivery system) was used. Transmyocardial channels (2 - 3 pulses, distribution 1  $\text{cm}^2$ , diameter 1 mm, laser delivery synchronized to electrocardiographic R wave) were drilled from the epicardium

to the endocardium in anterior, lateral and inferior walls. Myocardium was visually inspected by the surgeon to ensure that only areas devoid of fibrous material, i.e. scar tissue, were lased. The site and number of channels delivered were recorded.

#### **7.4.2.2 Thoracic sympathectomy**

TS was performed via a mini left anterior thoracotomy at the level of the second intercostal space. A mediastinoscope was used to visualize the sympathetic ganglia at thoracic level 2 - 4. Ablation of the sympathetic chain was achieved by diathermy skeletonization of ganglia from the left border of the vertebral bodies and posterior thirds of the second to the fourth rib.

#### **7.4.3 Exercise electrocardiography**

A standard Bruce protocol was utilized for exercise electrocardiography. Beta-blocker medication was withheld for 48 hours prior to the test. Indications to terminate the test were symptoms of ischaemia accompanied by electrocardiographic changes, sustained arrhythmias, limiting dyspnoea or fatigue. Total exercise time in seconds was recorded.

#### **7.4.4 Magnetic resonance imaging**

The dual adenosine stress protocol was employed (Section 2.7). For comparison of regional perfusion and function parameters, regions of interest (ROI) were divided into three treatment groups:

- a. ROI receiving transmural laser channels;
- b. ROI remote from those receiving transmural laser channels (control regions to lased areas);
- c. ROI in myocardium from patients undergoing TS.

#### **7.4.4.1 Myocardial perfusion**

First pass contrast-enhanced MRI was performed during adenosine stress and at rest to assess myocardial perfusion. Each myocardial short axis slice was divided radially into 4 equal regions of interest (ROI), representing anterior, lateral, inferior and septal walls respectively (Figure 2.7c). Myocardial perfusion parameters were evaluated with the use of qualitative and quantitative image analytical techniques. The unidirectional transport coefficient for gadodiamide over the capillary membrane,  $K_i$ , was calculated for each ROI (Section 2.5.4). Stress/rest  $K_i$  ratios were calculated to give an index of myocardial perfusion reserve (MPRI) for each ROI. Correction for the extraction fraction of gadodiamide over the capillary membrane,  $E$ , was applied. An experienced radiologist, blinded to clinical and angiographic data, performed qualitative image analysis (Section 2.5.5).

#### **7.4.4.2 Delayed hyperenhancement**

In the TMR patients, the increase in regional baseline  $R_1$  values during rest imaging compared with stress was calculated to determine the presence of any delayed hyperenhancement (Section 2.5.4.7). Regional differences between initial and follow-up imaging scans for lased and non-lased ROI were compared.

#### **7.4.4.3 Myocardial function**

Functional cine imaging was acquired at rest and during a multi-step dobutamine protocol. Overall ejection fraction, left ventricular end-diastolic, end-systolic and stroke volumes were obtained at each visit (Section 2.6.4). A second independent radiologist, blinded to clinical and operative data, reported regional systolic wall thickening at rest and during dobutamine stress according to a wall motion score (Section 2.6.5.1, Table 2.8). Each myocardial ROI was characterized as being predominantly composed of normal, ischaemic or scar tissue (Section 2.6.5.2, Table 2.9).

## 7.4.5 Statistics

Data are expressed as mean  $\pm$  standard deviation. Paired Student's *t* tests were used to compare pre-and post-operative clinical data, exercise tolerance, MRI haemodynamic data and quantitative functional cine data. Two way analysis of variance was used for comparison of pre-and post-operative quantitative perfusion and delayed hyperenhancement results. Qualitative data are presented with 95% confidence intervals for proportions.

## 7.5 Results

### 7.5.1 Patient demographics

Demographic data of the two groups of patients were similar (Table 7.1).

	TMR (n = 10)	TS (n = 10)
Male:Female	8:2	8:2
Age (years)	65 $\pm$ 7.6	66 $\pm$ 5.4
Body mass index	27.4 $\pm$ 1.8	25.8 $\pm$ 3.6
Previous CABG x1, x2	7	8
Previous PTCA	3	1
Previous myocardial infarction	7	5
NYHA class angina	3.5 $\pm$ 0.8	3.2 $\pm$ 1.3

*Table 7.1. Patient demographics. TMR = transmyocardial laser revascularization; TS = thoracic sympathectomy; CABG = coronary artery bypass grafting; PTCA = percutaneous transluminal coronary angioplasty; NYHA = New York Heart Association.*

### 7.5.2 Revascularization

All operative procedures were without complication. No mortality occurred peri-operatively or during the six months follow-up. As expected, patients undergoing TMR required a longer hospital stay than those receiving TS, i.e. 6.7  $\pm$  4.2 vs. 3.6  $\pm$  1.7 days, respectively ( $p < 0.05$ ).

### 7.5.2.1 Transmyocardial laser revascularization

The mean number of lased channels per patient in the TMR group was  $42 \pm 11$ . Myocardial channels were drilled in anterior, lateral and inferior walls in 8 patients, to lateral and inferior walls in 1 patient and to the inferior wall only in 1 patient (Table 7.2).

Patient ID	Anterior wall	Lateral wall	Inferior wall
TMR1	12	10	10
TMR3	0	17	15
TMR5	24	13	11
TMR6	12	9	15
TMR7	14	12	14
TMR8	14	12	12
TMR14	18	12	19
TMR15	20	15	19
TMR17	8	17	23
TMR18	0	0	24

Table 7.2. Number and site of transmyocardial channels lased.

### 7.5.2.2 Thoracic sympathectomy

No complications occurred with TS. In particular no Horner's syndrome was encountered.

## 7.5.3 Clinical outcome

### 7.5.3.1 Symptom perception

Changes in patient perception of angina are shown in Table 7.3. Subjective assessment of angina with the use of the NYHA score was similar in both groups prior to surgery. Post-operatively, patients receiving TMR reported an overall improvement in symptoms of ischaemia ( $p < 0.01$ ). A trend towards amelioration of angina was seen following TS but this was not statistically significant.

Visit	TMR		TS	
	A	B	A	B
NYHA class angina	3.5 ± 0.8	1.9 ± 1.4 <sup>†</sup>	3.1 ± 1.4	1.9 ± 1.8
Exercise tolerance (sec)	281 ± 161	352 ± 110	290 ± 154	266 ± 83

*Table 7.3. Clinical outcome data showing New York Heart Association (NYHA) criteria for angina and exercise tolerance (Bruce protocol, sec). <sup>†</sup>p < 0.01. TMR = transmyocardial revascularization; TS = thoracic sympathectomy.*

### **7.5.3.2 Exercise tolerance test**

The Bruce protocol was attempted by 15 patients (TS = 7; TMR = 8). Five patients were unable to exercise for the following reasons: limiting lower limb arthritis (n = 3), femoral aneurysm (n = 1), patient refusal (n = 1). No change in exercise tolerance was seen in the TS group. A trend towards improvement was seen in patients undergoing TMR but this difference failed to achieve statistical significance (Table 7.3).

### **7.5.4 Magnetic resonance imaging**

Seventeen patients completed MRI follow-up. Two patients from the TS group were withdrawn because of claustrophobia (n = 1) and onset of rest angina prior to commencing MRI (n = 1). A recipient of TMR withdrew because of adenosine intolerance.

#### **7.5.4.1 Haemodynamic data**

No significant difference in haemodynamic parameter changes in response to the stressors occurred between the two treatment groups (Table 7.4).

Stressor	Pt Group	P	SBP	DBP	MAP	P*SBP
Rest	All	72 ± 12	141 ± 34	78 ± 15	105 ± 16	10160 ± 2928
	TMR	76 ± 13	139 ± 25	79 ± 17	105 ± 18	10543 ± 2455
	TS	67 ± 9	140 ± 45	77 ± 12	104 ± 17	9552 ± 3732
Adenosine	All	85 ± 14 <sup>‡</sup>	130 ± 24 <sup>†</sup>	73 ± 14 <sup>‡</sup>	93 ± 17 <sup>‡</sup>	10870 ± 3774
	TMR	87 ± 12 <sup>†</sup>	126 ± 21 <sup>†</sup>	73 ± 14 <sup>†</sup>	93 ± 17 <sup>†</sup>	11007 ± 2948
	TS	79 ± 12 <sup>‡</sup>	133 ± 24	69 ± 11 <sup>†</sup>	90 ± 16 <sup>†</sup>	10532 ± 2907
Dobutamine	All	100 ± 21 <sup>‡</sup>	143 ± 28	75 ± 13 <sup>*</sup>	95 ± 22 <sup>*</sup>	11483 ± 6349 <sup>‡</sup>
	TMR	101 ± 20 <sup>‡</sup>	134 ± 25	74 ± 15	95 ± 17 <sup>*</sup>	13560 ± 3710 <sup>†</sup>
	TS	102 ± 20 <sup>‡</sup>	156 ± 29	75 ± 9	93 ± 30	15452 ± 2073 <sup>†</sup>

Table 7.4. Haemodynamic data in response to adenosine and dobutamine stressors for pre-operative and post-operative scans. Statistical significance is shown compared with resting data. P = pulse; SBP = systolic blood pressure; DBP = diastolic blood pressure; MAP = mean arterial pressure; P\*SBP = rate-pressure product; TMR = transmyocardial revascularization; TS = thoracic sympathectomy. \* $p < 0.05$ , <sup>†</sup> $p < 0.01$ , <sup>‡</sup> $p < 0.001$ .

#### 7.5.4.2 Myocardial perfusion

##### 7.5.4.2.1 Quantitative analysis

Perfusion images were of sufficient quality for analysis in 15 / 17 patients. In two patients from the TMR group, two sets of resting perfusion images had to be discarded because of failure of the gradient coils to reset following acquisition of the initial proton density image. Only stress data were available in these patients and so they were excluded from the following data.

Perfusion values in the three treatment groups are presented in Table 7.5. There was no significant difference in perfusion at rest or on stress between the three groups. No change in any perfusion parameters was seen in any of the treatment arms.

ROI	Visit	Stress $K_i$	Rest $K_i$	MPRI	Stress F	Rest F	MPR
TMR treated	A	46.4 ± 17.9	42.0 ± 17.1	1.31 ± 0.74	116.0 ± 44.8	84.0 ± 34.3	1.64 ± 0.92
	B	50.2 ± 17.9	46.6 ± 23.6	1.20 ± 0.43	125.6 ± 44.9	93.3 ± 47.3	1.50 ± 0.54
TMR Control	A	58.5 ± 26.4	41.6 ± 12.0	1.48 ± 0.67	146.4 ± 66.1	83.1 ± 24.1	1.85 ± 0.82
	B	71.6 ± 38.4	44.2 ± 29.1	1.99 ± 1.27	179.0 ± 96.0	88.3 ± 58.3	2.49
TS	A	59.2 ± 32.9	55.2 ± 35.2	1.33 ± 0.99	148.0 ± 82.3	110.3 ± 70.4	1.66 ± 1.23
	B	54.6 ± 25.9	40.9 ± 15.1	1.55 ± 0.98	136.5 ± 64.9	81.8 ± 30.3	1.94 ± 1.22

Table 7.5. Mean ± SD stress and rest  $K_i$  ( $ml\ 100g^{-1}\ min^{-1}$ ), estimate of flow (F) during stress and rest ( $ml\ 100g^{-1}\ min^{-1}$ ), myocardial perfusion reserve index (MPRI) and estimate of absolute myocardial perfusion reserve (MPR) from (A) preoperative and (B) postoperative MRI scans. Data are shown for the regions of interest (ROI) that received laser treatment (TMR treated), for the non-lased ROI (TMR control) and for ROI from patients who had thoracic sympathectomy (TS). TMR = transmyocardial laser revascularization.

Perfusion Characteristic	TMR Lased		TMR Control / Non-lased		TS	
	A	B	A	B	A	B
Normal	17.9 (11.1 - 27.4)	10.7 (5.70 - 19.1)	20.0 (9.50 - 37.3)	10.0 (3.50 - 25.6)	22.9 (15.6 - 32.3)	19.8 (13.1 - 28.9)
Reversible SE	32.1 (23.1 - 42.7)	38.1 (28.4 - 48.8)	23.3 (11.8 - 40.9)	40.0 (24.6 - 57.7)	45.8 (36.2 - 55.8)	18.8 (12.2 - 27.7)
Reversible TM	02.4 (0.70 - 8.30)	00.0 (0.00 - 4.40)	03.3 (0.60 - 16.7)	00.0 (0.00 - 14.4)	09.4 (5.00 - 16.9)	08.3 (4.30 - 15.6)
Fixed SE	21.4 (14.0 - 31.3)	19.0 (28.7 - 12.1)	26.7 (14.2 - 44.4)	16.7 (7.30 - 36.6)	15.6 (24.2 - 9.70)	30.2 (21.9 - 40.0)
Fixed TM	26.2 (18.0 - 36.5)	32.1 (23.1 - 42.7)	26.7 (14.2 - 44.4)	33.3 (19.2 - 51.2)	6.30 (2.90 - 13.0)	22.9 (15.6 - 32.3)

Table 7.6. The percentage of ROI/total ROI for each group demonstrating normal perfusion, reversible or fixed perfusion deficits (expressed as mean ± 95% confidence intervals for proportions) as reported by visual rating pre- (A) and post-operatively (B). SE = subendocardial; TM = transmural; TMR = transmyocardial revascularization; TS = thoracic sympathectomy.

#### 7.5.4.2.2 *Qualitative analysis*

Similarly, no improvement in perfusion was seen with either intervention by qualitative assessment of the images (Table 7.6). In particular, evaluation of the subendocardial layer revealed no change in distribution of myocardial blood flow.

#### 7.5.4.2.3 *Delayed hyperenhancement*

Table 7.7 shows the percent increase in hyperenhancement between initial and follow-up scans for lased and control ROI in the TMR patients. An increase in gadodiamide accumulation on delayed imaging was seen post-operatively in ROI in which laser channels were created ( $p < 0.05$ ). No increase was seen in the control ROI.

Patient group	n	DHE A	DHE B
TMR lased ROI	18	$0.22 \pm 0.05$	$0.26 \pm 0.07^*$
TMR control ROI	10	$0.24 \pm 0.11$	$0.24 \pm 0.06$

*Table 7.7. Change in delayed hyperenhancement (DHE) between pre-operative (A) and post-operative (B) scans for regions of interest (ROI) in patients receiving transmyocardial revascularization (TMR). \* $p < 0.05$ ; n = number of ROI.*

#### 7.5.4.3 *Functional cine imaging*

Details of patient completion of the dobutamine stress protocol are shown in Table 7.8. The majority of patients receiving TMR (7/10) completed the protocol at both visits. Pre-operatively, dobutamine was withheld because of chest pain at rest prior to the infusion. Dobutamine was terminated at  $10 \mu\text{g}^{-1} \text{kg}^{-1} \text{min}$  in 2 patients owing to development of ischaemia ( $n = 1$ ) and failure of the electrocardiogram to trigger imaging ( $n = 1$ ). Postoperatively, dobutamine was also terminated at  $10 \mu\text{g}^{-1} \text{kg}^{-1} \text{min}$  in 2 patients, because of ischaemia ( $n = 1$ ) and onset of ventricular tachycardia ( $n = 1$ ). One patient withdrew because of severe side effects with adenosine.

In the sympathectomy group, a lower proportion of patients completed the stress cine imaging (4/10 pre-operatively and 3/10 post-operatively). Pre-operatively, dobutamine was withheld in two

patients because of extremely poor image quality owing to poor electrocardiogram triggering for image acquisition. Dobutamine was terminated at  $10 \mu\text{g}^{-1} \text{kg}^{-1} \text{min}$  because of ischaemia in 4 patients pre-operatively, and in 1 patient post-operatively. Post-operatively, dobutamine was electively withheld from 5 patients because of unstable symptoms at rest. A further patient withdrew because of claustrophobia.

Patient group	Final		Scan A		Scan B	
	Db Dose	n	Termination reason	n	Termination reason	
TMR	0	1	CP at rest	1	Withdrew*	
	10	2	ECG trigger = 1, CP = 1	2	CP = 1, VT = 1	
	20	7	Completed protocol	7	Completed protocol	
TS	0	2	ECG trigger	6	CP/SOB at rest = 5, withdrew** = 1	
	10	4	SOB = 2, CP = 2	1	CP	
	20	4	Completed protocol	3	Completed protocol	

*Table 7.8. Details of patient completion of dobutamine stress protocol pre (A) and post (B) operatively for the two treatment arms. The dobutamine dose is the final dose at which images were acquired. Where this is 0, no dobutamine was given. Reasons for termination at each level are given. n = number of patients; CP = chest pain; SOB = dyspnoea; ECG trigger = unable to trigger cine MRI; VT = ventricular tachycardia; \*vomited with adenosine and unable to complete remainder of scan; \*\*claustrophobic; TMR = transmyocardial revascularization; TS = thoracic sympathectomy.*

#### **7.5.4.3.1 Resting ejection fraction and left ventricular volumes**

No significant difference in ejection fraction or left ventricular chamber volumes was seen between the two treatment groups at visit A (Table 7.9). There was no change in any of these parameters following either procedure.

Patient group	Visit	EF	EDV	ESV	SV
TMR	A	51.6 ± 14.8	63.9 ± 24.2	31.4 ± 15.2	32.5 ± 13.7
	B	54.1 ± 16.2	63.5 ± 20.5	29.7 ± 13.5	33.7 ± 13.1
TS	A	63.0 ± 11.4	66.2 ± 25.5	25.9 ± 15.9	40.3 ± 11.9
	B	56.6 ± 22.6	67.2 ± 25.9	34.0 ± 29.4	33.2 ± 8.3

*Table 7.9. Resting left ventricular ejection fraction (EF), end-diastolic (EDV), end-systolic (ESV) and stroke (SV) volumes shown for patients receiving transmyocardial laser revascularization (TMR) and thoracic sympathectomy (TS) for visits A and B.*

#### **7.5.4.3.2 Characterization of myocardium from rest/stress scans**

There appeared to be a similar ischaemic burden in the two groups pre-operatively as judged from the proportion of ischaemic segments defined by regional wall motion studies. It is difficult to compare the results of the two interventions as so few sympathectomy patients were able to withstand the dobutamine stress protocol at follow-up. The proportion of the differing myocardial types from the data available at each visit for the two patient groups is shown in Table 7.10.

Patient group	TMR		TS		
	Visit	A (n = 328)	B (n = 304)	A (n = 307)	B (n = 88)
Normal		54.9 (49.5 - 60.2)	46.4 (40.9 - 52)	55.4 (49.8 - 60.8)	73.9 (63.8 - 81.9)
Ischaemia		42.1 (36.9 - 47.5)	47.4 (41.8 - 53)	37.8 (32.5 - 43.3)	25 (17.1 - 35)
Scar		3 (1.7 - 5.5)	6.3 (4 - 9.6)	2.9 (1.5 - 5.5)	1.1 (0.2 - 6.2)
NA		4.7 (2.9 - 7.4)	11.6 (8.7 - 15.4)	10.5 (7.1 - 13.1)	73.4 (68.4 - 77.9)

*Table 7.10. The percentage (95% confidence intervals) of the differing myocardial types for the two patient groups. n = number of ROI within each patient group for which dobutamine cine data were available; TMR = transmyocardial revascularization; TS = thoracic sympathectomy.*

## **7.6 Discussion**

This is one of the first studies to compare the clinical efficacy of TMR and TS and to use MRI to evaluate the effect of the two interventions on myocardial function and perfusion. The study has shown that TMR produces greater perceptual relief of angina than TS. However, this is not paralleled by detectable improvement in global left ventricular function, regional wall motion or myocardial perfusion despite inspection of the subendocardial layer.

### **7.6.1 Clinical outcome**

The findings of improved subjective benefit of symptom reduction and trend towards improved exercise tolerance are consistent with previously reported clinical outcome data following TMR. (Allen *et al.*, 1999; Burkhoff *et al.*, 1999; Frazier *et al.*, 1999; Schofield *et al.*, 1999). In contrast to this, the symptom relief obtained by patients undergoing TS failed to reach statistical significance and there was no suggestion of improved exercise tolerance from the data. This implies that the clinical effect of TMR is not mediated through incidental partial or total cardiac denervation. However, although sympathetic afferents contribute to the majority of anginal pain, Meller demonstrated in a series of studies that the removal of the superior cervical ganglia, stellate ganglia or cervical thoracic trunk and the sympathetic chain obtained complete relief from angina in 50% of the patients treated, partial relief in 30% and no relief in 20% (Meller & Gebhart, 1992). Given this variability in clinical outcome from TS, this study may be underpowered for clinical assessment. In addition, the technique employed for TS may have been suboptimal as only isolated left thoracic sympathectomy was performed. Since thermal sympathectomy was utilized no pathology specimens were obtained to confirm the success of the procedure.

## **7.6.2 Magnetic resonance imaging**

### **7.6.2.1 Myocardial perfusion**

The severe nature of ischaemia in all patients participating in this study is clear from the poor myocardial perfusion reserve detected at outset. No improvement in perfusion parameters was seen with either quantitative image analysis or by visual inspection. This is in contrast to the MRI findings following percutaneous transluminal angioplasty where improvement in myocardial perfusion following revascularization was seen with both methods of analysis (Chapter 6).

Conflicting reports regarding the effect of TMR on perfusion have been presented. Rimoldi *et al.* failed to show improved myocardial perfusion with <sup>15</sup>O-labelled water positron emission tomography at either two or seven months following the procedure (Rimoldi *et al.*, 1999). Similar results were obtained with thallium scintigraphy (Allen *et al.*, 1999). However, Frazier's group have demonstrated some improvement in myocardial perfusion (Frazier *et al.*, 1995; Horvath *et al.*, 1997; Frazier *et al.*, 1999). They describe use of positron emission tomography to assess the ratio of subendocardial to subepicardial perfusion and found a modest improvement in this ratio in laser myocardial segments (Frazier *et al.*, 1995). However, the spatial resolution of positron emission tomography is not optimal for this detailed transmural assessment. Thallium scintigraphy identified no change in perfusion in the same group of patients. Although it could be argued that the MRI technique employed in this study was not sufficiently sensitive to pick up microvascular changes, lack of demonstrable perfusion change with MRI supports the data that suggest that TMR has no beneficial effect on myocardial perfusion reserve or subendocardial flow. This would be against a significant contribution of neoangiogenesis to the mechanism of action of TMR.

### **7.6.2.2 Delayed hyperenhancement**

The quantitative perfusion data from this study facilitated the comparison of pre-operative and post-operative delayed hyperenhancement in the TMR patients between ROI that received laser channels and the control ROI. There was an increase in delayed hyperenhancement seen post-

operatively in the lased areas. This parameter is suggestive of myocardial scar tissue, as described in Chapter 5. This finding implies that myocardial fibrosis may be induced following laser application, reflecting possible laser-induced injury or myocardial channel healing with scar formation (Gassler & Stubbe, 1997). Such changes have the potential to have deleterious consequences on myocardial perfusion and function in the longterm.

### **7.6.2.3 Functional cine imaging**

Insufficient regional dobutamine MRI data were obtained in this study to comment on change in the extent of inducible myocardial ischaemia following these procedures. The large ischaemic burden present in these patients was evident with the poor tolerance of dobutamine for cine imaging. This occurred particularly post-operatively in the group that had undergone TS with five patients presenting with unstable symptoms of ischaemia contra-indicating use of the stressor. Although this observation cannot be tested statistically it supports the clinical assessment of a less successful outcome in patients undergoing TS rather than with TMR.

### **7.6.2.4 Placebo effect**

Preliminary reports of a study evaluating the effect of percutaneous laser therapy have suggested that some of the clinical efficacy may be owing to placebo effect (Direct myocardial revascularization in regeneration of endomyocardial channels trial (DIRECT), presented by Martin Leon, American College of Cardiology annual meeting, 2001). Both patient groups in the study presented here underwent some form of thoracotomy, but the surgical approach was different for each procedure. Neither patients nor doctors could be blinded to the intervention because of the difference in thoracotomy scar. This is an issue that will not be resolved until blind studies with proper controls for the TMR treatment, i.e. the performance of an identical thoracotomy without intervention, are carried out. Such studies for surgical laser revascularization would be unlikely to gain ethical approval.

## **7.7 Conclusion**

TMR produces a superior clinical outcome to unilateral TS in perception of angina in patients with diffuse coronary artery disease that cannot receive percutaneous transluminal angioplasty or coronary artery bypass graft surgery. However, this is not paralleled by detectable improvement with MRI in global left ventricular function, regional wall motion or myocardial perfusion despite inspection of the subendocardial layer. These results do not support the hypothesis that neoangiogenesis is the main mechanism underlying the therapeutic effect of TMR. Similarly, it implies that partial or total cardiac denervation alone cannot be entirely responsible for the perceived benefit. The possibility that a placebo effect may play a role in the mechanism underlying TMR cannot be ignored but would be difficult to prove. Further clinical and MRI studies would be of value on larger cohorts of patients.

---

## **Chapter 8**

### **Conclusions and Future Perspectives**

---

## 8.1 Conclusions

The main objectives of the studies presented within this thesis were to customize the current state of the art MRI techniques and to apply them to a range of clinical applications in patients with coronary artery disease. The practical part of this work was carried out between October 1998 and October 2000 with the use of the 1.5 Tesla *Vision*<sup>TM</sup> imager recently installed at Glenfield. The higher specifications of this scanner compared with the 1.0 *Magnetom*<sup>TM</sup> previously used by the department facilitated faster imaging times and acquisition of images with notably improved quality.

The faster image acquisition speed permitted upgrade of the dynamic inversion-recovery snapshot-FLASH sequence (Chapter 3). Image acquisition with a constant total repetition time was shown to have increased temporal resolution compared with image acquisition gated to the electrocardiogram. In the majority of clinical situations the variation in image placement within the cardiac cycle with the former method was similar to the errors that could occur when the sequence was cardiac gated. No subjective loss of image quality was appreciated despite use of low dose contrast agent bolus. The myocardial relaxation rate, calculated from either non cardiac gated or cardiac gated images had similar levels of agreement to that obtained by multiple inversion imaging, suggesting that quantitative data were not compromised by this technique.

The reproducibility of calculation of the extraction fraction of gadolinium across the capillary membrane,  $K_i$ , was examined. There was some variation in values obtained particularly between examinations on different days. A higher level of agreement was seen within repeated scans at the same examination. The variation obtained was considered to be acceptable for evaluation in the context of the addition of stress, where the likely four-fold variation between stress and rest values would be greater than the inter-study variation demonstrated.

The potential diagnostic accuracy of the dynamic perfusion technique for the identification of significant angiographic coronary artery stenosis was evaluated in Chapter 4. Myocardial perfusion

reserve index could be used to identify areas of myocardium subtended by diseased vessels. A myocardial perfusion reserve index of  $\leq 2$  was identified as a potential cut-off value, giving rise to sensitivity and specificity of 79% and 68% in patients with normal left ventricular function. Since quantitative analysis was labour-intensive, a more rapid qualitative reporting method was developed. In a cohort of 30 patients, diagnostic sensitivity and specificity for detection of angiographic coronary artery disease from visual inspection was 93% and 60%.

In Chapter 5, the adenosine perfusion protocol was successfully combined with a stress function imaging sequence to create the dual adenosine-dobutamine stress protocol. This was designed to optimize the assessment of myocardial perfusion, function and hibernation in a single examination in patients with left ventricular function being considered for revascularization. The technique was well tolerated in a pilot group of patients. In a definitive study, proposed MRI parameters of myocardial hibernation were examined for their ability to predict regional and global left ventricular recovery. Respective sensitivities and specificities for the prediction of regional myocardial recovery were: end-diastolic wall thickness, 70% and 68%; dobutamine-induced contractile reserve 77% and 74%; rest  $K_i$ , 78% and 42%; delayed hyperenhancement, 68% and 56%; thallium scintigraphy, 44% and 48%. For prediction of improvement in ejection fraction, an individual had to demonstrate the parameter in a minimal percentage of dysfunctional myocardium (sensitivity, specificity), i.e. for preserved end-diastolic wall thickness in  $\geq 80\%$  (80%, 82%), contractile reserve in  $\geq 30\%$  (100%, 73%), delayed hyperenhancement in  $\geq 50\%$  (70%, 73%) or viability with thallium scintigraphy in 100% (80%, 80%), respectively.

The potential use of the adenosine perfusion protocol in evaluating serial perfusion changes following revascularization with percutaneous transluminal angioplasty was explored (Chapter 6). Both methods of image analysis, i.e. quantitative and qualitative, were sensitive to early changes in myocardial perfusion following revascularization. Late assessment demonstrated persisting perfusion improvement. In addition, the findings suggested that in-stent restenosis may be detected and this application merits further study.

The final study made use of the combined perfusion and function protocol to evaluate the effects of less conventional treatments for refractory angina, i.e. transmyocardial laser revascularization and thoracic sympathectomy (Chapter 7). No change in myocardial perfusion or ischaemic burden was demonstrated following either technique. This may represent the fact that the mechanism underlying the clinical efficacy of these procedures is remote from the heart. Alternatively, the MRI techniques used could be insufficiently sensitive to demonstrate any subtle changes in myocardial perfusion and function.

In conclusion, MRI techniques were customized to provide comprehensive assessments of myocardial function and perfusion. The findings in the studies presented suggest that MRI has varied applications in the clinical assessment of patients with coronary artery disease. Larger prospective multi-centre trials are necessary to establish databases of normal values, to fully elucidate the diagnostic potential of MRI to detect *de novo* or recurrent myocardial ischaemia and hibernation, and to optimally apply MRI information to guide and assess clinical therapy. The use of combined imaging to evaluate myocardial function, perfusion and viability may facilitate greater understanding of the pathophysiology of coronary artery disease.

## 8.2 Future Perspectives

The studies presented in this thesis were performed on a whole body imager with optional cardiac sequences. The rapid growth of interest in cardiac MRI in the last few years has stimulated manufacturers to produce imagers with cardiac dedicated specifications. An example is the *Sonata* imager (Siemens, Erlangen, Germany) with gradient system of up to 40 mTesla  $m^{-1}$ . This imager has a short, wide bore to maximize patient comfort and to improve examination tolerance. Cardiac circular polarized array coils provide an optimal image signal, increasing image quality and spatial resolution.

Increased imager specifications have facilitated the development of improved image acquisition sequences to evaluate myocardial perfusion, function and viability. The true fast imaging with

steady state precession (FISP) sequence has superseded segmented gradient echo cine sequences for assessment of myocardial function (Carr *et al.*, 2001). Ultrafast imaging times now permit interactive real time imaging for easy and rapid manoeuvring between planes (Nagel *et al.*, 2000). Tagging techniques can be used to track the in-plane, through-plane and rotational displacement of the ventricle through the cardiac cycle (McVeigh, 1996; Carr *et al.*, 2001). Hybrid echo planar imaging for myocardial perfusion retains the image quality of the inversion recovery snapshot-FLASH sequence whilst reducing scan time sufficiently to allow ECG-gated multiple slice acquisition within a given repetition time (Reeder *et al.*, 1999). Clinical trials are underway to evaluate intravascular and infarct avid contrast agents (McVeigh & Bolster, Jr., 1998). Much research is directed towards visualization of the coronary arterial tree (Saeed *et al.*, 2000; Fayad & Fuster, 2001). The challenges facing MRI include the high spatial resolution required, the tortuous anatomical course of the coronary vessels and the sensitivity of the images to cardiac and respiratory motion.

Progress in the development of cardiac dedicated scanners, image quality and acquisition speed of imaging sequences over the last few years has been exponential. It has resulted from collaborations between clinicians, researchers, physicists, and industry. Numerous clinical studies are in progress. The need for prospective multi-centre research has been recognized. As cardiologists and radiologists become more familiar with current MRI techniques and their clinical applications in patients with coronary artery disease, integrated cardiac examination by magnetic resonance is likely to become a clinical investigation of choice in the foreseeable future.

---

## **Appendix**

**Publications and presentations arising from this  
thesis**

---

## **Papers**

Sensky, P.R., Jivan, A., Hudson, N., Keal, R.P., Morgan, B., Tranter, J., de Bono, D., Samani, N.J.

& Cherryman, G.R. (2000). Coronary artery disease: combined stress MR imaging protocol – one-stop evaluation of myocardial perfusion and function. *Radiology* 215:608-614.

Sensky, P.R., Hudson, N., Keal, R.P., Samani, N.J. & Cherryman, G.R. (2002). Interpreting regional myocardial magnetic resonance imaging data: a method for collation with angiographic findings in patients with coronary artery disease. *Clin Radiol* 57 (6):498-501. (2002)

Sensky, P.R., Reek, C., Samani, N.J. & Cherryman, G.R. (2002). Magnetic resonance perfusion imaging in patients with coronary artery disease: a qualitative approach. *Int J Card Imaging* 18: 373-383.

Sensky, P.R., Samani, N.J., Horsfield, M.A. & Cherryman, G.R. (2002). Restoration of myocardial blood flow following percutaneous coronary balloon dilatation and stent implantation: assessment with qualitative and quantitative contrast enhanced magnetic resonance imaging. *Clin Radiol* 57(7):593-599.

## **Book Chapters**

Sensky, P.R. & Cherryman, G.R. (2002). What is the role of MRI in coronary syndromes? In “Challenges in acute coronary syndromes”. Ed. de Bono, D., Sobel B., *Blackwell Science*, pp. 133-147.

Sensky, P.R. & Cherryman, G.R. (2003) Myocardial perfusion in ischaemic heart disease. In “Cardiovascular MRI and MRA”. Ed. Higgins C.B., de Roos A., *Lippincott, Williams & Wilkins*, pp. 173-190.

## **Submitted Papers**

Galinares, M., Sensky, P.R., Loubani, M., Cherryman, G.R., Samani, N.J. & Leverment, J.N.

Transmyocardial myocardial revascularization versus cardiac denervation with thoracic sympathectomy for relief of refractory angina: effect on myocardial perfusion? *Heart*, Aug 2002.

Sensky, P.R., Cherryman, G.R., Keal, R.P., Hudson, N. & Samani, N.J. Magnetic resonance imaging prediction of contractile recovery in dysfunctional myocardial segments following revascularization: translation into clinical benefit. *Heart*, Dec 2002.

Sensky, P.R., Horsfield, M.A., Samani, N.J. & Cherryman, G.R. First pass contrast-enhanced MRI for the assessment of myocardial blood flow: is cardiac gating beneficial? *Br J Radiol*, May 2002.

Sensky, P.R., Horsfield, M.A., Samani, N.J. & Cherryman, G.R. Unidirectional transfer coefficient of gadodiamide,  $K_1$ : reproducibility and diagnostic potential for detection of myocardial blood flow. *Br J Radiol*, May 2002.

## **Abstracts**

Sensky, P.R., Jivan, A., Cherryman, G.R., Hudson, N., Keal, R.P., Morgan, B. & Samani, N.J. Stress magnetic resonance imaging for the evaluation of hibernating myocardium: a one-stop assessment of regional left ventricular function and perfusion. *Proc Int Soc Magn Reson Med* 1999; 8:P24.

*Presented at the International Society Magnetic Resonance in Medicine, Philadelphia, May 1999.*

Sensky, P.R., Jivan, A., Hudson, N., Keal, R.P., Samani, N.J. & Cherryman, G.R. Dobutamine/adenosine double stress (DADS) MRI in patients with coronary artery disease (CAD): a one-stop assessment of myocardial perfusion, hibernation and left ventricular (LV) function. *J Cardiovasc Magn Reson* 1999; 1(4):366.

*Presented at the Society Cardiovascular Magnetic Resonance, Atlanta, January 2000.*

Cherryman, G.R., Sensky, P.R., Jivan, A., Reek, C. & Samani, N.J. Qualitative myocardial perfusion magnetic resonance imaging (MRI): detection of angiographic coronary artery disease. *J Cardiovasc Magn Reson* 1999; 1(4):366.

*Presented at the Society Cardiovascular Magnetic Resonance, Atlanta, January 2000.*

Sensky, P.R., Jivan, A., Reek, C., Samani, N.J. & Cherryman, G.R. Qualitative magnetic resonance imaging in patients with coronary artery disease. *Proc Int Soc Magn Reson Med* 2000; **8**:1560.

*Presented at the International Society Magnetic Resonance in Medicine, Denver, April 2000.*

Sensky, P.R., Cherryman, G.R., Jivan, A., Reek, C. & Samani, N.J. Adenosine perfusion MRI (PMRI): a clinical approach for the detection of coronary artery disease (CAD). *Heart* 2000; **83** (suppl 1):10.

*Presented at the British Cardiac Society, Glasgow, May 2000.*

Sensky, P.R., Jivan, A., Cherryman, G.R. & Samani, N.J. Pre-operative assessment of patients with coronary artery disease and low ejection fraction: a dual adenosine/dobutamine stress (DADS) magnetic resonance imaging protocol. *Heart* 2000; **83** (suppl 1):10.

*Presented at the British Cardiac Society, Glasgow, May 2000.*

Sensky, P.R., Keal, R., Samani, N.J. & Cherryman, G.R. Comparison of delayed contrast-enhanced MRI and dobutamine cine-MRI in the identification of regional left ventricular (LV) recovery following coronary artery bypass grafting (CABG) in patients with poor ejection fraction. *J Cardiovasc Magn Reson* 2000; **2**(4):298.

*Presented at the European Society of Cardiac Magnetic Resonance, Amsterdam, May 2000.*

Sensky, P.R., Reek, C., Samani, N.J. & Cherryman, G.R. A clinical qualitative approach to perfusion MRI for the detection of coronary artery disease. *J Cardiovasc Magn Reson* 2000; **2**(4):290.

*Presented at the European Society of Cardiac Magnetic Resonance, Amsterdam, May 2000.*

Sensky, P.R., Cherryman, G.R., Keal, R. & Samani, N.J. Accuracy of dobutamine cine-MRI and delayed contrast-enhanced MRI in the prediction of regional left ventricular recovery following surgical revascularization in patients with low ejection fraction. *Eur Heart J* 2000; **21** (Suppl):86.

*Presented at the European Society of Cardiology, Amsterdam, August 2000.*

Sensky, P.R., Horsfield, M.A., Samani, N.J. & Cherryman, G.R. Is cardiac gating beneficial for myocardial perfusion imaging? A non ECG-gated model and diagnostic performance evaluation in patients with coronary artery disease (CAD). *J Cardiovasc Magn Reson* 2001; **3(2)**:108-109.

*Presented at the Society Cardiovascular Magnetic Resonance, Atlanta, January 2001.*

Sensky, P.R., Horsfield, M.A., Samani, N.J. & Cherryman, G.R. A non ECG-gated model for myocardial perfusion imaging; evaluation of diagnostic performance evaluation in patients with coronary artery disease (CAD). *Proc Int Soc Magn Reson Med* 2001; **9**:1899.

*Presented at the International Society Magnetic Resonance in Medicine, Glasgow, April 2001.*

Sensky, P.R., Samani, N.J. & Cherryman, G.R. Serial first pass contrast perfusion MRI following coronary artery angioplasty (PTCA) in patients with single vessel disease: qualitative and quantitative image analysis. *Proc Int Soc Magn Reson Med* 2001; **9**:1897.

*Presented at the International Society Magnetic Resonance in Medicine, Glasgow, April 2001.*

Sensky, P.R., Samani, N.J., Horsfield, M.A. & Cherryman, G.R. Early restoration of myocardial perfusion after percutaneous angioplasty and stenting (PTCA): delineation with magnetic resonance imaging (MRI). *Heart* 2001; **85 (suppl 1)**:12.

*Presented at the British Cardiac Society, Manchester, May 2001.*

Galinares, M., Sensky, P.R., Loubani, M., Cherryman, G.R., Samani, N.J. & Leverment, J.N. TMR vs. cardiac denervation with thoracic sympathectomy for the relief of refractory angina. *Circulation* 2001; **104 (suppl II)**:362.

*Presented at the American Heart Association, Anaheim, November 2001.*

Sensky, P.R., Samani, N.J. & Cherryman, G.R. Can MRI establish whether the clinical effects of transmyocardial laser revascularization are really placebo? *Proc Euro CMR*, 2002:13.

*Presented at the European Society of Cardiac Magnetic Resonance, Basle, June 2002.*

Sensky, P.R., Cherryman, G.R., Keal, R. Hudson, N.M. & Samani, N.J. MRI prediction of contractile recovery of dysfunctional myocardial segments following revascularization: can

regional data be translated into individual patient benefit? *J Cardiovasc Magn Reson*, 2003 (in press).

*To be presented at Society Cardiovascular Magnetic Resonance, Florida, February 2003.*

Sensky, P.R., Samani, N.J. & Cherryman, G.R. Improvement in ejection fraction following revascularization in patients with ischaemic left ventricular dysfunction: is this correlated with improved perfusion? *J Cardiovasc Magn Reson*, 2003 (in press).

*To be presented at Society Cardiovascular Magnetic Resonance, Florida, February 2003.*

Sensky, P.R., Samani, N.J. & Cherryman, G.R. Reproducibility of quantitative measurements of myocardial perfusion in volunteers. *J Cardiovasc Magn Reson*, 2003 (in press).

*To be presented at Society Cardiovascular Magnetic Resonance, Florida, February 2003.*

Sensky, P.R., Samani, N.J. & Cherryman, G.R. Does transmyocardial laser revascularization (tmr) give rise to myocardial fibrosis? *J Cardiovasc Magn Reson*, 2003 (in press).

*To be presented at Society Cardiovascular Magnetic Resonance, Florida, February 2003.*

---

## **References**

---

- Afridi, I., Kleiman, N.S., Raizner, A.E. & Zoghbi, W.A. (1995). Dobutamine echocardiography in myocardial hibernation. Optimal dose and accuracy in predicting recovery of ventricular function after coronary angioplasty. *Circulation* **91**:663-670.
- Al-Saadi, N., Nagel, E., Gross, M., Bornstedt, A., Schnackenburg, B., Klein, C., Klimek, W., Oswald, H. & Fleck, E. (2000). Noninvasive detection of myocardial ischemia from perfusion reserve based on cardiovascular magnetic resonance. *Circulation* **101**:1379-1383.
- Al-Saadi, N., Nagel, E., Gross, M., Klein, C., Schalla, B., Schnackenburg, B. & Fleck, E. (1999). Myocardial perfusion reserve early after successful revascularisation: comparison of stent and balloon by cardiac MR. *Proc Soc Exp Biol Med* **1**:324-325.
- Al-Sheikh, T., Allen, K.B., Straka, S.P., Heimansohn, D.A., Fain, R.L., Hutchins, G.D., Sawada, S.G., Zipes, D.P. & Engelstein, E.D. (1999). Cardiac sympathetic denervation after transmyocardial laser revascularization. *Circulation* **100**:135-140.
- Alderman, E.L., Fisher, L.D., Litwin, P., Kaiser, G.C., Myers, W.O., Maynard, C., Levine, F. & Schloss, M. (1983). Results of coronary artery surgery in patients with poor left ventricular function (CASS). *Circulation* **68**:785-795.
- Allen, K.B., Dowling, R.D., Fudge, T.L., Schoettle, G.P., Selinger, S.L., Gangahar, D.M., Angell, W.W., Petracek, M.R., Shaar, C.J. & O'Neill, W.W. (1999). Comparison of transmyocardial revascularization with medical therapy in patients with refractory angina. *N Engl J Med* **341**:1029-1036.
- Anonymous (1983). Risk stratification and survival after myocardial infarction. *N Engl J Med* **309**: 331-336.
- Arai, A.E., Epstein, F.H., London, J., Weiss, C.R., Kannel, N., Moalemi, A., Dilsizian, V. & Balaban, R.S. (1999). Dipyridamole stress MRI perfusion: clinical evaluation using high contrast dose, multislice imaging and a novel read technique. *Proc Int Soc Magn Reson Med* **7**:304.
- Armstrong, W.F. & Bossone, E. (1997). Evaluation of myocardial viability using stress echocardiography. *Prog Cardiovasc Dis* **39**:555-566.

- Atkinson, D.J., Burstein, D. & Edelman, R.R. (1990). First-pass cardiac perfusion: evaluation with ultrafast MR imaging. *Radiology* 174:757-762.
- Austin, R.E.J., Aldea, G.S., Coggins, D.L., Flynn, A.E. & Hoffman, J.I. (1990). Profound spatial heterogeneity of coronary reserve. Discordance between patterns of resting and maximal myocardial blood flow. *Circ Res* 67:319-331.
- Bach, R.G., Donohue, T.J. & Kern, M.J. (1995). Intracoronary Doppler flow velocity measurements for the evaluation and treatment of coronary artery disease. *Curr Opin Cardiol* 10:434-442.
- Bache, R.J. & Schwartz, J.S. (1982). Effect of perfusion pressure distal to a coronary stenosis on transmural myocardial blood flow. *Circulation* 65:928-935.
- Badimon, J.J., Ortiz, A.F., Meyer, B., Mailhac, A., Fallon, J.T., Falk, E., Badimon, Chesebro, J.H. & Fuster, V. (1998). Different response to balloon angioplasty of carotid and coronary arteries: effects on acute platelet deposition and intimal thickening. *Atherosclerosis* 140:307-314.
- Baer, F.M., Theissen, P., Crnac, J., Schmidt, M., Jochims, M. & Schicha, H. (1999a). MRI assessment of coronary artery disease. *Rays* 24:46-59.
- Baer, F.M., Theissen, P., Schneider, C.A., Kettering, K., Voth, E., Sechtem, U. & Schicha, H. (1999b). MRI assessment of myocardial viability: comparison with other imaging techniques. *Rays* 24:96-108.
- Baer, F.M., Theissen, P., Schneider, C.A., Voth, E., Sechtem, U., Schicha, H. & Erdmann, E. (1998). Dobutamine magnetic resonance imaging predicts contractile recovery of chronically dysfunctional myocardium after successful revascularization. *J Am Coll Cardiol* 31:1040-1048.
- Baer, F.M., Voth, E., Deutsch, H.J., Schneider, C.A., Horst, M., de Vivie, E.R., Schicha, H., Erdmann, E. & Sechtem, U. (1996a). Predictive value of low dose dobutamine transesophageal echocardiography and fluorine-18 fluorodeoxyglucose positron emission tomography for recovery of regional left ventricular function after successful revascularization. *J Am Coll Cardiol* 28:60-69.

- Baer, F.M., Voth, E., La Rosee, K., Schneider, C.A., Theissen, P., Deutsch, H.J., Schicha, H., Erdmann, E. & Sechtem, U. (1996b). Comparison of dobutamine transesophageal echocardiography and dobutamine magnetic resonance imaging for detection of residual myocardial viability. *Am J Cardiol* 78:415-419.
- Baer, F.M., Voth, E., Schneider, C.A., Theissen, P., Schicha, H. & Sechtem, U. (1995). Comparison of low-dose dobutamine-gradient-echo magnetic resonance imaging and positron emission tomography with [18F]fluorodeoxyglucose in patients with chronic coronary artery disease. A functional and morphological approach to the detection of residual myocardial viability. *Circulation* 91:1006-1015.
- Bassingthwaighe, J.B., King, R.B. & Roger, S.A. (1989). Fractal nature of regional myocardial blood flow heterogeneity. *Circ Res* 65:578-590.
- Bax, J.J., Cornel, J.H., Visser, F.C., Fioretti, P.M., Huitink, J.M., van Lingen, A., Sloof, G.W. & Visser, C.A. (1997a). F18-fluorodeoxyglucose single-photon emission computed tomography predicts functional outcome of dyssynergic myocardium after surgical revascularization. *J Nucl Cardiol* 4:302-308.
- Bax, J.J., Cornel, J.H., Visser, F.C., Fioretti, P.M., van Lingen, A., Huitink, J.M., Kamp, O., Nijland, F., Roelandt, J.R. & Visser, C.A. (1997b). Prediction of improvement of contractile function in patients with ischemic ventricular dysfunction after revascularization by fluorine-18 fluorodeoxyglucose single-photon emission computed tomography. *J Am Coll Cardiol* 30:377-383.
- Beanlands, R.S., Hendry, P.J., Masters, R.G., de Kemp, R.A., Woodend, K. & Ruddy, T.D. (1998). Delay in revascularization is associated with increased mortality rate in patients with severe left ventricular dysfunction and viable myocardium on fluorine 18-fluorodeoxyglucose positron emission tomography imaging. *Circulation* 98 (suppl II):51-56.
- Bellenger, N.G., Ceri Davies, L., Francis, J.M., Coats, A.J.S. & Pennell, D.J. (2000). Reduction in sample size for studies of remodeling in heart failure by the use of cardiovascular magnetic resonance. *J Cardiovasc Magn Reson* 2:271-278.

- Bergmann, S.R., Herrero, P., Markham, J., Weinheimer, C.J. & Walsh, M.N. (1989). Noninvasive quantitation of myocardial blood flow in human subjects with oxygen-15-labeled water and positron emission tomography. *J Am Coll Cardiol* 14:639-652.
- Bland, J.M. & Altman, D.G. (1986). Statistical methods for assessing agreement between two methods of clinical measurement. *Lancet* 1 (8476):307-310.
- Blomley, M.J., Coulden, R., Bufkin, C., Lipton, M.J. & Dawson, P. (1993). Contrast bolus dynamic computed tomography for the measurement of solid organ perfusion. *Invest Radiol* 28 (suppl 5):S72-S77.
- Bourdarias, J.P. (1995). Coronary reserve: concept and physiological variations. *Eur Heart J* 16 (suppl I):2-6.
- Brandt, P.W., Partridge, J.B. & Wattie, W.J. (1977). Coronary arteriography; method of presentation of the arteriogram report and a scoring system. *Clin Radiol* 28:361-365.
- Brasch, R.C. (1992). New directions in the development of MR imaging contrast media. *Radiology* 183:1-11.
- Bremerich, J., Buser, P., Bongartz, G., Muller-Brand, J., Gradel, C., Pfisterer, M.E. & Steinbrich, W. (1997). Noninvasive stress testing of myocardial ischemia: comparison of GRE-MRI perfusion and wall motion analysis to 99 mTc-MIBI-SPECT, relation to coronary angiography. *Eur Radiol* 7:990-995.
- Brown, K.A. (1995). Prognostic value of cardiac imaging in patients with known or suspected coronary artery disease: comparison of myocardial perfusion imaging, stress echocardiography, and positron emission tomography. *Am J Cardiol* 75:35D-41D.
- Burkhoff, D., Schmidt, S., Schulman, S.P., Myers, J., Resar, J., Becker, L.C., Weiss, J. & Jones, J.W. (1999). Transmyocardial laser revascularisation compared with continued medical therapy for treatment of refractory angina pectoris: a prospective randomised trial. ATLANTIC Investigators. Angina Treatments-Lasers and Normal Therapies in Comparison. *Lancet* 354:885-890.

- Carr, J.C., Simonetti, O., Bundy, J., Li, D., Pereles, S. & Finn, J.P. (2001). Cine MR angiography of the heart with segmented true fast imaging with steady-state precession. *Radiology* **219**:828-834.
- Chan, S.Y., Brunken, R.C., Czernin, J., Porenta, G., Kuhle, W., Krivokapich, J., Phelps, M.E. & Schelbert, H.R. (1992). Comparison of maximal myocardial blood flow during adenosine infusion with that of intravenous dipyridamole in normal men. *J Am Coll Cardiol* **20**:979-985.
- Cherryman, G.R., Sensky, P.R., Jivan, A., Tranter, J., Horsfield, M.A., Hudson, N.M., Pennell, D.J., Dendale, P., de Roos, A., Woods, K.L., Barnett, D.B. & Pirovano, G.P. (1999a). Comparison of first pass magnetic resonance (MR) perfusion and thallium-201 (Tl-201) imaging in acute myocardial infarction (AMI). *Heart* **81 (suppl 1)**:P40.
- Cherryman, G.R., Sensky, P.R., Tranter, J., Jivan, A., Hudson, N.M., Keal, R.P., McCullough, A., Dendale, P., de Roos, A., Pennell, D.J., Woods, K.L., Barnett, D.B., Pirovano, G.P. & Spinazzi, A. (1999b). Contrast enhanced MRI in the diagnosis of acute myocardial infarction. *Eur Radiol* **9 (suppl)**:288.
- Choi, K.M., Kim, R.J., Gubernikoff, G., Vargas, J.D., Parker, M. & Judd, R.M. (2001). Transmural extent of acute myocardial infarction predicts long-term improvement in contractile function. *Circulation* **104**:1101-1107.
- Cigarroa, C.G., de Filippi, C.R., Brickner, M.E., Alvarez, L.G., Wait, M.A. & Grayburn, P.A. (1993). Dobutamine stress echocardiography identifies hibernating myocardium and predicts recovery of left ventricular function after coronary revascularization. *Circulation* **88**:430-436.
- Claes, G., Drott, C., Wettervik, C., Tygesen, H., Emanuelsson, H., Lomsky, M. & Radberg, G. (1996). Angina pectoris treated by thoracoscopic sympathectomy. *Cardiovasc Surg* **4**:830-831.
- Clough, A.V., al-Tinawi, A., Linehan, J.H. & Dawson, C.A. (1994). Regional transit time estimation from image residue curves. *Ann Biomed Eng* **22**:128-143.
- Crone, C. (1963). The permeability of the capillaries in various organs determined by use of the indicator diffusion method. *Acta Physiol Scand* **58**:292-305.

- Cullen, J.H., Cherryman, G.R., Samani, N.J., Tranter, J., Jivan, A., Horsfield, M.A., Woods, K.L. & Barnett, D.B. (1999a). Mechanism and clinical significance of precordial ST depression in inferior myocardial infarction: evaluation by contrast-enhanced dynamic myocardial perfusion magnetic resonance imaging. *J Cardiovasc Magn Reson* 1: 121-130.
- Cullen, J.H., Horsfield, M.A., Reek, C.R., Cherryman, G.R., Barnett, D.B. & Samani, N.J. (1999b). A myocardial perfusion reserve index in humans using first-pass contrast-enhanced magnetic resonance imaging. *J Am Coll Cardiol* 33:1386-1394.
- Di Carli, M.F., Asgarzadie, F., Schelbert, H.R., Brunken, R.C., Laks, H., Phelps, M.E. & Maddahi, J. (1995). Quantitative relation between myocardial viability and improvement in heart failure symptoms after revascularization in patients with ischemic cardiomyopathy. *Circulation* 92:3436-3444.
- Di Carli, M.F., Maddahi, J., Rokhsar, S., Schelbert, H.R., Bianco-Batlles, D., Brunken, R.C. & Fromm, B. (1998). Long-term survival of patients with coronary artery disease and left ventricular dysfunction: implications for the role of myocardial viability assessment in management decisions. *J Thorac Cardiovasc Surg* 116:997-1004.
- Diesbourg, L.D., Prato, F.S., Wisenberg, G., Drost, D.J., Marshall, T.P., Carroll, SE & O'Neill, B. (1992). Quantification of myocardial blood flow and extracellular volumes using a bolus injection of Gd-DTPA: kinetic modeling in canine ischemic disease. *Magn Reson Med* 23:239-253.
- Donovan, C.L., Landolfo, K.P., Lowe, J.E., Clements, F., Coleman, R.B. & Ryan, T. (1997). Improvement in inducible ischemia during dobutamine stress echocardiography after transmyocardial laser revascularization in patients with refractory angina pectoris. *J Am Coll Cardiol* 30:607-612.
- Eagle, K.A., Guyton, R.A., Davidoff, R., Ewy, G.A., Fonger, J., Gardner, T.J., Gott, J.P., Herrmann, H.C., Marlow, R.A., Nugent, W.C., O'Connor, G.T., Orszulak, T.A., Rieselbach, R.E., Winters, W.L., Yusuf, S., Gibbons, R.J., Alpert, J.S., Garson, A.J., Gregoratos, G., Russell, R.O. & Smith, S.C., Jr. (1999). ACC/AHA Guidelines for Coronary Artery Bypass

- Graft Surgery: A Report of the American College of Cardiology/American Heart Association Task Force on Practice Guidelines (Committee to Revise the 1991 Guidelines for Coronary Artery Bypass Graft Surgery). American College of Cardiology/American Heart Association. *J Am Coll Cardiol* **34**:1262-1347.
- Eichenberger, A.C., Schuiki, E., Kochli, V.D., Amann, F.W., McKinnon, G.C. & von Schulthess, G.K. (1994). Ischemic heart disease: assessment with gadolinium-enhanced ultrafast MR imaging and dipyridamole stress. *J Magn Reson Imaging* **4**:425-431.
- Elefteriades, J.A., Tolis, G.J., Levi, E., Mills, L.K. & Zaret, B.L. (1993). Coronary artery bypass grafting in severe left ventricular dysfunction: excellent survival with improved ejection fraction and functional state. *J Am Coll Cardiol* **22**:1411-1417.
- Falsetti, H.L., Carroll, R.J. & Marcus, M.L. (1975). Temporal heterogeneity of myocardial blood flow in anesthetized dogs. *Circulation* **52**:848-853.
- Fayad, Z.A. & Fuster, V. (2001). Clinical imaging of the high-risk or vulnerable atherosclerotic plaque. *Circ Res* **89**:305-316.
- Ferrari, R., Ceconi, C., Curello, S., Percoco, G., Toselli, T. & Antonioli, G. (1999). Ischemic preconditioning, myocardial stunning, and hibernation: basic aspects. *Am Heart J* **138**:S61-S68.
- Fieno, D.S., Kim, R.J., Chen, E.L., Lomasney, J.W., Klocke, F.J. & Judd, R.M. (2000). Contrast-enhanced magnetic resonance imaging of myocardium at risk: distinction between reversible and irreversible injury throughout infarct healing. *J Am Coll Cardiol* **36**:1985-1991.
- Fisher, M.R., von Schulthess, G.K. & Higgins, C.B. (1985). Multiphasic cardiac magnetic resonance imaging: normal regional left ventricular wall thickening. *Am J Roentgenol* **145**: 27-30.
- Frazier, O.H., Cooley, D.A., Kadipasaoglu, K.A., Pehlivanoglu, S., Lindenmeir, M., Barasch, E., Conger, J.L., Wilansky, S. & Moore, W.H. (1995). Myocardial revascularization with laser. Preliminary findings. *Circulation* **92**:II58-II65.

- Frazier, O.H., March, R.J. & Horvath, K.A. (1999). Transmyocardial revascularization with a carbon dioxide laser in patients with end-stage coronary artery disease. *N Engl J Med* **341**:1021-1028.
- Fritz-Hansen, T., Rostrup, E., Sondergaard, L., Ring, P.B., Amtorp, O. & Larsson, H.B. (1998). Capillary transfer constant of Gd-DTPA in the myocardium at rest and during vasodilation assessed by MRI. *Magn Reson Med* **40**:922-929.
- Fuster, V., Badimon, L., Badimon, J.J. & Chesebro, J.H. (1992). The pathogenesis of coronary artery disease and the acute coronary syndromes (1). *N Engl J Med* **326**:242-250.
- Ganong W.F. (2000). The Heart as a Pump. In *Review of Medical Physiology*, pp. 451-461. Lange Medical Publications.
- Gassler, N. & Stubbe, H.M. (1997). Clinical data and histological features of transmyocardial revascularization with CO<sub>2</sub>-laser. *Eur J Cardiothorac Surg* **12**:25-30.
- Gensini, G.F., Comeglio, M. & Falai, M. (1999). Advances in antithrombotic therapy of acute myocardial infarction. *Am Heart J* **138**:S171-S176.
- Georgiou, D., Wolfkiel, C. & Brundage, B.H. (1994). Ultrafast computed tomography for the physiological evaluation of myocardial perfusion. *Am J Card Imaging* **8**:151-158.
- Gewirtz, H., Fischman, A.J., Abraham, S., Gilson, M., Strauss, H.W. & Alpert, N.M. (1994). Positron emission tomographic measurements of absolute regional myocardial blood flow permits identification of nonviable myocardium in patients with chronic myocardial infarction. *J Am Coll Cardiol* **23**:851-859.
- Go, R.T., Marwick, T.H., MacIntyre, W.J., Saha, G.B., Neumann, D.R., Underwood, D.A. & Simpfendorfer, C.C. (1990). A prospective comparison of rubidium-82 PET and thallium-201 SPECT myocardial perfusion imaging utilizing a single dipyridamole stress in the diagnosis of coronary artery disease. *J Nucl Med* **31**:1899-1905.
- Goldman, L. (1995). Cost and quality of life: thrombolysis and primary angioplasty. *J Am Coll Cardiol* **25**:38S-41S.

- Goldman, L., Hashimoto, B., Cook, E.F. & Loscalzo, A. (1981). Comparative reproducibility and validity of systems for assessing cardiovascular functional class: advantages of a new specific activity scale. *Circulation* **64**:1227-1234.
- Goldstein, R.A., Kirkeeide, R.L., Demer, L.L., Merhige, M., Nishikawa, A., Smalling, R.W., Mullani, N.A. & Gould, K.L. (1987). Relation between geometric dimensions of coronary artery stenoses and myocardial perfusion reserve in man. *J Clin Invest* **79**:1473-1478.
- Gould, K.L. (1988). Percent coronary stenosis: battered gold standard, pernicious relic or clinical practicality? *J Am Coll Cardiol* **11**:886-888.
- Gould, K.L. & Lipscomb, K. (1974). Effects of coronary stenoses on coronary flow reserve and resistance. *Am J Cardiol* **34**:48-55.
- Gruning, T., Kropp, J., Wiener, S., Franke, W.G., Tugtekin, S.M., Gulielmos, V. & Schuler, S. (1999). Evaluation of transmyocardial laser revascularization (TMLR) by gated myocardial perfusion scintigraphy. *Ann Nucl Med* **13**:361-366.
- Gunning, M.G., Anagnostopoulos, C., Davies, G., Knight, C.J., Pennell, D.J., Fox, K.M., Pepper, J. & Underwood, S.R. (1999). Simultaneous assessment of myocardial viability and function for the detection of hibernating myocardium using ECG-gated <sup>99</sup>Tcm-tetrofosmin emission tomography: a comparison with <sup>201</sup>Tl emission tomography combined with cine magnetic resonance imaging. *Nucl Med Commun* **20**:209-214.
- Haase, A. (1990). Snapshot FLASH MRI. Applications to T1, T2, and chemical-shift imaging. *Magn Reson Med* **13**:77-89.
- Haase, J., Escaned, J., van Swijndregt, E.M., Ozaki, Y., Gronenschild, E., Slager, C.J. & Serruys, P.W. (1993). Experimental validation of geometric and densitometric coronary measurements on the new generation Cardiovascular Angiography Analysis System (CAAS II). *Catheter Cardiovasc Diag* **30**:104-114.
- Haque, T., Furukawa, T., Takahashi, M. & Kinoshita, M. (1995). Identification of hibernating myocardium by dobutamine stress echocardiography: comparison with thallium-201 reinjection imaging. *Am Heart J* **130**:553-563.

- Hartnell, G., Cerel, A., Kamalesh, M., Finn, J.P., Hill, T., Cohen, M., Tello, R. & Lewis, S. (1994). Detection of myocardial ischemia: value of combined myocardial perfusion and cineangiographic MR imaging. *Am J Roentgenol* **163**:1061-1067.
- Haude, M., Caspari, G., Baumgart, D., Brennecke, R., Meyer, J. & Erbel, R. (1996). Comparison of myocardial perfusion reserve before and after coronary balloon predilatation and after stent implantation in patients with postangioplasty restenosis. *Circulation* **94**:286-297.
- Hawkes, R.C., Holland, G.N., Moore, W.S., Roebuck, E.J. & Worthington, B.S. (1981). Nuclear magnetic resonance (NMR) tomography of the normal heart. *J Comput Assist Tomogr* **5**:605-612.
- Heusch, G. & Schulz, R. (1996). Hibernating myocardium: a review. *J Mol Cell Cardiol* **28**:2359-2372.
- Higgins, C.B., Saeed, M., Wendland, M., Yu, K., Lauerma, K., Dulce, M. & Kanth, N. (1993). Contrast media for cardiothoracic MR imaging. *J Magn Reson Imaging* **3**:265-276.
- Higgins, C.B. & Sakuma, H. (1996). Heart disease: functional evaluation with MR imaging. *Radiology* **199**:307-315.
- Hilton, T.C., Thompson, R.C., Williams, H.J., Saylor, R., Fulmer, H. & Stowers, S.A. (1994). Technetium-99m sestamibi myocardial perfusion imaging in the emergency room evaluation of chest pain. *J Am Coll Cardiol* **23**:1016-1022.
- Hoffman, J.I. (1987). Transmural myocardial perfusion. *Prog Cardiovasc Dis* **29**:429-464.
- Hoffmann, R., Lethen, H., Marwick, T., Arnese, M., Fioretti, P., Pingitore, A., Picano, E., Buck, T., Erbel, R., Flachskampf, F.A. & Hanrath, P. (1996). Analysis of interinstitutional observer agreement in interpretation of dobutamine stress echocardiograms. *J Am Coll Cardiol* **27**:330-336.
- Hollman, J.L. (1992). Myocardial revascularization. Coronary angioplasty and bypass surgery indications. *Med Clin North Am* **76**:1083-1097.
- Hor, G. (1988). Myocardial scintigraphy - 25 years after start. *Eur J Nucl Med* **13**:619-636.

- Horvath, K.A., Cohn, L.H., Cooley, D.A., Crew, J.R., Frazier, O.H., Griffith, B.P., Kadipasaoglu, K., Lansing, A., Mannting, F., March, R., Mirhoseini, M.R. & Smith, C. (1997). Transmyocardial laser revascularization: results of a multicenter trial with transmyocardial laser revascularization used as sole therapy for end-stage coronary artery disease. *J Thorac Cardiovasc Surg* **113**:645-653.
- Hughes, G.C., Abdel-aleem, S., Biswas, S.S., Landolfo, K.P. & Lowe, J.E. (1999). Transmyocardial laser revascularization: experimental and clinical results. *Can J Cardiol* **15**:797-806.
- Iliceto, S. (1995). Pharmacological agents for stress testing in the diagnosis of coronary artery disease. *Eur Heart J* **16 (suppl M)**:1-2.
- Iskander, S. & Iskandrian, A.E. (1998). Risk assessment using single-photon emission computed tomographic technetium-99m sestamibi imaging. *J Am Coll Cardiol* **32**:57-62.
- Iskandrian, A.S., Verani, M.S. & Heo, J. (1994). Pharmacologic stress testing: mechanism of action, hemodynamic responses, and results in detection of coronary artery disease. *J Nucl Cardiol* **1**:94-111.
- Jerosch-Herold, M. & Wilke, N. (1997). MR first pass imaging: quantitative assessment of transmural perfusion and collateral flow. *Int J Card Imaging* **13**:205-218.
- Jerosch-Herold, M., Wilke, N. & Stillman, A.E. (1998). Magnetic resonance quantification of the myocardial perfusion reserve with a Fermi function model for constrained deconvolution. *Med Phys* **25**:73-84.
- Jivan, A., Horsfield, M.A., Moody, A.R. & Cherryman, G.R. (1997). Dynamic T1 measurement using snapshot-FLASH MRI. *J Magn Reson* **127**:65-72.
- Johnson, L.W. & Krone, R. (1993). Cardiac catheterization 1991: a report of the Registry of the Society for Cardiac Angiography and Interventions (SCA&I). *Catheter Cardiovasc Diag* **28**:219-220.

- Jones, E.L., Craver, J.M., Kaplan, J.A., King, S.B., Douglas, J.S., Morgan, E.A. & Hatcher, C.R., Jr. (1978). Criteria for operability and reduction of surgical mortality in patients with severe left ventricular ischemia and dysfunction. *Ann Thorac Surg* **25**: 413-424.
- Judkins, M.P. (1967). Selective coronary arteriography. I. A percutaneous transfemoral technique. *Radiology* **89**:815-824.
- Kaul, S., Glasheen, W.P., Oliner, J.D., Kelly, P. & Gascho, J.A. (1991). Relation between anterograde blood flow through a coronary artery and the size of the perfusion bed it supplies: experimental and clinical implications. *J Am Coll Cardiol* **17**:1403-1413.
- Keijer, J.T., Bax, J.J., van Rossum, A.C., Visser, F.C. & Visser, C.A. (1997). Myocardial perfusion imaging: clinical experience and recent progress in radionuclide scintigraphy and magnetic resonance imaging. *Int J Card Imaging* **13**:415-431.
- Keijer, J.T., van Rossum, A.C., Eenige, M.J., Bax, J.J., Visser, F.C., Teule, J.J. & Visser, C.A. (2000). Magnetic resonance imaging of regional myocardial perfusion in patients with single-vessel coronary artery disease: quantitative comparison with 201-thallium-SPECT and coronary angiography. *J Magn Reson Imaging* **11**:607-615.
- Keijer, J.T., van Rossum, A.C., van Eenige, M.J., Karreman, A.J., Hofman, M.B., Valk, J. & Visser, C.A. (1995). Semiquantitation of regional myocardial blood flow in normal human subjects by first-pass magnetic resonance imaging. *Am Heart J* **130**:893-901.
- Kety, S.S. (1951). The theory and application of the exchange of inert gas in lung and tissues. *Pharmacology* **3**:1-41.
- Kim, R.J., Chen, E.L., Lima, J.A. & Judd, R.M. (1996). Myocardial Gd-DTPA kinetics determine MRI contrast enhancement and reflect the extent and severity of myocardial injury after acute reperfused infarction. *Circulation* **94**:3318-3326.
- Kim, R.J., Fieno, D.S., Parrish, T.B., Harris, K., Chen, E.L., Simonetti, O., Bundy, J., Finn, J.P., Klocke, F.J. & Judd, R.M. (1999). Relationship of MRI delayed contrast enhancement to irreversible injury, infarct age, and contractile function. *Circulation* **100**:1992-2002.

- Kim, R.J., Wu, E., Rafael, A., Chen, E.L., Parker, M.A., Simonetti, O., Klocke, F.J., Bonow, R.O. & Judd, R.M. (2000). The use of contrast-enhanced magnetic resonance imaging to identify reversible myocardial dysfunction. *N Engl J Med* **343**:1445-1453.
- Klein, C., Nekolla, S., Bengel, F.M., Momose, M., Sammer, A., Haas, F., Shnackenburg, B., Delius, W., Mudra, H., Wolfram, D. & Schwaiger, M. (2002). Assessment of myocardial viability with contrast-enhanced magnetic resonance imaging: comparison with positron emission tomography. *Circulation* **105**:162-167.
- Klein, M.A., Collier, B.D., Hellman, R.S. & Bamrah, V.S. (1993). Detection of chronic coronary artery disease: value of pharmacologically stressed, dynamically enhanced turbo-fast low-angle shot MR images. *Am J Roentgenol* **161**:257-263.
- Kohmoto, T., De Rosa, C.M., Yamamoto, N., Fisher, P.E., Failey, P., Smith, C.R. & Burkhoff, D. (1998). Evidence of vascular growth associated with laser treatment of normal canine myocardium. *Ann Thorac Surg* **65**:1360-1367.
- Kosa, I., Blasini, R., Schneider-Eicke, J., Dickfeld, T., Neumann, F.J., Ziegler, S.I., Matsunari, I., Nerverve, J., Schomig, A. & Schwaiger, M. (1999). Early recovery of coronary flow reserve after stent implantation as assessed by positron emission tomography. *J Am Coll Cardiol* **34**:1036-1041.
- Krahwinkel, W., Ketteler, T., Godke, J., Wolfertz, J., Ulbricht, L.J., Krakau, I. & Gulker, H. (1997a). Dobutamine stress echocardiography. *Eur Heart J* **18 (suppl D)**:D9-D15.
- Krahwinkel, W., Ketteler, T., Wolfertz, J., Godke, J., Krakau, I., Ulbricht, L.J., Mecklenbeck, W. & Gulker, H. (1997b). Detection of myocardial viability using stress echocardiography. *Eur Heart J* **18 (suppl D)**:D111-D116.
- Kramer, C.M., Rogers, W.J., Theobald, T.M., Power, T.P., Petruolo, S. & Reichek, N. (1996). Remote noninfarcted region dysfunction soon after first anterior myocardial infarction. A magnetic resonance tagging study. *Circulation* **94**:660-666.

- Kuijjer, J.P., Marcus, J.T., Gotte, M.J., van Rossum, A.C. & Heethaar, R.M. (1999). Simultaneous MRI tagging and through-plane velocity quantification: a three-dimensional myocardial motion tracking algorithm. *J Magn Reson Imaging* 9:409-419.
- Kurz, D.J., Naegeli, B. & Bertel, O. (2000). A double-blind, randomized study of the effect of immediate intravenous nitroglycerin on the incidence of postprocedural chest pain and minor myocardial necrosis after elective coronary stenting. *Am Heart J* 139:35-43.
- Kwong, K.F., Kanellopoulos, G.K., Nickols, J.C., Pogwizd, S.M., Saffitz, J.E., Schuessler, R.B. & Sundt, T.M. (1997). Transmyocardial laser treatment denervates canine myocardium. *J Thorac Cardiovasc Surg* 114:883-889.
- Laham, R.J., Sellke, F.W., Edelman, E.R., Pearlman, J.D., Ware, J.A., Brown, D.L., Gold, J.P. & Simons, M. (1999). Local perivascular delivery of basic fibroblast growth factor in patients undergoing coronary bypass surgery: results of a phase I randomized, double-blind, placebo-controlled trial. *Circulation* 100:1865-1871.
- Lamas, G.A., Flaker, G.C., Mitchell, G., Smith, S.C.J., Gersh, B.J., Wun, C.C., Moye, L., Rouleau, J.L., Rutherford, J.D. & Pfeffer, M.A. (1995). Effect of infarct artery patency on prognosis after acute myocardial infarction. The Survival and Ventricular Enlargement Investigators. *Circulation* 92:1101-1109.
- Lanzer, P., Barta, C., Botvinick, E.H., Wiesendanger, H.U., Modin, G. & Higgins, C.B. (1985). ECG-synchronized cardiac MR imaging: method and evaluation. *Radiology* 155:681-686.
- Larsson, H.B., Fritz-Hansen, T., Rostrup, E., Sondergaard, L., Ring, P. & Henriksen, O. (1996). Myocardial perfusion modeling using MRI. *Magn Reson Med* 35:716-726.
- Larsson, H.B., Stubgaard, M., Sondergaard, L. & Henriksen, O. (1994). In vivo quantification of the unidirectional influx constant for Gd-DTPA diffusion across the myocardial capillaries with MR imaging. *J Magn Reson Imaging* 4:433-440.
- Lauerma, K., Virtanen, K.S., Sipila, L.M., Hekali, P. & Aronen, H.J. (1997). Multislice MRI in assessment of myocardial perfusion in patients with single-vessel proximal left anterior

- descending coronary artery disease before and after revascularization. *Circulation* **96**:2859-2867.
- Lauffer, R.B. (1987). Paramagnetic metal complexes as water proton relaxation agents for NMR imaging: theory and design. *Chem Rev* **87**:901-927.
- Lieu, T.A., Gurley, R.J., Lundstrom, R.J. & Parmley, W.W. (1996). Primary angioplasty and thrombolysis for acute myocardial infarction: an evidence summary. *J Am Coll Cardiol* **27**:737-750.
- Lomboy, C.T., Schulman, D.S., Grill, H.P., Flores, A.R., Orié, J.E. & Granato, J.E. (1995). Redistribution thallium-201 scintigraphy to determine myocardial viability early after myocardial infarction. *J Am Coll Cardiol* **25**:210-217.
- Losordo, D.W., Vale, P.R. & Isner, J.M. (1999). Gene therapy for myocardial angiogenesis. *Am Heart J* **138**:S132-S141.
- Lutter, G., Sarai, K., Nitzsche, E., Saurbier, B., Frey, M., Hoegerle, S., Martin, J., Zipfel, M., Spillner, G. & Beyersdorf, F. (2000). Evaluation of transmyocardial laser revascularization by following objective parameters of perfusion and ventricular function. *Thorac Cardiovasc Surg* **48**:79-85.
- Manning, W.J., Atkinson, D.J., Grossman, W., Paulin, S. & Edelman, R.R. (1991). First-pass nuclear magnetic resonance imaging studies using gadolinium-DTPA in patients with coronary artery disease. *J Am Coll Cardiol* **18**:959-965.
- Martin, E.T., Fuisz, A.R. & Pohost, G.M. (1998). Imaging cardiac structure and pump function. *Cardiol Clin* **16**:135-160.
- Matheijssen, N.A., Louwerenburg, H.W., van Ruge, F.P., Arens, R.P., Kauer, B., de Roos, A. & van der Wall, E.E. (1996). Comparison of ultrafast dipyridamole magnetic resonance imaging with dipyridamole SestaMIBI SPECT for detection of perfusion abnormalities in patients with one-vessel coronary artery disease: assessment by quantitative model fitting. *Magn Reson Med* **35**:221-228.

- Matter, C., Nagel, E., Stuber, M., Boesiger, P. & Hess, O.M. (1996). Assessment of systolic and diastolic LV function by MR myocardial tagging. *Basic Res Cardiol* **91** (suppl 2): 23-28.
- McVeigh, E.R. (1996). MRI of myocardial function: motion tracking techniques. *Magn Reson Imaging* **14**:137-150.
- McVeigh, E.R. & Bolster, B.D., Jr. (1998). Improved sampling of myocardial motion with variable separation tagging. *Magn Reson Med* **39**:657-661.
- Melin, J.A., Wijns, W., Keyeux, A., Gurne, O., Cogneau, M., Michel, C., Bol, A., Robert, A., Charlier, A. & Pouleur, H. (1988). Assessment of thallium-201 redistribution versus glucose uptake as predictors of viability after coronary occlusion and reperfusion. *Circulation* **77**:927-934.
- Meller, S.T. & Gebhart, G.F. (1992). A critical review of the afferent pathways and the potential chemical mediators involved in cardiac pain. *Neuroscience* **48**:501-524.
- Merlet, P., Mazoyer, B., Hittinger, L., Valette, H., Saal, J.P., Bendriem, B., Crozatier, B., Castaigne, A., Syrota, A. & Rande, J.L. (1993). Assessment of coronary reserve in man: comparison between positron emission tomography with oxygen-15-labeled water and intracoronary Doppler technique. *J Nucl Med* **34**:1899-1904.
- Milano, A., Pratali, S., Tartarini, G., Mariotti, R., De Carlo, M., Paterni, G., Boni, G. & Bortolotti, U. (1998). Early results of transmyocardial revascularization with a holmium laser. *Ann Thorac Surg* **65**:700-704.
- Mirhoseini, M. & Cayton, M.M. (1981). Revascularization of the heart by laser. *J Microsurg* **2**:253-260.
- Misra, V.K., Agirbasli, M. & Fischell, T.A. (1997). Coronary artery vasomotion after percutaneous transluminal coronary angioplasty. *Clin Cardiol* **20**:915-922.
- Mulvagh, S.L. (2000). Myocardial perfusion by contrast echocardiography: diagnosis of coronary artery disease using contrast-enhanced stress echocardiography and assessment of coronary anatomy and flow reserve. *Coron Artery Dis* **11**:243-251.

- Muzik, O., Duvernoy, C., Beanlands, R.S., Sawada, S., Dayanikli, F., Wolfe, E.R., Jr & Schwaiger, M. (1998). Assessment of diagnostic performance of quantitative flow measurements in normal subjects and patients with angiographically documented coronary artery disease by means of nitrogen-13 ammonia and positron emission tomography. *J Am Coll Cardiol* **31**:534-540.
- Nagel, E., Lehmkuhl, H.B., Bocksch, W., Klein, C., Vogel, U., Frantz, E., Ellmer, A., Dreysse, S. & Fleck, E. (1999). Noninvasive diagnosis of ischemia-induced wall motion abnormalities with the use of high-dose dobutamine stress MRI: comparison with dobutamine stress echocardiography. *Circulation* **99**:763-770.
- Nagel, E., Schneider, U., Schalla, S., Ibrahim, T., Schnackenburg, B., Bornstedt, A., Klein, C., Lehmkuhl, H.B. & Fleck, E. (2000). Magnetic resonance real-time imaging for the evaluation of left ventricular function. *J Cardiovasc Magn Reson* **2**:7-14.
- Nesto, R.W. & Kowalchuk, G.J. (1987). The ischemic cascade: temporal sequence of hemodynamic, electrocardiographic and symptomatic expressions of ischemia. *Am J Cardiol* **59**:23C-30C.
- Ofili, E.O., Labovitz, A.J. & Kern, M.J. (1993). Coronary flow velocity dynamics in normal and diseased arteries. *Am J Cardiol* **71**:3D-9D.
- Orlandi, C. (1996). Pharmacology of coronary vasodilation: a brief review. *J Nucl Cardiol* **3**:S27-S30.
- Owen, A.R. & Stables, R.H. (2000). Myocardial revascularisation by laser. *Int J Cardiol* **72**:215-220.
- Pagley, P.R., Beller, G.A., Watson, D.D., Gimble, L.W. & Ragosta, M. (1997). Improved outcome after coronary bypass surgery in patients with ischemic cardiomyopathy and residual myocardial viability. *Circulation* **96**:793-800.
- Patlak, C.S., Blasberg, R.G. & Fenstermacher, J.D. (1983). Graphical evaluation of blood-to-brain transfer constants from multiple-time uptake data. *J Cereb Blood Flow Metab* **3**:1-7.

- Pelletier, M.P., Giaid, A., Sivaraman, S., Dorfman, J., Li, C.M., Philip, A. & Chiu, R.C. (1998). Angiogenesis and growth factor expression in a model of transmural revascularization. *Ann Thorac Surg* 66:12-18.
- Penzkofer, H., Wintersperger, B.J., Knez, A., Weber, J. & Reiser, M. (1999). Assessment of myocardial perfusion using multisection first-pass MRI and color-coded parameter maps: a comparison to <sup>99m</sup>Tc Sesta MIBI SPECT and systolic myocardial wall thickening analysis. *Magn Reson Imaging* 17:161-170.
- Picano, E., Bento de Sousa, M., de Moura Duarte, L., Pingitore, A. & Sicari, R. (1994). Detection of viable myocardium by dobutamine and dipyridamole stress echocardiography. *Herz* 19:204-209.
- Picano, E., Lattanzi, F., Sicari, R., Silvestri, O., Polimeno, S., Pingitore, A., Petix, N., Margaria, F., Magaia, O., Mathias, W.J., Lowenstein, J., Minardi, G., Coletta, C. & Borges, A. (1997). Role of stress echocardiography in risk stratification early after an acute myocardial infarction. EPIC (Echo Persantin International Cooperative) and EDIC (Echo Dobutamine International Cooperative) Study Groups. *Eur Heart J* 18 (suppl D):D78-D85.
- Pigott, J.D., Kouchoukos, N.T., Oberman, A. & Cutter, G.R. (1985). Late results of surgical and medical therapy for patients with coronary artery disease and depressed left ventricular function. *J Am Coll Cardiol* 5:1036-1045.
- Prato, F.S., Wisenberg, G., Marshall, T.P., Uksik, P. & Zabel, P. (1988). Comparison of the biodistribution of gadolinium-153 DTPA and technetium-99m DTPA in rats. *J Nucl Med* 29:1683-1687.
- Qian, J., Ge, J., Baumgart, D., Sack, S., Haude, M. & Erbel, R. (1999). Prevalence of microvascular disease in patients with significant coronary artery disease. *Herz* 24:548-557.
- Rahimtoola, S.H. (1989). The hibernating myocardium. *Am Heart J* 117:211-221.
- Rahimtoola, S.H. (1995). From coronary artery disease to heart failure: role of the hibernating myocardium. *Am J Cardiol* 75:16E-22E.

- Reeder, S.B., Atalar, E., Faranesh, A.Z. & McVeigh, E.R. (1999). Multi-echo segmented k-space imaging: an optimized hybrid sequence for ultrafast cardiac imaging. *Magn Reson Med* **41**:375-385.
- Reid, P.G., Fraser, A.G., Watt, A.H., Henderson, A.H. & Routledge, P.A. (1990). Acute haemodynamic effects of intravenous infusion of adenosine in conscious man. *Eur Heart J* **11**: 1018-1028.
- Renkin, E.M. (1959). Transport of potassium-42 from blood to tissue in isolated mammalian skeletal muscles. *Am J Physiol* **197**:1205-1210.
- Rimoldi, O., Burns, S.M., Rosen, S.D., Wistow, T.E., Schofield, P.M., Taylor, G. & Camici, P.G. (1999). Measurement of myocardial blood flow with positron emission tomography before and after transmural laser revascularization. *Circulation* **100**:II134-II138.
- Rongen, G.A., Brooks, S.C., Pollard, M.J., Ando, S., Dajani, H.R., Notarius, C.F. & Floras, J.S. (1999). Effect of adenosine on heart rate variability in humans. *Clin Sci* **96**:597-604.
- Ross, J., Jr. (1986). Assessment of ischemic regional myocardial dysfunction and its reversibility. *Circulation* **74**:1186-1190.
- Roth, J.L., Nugent, M., Gray, J.E., Julsrud, P.R., Berquist, T.H., Sill, J.C. & Kispert, D.B. (1985). Patient monitoring during magnetic resonance imaging. *Anesthesiology* **62**:80-83.
- Sabia, P.J., Powers, E.R., Jayaweera, A.R., Ragosta, M. & Kaul, S. (1992). Functional significance of collateral blood flow in patients with recent acute myocardial infarction. A study using myocardial contrast echocardiography. *Circulation* **85**:2080-2089.
- Saeed, M., Wendland, M.F., Watzinger, N., Lund, G., Akbari, H. & Higgins, C.B. (2000). Contrast enhanced magnetic resonance imaging for characterization of myocardial and coronary artery disease. *Radiol Med* **100**:201-215.
- Salustri, A., Fioretti, P.M., McNeill, A.J., Pozzoli, M.M. & Roelandt, J.R. (1992). Pharmacological stress echocardiography in the diagnosis of coronary artery disease and myocardial ischaemia: a comparison between dobutamine and dipyridamole. *Eur Heart J* **13**:1356-1362.

- Sambuceti, G., Parodi, O., Marcassa, C., Neglia, D., Salvadori, P., Giorgetti, A., Bellina, R.C., Di Sacco, S., Nista, N. & Marzullo, P. (1993). Alteration in regulation of myocardial blood flow in one-vessel coronary artery disease determined by positron emission tomography. *Am J Cardiol* 72:538-543.
- Sandstede, J.J., Bertsch, G., Beer, M., Kenn, W., Werner, E., Pabst, T., Lipke, C., Kretschmer, S., Neubauer, S. & Hahn, D. (1999). Detection of myocardial viability by low-dose dobutamine Cine MR imaging. *Magn Reson Imaging* 17:1437-1443.
- Schaefer, S., van Tyen, R. & Saloner, D. (1992). Evaluation of myocardial perfusion abnormalities with gadolinium-enhanced snapshot MR imaging in humans. Work in progress. *Radiology* 185:795-801.
- Schmermund, A., Bell, M.R., Lerman, L.O., Ritman, E.L. & Rumberger, J.A. (1997). Quantitative evaluation of regional myocardial perfusion using fast X-ray computed tomography. *Herz* 22:29-39.
- Schofield, P.M., Sharples, L.D., Caine, N., Burns, S., Tait, S., Wistow, T., Buxton, M. & Wallwork, J. (1999). Transmyocardial laser revascularisation in patients with refractory angina: a randomised controlled trial. *Lancet* 353:519-524.
- Schwaiger, M. (1994). Myocardial perfusion imaging with PET. *J Nucl Med* 35:693-698.
- Schwaiger, M. & Hutchins, G. (1995). Quantification of regional myocardial perfusion by PET: rationale and first clinical results. *Eur Heart J* 16 (suppl J):84-91.
- Schwaiger, M. & Muzik, O. (1991). Assessment of myocardial perfusion by positron emission tomography. *Am J Cardiol* 67:35D-43D.
- Schwitzer, J., Nanz, D., Kneifel, S., Bertschinger, K., Buchi, M., Knusel, P.R., Marincek, B., Luscher, T.F. & von Schulthess, G.K. (2001). Assessment of myocardial perfusion in coronary artery disease by magnetic resonance: a comparison with positron emission tomography and coronary angiography. *Circulation* 103:2230-2235.

- Sechtem, U., Pflugfelder, P.W., White, R.D., Gould, R.G., Holt, W., Lipton, M.J. & Higgins, C.B. (1987). Cine MR imaging: potential for the evaluation of cardiovascular function. *Am J Roentgenol* **148**:239-246.
- Senior, R., Kaul, S., Soman, P. & Lahiri, A. (2000). Power doppler harmonic imaging: a feasibility study of a new technique for the assessment of myocardial perfusion. *Am Heart J* **139**:245-251.
- Senior, R., Sridhara, B.S., Anagnostou, E., Handler, C., Raftery, E.B. & Lahiri, A. (1994). Synergistic value of simultaneous stress dobutamine sestamibi single-photon-emission computerized tomography and echocardiography in the detection of coronary artery disease. *Am Heart J* **128**:713-718.
- Sensky, P.R. & Cherryman, G.R. (2000). What is the role of MRI in coronary syndromes? In *Challenges in acute coronary syndromes*, eds. de Bono, D.P. & Sobel, B., pp. 133-147. Blackwell Science.
- Sensky, P.R., Jivan, A., Hudson, N.M., Keal, R.P., Morgan, B., Tranter, J., de Bono, D.P., Samani, N.J. & Cherryman, G.R. (2000). Coronary artery disease: combined stress MR imaging protocol - one-stop evaluation of myocardial perfusion and function. *Radiology* **215**:608-614.
- Sheiban, I., Tonni, S., Marini, A. & Trevisani, G. (1995). Clinical and therapeutic implications of chronic left ventricular dysfunction in coronary artery disease. *Am J Cardiol* **75**: 23E-30E.
- Shroder K., Schultheiss H.-P. (1997). Coronary artery disease – diagnosis of ischaemia and general considerations. *Eur Heart J* **18**: D57-D62.
- Simonetti, O.P., Kim, R.J., Fieno, D.S., Hillenbrand, H.B., Wu, E., Bundy, J.M., Finn, J.P. & Judd, R.M. (2001). An improved MR imaging technique for the visualization of myocardial infarction. *Radiology* **218**:215-223.
- Sinitsyn, V. (2001). Magnetic resonance imaging in coronary heart disease. *European Journal of Radiology* **38**:191-199.
- Sinnaeve, P., Varenne, O., Collen, D. & Janssens, S. (1999). Gene therapy in the cardiovascular system: an update. *Cardiovasc Res* **44**:498-506.

- Spaan, J.A., Breuls, N.P. & Laird, J.D. (1981). Forward coronary flow normally seen in systole is the result of both forward and concealed back flow. *Basic Res Cardiol* **76**:582-586.
- Stein, P.K. & Kleiger, R.E. (1999). Insights from the study of heart rate variability. *Annu Rev Med* **50**:249-261.
- Strich, G., Hagan, P.L., Gerber, K.H. & Slutsky, R.A. (1985). Tissue distribution and magnetic resonance spin lattice relaxation effects of gadolinium-DTPA. *Radiology* **154**:723-726.
- Svendsen, J.H., Efsen, F. & Haunso, S. (1992). Capillary permeability of <sup>99m</sup>Tc-DTPA and blood flow rate in the human myocardium determined by intracoronary bolus injection and residue detection. *Cardiology* **80**:18-27.
- Tamaki, N., Kawamoto, M., Tadamura, E., Magata, Y., Yonekura, Y., Nohara, R., Sasayama, S., Nishimura, K., Ban, T. & Konishi, J. (1995). Prediction of reversible ischemia after revascularization. Perfusion and metabolic studies with positron emission tomography. *Circulation* **91**:1697-1705.
- Tanabe, M., Fujiwara, S., Ohta, N., Shimamoto, N. & Hirata, M. (1980). Pathophysiological significance of coronary collaterals for preservation of the myocardium during coronary occlusion and reperfusion in anaesthetised dogs. *Cardiovasc Res* **14**:288-294.
- Tong, C.Y., Prato, F.S., Wisenberg, G., Lee, T.Y., Carroll, E., Sandler, D., Wills, J. & Drost, D. (1993). Measurement of the extraction efficiency and distribution volume for Gd-DTPA in normal and diseased canine myocardium. *Magn Reson Med* **30**:337-346.
- Trent, R.J., Waiter, G.D., Hillis, G.S., McKiddie, F.I., Redpath, T.W. & Walton, S. (2000). Dobutamine magnetic resonance imaging as a predictor of myocardial functional recovery after revascularisation. *Heart* **83**:40-46.
- Tweedle, M.F., Gaughan, G.T., Hagan, J., Wedeking, P.W., Sibley, P., Wilson, L.J. & Lee, D.W. (1988). Considerations involving paramagnetic coordination compounds as useful NMR contrast agents. *Int J Radiat Appl Instrum* **15**:31-36.

- Uren, N.G., Melin, J.A., De Bruyne, B., Wijns, W., Baudhuin, T. & Camici, P.G. (1994). Relation between myocardial blood flow and the severity of coronary-artery stenosis. *N Engl J Med* 330:1782-1788.
- Vallee, J.P., Sostman, H.D., MacFall, J.R., De Grado, T.R., Zhang, J., Sebbag, L., Cobb, F.R., Wheeler, T., Hedlund, L.W., Turkington, T.G., Spritzer, C.E. & Coleman, R.E. (1998). Quantification of myocardial perfusion by MRI after coronary occlusion. *Magn Reson Med* 40:287-297.
- Vallee, J.P., Sostman, H.D., MacFall, J.R., Wheeler, T., Hedlund, L.W., Spritzer, C.E. & Coleman, R.E. (1997). MRI quantitative myocardial perfusion with compartmental analysis: a rest and stress study. *Magn Reson Med* 38:981-989.
- van der Wall, E.E., Vliegen, H.W., de Roos, A. & Bruschke, A.V. (1995). Magnetic resonance imaging in coronary artery disease. *Circulation* 92:2723-2739.
- van Ruge, F.P., Holman, E.R., van der Wall, E.E., de Roos, A., van der Laarse, A. & Bruschke, A.V. (1993). Quantitation of global and regional left ventricular function by cine magnetic resonance imaging during dobutamine stress in normal human subjects. *Eur Heart J* 14:456-463.
- van Ruge, F.P., van der Wall, E.E., Spanjersberg, S.J., de Roos, A., Matheijssen, NA, Zwinderman, A.H., van Dijkman, P.R., Reiber, J.H. & Bruschke, A.V. (1994). Magnetic resonance imaging during dobutamine stress for detection and localization of coronary artery disease. Quantitative wall motion analysis using a modification of the centerline method. *Circulation* 90:127-138.
- Versaci, F., Tomai, F., Nudi, F., Gaspardone, A., De Fazio, A., Ciavolella, M., Crea, F., Mango, L., Chiariello, L. & Gioffre, P.A. (1996). Differences of regional coronary flow reserve assessed by adenosine thallium-201 scintigraphy early and six months after successful percutaneous transluminal coronary angioplasty or stent implantation. *Am J Cardiol* 78:1097-1102.
- Watada, H., Ito, H., Oh, H., Masuyama, T., Aburaya, M., Hori, M., Iwakura, M., Higashino, Y., Fujii, K. & Minamino, T. (1994). Dobutamine stress echocardiography predicts reversible

- dysfunction and quantitates the extent of irreversibly damaged myocardium after reperfusion of anterior myocardial infarction. *J Am Coll Cardiol* 24:624-630.
- Watzinger, N., Saeed, M., Wendland, M.F., Akbari, H., Lund, G. & Higgins, C.B. (2001). Myocardial viability: magnetic resonance assessment of functional reserve and tissue characterization. *J Cardiovasc Magn Reson* 3:195-208.
- Weiner, D.A., Ryan, T.J., McCabe, C.H., Chaitman, B.R., Sheffield, L.T., Fisher, L.D. & Tristani, F. (1987). Value of exercise testing in determining the risk classification and the response to coronary artery bypass grafting in three-vessel coronary artery disease: a report from the Coronary Artery Surgery Study (CASS) registry. *Am J Cardiol* 60:262-266.
- Weinmann, H.J., Brasch, R.C., Press, W.R. & Wesbey, G.E. (1984). Characteristics of gadolinium-DTPA complex: a potential NMR contrast agent. *Am J Roentgenol* 142:619-624.
- Weinmann, H.J., Press, W.R. & Gries, H. (1990). Tolerance of extracellular contrast agents for magnetic resonance imaging. *Invest Radiol* 25 (suppl 1):S49-S50.
- Wendland, M.F., Saeed, M., Lund, G. & Higgins, C.B. (1999). Contrast-enhanced MRI for quantification of myocardial viability. *J Magn Reson Imaging* 10:694-702.
- White, C.W., Wright, C.B., Doty, D.B., Hiratza, L.F., Eastham, C.L., Harrison, D.G. & Marcus, M.L. (1984). Does visual interpretation of the coronary arteriogram predict the physiologic importance of a coronary stenosis? *N Engl J Med* 310:819-824.
- Wieneke, H., Zander, C., Eising, E.G., Haude, M., Bockisch, A. & Erbel, R. (1999). Non-invasive characterization of cardiac microvascular disease by nuclear medicine using single-photon emission tomography. *Herz* 24:515-521.
- Wilke, N. (1998). MR measurement of myocardial perfusion. *Magma* 6:147
- Wilke, N., Jerosch-Herold, M., Stillman, A.E., Kroll, K., Tsekos, N., Merkle, H., Parrish, T., Hu, X., Wang, Y. & Bassingthwaighe, J. (1994). Concepts of myocardial perfusion imaging in magnetic resonance imaging. *Magn Reson Q* 10:249-286.

- Wilke, N., Jerosch-Herold, M., Wang, Y., Huang, Y., Christensen, B.V., Stillman, A.E., Ugurbil, K., McDonald, K. & Wilson, R.F. (1997). Myocardial perfusion reserve: assessment with multisection, quantitative, first-pass MR imaging. *Radiology* **204**:373-384.
- Wilke, N., Simm, C., Zhang, J., Ellermann, J., Ya, X., Merkle, H., Path, G., Ludemann, H., Bache, R.J. & Ugurbil, K. (1993). Contrast-enhanced first pass myocardial perfusion imaging: correlation between myocardial blood flow in dogs at rest and during hyperemia. *Magn Reson Med* **29**:485-497.
- Wolff, S.D., Day, R.A., Santiago, L., Macaluso, F., Carey, R., Chalmers, D., Slavin, G., Gulotta, S.J. & Hershman, R.A. (1999). Assessment of first-pass myocardial perfusion imaging during rest and adenosine stress: comparison with cardiac catheterization. *Proc Int Soc Magn Reson Med* **7**:305.
- Zipes, D.P. (2000). Specific Arrhythmias: Diagnosis and Treatment. In *Heart Disease*, ed. Brunswald A, pp. 640-704. Saunders WB.

